Aus dem Dr. von Haunerschen Kinderspital

Klinik der Universität München

Vorstand: Prof. Dr. med. Dr. sci. nat. Christoph Klein

Blast – T cell – interaction in pediatric acute myeloid leukemia

Dissertation

zum Erwerb des Doktorgrades der Medizin

an der Medizinischen Fakultät der

Ludwigs-Maximilians-Universität zu München

vorgelegt von Paula Rothämel aus München

2022

Mit Genehmigung der Medizinischen Fakultät
der Universität München

Berichterstatter:	Prof. Dr. med. Tobias Feuchtinger
Mitberichterstatter:	Prof. Dr. med. Philip Greif apl. Prof. Dr. med. Marcus Hentrich PD Dr. rer. nat. Hanna-Mari Baldauf
Mitbetreuung durch den promovierten Mitarbeiter:	Dr. med. Semjon Willier
Dekan:	Prof. Dr. med. Thomas Gudermann
Tag der mündlichen Prüfung:	22.12.2022

Eidesstattliche Versicherung

Rothämel, Paula

_____

Name, Vorname

Ich erkläre hiermit an Eides statt, dass ich die vorliegende Dissertation mit dem Titel

Blast – T cell – interaction in pediatric acute myeloid leukemia

selbständig verfasst, mich außer der angegebenen keiner weiteren Hilfsmittel bedient und alle Erkenntnisse, die aus dem Schrifttum ganz oder annähernd übernommen sind, als solche kenntlich gemacht und nach ihrer Herkunft unter Bezeichnung der Fundstelle einzeln nachgewiesen habe.
Ich erkläre des Weiteren, dass die hier vorgelegte Dissertation nicht in gleicher oder in ähnlicher Form bei einer anderen Stelle zur Erlangung eines akademischen Grades eingereicht wurde.

München, 03.01.2023	Paula Rothämel
Ort, Datum	Unterschrift Doktorand

1 Abbreviations

2B4	Natural killer cell receptor 2B4
AAAs	AML associated antigens
ALL	Acute lymphoblastic leukemia
Allo-HSCT	Allogeneic hematopoietic stem cell transplantation
AML	Acute myeloid leukemia
APCs	Antigen-presenting cells
ASNAs	AML-specific neo-antigens
ATAC	Assay for Transposase accessible chromatin
B3GAT1	Beta-1,3-Glucuronyltransferase 1
B-ALL	B-cell acute lymphoblastic leukemia
BM	Bone marrow
bmT cells	Bone marrow T cells
bp	Base pair
CAR	Chimeric antigen receptor
cCAR	Compound CAR
CCR1	C-C chemokine receptor type 1
CCR4	C-C chemokine receptor type 4
CD	Cluster of differentiation
cDNA	Complementary DNA
CLL1	C-type lectin-like molecule-1
CNS	Central nervous system
CREM	CAMP responsive element modulator
CTLA-4	Cytotoxic T-lymphocyte-associated protein 4
CXCR3	CXC-motive-chemokine receptor 3
DMSO	Dimethyl sulfoxide
DNA	Deoxyribonucleic acid
DNAseI	Desoxyribonuclease I
DYNLT1	Dynein light chain Tctex-type 1
Ec	Extracellularly stained
EMR2	EGF-like module-containing mucin-like hormone receptor-like 2
ENTPD1	Ectonucleoside triphosphate diphosphohydrolase 1
FAB classification	French American British association
FACS	Fluorescence-activated cell sorting
FC	Fold change

Fc	Fragment, crystallizable region
FcR	Fc receptor
FCS	Fetal bovine serum
FMF	Fluorenscence-minus-five
FMS	Fluorenscence-minus-six
Foxp3	Forkhead-box-protein P3
FR	Future relapse
FSC-A	Forward scatter-area
FSC-H	Forward scatter-height
FU	Fluorescence unit
GAL-9	Galectin-9
GITR	Glucocorticoid-induced TNFR-related protein
GZMB	Granzyme B
HAVCR2	Hepatitis A virus cellular receptor 2
HD	Healthy bone marrow donor
Healthy BMD	Healthy bone marrow donor
HVEM	Herpesvirus entry mediator
I	Inductor antigen
IC panel	Intracellular panel
ICOS	Inducible T-cell co-stimulator
ICOSL	Inducible T-cell co-stimulator ligand
ID	Initial diagnosis
IFN	Interferon
IFRD1	Interferon related developmental regulator 1
Ig	Immunoglobulin
IgG	Immunoglobulin G
IL2	Interleukin 2
IL21	Interleukin 21
IL21R	Interleukin 21 receptor
Initial Dx	Initial diagnosis
Int	Intermediate
Isotype Ctrl	Isotype control
LAG3	Lymphocyte-activation gene 3
LSCs	Leukemic stem cells
mAb	Monoclonal antibody
MD	Doctor of Medicine (Medicinae Doctor)
MDS	Myelodysplastic syndrome
MFI	Mean fluorescence intensity

mRNA	Messenger-RNA
MUC1 5E10	Mucin-1 5E10
MUC1 5E5	Mucin-1 5E5
NF-κB	Nuclear factor kappa-light-chain-enhancer of activated B cells
NFKBIA	NF-κB inhibitor alpha
NFR	No future relapse
NK cells	Natural killer cells
NKT cells	Natural killer T cells
NP40	Nonidet P40
Nt	Nucleotide
NT5E	5'-Nucleotidase ecto
OX-40	OX40 receptor
OX-40L	OX40 receptor-ligand
PBMCs	Peripheral blood mononuclear cells
PBS	Phosphate-buffered saline
PCR	Polymerase chain reaction
PD-1	Programmed cell death protein 1
PD-L1	Programmed cell death-ligand 1
PDCD1	Programmed cell death 1
Pen-Strep	Penicillin-Streptomycin
PRF1	Perforin 1
R	Relapse
RARA	Retinoic acid receptor alpha
RFS	Relapse-free survival
RIN	RNA integrity number
RNA	Ribonucleic acid
RNA-seq	RNA sequencing
RPKM	Reads per kilo base per million mapped reads
RPM	Rounds per minute
RPMI medium	Roswell Park Memorial Institute medium
scFv	Single chain variable fragment
SSC-A	Side scatter-area
synNotch receptor	Synthetic Notch receptor
T	Target antigen
T_{CM}	Central memory T cells
TCRγ/δ	T-cell receptor γ/δ

TD buffer	DNA tagmentation buffer
T_{EFF}	Effector T cells
T_{EM}	Effector memory T cells
TF	Transcription factor
Th cells	T helper cells
TIGIT	T-cell immunoreceptor with Ig and ITIM domains
TILs	Tumor-infiltrating lymphocytes
TIM-3	T-cell immunoglobulin and mucin-domain containing-3
TME	Tumor microenvironment
T_N	Naïve T cells
TNFRSF18	TNF receptor superfamily member 18
TNFRSF4	TNF receptor superfamily member 4
T_{regs}	Regulatory T cells
TRIM39	Tripartite motif containing 39
T_{SCM}	Stem cell-like memory T cells

2 Introduction

2.1 Pediatric acute myeloid leukemia

Acute myeloid leukemia (AML) is an aggressive type of hematological malignancy caused by the abnormal proliferation of immature myeloid cells (Austin et al., 2016). While acute lymphoblastic leukemia (ALL) is the most common form of cancer in children, AML mainly affects adults. Nevertheless, AML still accounts for approximately 15 % of pediatric leukemia (Klein et al., 2018).

Due to intensified treatment regimens and advancements in supportive care, the outcome for pediatric AML patients has improved substantially over the past years with current survival rates up to 75 % in high-income countries (Zwaan et al., 2015; Elgarten and Aplenc, 2020). Nonetheless, most treatment regimens still rely on conventional chemotherapeutic agents associated with significant toxicity (Fidler et al., 2016; Klein et al., 2018) and relapse rates remain high with 25-35 % (Zwaan et al., 2015). Therefore, AML is still one of the poorest prognosis pediatric cancers (Figure 1).

In view of those circumstances, central objective should be the development of more specific therapy measures. Here, immunotherapy provides important opportunities.

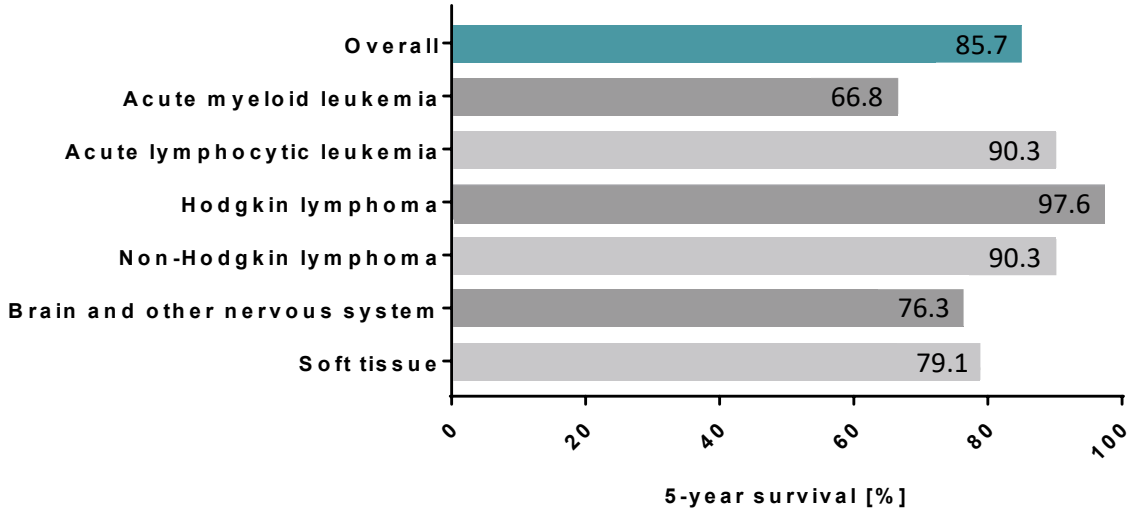

Figure 1: 5-year survival rate of pediatric cancer, Ages 0-19, 2009-2015. AML is still one of the poorest prognosis pediatric cancer (SEER Cancer Statistic Review, 1975-2016, Howlader et al., 2019).

2.2 Cancer immunotherapy

Over the last decades, immunotherapy has developed from a promising therapeutic option to a robust clinical reality for treating cancer patients.

In cancer formation, tumor cells develop certain strategies in order to escape immunosurveillance, for example by upregulation of co-inhibitory molecules on the surface and therefore negatively impacting the activity of tumor infiltrating lymphocytes (Austin et al., 2016). Preventing such escape mechanisms (immunoescape) and therefore enabling T cell mediated cytotoxity by using so-called *immune response amplifiers* (e.g. Checkpoint inhibitors) is a strategy used in anti-cancer immunotherapy (Majzner et al., 2017).

Another approach in immunotherapy of malignancies is the generation of a yet not existing immune response against tumor cells by using *synthetic immunotherapies*. These include monoclonal antibodies against surface structures of malignant cells, as well as the adoptive immunotherapy with T cells expressing chimeric antigen receptors (CARs, Majzner et al., 2017).

Recently, especially the monoclonal antibodies Ipilimumab (anti-CTLA-4) and Nivolumab (anti-PD-1) could achieve brilliant success in improving survival of metastatic melanoma patients (Austin et al., 2016; Larkin et al., 2019).

In synthetic immunotherapy CAR T cells targeting the B-ALL associated antigen CD19 have yielded high remission rates particularly in pediatric patients (Maude et al., 2014, 2018).

Mutational load is thought to be a prerequisite for effective immune response amplification by e.g. checkpoint inhibition (Samstein et al., 2019). However, synthetic immunotherapy e.g. by CAR T cells does not necessitate mutations, as it does not rely on previously primed T cells that specifically recognize cancer cells in contrast to immune response amplifiers (Hegde and Chen, 2020). B-ALL serves here as an example that a low mutational load malignancy, which is probably not accessible to immune response amplification, can be efficiently treated by synthetic immunotherapy.

This is of particular relevance in view of the widely shared supposition that a high tumor mutational burden is essential for tumor cell immunogenicity and therefore fundamental for a relevant response to immunotherapy (Austin et al., 2016).

2.3 Immunotherapy of pediatric AML

Immunotherapeutic approaches in AML have been much less successful so far. This is primarily due to the lack of appropriate AML specific target structures suitable for immunotherapy (Mardiana and Gill, 2020). Considering AML as malignant entity with one of the lowest mutational burden, targeting of AML-specific neo-antigens arising from genetic mutations may not be effective (Austin et al., 2016). Furthermore, immune recognition is less likely to respond to immune checkpoint blockade due to the unclear immunogenicity of the AML cells (Perna et al., 2017).

AML associated antigens (AAAs), which are self-antigens that are abnormally expressed by AML cells, might represent more promising immune targets e.g. for CAR T-cell therapy (Austin et al., 2016). But

as the majority of reported AAAs like CD33, CD123 and CLL1 is also expressed in healthy tissues, single targeting approaches could lead to severe on-target off-leukemia toxicity (Haubner et al., 2019; Lamble and Tasian, 2019).

Combinatorial CAR T-cell therapies (e.g. Tandem-CARs, synNotch-gated CARs) might enhance efficacy of this immunotherapeutic approach without increasing on-target off-leukemia effects (Daver et al., 2021; Perna et al., 2017). Here, a Tandem-Car contains two extracellular antigen-binding domains against two different antigens, joined in tandem via a linker molecule, with a common intracellular domain (Figure 2). Therefore, target cells need to express both antigens at the same time in order to activate the CAR T cells (Navai and Ahmed, 2016). In case of the synNotch-gated CAR T-cell approach (Figure 3) a synNotch receptor for one antigen (inductor antigen) controls the inducible expression of a CAR for a second antigen (target antigen, Roybal et al., 2016).

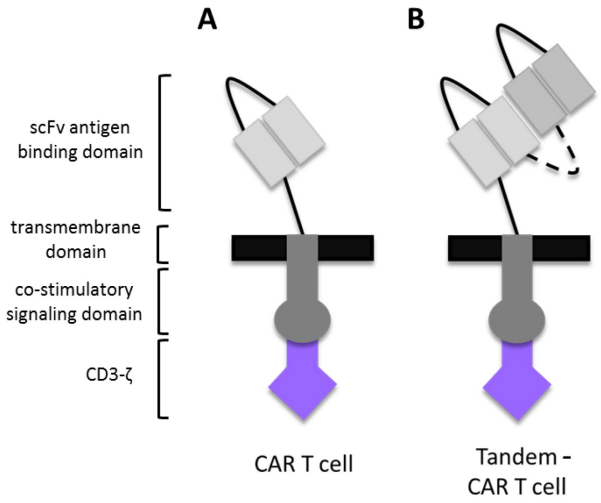

Figure 2: CAR constructs. A) Single-targeting second generation CAR contains an intracellular CD3-ζ or Fc receptor-γ signaling domain and an intracellular co-stimulatory domain. **B)** Tandem-CAR contains two extracellular antigen-binding domains against two different antigens, joined in tandem via a linker molecule, with a common intracellular domain (Figure adapted from Navai and Ahmed, 2016).

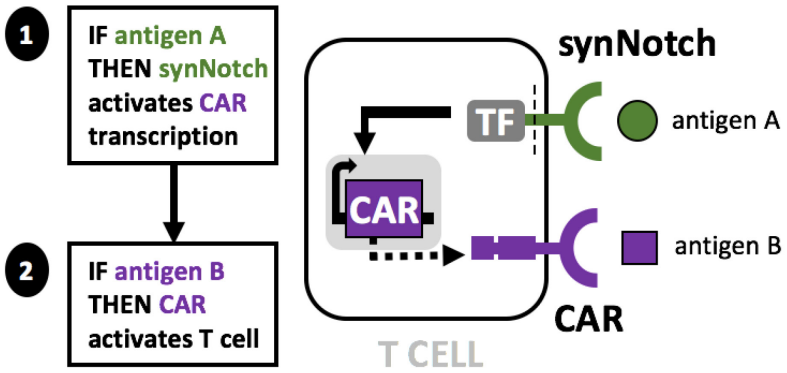

Figure 3: Design of a synNotch-gated CAR T-cell construct. After binding antigen A the synNotch receptor leads to expression of a CAR targeting antigen B via releasing of a transcription factor (Figure adapted from Roybal et al., 2016).

Furthermore, AML cells employ various mechanisms in order to impair anti-leukemic immune responses as immunoescape mechanism, which is of particular relevance for any T cell-based AML immunotherapy. Several receptor-ligand pairs with conserved functions in physiologic immunology could be potentially involved in the AML – T cell crosstalk possibly leading to immunoescape. High levels of CD80 or CD86 on AML cells may induce immunosuppression via the engagement of

co-inhibitory receptor CTLA-4 on T cells (Austin et al., 2016). Additionally, AML blasts were reported to express high levels of CD112 and CD155, which was correlated with a downregulation of their stimulatory receptor CD226 on NK (Sanchez-Correa et al., 2012) and T cell side (Wang et al., 2018) and led to an impaired prognosis. To sum up, AML blasts may develop specific strategies in order to create environmental conditions favorable for leukemia progression by counteracting T cell mediated cytotoxicity (Austin et al., 2016).

Nevertheless, it remains unclear, which mechanisms in the interaction of AML blasts and T cells contribute to immunoescape in pediatric AML, as mentioned results were mainly obtained in adults (Kaspers and Creutzig, 2005).

3 Aims and objectives of this study

Although immunotherapy has developed from a promising therapeutic option to a robust clinical reality for treating cancer patients over the last decades, pediatric AML patients did not profit so far from this development. This is due to the unknown immunogenicity of AML, lacking feasible AML-specific target antigens and low patient numbers that make clinical studies cumbersome.

In order to analyze the immunologic landscape within the AML bone marrow and to identify possible target antigens for combinatorial CAR-T cell therapy, bmT cells (T cells within the bone marrow), AML blasts, NK and NKT cells within bone marrow samples of 29 pediatric AML patients and 9 healthy bone marrow (BM) donors were assayed by flow cytometry, RNA-sequencing and ATAC-sequencing. Subsequently, three differential analyzes were most relevant to us:

(1) AML patients vs. healthy controls: what is the effect of AML disease on healthy bone marrow immune populations such as T cells?
(2) Initial AML samples with future relapse vs. initial AML samples without future relapse: can we define prognostic factors at time of primary diagnosis?
(3) Initial AML samples vs. relapsed AML samples: what changes occur both on the side of leukemia and bmT cells during the course of AML relapse?

Finally, we examined whether the observed changes in phenotype of physiologic immune cells were linked to blast phenotype by integrating results from both populations. Thus, to determine whether AML blasts do induce e.g. T cell phenotype changes we analyzed two common axes of interaction between antigen-presenting cells (APCs) and T cells in the context of AML. To that end, we correlated the expression of CD86 and CD112/CD155 on AML blasts to the respective expression of CTLA-4/CD28 on bmT cells and TIGIT/CD226 on bmT cells, NK and NKT cells.

4 Materials

4.1 Equipment and software

Equipment/software	Name, Manufacturer
Cell counting auxiliaries	Cell Counting Chamber Neubauer, Chamber Depth 0.1 mm, Paul Marienfeld, Lauda-Königshofen, Germany
Centrifuges	Mini Centrifuge Fresco 17, Heraeus, Hanau, Germany
	Centrifuge 5810R, Eppendorf, Hamburg, Germany
Cooling units	Cooler (4 °C) Comfort No Frost, Liebherr, Biberach an der Riß, Germany
	Freezer (-20 °C) Premium No Frost, Liebherr, Biberach an der Riß, Germany
	Freezer (-86 °C) HERAfreeze HFC Series, Heraeus, Hanau, Germany
	Thermo Scientific Cryo 200 liquid nitrogen dewar, Thermo Fisher Scientific, Waltham, Massachusetts, USA
Flow cytometer	BD FACSAria III, BD, Franklin Lakes, New Jersey, USA
	BD LSRFortessa Cell Analyzer, BD, Franklin Lakes, New Jersey, USA
Heat block	Eppendorf ThermoMixer comfort, Eppendorf, Hamburg, Germany
Incubator	HERAcell 240, 150i CO_2 Incubator, Thermo Fisher, Waltham, Massachusetts, USA
Laminar flow hood	HERAsafe, Thermo Fisher, Waltham, Massachusetts, USA
Cleaner Box	UVC/T-M-AR, DNA-/RNA UV-cleaner box, Biosan, Riga, Latvia
Vortexer	Vortex Genie 3, IKA-Werke, Staufen, Germany
Microscope	Leica DM IL, Leica Microsysteme, Wetzlar, Germany
Agilent 2100 Bioanalyzer	Agilent Technologies, Santa Clara, California, USA
Pipettes (manual)	2,5 µl, 20 µl, 200 µl, 1000 µl Eppendorf Research, Eppendorf, Hamburg, Germany
Software	BD FACSDiva 8.0.1, BD Biosciences, Franklin Lakes, New Jersey, USA
	FlowJo 10.0.7r2, Ashland, Oregon, USA
	GraphPad PRISM 7.0, La Jolla, California, USA
	Microsoft Office 2010, Redmond, Washington, USA
	2100 Bioanalyzer Expert, Agilent Technologies, Santa Clara, California, USA
	DNASTAR – Lasergene, DNASTAR, Madison, Wisconsin, USA
	Arraystar 15, DNASTAR, Madison, Wisconsin, USA
Sequencer	NextSeq500 & NextSeq550, Illumina, San Diego, California, USA
Thermocycler	peqSTAR 96 Universal Gradient, Isogen, Utrecht, Netherlands
Vacuum pump	Vakuumsytem BVC 21 NT, Vacuubrand, Wertheim, Germany
Water bath	3043, Köttermann, Uetze/Hänigsen, Germany
Freezing container	Nalgene Mr. Frosty, Thermo Fisher Scientific, Waltham, USA

Pipettes (electrical)	Easypet 3, Easypet Original, Eppendorf, Hamburg, Germany
Scale	R 200 D, Sartorius AG, Göttingen, Germany

4.2 Solutions, media and sera for cell culture

Solution/Medium/Serum	Order number	Manufacturer
Compensation beads	552843	BD Biosciences, San Diego, California, USA
Fetal Bovine Serum	F0804	Sigma-Aldrich CHEMIE, Steinheim, Germany
FIX & PERM™ Cell Permeabilization Kit	GAS004	Life Technologies, Frederick, Maryland, USA
L-Glutamine 200 mM	K 0283	Biochrom, Berlin, Germany
Penicillin/Streptomycin	15140-122	Gibco, Life Technologies, Darmstadt, Germany
Trypan blue	15250-061	Gibco, Life Technologies, Darmstadt, Germany
Tween 20	11332465001	Sigma-Aldrich, St.Louis, Missouri, USA
VLE RPMI 1640 Medium	F1415	Biochrom, Berlin, Germany
Nonidet P40 Substitute	11332473001	Sigma-Aldrich, St.Louis, Missouri, USA
PBS	14190-250	Invitrogen, Carlsbad, California, USA
Quick-RNA™ Microprep	R1051	Zymo, Irvine, California, USA
Human BD Fc Block™	564220	Becton, Dickinson and Company (BD), Franklin Lakes, New Jersey, USA
DNAse I	18047-019	Invitrogen, Carlsbad, California, USA
Bioanalyzer High Sensitivity DNA Analysis Kit	5067-4626	Agilent Technologies, Santa Clara, California, USA
Agilent RNA 6000 Pico Kit	5067-1513	Agilent Technologies, Santa Clara, California, USA
Digitonin	G9441	Promega, Fitchburg, Wisconsin, USA
Illumina NextSeq 500 Mid	FC-404-2001	Illumina, San Diego, California, USA
Nextera DNA Library Kit	FC-121-1030	Illumina, San Diego, California, USA
RNAse free Tubes	20170-038	VWR International, Radnor, Pennsylvania, USA
DNA Clean & Concentrator™ -5	D4014	Zymo Research Corp., Irvine, California, USA
DMSO	4720.4	Carl Roth, Karlsruhe, Germany
NEBNext® Ultra™ II Directional RNA Library Prep Kit for Illumina	E7760S	New England Biolabs, Ipswich, Massachusetts, USA
NEBNext® Poly(A) mRNA Magnetic Isolation Module	S7490S	New England Biolabs, Ipswich, Massachusetts, USA
NEBNext® Multiplex Oligos for Illumina® (Dual Index Primers Set 1)	E7600S	New England Biolabs, Ipswich, Massachusetts, USA
NextSeq 500/550 High Output Kit v2.5 (150 Cycles)	20024907	Illumina, San Diego, California, USA

4.3 Consumables

Consumable	Order number	Name, Manufacturer
Cannula	851.638.235	Safety-Multifly-Needle, Sarstedt, Nümbrecht, Germany
Cell culture dish	664 160	Cellstar Greiner Labortechnik, Kremsmünster, Austria
Cell culture flasks with ventilation caps	83.3910.002, 83.3911.002, 83.3912.002	T25, T75, T175, Sarstedt, Nümbrecht, Germany
Compresses	18507	Gauze Compresses 10 x 10 cm, Nobamed Paul Danz, Wetter, Germany
Cover slips	C10143263NR1	Menzel-Gläser 20 x 20 mm, Gerhard Menzel, Braunschweig, Germany
FACS buffers and solutions	340345, 340346, 342003	FACS clean/rinse/flow, Becton, Dickinson and Company (BD), Franklin Lakes, New Jersey, USA
Freezing tubes	72.379	Cryo Pure Gefäß 1.8 ml, Sarstedt, Nümbrecht, Germany
Pasteur pipettes	747720	Glass Pasteur Pipettes 230 mm, Brand, Wertheim, Germany
Pipette tips	70.1130.217, 70.760.213, 70.760.212, 70.762.211	0.1-2.5 µl, 10 µl, 20 µl, 100 µl, 2-200 µl, 1000 µl, Sarstedt, Nümbrecht, Germany
Reaction vessels	62.554.502	15 ml, Sarstedt, Nümbrecht, Germany
	4440100	50 ml, Orange Scientific, Braine-l'Alleud, Belgium
	72.690.550	1.5 ml, Sarstedt, Nümbrecht, Germany
	72.737	Multiply-Pro 0,2ml Biosphere, Sarstedt, Nümbrecht, Germany
Round bottom tubes with cell strainer snap cap	352235	5 ml Polystyrene Round Bottom Tube, Falcon, Corning Science, Taumaulipas, Mexico
Safety gloves	9209817	Vaso Nitril Blue, B. Braun Melsungen, Melsungen, Germany
Serological pipettes	86.1685.001, 86.1253.001, 86.1254.001	5 ml, 10 ml, 25ml Serological Pipette, Sarstedt, Nümbrecht, Germany
Skin disinfectant	975512, 306650	Sterilium Classic Pure, Sterilium Virugard, Hartmann, Heidenheim, Germany
Surface disinfectant	CLN-1006.5000	Ethanol 80 % MEK/Bitrex, CLN, Niederhummel, Germany
RNAse AWAY	A998.4	Molecular bioproducts

4.4 Antibodies

Fluoro-chrome	Antigen	Clone	Order number	Manufacturer
AF 488	CCR1	5F10B29	362906	Biolegend, San Diego, California, USA
AF647	EMR2	494025	564342	Becton, Dickinson and Company (BD), Franklin Lakes, New Jersey, USA

APC	2B4	C1.7	329511	Biolegend, San Diego, California, USA
APC	CD28	CD28.2	561792	Becton, Dickinson and Company (BD), Franklin Lakes, New Jersey, USA
APC	CCR4	REA297	130-103-883	Miltenyi Biotec, Bergisch Gladbach, Germany
APC	CD57	TB03	130-099-748	Miltenyi Biotec, Bergisch Gladbach, Germany
APC	HVEM	122	318808	Biolegend, San Diego, California, USA
APC	CD80	2D10	305219	Biolegend, San Diego, California, USA
APC	CTLA-4	BNI3	555855	Becton, Dickinson and Company (BD), Franklin Lakes, New Jersey, USA
APC	CD8	SK1	345775	Becton, Dickinson and Company (BD), Franklin Lakes, New Jersey, USA
APC	MUC1	5E5	by MTA	obtained by MTA with the university of Copenhagen
APC-eFluor780	Viability Dye	730804	FAB71261A	eBioscience, Waltham, Massachusetts, USA
BB515	TIM-3	7D3	565568	Becton, Dickinson and Company (BD), Franklin Lakes, New Jersey, USA
BB515	CD27	M-T271	564643	Becton, Dickinson and Company (BD), Franklin Lakes, New Jersey, USA
BB515	CD196	11A9	564479	Becton, Dickinson and Company (BD), Franklin Lakes, New Jersey, USA
BB515	CD96	6F9	564774	Becton, Dickinson and Company (BD), Franklin Lakes, New Jersey, USA
BUV395	CD45RO	UCHL1	564292	Becton, Dickinson and Company (BD), Franklin Lakes, New Jersey, USA
BUV395	CD45	HI30	563792	Becton, Dickinson and Company (BD), Franklin Lakes, New Jersey, USA
BUV496	CD4	SK3	564651	Becton, Dickinson and Company (BD), Franklin Lakes, New Jersey, USA
BUV496	CD38	HIT2	564658	Becton, Dickinson and Company (BD), Franklin Lakes, New Jersey, USA
BUV737	CD3	UCHT1	564308	Becton, Dickinson and Company (BD), Franklin Lakes, New Jersey, USA
BV421	PD-1	EH12.2H7	329919	Biolegend, San Diego, California, USA
BV421	GITR	108-17	371208	Biolegend, San Diego, California, USA
BV421	TCRγ/δ	B1	331217	Biolegend, San Diego, California, USA
BV421	TIGIT	A15153G	372709	Biolegend, San Diego, California, USA
BV421	CD371	50C1	742929	Becton, Dickinson and Company (BD), Franklin Lakes, New Jersey, USA
BV421	PD-L1	29E.2A3	329714	Biolegend, San Diego, California, USA
BV421	CD275	2D3 B7-H2	564276	Becton, Dickinson and Company (BD), Franklin Lakes, New Jersey, USA
BV650	CD62L	DREG-56	563808	Becton, Dickinson and Company (BD), Franklin Lakes, New Jersey, USA
BV650	CD33	WM53	303429	Biolegend, San Diego, California, USA
BV650	PD-1	EH12.2H7	329949	Biolegend, San Diego, California, USA
BV785	LAG3	11C3C65	369322	Biolegend, San Diego, California, USA
BV786	CD127	HIL-7R-M21	563324	Becton, Dickinson and Company (BD), Franklin Lakes, New Jersey, USA

BV785	CD155	TX24	744720	Becton, Dickinson and Company (BD), Franklin Lakes, New Jersey, USA
BV785	CD86	IT2.2	305441	Biolegend, San Diego, California, USA
BV785	TIM-3	F38-2E2	345031/345032	Biolegend, San Diego, California, USA
BV785	CD3	Oct-03	317330	Biolegend, San Diego, California, USA
BV786	CTLA-4	BNI3	563931	Becton, Dickinson and Company (BD), Franklin Lakes, New Jersey, USA
BV786	ICOS	C398.4A	313534	Biolegend, San Diego, California, USA
BV786	CD226	DX11	742497	Becton, Dickinson and Company (BD), Franklin Lakes, New Jersey, USA
BV786	CD123	6H6	306031	Biolegend, San Diego, California, USA
FITC	CD16	REA423	130-106-761	Miltenyi Biotec, Bergisch Gladbach, Germany
FITC	CD73	AD2	344016	Biolegend, San Diego, California, USA
PE	CD160	BY55	341205	Biolegend, San Diego, California, USA
PE	OX-40	Ber-ACT35	350003	Biolegend, San Diego, California, USA
PE	CD25	M-A251	356103/356104	Biolegend, San Diego, California, USA
PE	CD56	REA196	130-100-653	Miltenyi Biotec, Bergisch Gladbach, Germany
PE	CD85d	42D1	338706	Biolegend, San Diego, California, USA
PE	CD112	TX31	337410	Biolegend, San Diego, California, USA
PE	OX-40L	ik-1	558164	Becton, Dickinson and Company (BD), Franklin Lakes, New Jersey, USA
PE	LAG-3	11C3C65	369306	Biolegend, San Diego, California, USA
PE	MUC1	5E10	By MTA	obtained by MTA with the university of Copenhagen
PE-CF594	CXCR3	1C6/CXCR3	562451	Becton, Dickinson and Company (BD), Franklin Lakes, New Jersey, USA
PE-CF594	CD45	HI30	562312	Becton, Dickinson and Company (BD), Franklin Lakes, New Jersey, USA
PE-Cy7	CD39	A1	328211	Biolegend, San Diego, California, USA
PerCP-Cy5.5	CD135	BV10A4H2	313316	Biolegend, San Diego, California, USA
PerCP-Cy5.5	CD47	CC2C6	323109	Biolegend, San Diego, California, USA
PerCP-Cy5.5	CD70	113-16	355107/355108	Biolegend, San Diego, California, USA
PerCP-Cy5.5	CD8	SK1	344709	Biolegend, San Diego, California, USA
PEVio770	CD95	DX2	130-104-232	Miltenyi Biotec, Bergisch Gladbach, Germany
PEVio770	CD34	AC136	130-100-844	Miltenyi Biotec, Bergisch Gladbach, Germany
VioBlue	CD45	5B1	130-092-880	Miltenyi Biotec, Bergisch Gladbach, Germany
Viobright FITC	CD4	REA623	130-109-457	Miltenyi Biotec, Bergisch Gladbach, Germany
Viobright FITC	CD4	REA623	130-113-229	Miltenyi Biotec, Bergisch Gladbach, Germany

4.5 Isotype controls

Fluorochrome	Isotype control	Order number	Company
APC	Mouse IgG1, k	400121	Biolegend, San Diego, California, USA
APC	Mouse IgG2a k	552893	Becton, Dickinson and Company (BD), Franklin Lakes, New Jersey, USA
BB515	Mouse, IgG1, k	564416	Becton, Dickinson and Company (BD), Franklin Lakes, New Jersey, USA
BV421	Mouse IgG2b, k	562748	Becton, Dickinson and Company (BD), Franklin Lakes, New Jersey, USA
BV421	Mouse IgG1, k	400158	Biolegend, San Diego, California, USA
BV786	Mouse IgG1, k	563330	Becton, Dickinson and Company (BD), Franklin Lakes, New Jersey, USA
FITC	Mouse IgG1, k	130-098-105	Miltenyi Biotec, Bergisch Gladbach, Germany
FITC	Mouse IgG1, k	400109	Biolegend, San Diego, California, USA
PE	Mouse IgG1, k	400113	Biolegend, San Diego, California, USA
PE-Cy7	Mouse IgG1, k	400125	Biolegend, San Diego, California, USA
PerCP-Cy5.5	Mouse IgG1, k	400149	Biolegend, San Diego, California, USA

5 Methods

5.1 Selection of bone marrow samples for analysis

36 bone marrow samples (BM samples) of pediatric AML patients at the time of primary diagnosis or at the time of relapse were selected from the biobank of the children's hospital. Furthermore, 9 samples of age-matched healthy bone marrow donors (healthy BM donors) were chosen from the same biobank in order to be used as a healthy control for the observations made in AML patients. The following criteria were taken into account for the selection of AML patient samples: (1) date of diagnosis, (2) age at the time of diagnosis, (3) gender, (4) therapy status (naïve or after treatment), (5) follow up, (6) initial white blood cell count and (7) bone marrow blast frequency. Samples from initial diagnosis had to be therapy naïve in order to be included in the study. Relapse samples were only included, if relapse treatment had not started yet, but independent of therapy status of initial diagnosis. Additionally, samples of patients diagnosed with acute promyelocytic leukemia (AML M3) were excluded. Sample selection and analysis was performed according to the guidelines of the HaunerHematologyBiobank (Projekt Nr: 17-163, Ethikkomission der LMU München). Patient samples (N=36) were anonymized and subsequently labelled according to their utilization in this project: samples of patients without relapse (A002 – A016, N=14), primary samples of relapse patients (A301-A306, N=7) and relapse samples (A401 – A410 for first relapse, N=10; A501, A503 for second relapse; A601 for third relapse; A701 for fourth relapse; A801 for fifth relapse). Samples of healthy BM donors (N=9) were equally anonymized and subsequently labelled (A101-A110). Further healthy BM donor and patient characteristics are presented in Figure 4 and Figure 5.

A

	Healthy BM donors	All cases
Samples, n	9	29
Age, mean (range)	7.3y (0.9-16.4)	7.6y (0.4-16.6)
Gender, n (%)		
Male	5 (56)	13 (45)
Female	4 (44)	16 (55)

B

	AML, all cases
Samples, n	29
FAB, n (%)	
M0	1 (3.4)
M1	2 (6.9)
M2	7 (24.1)
M3	0 (0)
M4	8 (27.6)
M4eo	3 (10.3)
M5	4 (13.8)
M6	1 (3.4)
M7	1 (3.4)
unknown	2 (6.9)
Age at initial Dx, mean (range)	7.6y (0.4-16.6)
Future relapse (%)	15 (51.7)
Time to relapse, mean (range)	1.3y (0.2-2.8)
Exitus letalis (%)	6 (20.7)
Monitoring period, mean (range)	6.7y (0.8-14.4)

Figure 4: Healthy bone marrow donor and AML patient characteristics. A) General information of healthy BM donors and AML patients. **B)** Detailed AML patient information including AML subtypes and age at time of diagnosis. Healthy BM donors: healthy BM donors, initial Dx: initial diagnosis.

Patient	Initial Dx	1st relapse	2nd relapse	3rd relapse	4th relapse	5th relapse
1	A301					
2	A302					
3	A303		A503			
4	A306	A406				
5	A307	A407				
6	A308	A408				
7	A309*	*				
8		A401				
9		A402				
10		A403				
11		A404				
12		A405				
13		A409				
14		A410				
15			A501	A601	A701	A801

Figure 5: Samples of relapsed pediatric AML patients. Measured samples with respective patient codes in green, unavailable samples in red. * indicates CNS relapse, blank cells indicate that the respective relapse did not occur. Initial Dx: Initial Diagnosis.

5.2 Cell culture methods

5.2.1 Cell culture

Cells cultures were stored in the HERAcell 240i CO_2 Incubator at 37 °C and 5 % CO_2. All cell culture related processes were performed under sterile bench conditions.

5.2.2 Thawing of cells

After being transported on dry ice to a sterile bench in the S1 area, samples were thawed by agitating them for about 2 min in a 37 °C water bath. Subsequently, 1.8 ml of sample volume was added to 13.2 ml of 37 °C RPMI-Medium (10 % FCS, 1 % Pen-strep, 1 % L-Glutamin) to which DNAseI had been added (100 U/ml) to prevent sample clotting. Live cells were counted in a Neubauer counting chamber using trypan blue to identify dead cells that were not counted. After 10 min of centrifugation at 300 g at room temperature the supernatant was aspirated and the remaining cell pellet resuspended in PBS+1 % FCS up to a maximal concentration of 10x10e7/ml.

In case of insufficient dissolving of the cell pellet after centrifugation DNAseI was added at an increased concentration (200 U/ml, in PBS+1 % FCS) and the cell suspension was incubated for

15 min at 37 °C (HERAcell 240i CO_2 Incubator). After centrifugation for 4 min at 400 g, the pellet was resuspended again in an appropriate amount of PBS+1 % FCS with regards to the cell count.

5.3 Immunological methods

5.3.1 Staining of patient samples with fluorochrome labelled monoclonal antibodies (mAb) for flow cytometry analysis

The following steps were performed in an unsterile environment. Prior to FACS staining all samples but samples A002-A010 and A101-A110 were treated with the Human BD Fc Block™ to reduce potential non-specific antibody staining caused by cellular receptors for IgG.

Subsequently, samples were analyzed in 8 single tubes by using 8 different 12- or 13-color panels (Figure 6). For cell type definition (e.g. AML blasts, CD3+ T cells in the bone marrow: bmT cells) and characterization of bmT cell maturation stage (e.g. CD62L-CD45RO-: effector bmT cells) 3 different 5- or 6-color backbone panels (Blast Panel, T cell Panel, IC panel; Figure 6) were employed. In addition, 5 to 6 other molecules were stained in each panel (Figure 6). For the latter isotype and fluorescence-minus-five (FMF) or fluorescence-minus-six (FMS) controls were performed.

After adding 25 µl of cell suspension (containing 1-10x10^5 cells in PBS+1 % FCS) to 25 µl of antibody mix, the mixture was incubated for 20 min in the dark at room temperature. Intracellular staining of CTLA-4 and PD-L1 was performed after extracellular staining by using the FIX & PERM™ Cell Permeabilization Kit by ThermoFisher according to the manufacturers´ protocol (4.2). Being stained, cells were washed once (400 g x 4 min), resuspended in 400 µl PBS+1 % FCS and stored in the dark at 4 °C. Prior to measurement, all samples were strained through a filter with 35 µm filtering capacity.

During the project some antigens had to be changed. As in samples A002-A010 and A101-A110 CTLA-4 could not be detected on the cell surface, BV786-CTLA-4 was replaced with BV785-LAG-3 for all other patients' samples (T1, Figure 6). Except one patient (Figure 7), MUC1 5E10 and MUC1 5E5 were only weakly expressed on AML blasts of patient samples A002-A010 in contrast to $CD45_{dim}$ cells of healthy BM donors' samples A101-A110, whereas CD96 was not only expressed on blasts, but also on bmT cells. Consequently, all three markers were not suited as CAR-targets and therefore replaced by three markers from the literature (CCR1, CD85d and EMR2, Perna et al., 2017). Those were stained in all other patient samples.

A

PerCP-Cy5.5	CD8
PE-Vio770	CD95
APC-eFluor780	live/dead
BV650	CD62L
BUV737	CD3
BUV496	CD4
BUV395	CD45RO

B

PE-Vio770	CD34
APC-eFluor780	live/dead
BV650	CD33
BUV737	CD3
BUV496	CD38
BUV395	CD45

C

PerCP-Cy5.5	CD8
APC-eFluor780	live/dead
BV650	PD-1
BUV737	CD3
BUV496	CD4
BUV395	CD45

D

T1: Exhaustion		T2: Stimulation	
BB515	TIM-3	BB515	CD27
PE	CD160	PE	OX40
APC	2B4	APC	CD28
BV786	CTLA-4	BV785	ICOS
BV421	PD-1	BV421	GITR
T3: T cell subsets		**T4: NK & NKT cell function**	
BB515	CCR6	FITC	CD16
PE-CF594	CXCR3	PE-CF594	CD45
PE	CD25	PE	CD56
APC	CCR4	APC	CD57
BV786	CD127	BV786	CD226
BV421	TCRγδ	BV421	TIGIT
B1: CAR targets		**B2: Inhibiton**	
PerCP-Cy5.5	CD135	PerCP-Cy5.5	CD47
BB515	CD96	BB515	TIM-3
PE	MUC1 5E10	PE	CD112
APC	MUC1 5E5	APC	HVEM
BV785	CD123	BV786	CD155
BV421	CLL1	BV421	PD-L1
B3: Stimulation		**IC: T cells and Blasts**	
PerCP-Cy5.5	CD70	FITC	CD73
BB515	CD27	PE/Cy7	CD39
PE	OX40-L	PE	LAG-3
APC	CD80	APC	CTLA-4
BV785	CD86	BV785	TIM-3
BV421	ICOS-L	BV421	PD-L1

E

T1: Exhaustion		T2: Stimulation	
BB515	TIM-3	BB515	CD27
PE	CD160	PE	OX40
APC	2B4	APC	CD28
BV785	LAG-3	BV785	ICOS
BV421	PD-1	BV421	GITR
T3: T cell subsets		**T4: NK & NKT cell function**	
BB515	CCR6	FITC	CD16
PE-CF594	CXCR3	PE-CF594	CD45
PE	CD25	PE	CD56
APC	CCR4	APC	CD57
BV786	CD127	BV786	CD226
BV421	TCRγδ	BV421	TIGIT
B1: CAR targets		**B2: Inhibiton**	
PerCP-Cy5.5	CD135	PerCP-Cy5.5	CD47
Alexa Fluor 488	CCR1	BB515	TIM-3
PE	CD85d	PE	CD112
Alexa Fluor 647	EMR2	APC	HVEM
BV785	CD123	BV786	CD155
BV421	CLL1	BV421	PD-L1
B3: Stimulation		**IC: T cells and Blasts**	
PerCP-Cy5.5	CD70	FITC	CD73
BB515	CD27	PE/Cy7	CD39
PE	OX40-L	PE	LAG-3
APC	CD80	APC	CTLA-4
BV785	CD86	BV785	TIM-3
BV421	ICOS-L	BV421	PD-L1

Intracellular staining
changed antigens

Figure 6: Flow cytometry panel design. A) T cell backbone panel. **B)** Blast backbone panel. **C)** IC backbone panel. **D)** T cell panels, Blast panels and Intracellular panel for A002-A010 and A101-A110. CTLA-4 and PD-L1 were stained intracellularly. **E)** T cell panels, Blast panels and Intracellular panel for A011-A016, A301-A309, A401-A410, A501, A601, A701 and A801. CTLA-4 and PD-L1 were stained intracellularly. T1-T4: T cell panels, B1-3: Blast panels, IC: Intracellular panel.

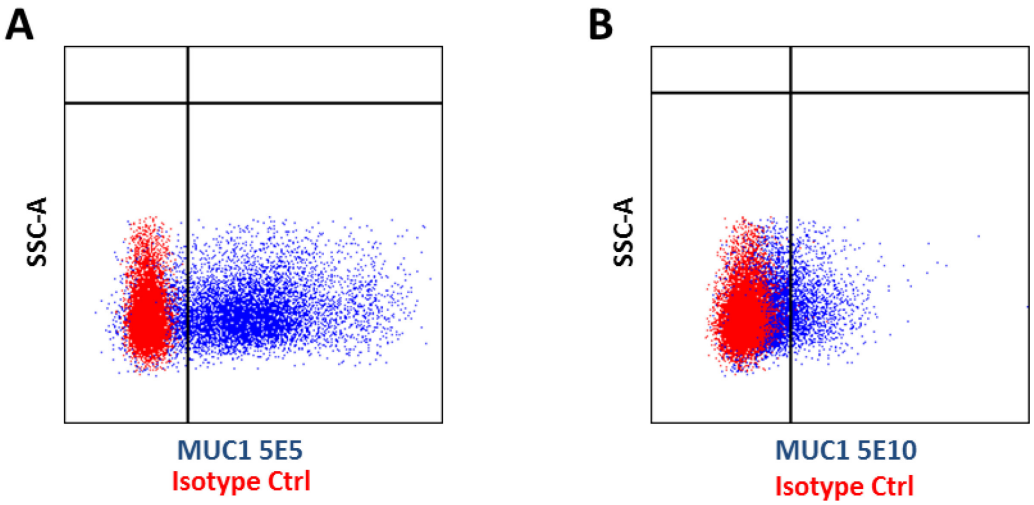

Figure 7: MUC1 5E5 and MUC1 5E10 expression on blasts of AML patient A005. Patient A005 showed the highest MUC1 5E5 (A: 79.4 %) and MUC1 5E10 (B: 18.8 %) expression levels on AML blasts of measured patients A002-A010. On blasts of the other patients, these antigens were only weakly expressed compared to $CD45_{dim}$ cells of healthy BM donors. Ctrl: Control.

5.3.2 Automated bead compensation

Prior to the measurement of BM samples automated bead compensation was performed. For this purpose, a single-stained compensation control tube was set up for each color used.

For all fluorochromes except for the viability dye APC-eFluor 780 positive (*BD™ CompBeads Anti-Mouse Ig, κ* particles) and negative (*BD™ CompBeads Negative Control* particles with no binding capacity) beads were used according to the BD LSRFortessa Cell Analyzer User's Guide (4.1). For the viability dye APC-eFluor 780 dead PBMCs (10 min at 65 °C) were used instead of positive beads.

Additionally, a tube containing negative beads and no fluorochrome labelled antibodies served as unstained control and two different *all in* tubes (with or w/o PE-CF594) containing both positive and negative beads, all antibodies and dead cells were prepared.

With a total volume of 50 µl (antibody + beads/PBMC or both + PBS+1 % FCS) the samples were incubated for 20 min in the dark at room temperature, washed once with PBS+1 % FCS and eluted in 400 µl PBS+1 % FCS. The spectral overlap of the fluorochromes was measured at the BD LSRFortessa and a compensation matrix was calculated by using the BD FACSDiva 8.0.1 software according to the BD LSRFortessa Cell Analyzer User's Guide. If necessary, voltages were adapted.

5.4 Sorting of bone marrow populations at the BD FACSAria III

Parallel to the staining process for flow cytometry analysis 50 µl of each sample's cell suspension was added to an antibody mixture containing 8 fluorochrome labelled antibodies: VioBright FITC-CD4,

PEVio770-CD34, PE-CD56, APC-eFluor780-live/dead, APC-CD8, BV785-CD3, BV650-CD33 and VioBlue-CD45.

After 20 min of incubation in the dark at room temperature 4 bone marrow populations per sample were sorted into tubes containing 100 % FCS at 4 °C in order to maximize cell viability: CD4+ bmT cells, CD8+ bmT cells, $CD45_{dim}$ cells (AML blasts/healthy control) and NK cells (Figure 8).

To document sample purity higher than 95 %, a post-sort was performed for 57 % of the sorted cell populations dependent on number of sorted cells (Figure 9).

Subsequently, sorted cell populations were processed further for downstream analysis: chromatin transposition, RNA and DNA isolation. Healthy BM donors` samples were treated equally. Compensation matrices for the sorting panel were generated regularly according to the manufacturers' protocol. Sorting at the BD FACSAria III was performed in cooperation with the working group of Prof. Dr. Dr. Klein.

5.5 Antibody titration

To determine the best antibody concentration for an optimized separation between the positive and the negative population, all antibodies were titrated prior to analysis of BM samples. Therefore, a known number of cells was stained with decreasing amounts of antibodies starting with the concentration recommended by the manufacturers. The antibody amount and concentration resulting in the highest signal-to-noise ratio was identified by eye in FlowJo 10.5.0 and subsequently used in the panel.

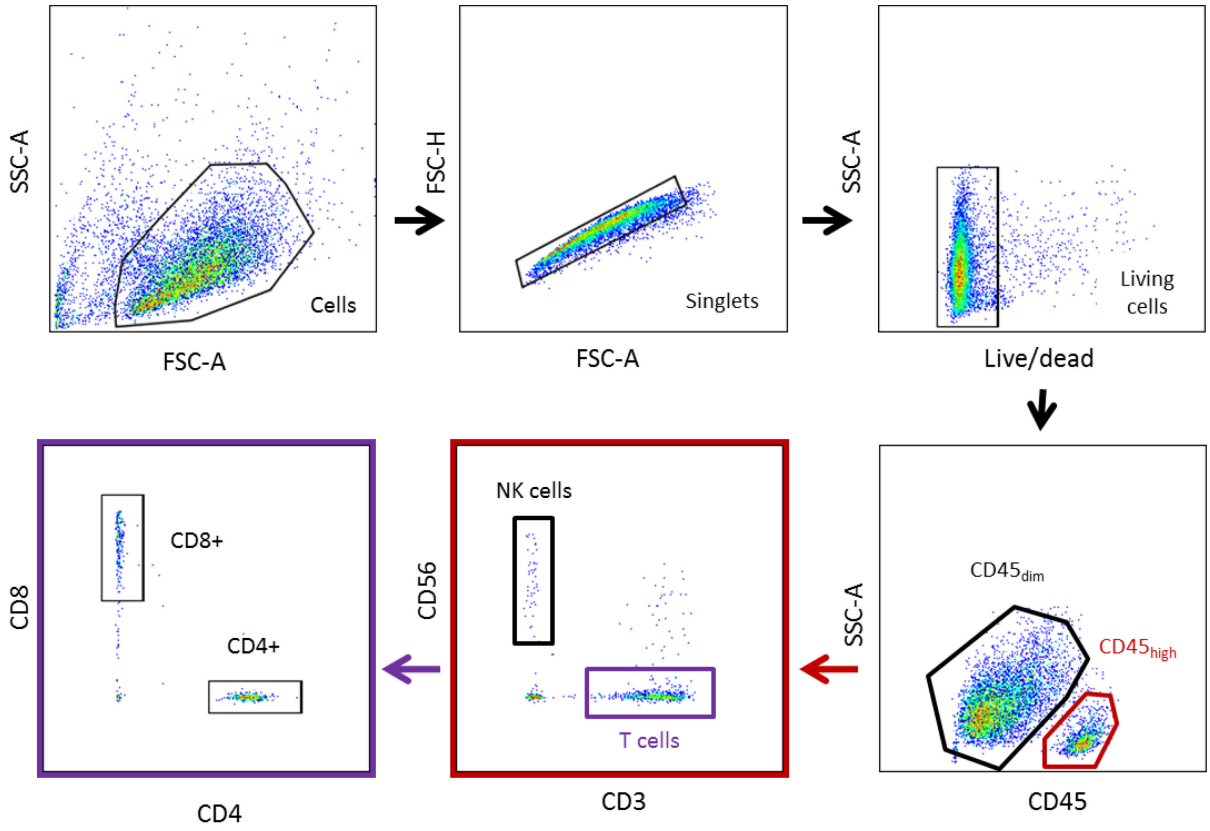

Figure 8: Sorting of bone marrow populations. Gating strategy for sorting as indicated by arrows between plots: (1) SSC-A vs. FSC-A: selection of cells by size and granularity, (2) FSC-H vs. FSC-A: excluding doublets, (3) SSC-A vs. live/dead: elimination of dead cells, (4) SSC-A vs. CD45: gating for $CD45_{dim}$ (AML blasts/healthy control) and $CD45_{high}$ cells, (5) CD56 vs. CD3: differentiation of $CD45_{high}$ cells in NK cells and bmT cells, (6) CD8 vs. CD4: differentiation of bmT cells in CD8+ and CD4+ bmT cells. The following bone marrow populations were sorted: $CD45_{dim}$ cells (AML blasts/healthy control), NK cells, CD8+ bmT cells and CD4+ bmT cells.

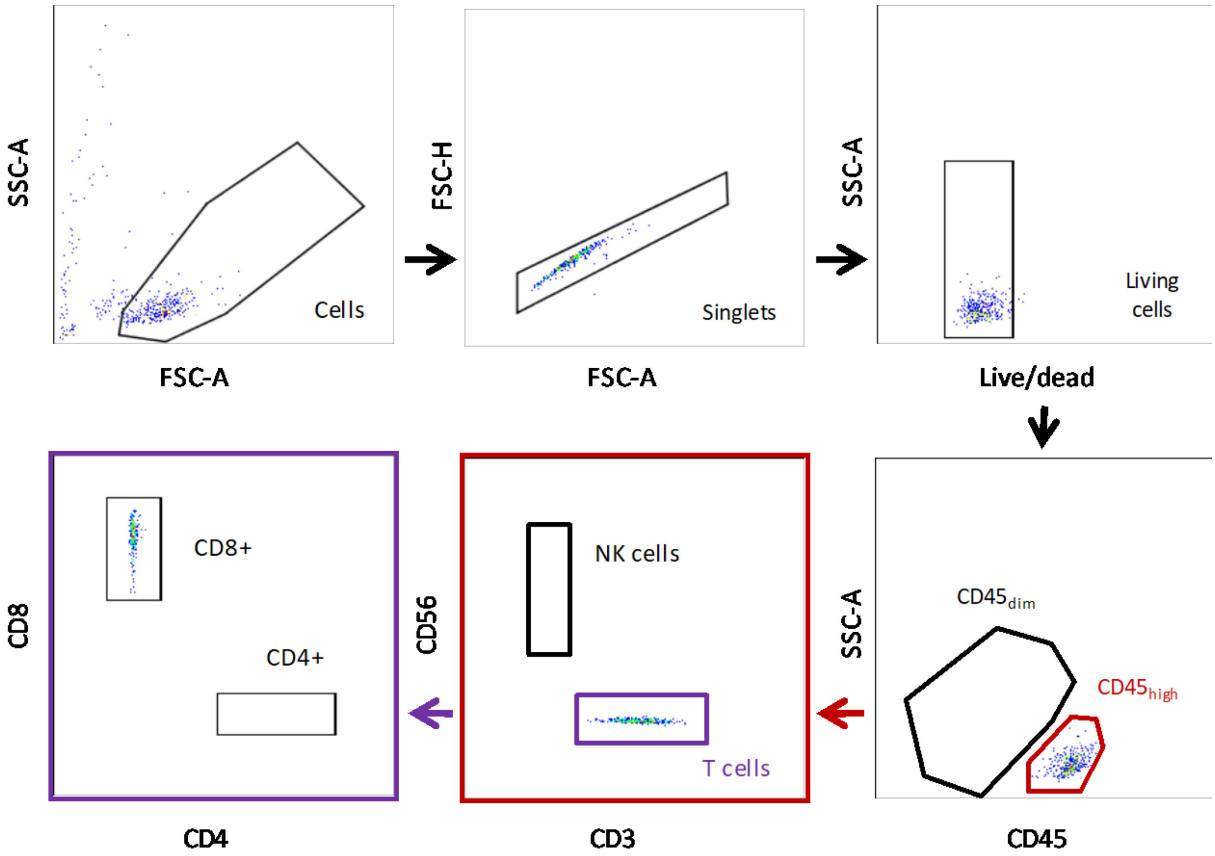

Figure 9: Exemplary post-sort of CD8+ bmT cells of patient A009. All measured cells are within the CD8+ bmT cells gate. The CD4+ bmT cells gate, the NK cells gate and the $CD45_{dim}$ cells gate (AML blasts/healthy control) are event-free. Therefore high sample purity of the sorted CD8+ bmT cell population is shown by using following gating strategy: (1) SSC-A vs. FSC-A: selection of cells by size and granularity, (2) FSC-H vs. FSC-A: excluding doublets, (3) SSC-A vs. live/dead: elimination of dead cells, (4) SSC-A vs. CD45: gating for $CD45_{dim}$ (AML blasts/healthy control) and $CD45_{high}$ cells, (5) CD56 vs. CD3: differentiation of $CD45_{high}$ cells in NK cells and bmT cells, (6) CD8 vs. CD4: differentiation of bmT cells in CD8+ and CD4+ bmT cells.

5.6 Flow cytometry data analysis

5.6.1 General gating strategies

To analyze the flow cytometry data generated at the BD LSRFortessa the software FlowJo 10.5.0 was used. In order to identify the cells of interest based on the relative size and complexity of the cells, while removing debris and other events that are not of interest, following steps were used as general gating strategy in the FlowJo files of all samples.

(1) SSC-A vs. FSC-A: selection of cells by size and granularity
(2) FSC-H vs. FSC-A: including singlets and excluding doublets
(3) SSC-A vs. APC-eFluor 780: elimination of dead cells from further analysis

Depending on the respective panel the living cells were differentiated into CD3+ bmT cells , further divided into CD3+CD4+ and CD3+CD8+ bmT cells (T cell panels, Figure 10), $CD45_{dim}$ cells (AML

blasts/healthy control, Blast panels, Figure 11), NK and NKT cells (Figure 12). For convenience, CD3+CD4+ and CD3+CD8+ bmT cells were referred to as CD4+ and CD8+ bmT cells.

The populations of CD3+ bmT cells in common, CD4+ bmT cells, CD8+ bmT cells, NKT and NK cells were analyzed for the expression of co-inhibitory and co-stimulatory molecules and for the expression of combinations out of these molecules.

By using CD62L, CD45RO and CD95 the bmT cell maturation stages could be further described (Figure 10): CD62L-CD45RO- cells were interpreted as effector bmT cells, CD62L-CD45RO+ cells as effector memory bmT cells and CD62L+CD45RO+ cells as central memory bmT cells. As naïve T cells are specified to be CD95-CD62L+CD45RO- cells and CD95+CD45RO-CD62L+ cells are defined as stem cell-like memory T cells, the CD95-CD62L+ population was interpreted as naïve bmT cell subpopulation and its percentage was subtracted from the percentage of the CD62L+CD45RO- population in order to define the stem cell-like memory bmT cells.

For the $CD45_{dim}$ cells (AML blasts/healthy control), CD38 vs. CD34 was used to define four distinguishable maturation stages of blasts (Figure 11). Here, CD38-CD34+ Blasts were defined as leukemic stem cells (LSCs) in case of the AML patients or as hematopoietic stem cells in case of the healthy BM donors. Moreover, expression levels of both stimulatory and inhibitory molecules, as well as the expression of possible target structures were measured on the blasts' surface.

In the Intracellular (IC) panel markers CD3, CD4 and CD8 for further evaluation of bmT cells were used together with CD45 to characterize $CD45_{dim}$ cells (AML blasts/healthy control).

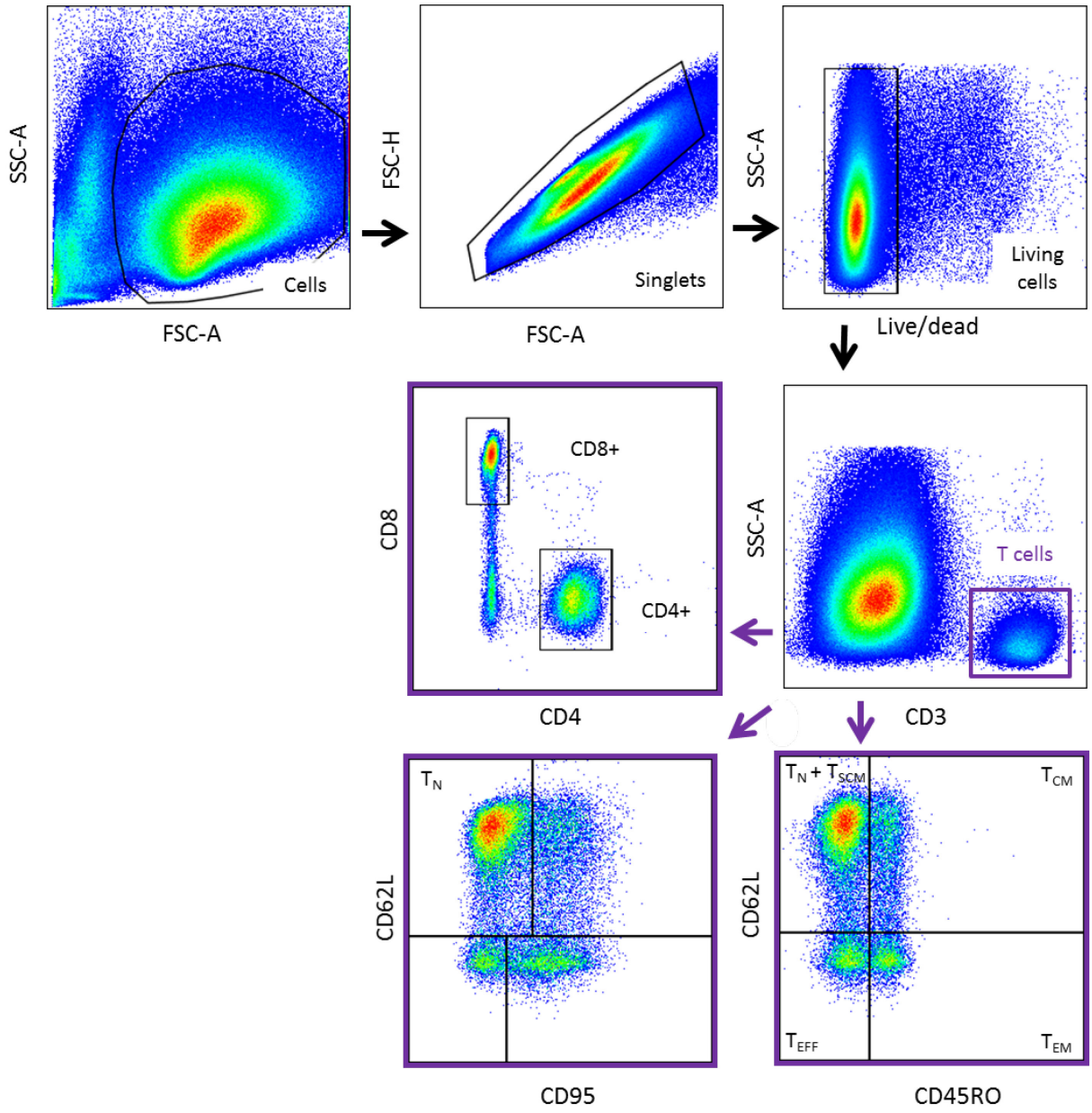

Figure 10: General FlowJo gating strategy for T cell panels (T1-T3, Figure 6). The following gating steps were performed in order to characterize CD4+ and CD8+ bmT cells**,** as well as the different maturation stages of bmT cells: (1) SSC-A vs. FSC-A: selection of cells by size and granularity, (2) FSC-H vs. FSC-A: excluding doublets, (3) SSC-A vs. Live/dead: elimination of dead cells, (4) SSC-A vs. CD3: gating for bmT cells, (5) CD8 vs. CD4: differentiation of bmT cells in CD4+ and CD8+ bmT cells, (6) CD62L vs. CD95 and CD62L vs. CD45RO: description of bmT cell maturation stages. CD62L-CD45RO- cells were interpreted as effector bmT cells (T_{EFF}), CD62L-CD45RO+ cells as effector memory bmT cells (T_{EM}), CD62L+CD45RO+ cells as central memory bmT cells (T_{CM}) and CD95-CD62L+ cells as naïve bmT cells (T_N). CD62L+CD45RO- were defined as sum out of naïve bmT cells (T_N) and stem cell-like memory bmT cells (T_{SCM}). T_N: naïve bmT cells, T_{SCM}: stem cell-like memory bmT cells, T_{CM}: central memory bmT cells, T_{EM}: effector memory bmT cells, T_{EFF}: effector bmT cells.

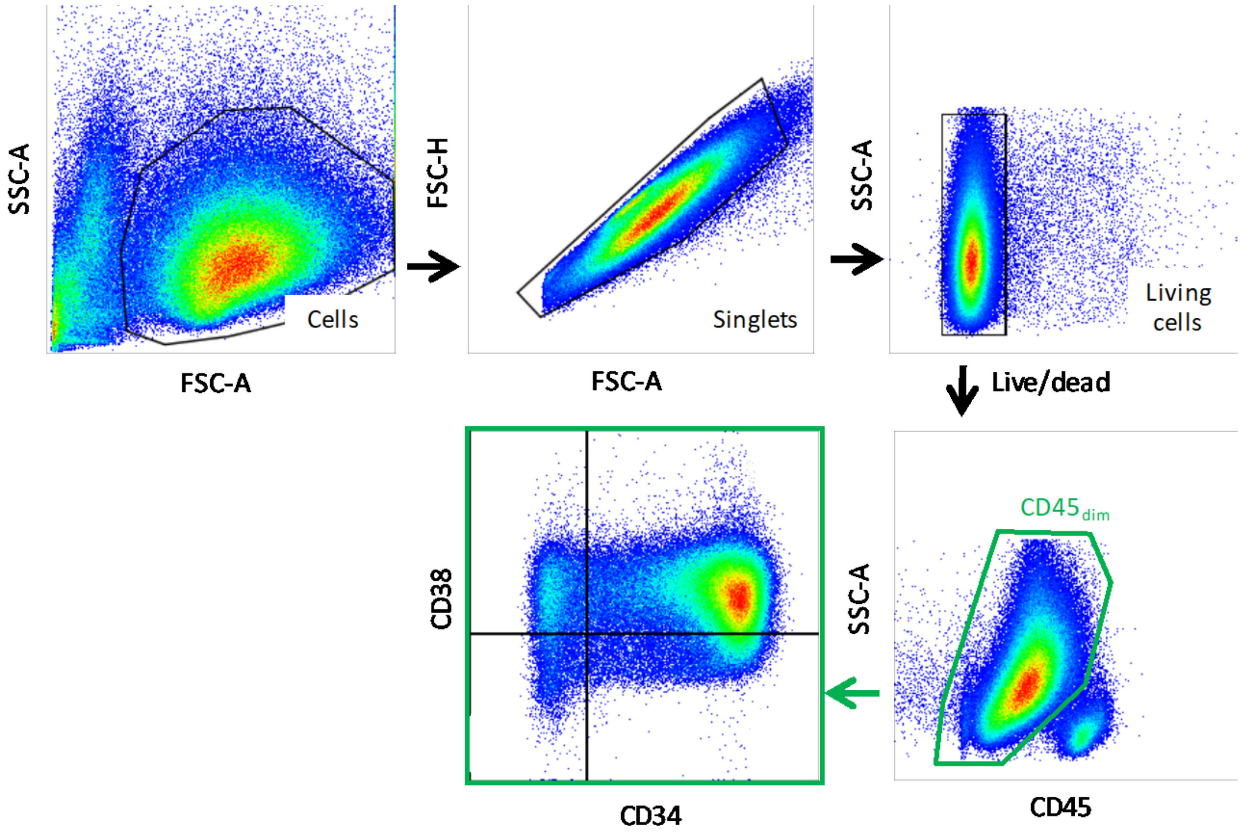

Figure 11: General FlowJo gating strategy for Blast panels (B1-B3, Figure 6). The following gating steps were performed in order to characterize $CD45_{dim}$ cells (AML blasts/healthy control), as well as the different maturation stages of $CD45_{dim}$ cells: (1) SSC-A vs. FSC-A: selection of cells by size and granularity, (2) FSC-H vs. FSC-A: excluding doublets, (3) SSC-A vs. Live/dead: elimination of dead cells, (4) SSC-A vs. CD45: gating for $CD45_{dim}$ cells (AML blasts/healthy control), (5) CD38 vs. CD34: differentiation of blasts in four distinguishable stages of maturation (CD34+CD38-: Leukemic Stem Cells).

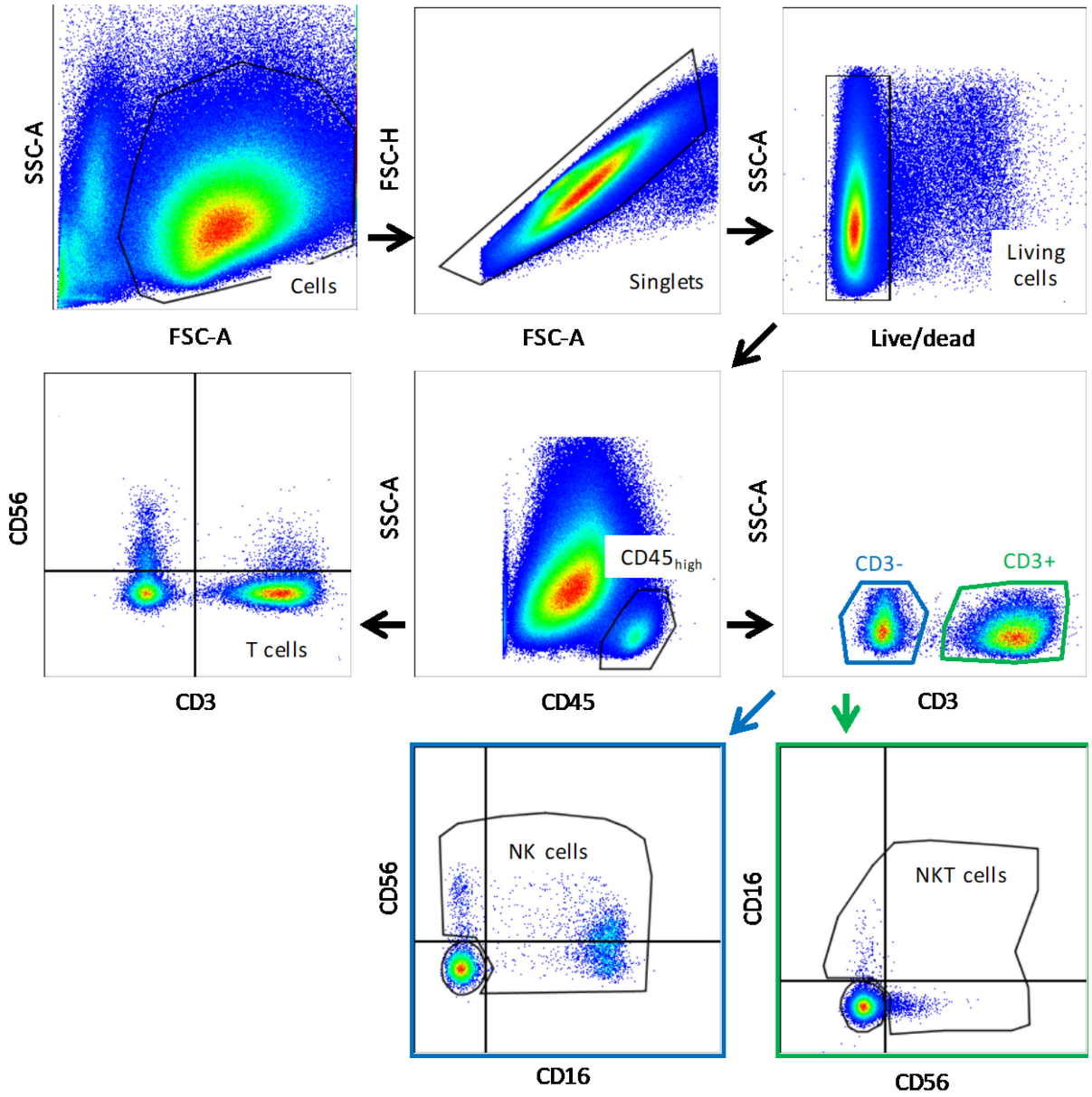

Figure 12: General FlowJo gating strategy for T4 Panel (Figure 6). The following gating steps were performed in order to characterize bmT cells, NK and NKT cells: (1) SSC-A vs. FSC-A: selection of cells by size and granularity, (2) FSC-H vs. FSC-A: excluding doublets, (3) SSC-A vs. Live/dead: elimination of dead cells, (4) SSC-A vs. CD45: gating for $CD45_{high}$ cells, (5) CD56 vs. CD3: gating for bmT cells, (6) SSC-A vs. CD3: differentiation in CD3- and CD3+ $CD45_{high}$ cells, (7) CD56 vs. CD16: gating for NK and NKT cells.

5.6.2 Analysis of bmT cell subsets

CXCR3, CCR6 and CCR4 (T3, Figure 6) were used to examine the proportional distribution of the different bmT cell subsets. After gating on naive CD4+ bmT cells (CD45RO-CD95-), CCR4-CCR6-CXCR3- cells were defined as Th0 T cells. Mature CD4+ T cells (CD45RO+CD95+) were further differentiated into the following 7 populations:

- CCR4-CCR6+CXCR3+ (Th1Th17),

- CCR4-CCR6+CXCR3- (CCR6+only),
- CCR4+CCR6+CXCR3- (Th17),
- CCR4+CCR6+CXCR3+ (CXCR3+Th17),
- CCR4+CCR6-CXCR3- (Th2),
- CCR4+CCR6-CXCR3+ (CXCR3+ Th2) and
- CCR4- CCR6- CXCR3+ cells (Th1), (Figure 13).

Regulatory bmT cells (bmT_{regs}) were characterized as $CD127_{low}/CD25_{high}$/CD4+ bmT cells (Figure 14).

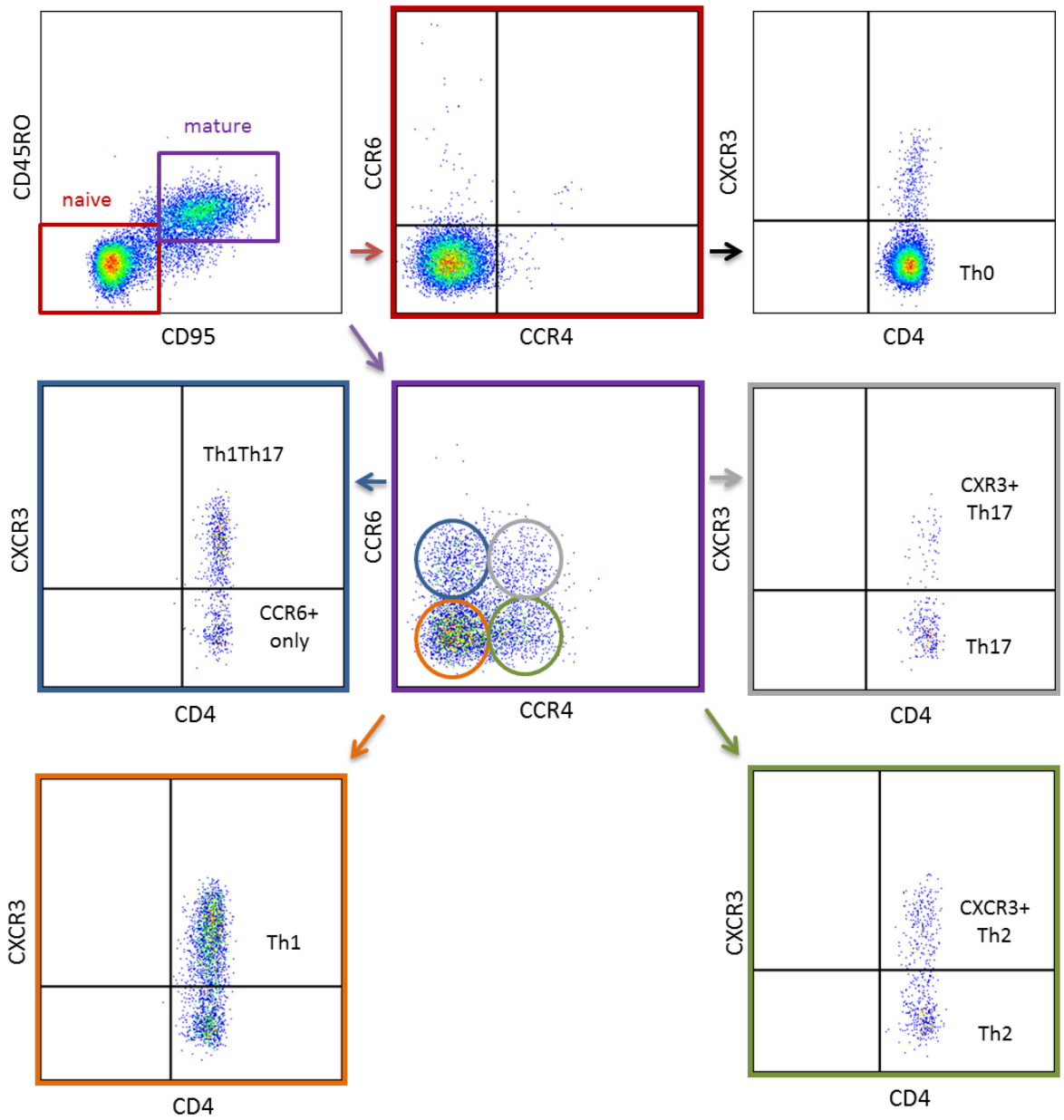

Figure 13: General FlowJo gating strategy for different bmT cell subsets (T3, Figure 6). After gating on CD4+ bmT cells, CD45RO-CD95- cells were defined as naïve CD4+ bmT cells and CD45RO+CD95+ cells were defined as mature CD4+ bmT cells. After gating on naïve CD4+ bmT cells CCR6-CCR4-CXCR3- cells were interpreted as Th0 cells, whereas after gating on mature CD4+ bmT cells CCR6+CCR4-CXCR3+ cells were characterized as Th1Th17, CCR4-CCR6+CXCR3- as CCR6+ only, CCR4+CCR6+CXCR3- as Th17, CCR4+CCR6+CXCR3+ as CXCR3+TH17, CCR4+CCR6-CXCR3- as Th2, CCR4+CCR6-CXCR3+ as CXCR3+ Th2 and CCR4- CCR6- CXCR3+ cells as Th1 cells.

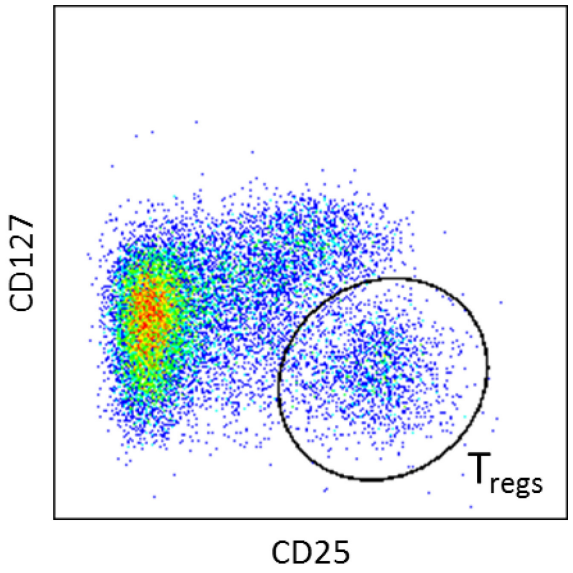

Figure 14: Representative dot plot of gating strategy for regulatory bmT cells (bmT_{regs}). bmT_{regs} were identified as $CD127_{low}/CD25_{high}/CD4+$ bmT cells using the following pregating steps: SSC-A vs. FSC-A, FSC-H vs. FSC-A, SSC-A vs. live/dead, SSC-A vs. CD3+, CD8 vs. CD4.

5.6.3 Gating strategies for surface and intracellular markers

5.6.3.1 Single-parameter

To analyze the single-parameter surface and intracellular expression, the gate was set according to populations, if possible (Figure 15). In a second step, also the Isotype control, the FMF/FMS control (fluorescence-minus-five/six) and the unstained control were taken into account. Later, all positive percentages of the Isotype controls (< 5 %) were subtracted from the positive percentages of the stained samples. In specific cases, it was not subtracted due to different reasons (see: Isotype control: Trouble shooting) or the mean value of the positive percentages of the Isotype controls of all other samples was subtracted instead.

Concerning markers, for which there was no *out-growing* positive population or two separate populations visible, gating was performed directly according to the Isotype control as this proved to be the strictest control (Figure 16). That applies particularly to $CD45_{dim}$ cells (AML blasts/healthy control). Here, the same strategy was equally used for analysis of both AML patients' samples and healthy BM donors to avoid analysis bias and ensure consistent flow cytometry data analysis.

In contrast, other working groups used different strategies to evaluate antigen expression intensity on AML blasts, e.g. MFI ratio: here, the MFI value of the antigen-specific antibody was divided by the MFI value of the respective isotype control (Haubner et al., 2019) to evaluate expression values. In order to check comparability, MFI ratio of TIM-3 expression on AML blasts was calculated, but the resulting expression levels were correlated with expression values calculated by gating according to

the Isotype control. Thus, the above-mentioned gating strategy was kept for *shifting* positive populations.

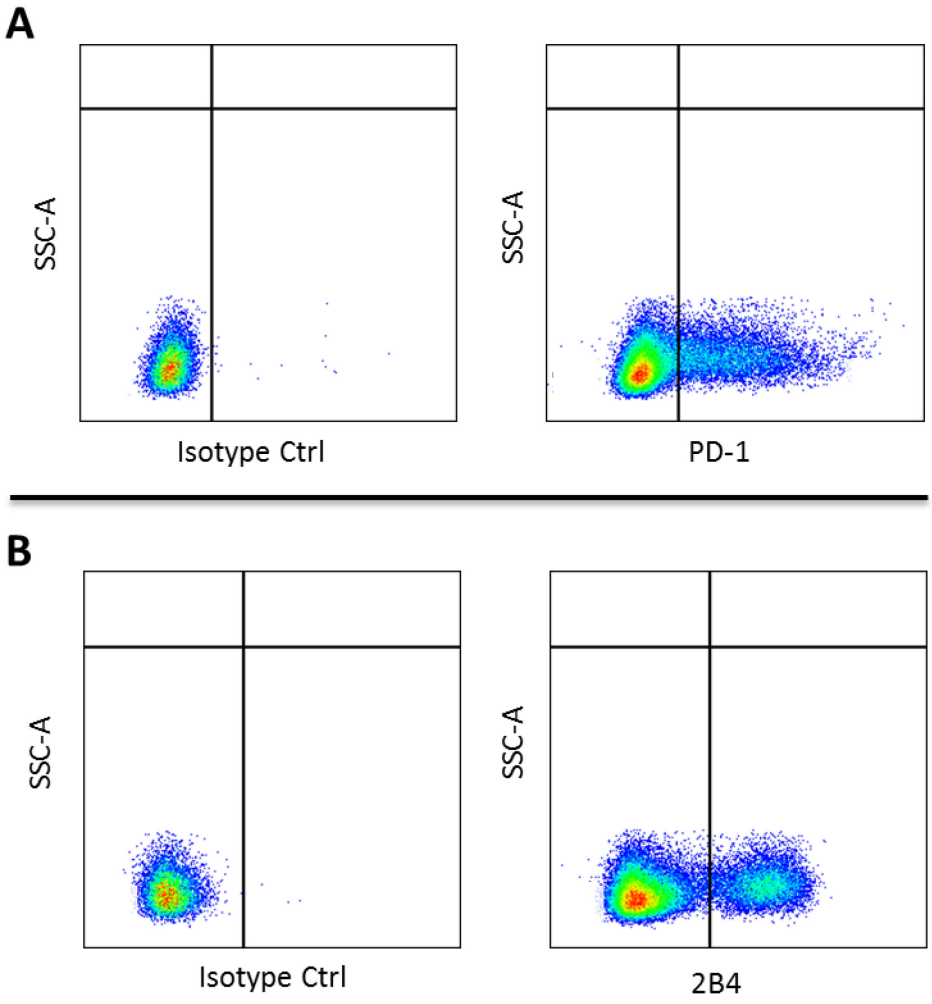

Figure 15: Representative dot plots of gating strategies for single-parameter surface and intracellular expression. A) *Out-growing* positive populations: To analyze the PD-1 expression on CD3+ bmT cells, the gate was set near to the negative population. In a second step, the Isotype control and other controls were taken into account. **B)** Two clear populations: To analyze the 2B4 expression on CD3+ bmT cells, the gating step was performed directly in the middle of both populations. In a second step, the Isotype control and other controls were taken into account. Ctrl: Control.

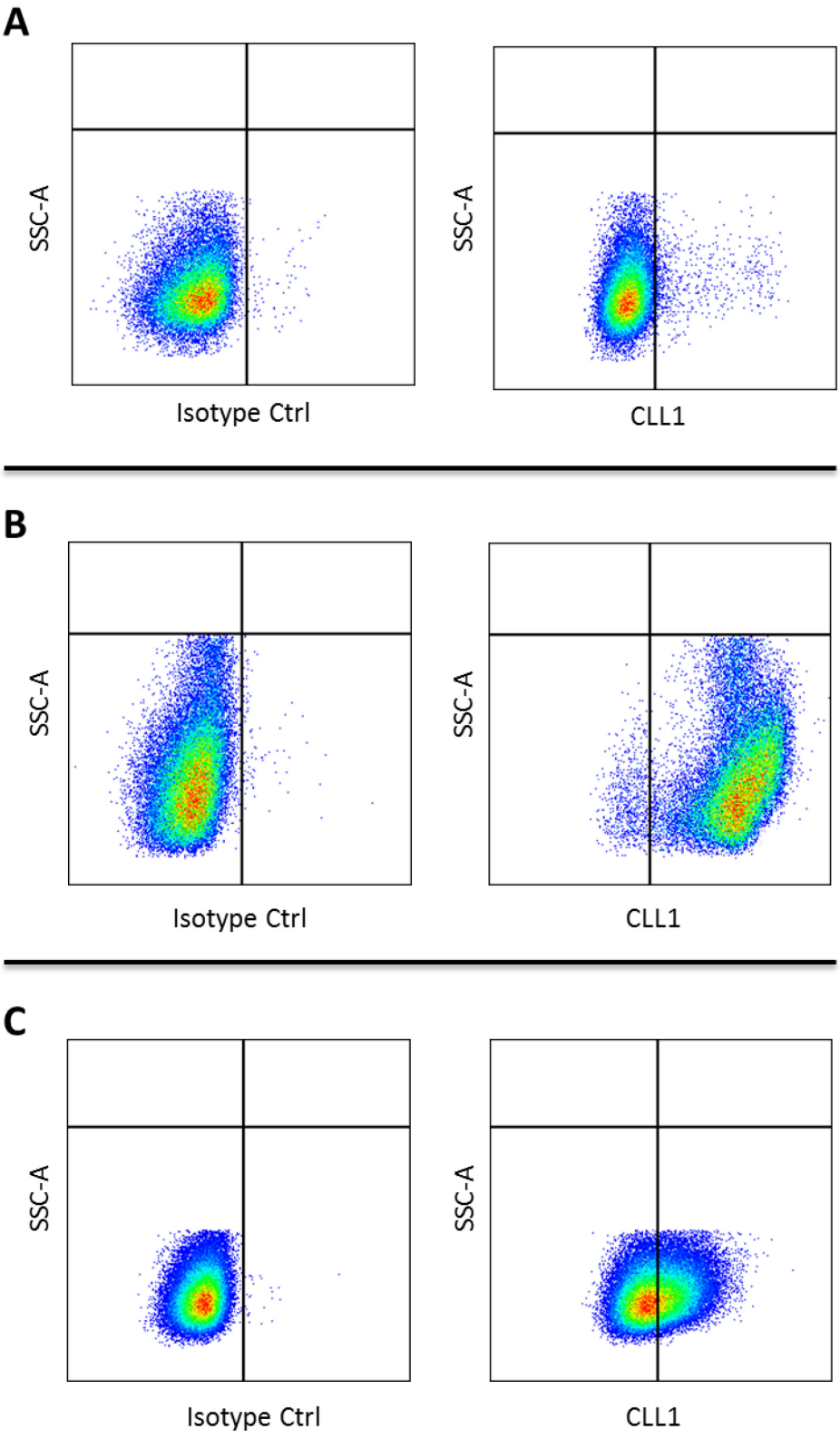

Figure 16: Gating strategy for single-markers with *shifting* positive populations. To analyze the CLL1 expression on $CD45_{dim}$ cells (AML blasts/healthy control) the gating strategy was based on the isotype control. **A)** $CLL1_{low}$ AML blasts of patient A801. **B)** $CLL1_{high}$ AML blasts of patient A011. **C)** $CLL1_{int}$ AML blasts of patient A014. Ctrl: Control, int: intermediate.

5.6.3.2 Two-parameter

To determine, if a cell does express two surface or intracellular markers at the same time, two-parameter dot-plots were used (Figure 17). Here, only the percentage of the double positive cells was exported and analyzed in accordance to the fitting isotype control. For gating the same strategies were used as with single-parameter analysis (5.6.3.1 and 5.6.4).

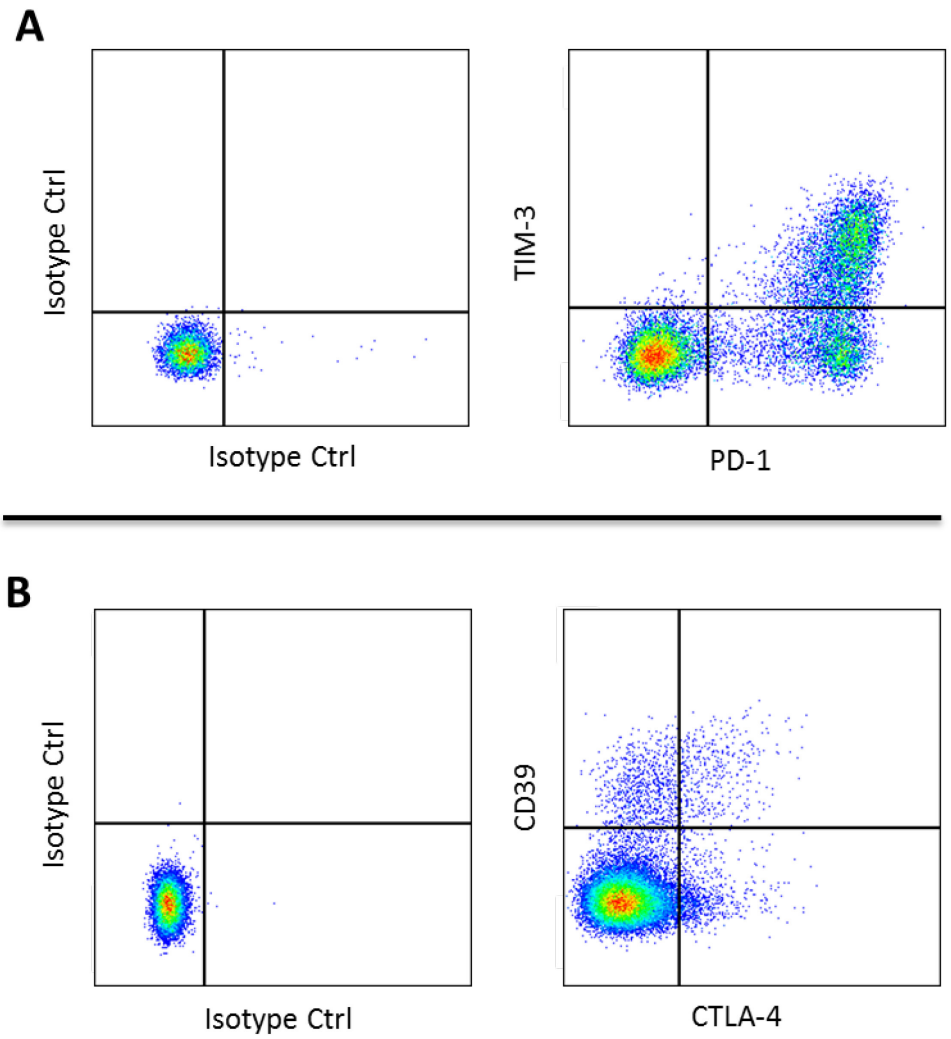

Figure 17: Representative dot plots of gating strategies for two-parameter surface and intracellular expression. A) TIM-3 vs. PD-1 was used in order to identify TIM-3, PD-1 double positive CD4+ bmT cells by using the following pregating steps: SSC-A vs. FSC-A, FSC-H vs. FSC-A, SSC-A vs. live/dead, SSC-A vs. CD3+, CD8 vs. CD4. **B)** CD39 vs. CTLA-4 was used in order to identify CD39, CTLA-4 double positive CD4+ bmT cells by using the following pregating steps: SSC-A vs. FSC-A, FSC-H vs. FSC-A, SSC-A vs. live/dead, SSC-A vs. CD3+, CD8 vs. CD4. Ctrl: Control.

5.6.4 Isotype control: Trouble shooting

The most appropriate isotype control would match the host species, the Ig subclass, the fluorophore and the manufacturer of the primary antibody as well as the antibody concentration. Due to low cell counts in AML patient samples and time management, these conditions could not be completely fulfilled in this project, as the performance of one single isotype control per panel was not possible. Instead, three different Isotype controls were used per patient sample: one Isotype control for all T cell panels (T1-4), one Isotype control for all Blast panels (B1-3) and one Isotype control for the IC Panel (Figure 18). In each of those three isotype controls the backbone antibodies were combined with the most appropriate isotype controls for all panels: for the T cell panels and Blast panels only mouse IgG1, k Isotype controls were used, whereas for the IC panel the Isotype controls could be directly adapted to the primary antibodies in case of host species, the Ig subclass and the fluorophore. As far as the fluorophore and the manufacturer of the primary antibodies are concerned, there had been made some compromises, which also leads to the fact that the isotype controls had to be interpreted with caution in some cases.

Usually, the positives percentages of the Isotype controls were subtracted from the positive percentages of the stained samples. In cases with positive percentages of the Isotype control more than 5 %, it was evaluated whether this was due to unspecific binding or only due to a shifting population in the Isotype control. In the latter case, the mean value of the positive percentages of the Isotype controls of all samples was subtracted instead.

A

PerCP-Cy5.5	CD8
BB515	IgG1, k Isotype control
PEvio770	CD95
PE	IgG1, k Isotype control
APC-eFlour780	Viability Dye
APC	IgG1, k Isotype control
BV786	IgG1, k Isotype control
BV650	CD62L
BV421	IgG1, k Isotype control
BUV737	CD3
BUV496	CD4
BUV395	CD45RO

B

PerCP-Cy5.5	IgG1, k Isotype control
BB515	IgG1, k Isotype control
PEvio770	CD34
PE	IgG1, k Isotype control
APC-eFlour780	Viability Dye
APC	IgG1, k Isotype control
BV786	IgG1, k Isotype control
BV650	CD33
BV421	IgG1, k Isotype control
BUV737	CD3
BUV496	CD38
BUV395	CD45

C

PerCP-Cy5.5	CD8
FITC	IgG1, k Isotype control
PE-Cy7	IgG1, k Isotype control
PE	IgG1, k Isotype control
APC-eFlour780	Viability Dye
APC	IgG2a, k Isotype control
BV786	IgG1, k Isotype control
BV650	PD1
BV421	IgG2b, k Isotype control
BUV737	CD3
BUV496	CD4
BUV395	CD45

Figure 18: Flow cytometry panel design of isotype controls. Extracellularly used isotype controls are marked in orange, whereas intracellularly stained isotype controls are highlighted in blue. **A)** Isotype control for all T cell panels. **B)** Isotype control for all Blast panels. **C)** Isotype control for the IC panel.

5.6.4.1 FITC-CD16

For the analysis of FITC-CD16 (T4, Figure 6) there was no isotype control taken into account for all samples, as in the other T cell panels only BB515 labeled antibodies were used, and therefore a BB515-IgG1 Isotype control was performed as an approximation for all T cell panels. While it is the case, that BB515 and FITC show very similar excitation and emission properties in flow cytometry, BB515 is a dye that is up to seven times brighter than FITC. Therefore, for FITC-CD16 this isotype control was ignored.

5.6.4.2 FITC-CD73

During the project the FITC Mouse IgG1, k Isotype control from Biolegend was exchanged by the FITC Mouse IgG1, k Isotype control from Miltenyi for organizational reasons. This lead to a shifting population in the Isotype control. Therefore, for analysis of CD73 expression (IC, Figure 6) the mean value of the positive percentages of the Isotype controls of all other samples was subtracted in all cases with an isotype control with a positive percentage more than 5 % (Figure 19).

5.6.4.3 PE-LAG-3

PE-LAG-3 (IC, Figure 6) was stained extracellularly, but in the IC Panel. This means, after extracellular staining cells were fixed and permeablized by using the FIX & PERM™ Cell Permeabilization Kit by ThermoFisher prior to intracellular staining. PE is a fluorophore with a relatively big mass. Bigger fluorophores are harder to get into the cell, but also harder to wash back out again if they are not bound to antigen. Due to this reason, in the isotype control often a positive population was observed with no similarity to the positive population in the stained. Therefore, the isotype control was ignored for analysis of LAG-3 expression (Figure 19).

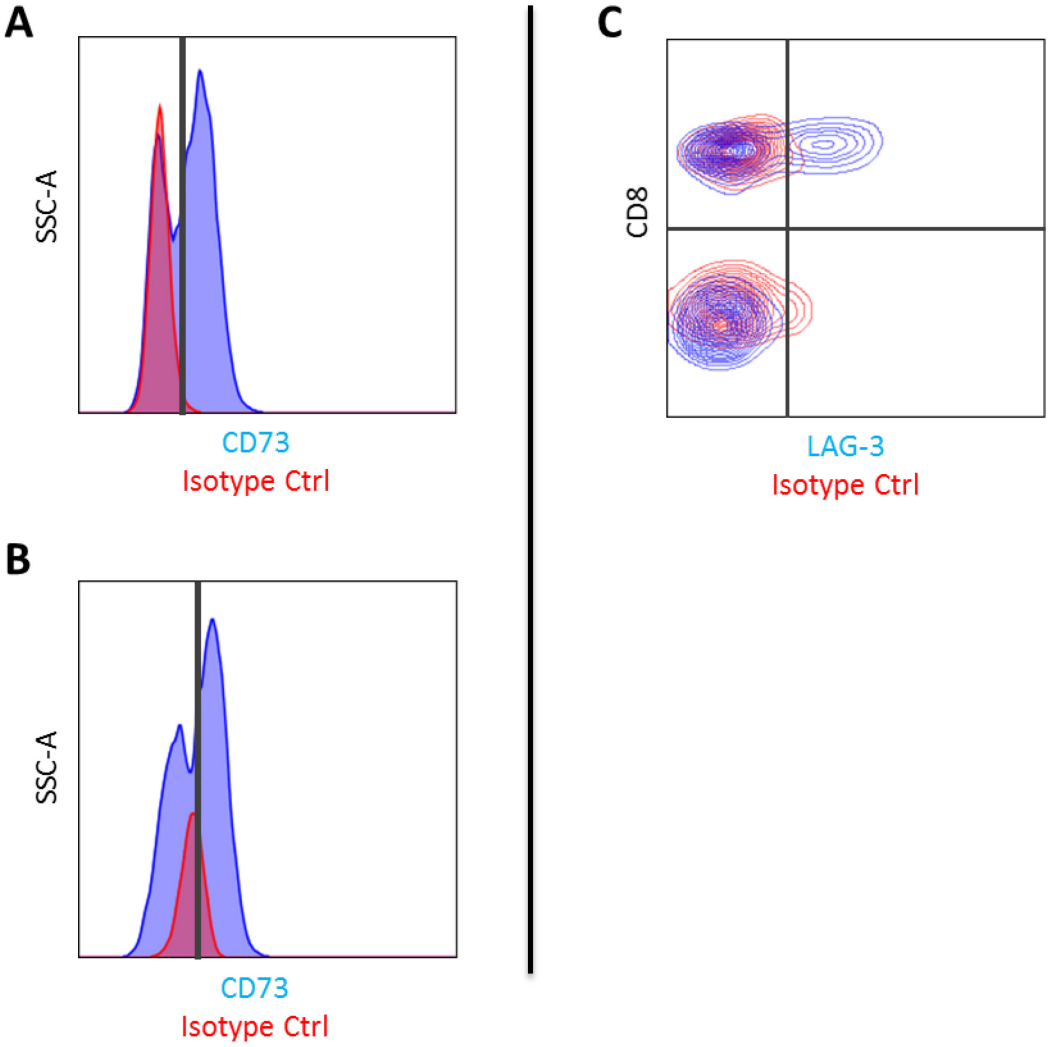

Figure 19: Exemplary histograms and dot plots for gating difficulties due to the isotype control. A) Usual gating strategy for CD73 was possible. Isotype control was event-free. **B)** Usual gating strategy for CD73 could not be performed without cutting the shifting population in the isotype control. In further analysis, the isotype control was ignored and not subtracted. The mean value of the positive percentages of all other samples was subtracted from the positive percentage of the stained sample instead. **C)** For PE-LAG-3 the isotype control showed positive populations with no similarity to the positive populations in the stained sample (CD8+ bmT cells were expressing more LAG-3 than CD4+ bmT cells in the stained sample) due to the process of intracellular staining. Unspecific binding of the antibody was excluded and the isotype control ignored for all samples.

5.7 RNA isolation

The RNA isolation of the sorted bone marrow populations was performed by using the Quick-RNA™ Microprep Kit from Zymo Research. Therefore, sorted cells were stored on ice for up to 4 hours and then pelleted by 5 min at 500 g. Afterwards, the supernatant was aspirated, the cell pellet resuspended in RNA lysis buffer and then frozen either at -20 °C or -80 °C.

After storage at -20 °C for a maximum of 7 days sample material was processed further according to the kit's manufacturers' protocol, including DNA in-column digestion prior to RNA isolation. When

stored at -80 °C, cell material was treated equally, with the exception, that samples could be stored more than 7 days prior to RNA isolation.

5.8 Quality control of RNA samples

Prior to sequencing, the quality of the isolated RNA was analyzed using the Agilent RNA 6000 Pico Kit and the Agilent Bioanalyzer 2100 according to the Agilent RNA 6000 Pico Kit Guide. For analysis, 1 µl of each 15 µl RNA sample was used; in case of samples generated from more than 100.000 cells a 1:10 dilution step with nuclease free water was performed prior to analysis to avoid overloading. Subsequently, the RNA 6000 Pico chip was loaded according to the Agilent RNA 6000 Pico Kit Guide. For quality assessment, the RIN (RNA integrity number) value (RIN-value > 7) and height of the 28S peak (> 18S peak) were taken into account (Figure 20).

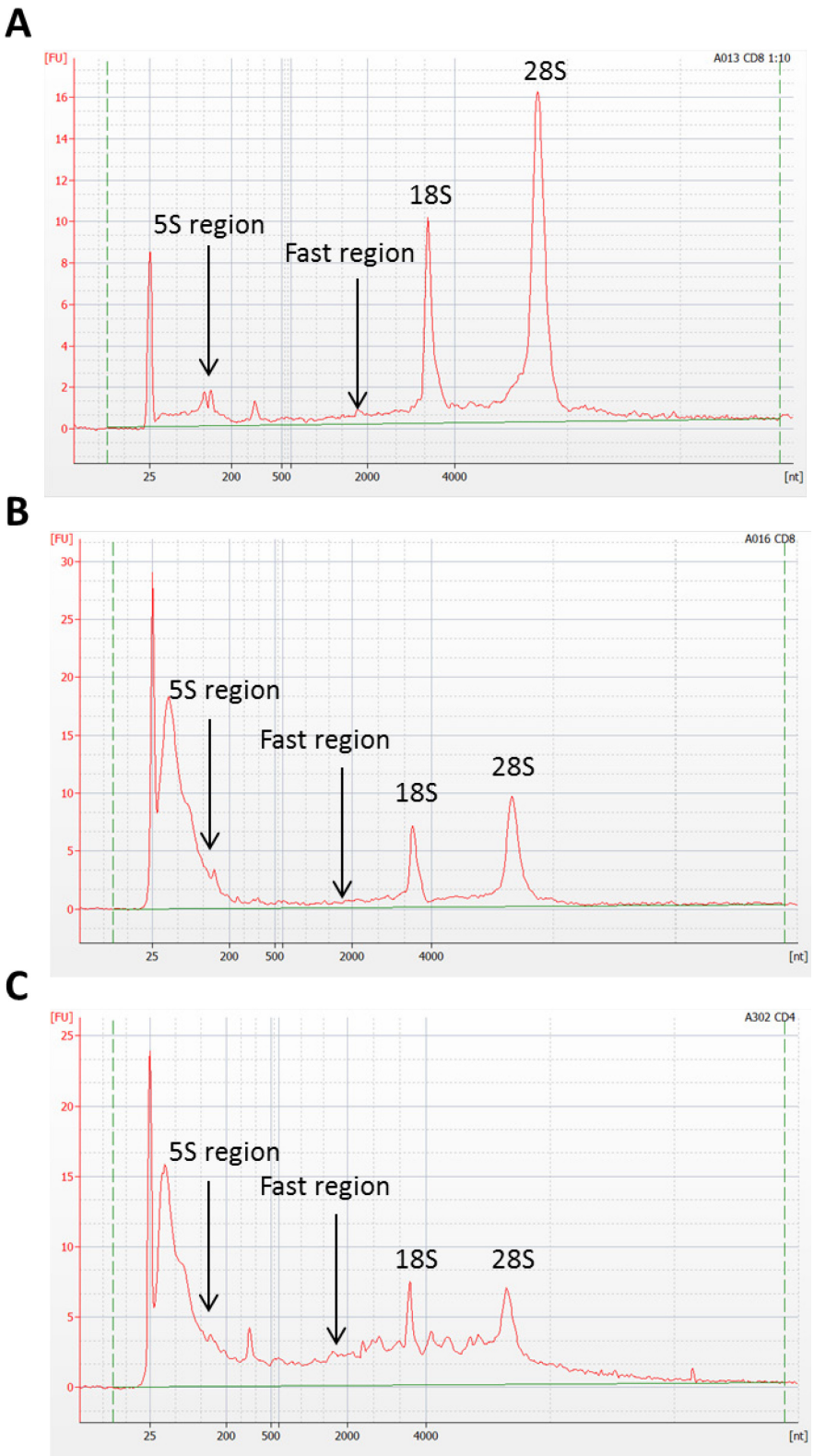

Figure 20: Representative electropherograms of RNA samples from CD8+ bmT cells produced by using the Agilent RNA 6000 Pico Kit and the Agilent Bioanalyzer 2100. A) Patient A013: With a RIN-value of 9.1 and no visible elevation of the curve in the fast region this sample could be used for RNA-seq. **B)** Patient A016: Despite the low RIN-value of 5.7 (under the threshold of RIN=7), the 28S and 18S peak were still visible and the elevation of the curve was limited to the 5S region. This indicated a high amount of Micro-RNA in the sample and not RNA degradation. Sample could be sequenced. **C)** Patient A302: Sample could not be sequenced due to a low RIN-value of 3.3 and an elevation within the fast region.

5.9 DNA isolation

In case of the blasts' population, a part of the cell suspension was kept for DNA isolation after sorting, if there were at least 3x10e4 blasts left after chromatin transposition. Therefore, after being pelleted by 5 min at 500 g, the cell pellet was resuspended in 200 µl PBS and then frozen at -20 °C. These frozen samples were saved for DNA isolation and further down-stream analysis in the future such as leukemia exome sequencing for mutational burden analysis.

5.10 Chromatin transposition

Chromatin transposition of the sorted bone marrow populations was performed according to the "Supplementary Protocol 1 – Omni-ATAC – An improved and broadly applicable ATAC-seq" published in Nature Methods 2017 by the Howard Chang Lab (Corces et al., 2017). After sorting at the BD FACSAria III 6.5-15x10e3 cells per sample (minimum: 13x10e3 sorted cells per sample in total) were resuspended in 100-200 µl RSB I (49,25 ml nuclease free water, 10 mM Tris-HCl pH 7.4, 10 mM NaCl, 3 mM $MgCl_2$) and pelleted for 5 min at 4 °C and 500 g. Afterwards, all supernatant was aspirated and the pellet was resuspended in 50 µl of RSB II (RSB I containing 0.1 % Tween-20, 0.1 % NP40 and 0.01 % Digitonin). After 3 min of incubation on ice 100µl of RSB III was added (RSB I containing 0.1 % Tween-20) and tubes were inverted. Then, nuclei were pelleted for 10 min at 4 °C and 500 g and supernatant was completely aspirated. Subsequently, the pellet was resuspended in 8 µl of freshly prepared transposition mix (70 % 2X TD buffer + 6.25 % Tn5 enzyme + 22.25 % PBS + 0.5 % Digitonin+ 1 % Tween-20) by pipetting up and down 6 times and then incubated at 37 °C for 30 min in the thermomixer with 1000 RPM mixing.

After incubation, a column-based DNA clean-up was performed using the Zymo DNA Clean & Concentrator™-5 Kit according to the DNA Clean & Concentrator™-5 INSTRUCTION MANUAL. Afterwards, DNA was eluted in 23.6 µl nuclease-free water and amplified via PCR. To that end, 1 µl each of a forward and a reverse primer was added to 25 µl of NEBNext 2x MasterMix and the purified transposed DNA. PCR was performed at the peqSTAR 96 Universal Gradient including the following cycles:

(1) 1 cycle of 72 °C for 5 min, 98 °C for 30 sec
(2) 9 cycles of 98 °C for 10 sec, 63 °C for 30 sec, 72 °C for 1 min

Prior to this project, 9 cycles of PCR had been determined as optimal in the context of 7.000-15.000 cells as input material and the described adapted OMNI-ATAC protocol. Thus, no real-time PCR for determination was performed as proposed by the original OMNI-ATAC protocol (Corces et al., 2017).

For samples A002-A010 and A101-A110 another clean-up reaction using the Zymo DNA Clean & Concentrator™-5 Kit was performed after PCR. Subsequently, the DNA was eluted in 11 µl

nuclease-free water and frozen at -20 °C. For all other patients, DNA was frozen immediately after amplification at -20 °C without another clean-up reaction until library preparation.

5.11 RNA Sequencing

The CD8+ bmT cell population showed the most promising effects in the flow cytometric analysis and was sequenced first.

RNA library preparation was performed according to the NEBNext® Ultra™ II Directional RNA Library Prep Kit for Illumina in combination with the NEBNext® Poly(A) mRNA Magnetic Isolation Module.

In brief, the following protocol was performed:

(1) Sample RNA (up to 100ng as available) was used as input material.
(2) Washed Oligo dT Beads were mixed with input RNA 1:1 (total 100µl).
(3) The RNA-Bead mix was denatured at 65°C for 4min and subsequently washed, eluted, rebound, rewashed and then eluted and fragmented by 15min at 94°C.
(4) Fragmented mRNA was subsequently used for first strand cDNA synthesis, then second strand synthesis.
(5) End Prep of cDNA Library was followed by Adaptor Ligation (100-fold dilution of adapters).
(6) Finally, adapter ligated cDNA library was enriched by 14 cycles of PCR using NEB primers for multiplexed sequencing.

Analysis of RNA-seq libraries was performed by DNA high sensitivity chip on the Bioanalyzer 2100. Pooling of 24 libraries for sequencing on a NextSeq 500/550 High Output Kit v2.5 (150 Cycles) was performed according to average library size and library concentration.

Pooled libraries were diluted and loaded on the NextSeq500 as described in the documentation of Illumina using paired end sequencing with 2 x 75 bp reads.

RNA sequencing was performed by Dr. med. Semjon Willier.

RNA-seq data of CD8+ bmT cells was available for AML patient samples and healthy BM donor samples, as listed in Figure 21. As healthy BM donors have been analyzed by both another MD student in the laboratory (Jonas Wilhelm) and me, healthy BM donor RNA-seq data was used as reference in both projects to have more reference samples.

Differential analysis as documented here was derived following the standard RNA-seq pipeline of the DNASTAR Lasergene: Arrayexpress.

Here, RNA-seq analysis focused on the question whether differences between healthy BM donors and AML patients could be seen and if so, whether (a) the molecules changed by flow cytometry

analysis could be confirmed as differentially expressed and (b) whether other molecules of functional relevance could be found to be differentially expressed.

The gene expression data was subjected to multiple testing correction and then filtered using the following criteria:

(1) RPKM≥2 in comparison group 1 (AML patient samples/initial samples without future relapse)
(2) RPKM≥2 in comparison group 2 (healthy BM donors/initial samples with future relapse)
(3) Fold change ≥2 in either group
(4) Statistics: $p<0.05$ (false discovery rate)

The filtered genes were researched and categorized by known function in CD8+ T cells. Genes with estimated relevance were colored in the volcano plots in subchapter 6.6. Genes that showed significant differences in flow cytometric analysis were also compared to their location in the volcano plots.

RNA-seq analysis was performed by me and Dr. med Semjon Willier.

A

	Healthy BM donors	All cases
Samples, n	14	20
Age, mean (range)	8.5y (1.7-13.0)	7.3y (0.4-16.6)
Gender, n (%)		
Male	7 (50)	9 (45)
Female	7 (50)	11 (55)

B

	NFR	FR
Samples, n	10	4
Age, mean (range)	8.0y (0.6-16.6)	6.4y (0.4-14.6)
Gender, n (%)		
Male	3 (30)	4 (100)
Female	7 (70)	0 (0)

C

Patient	Initial Dx	1st relapse	2nd relapse	3rd relapse	4th relapse	5th relapse
1	A002					
2	A003					
3	A004					
4	A005					
5	A006					
6	A007					
7	A009					
8	A010					
9	A011					
10	A012					
11	A013					
12	A014					
13	A015					
14	A016					
15	A301					
16	A302					
17	A303		A503			
18	A306	A406				
19	A307	A407				
20	A308	A408				
21	A309*	*				
22		A401				
23		A402				
24		A403				
25		A404				
26		A405				
27		A409				
28		A410				
29			A501	A601	A701	A801

Figure 21: RNA-seq data - healthy bone marrow donor and AML patient characteristics. A) General information of healthy BM donor and AML patient RNA samples. **B)** General information of initial AML RNA samples with and without future relapse. **C)** All AML samples with respective patient codes in green, unavailable samples in red. * indicates CNS relapse, blank cells indicate that the respective relapse did not occur. RNA samples available for RNA-seq analysis are marked in purple. Initial Dx: Initial Diagnosis, healthy BM donors: healthy BM donors, NFR: no future relapse, FR: future relapse.

5.12 Statistical Analysis

Statistical analysis was performed using GraphPad Prism 7. The significance of differences was determined by using the Mann–Whitney U test for unpaired values and the Wilcoxon matched-pairs signed rank test for paired values. Statistical significance was considered for $p<0.05$ (*), $p<0.01$ (**), $p<0.001$ (***) and $p<0.0001$ (****). In statistical analysis, only non-parametric tests were used in order to prevent false positive findings, as non-parametric tests tend to have less power than parametric tests. Multiple testing corrections were performed using the Original FDR method of Benjamini and Hochberg. Graphs were generated using GraphPad Prism 7.

5.12.1 Multiple testing correction

Multiple testing corrections for flow cytometry data were performed using the Original FDR method of Benjamini and Hochberg. P values were analyzed and corrected in separate groups with regard to cell type (CD3+, CD4+ and CD8+ bmT cells) and ways of comparison (AML vs. healthy BM donors, no future relapse vs. future relapse, initial diagnosis vs. relapse, Kaplan-Meier estimates for single antigens, Kaplan-Meier estimates for indices). In order to avoid any information loss, uncorrected, as well as corrected p values (q values) were listed at the end of each chapter. Unless otherwise stated, apart from that mentioned p values are uncorrected (note asterisks in figures).

5.12.2 Kaplan-Meier estimates

In context of Kaplan-Meier estimates, initial AML samples were categorized into two groups using the mean expression value of the respective marker/index on/of bmT cells of all AML patients (N=29) as cut-off value (6.2.8 and 6.2.9).

We also tried k-means clustering on SPSS in order to divide the AML patients into groups in consultation with our statistician: That did not work out with our patient cohort. Therefore, the above-mentioned method was maintained.

6 Results

Defined populations within bone marrow samples of pediatric AML patients and healthy bone marrow donors (healthy BM donors) were analyzed for protein expression by flow cytometry, for RNA expression by RNA-seq and for chromatin accessibility by ATAC-seq. Unless otherwise stated, for the following figures Mann-Whitney U test was used to calculate all p-values.

6.1 Flow cytometry analysis of cellular composition of AML bone marrow samples compared to healthy bone marrow donors

The frequency of cells in the *blast gate* ($CD45_{dim}$ cells) given as percentage of living cells was increased in AML patients in comparison to healthy controls (80.2 % vs. 23.7 %, mean values, $p<0.0001$, Figure 22A), whereas the number of $CD45_{high}$ cells was decreased in AML patients compared to healthy BM donors (12.6 % vs. 41.2 %, $p<0.0001$, Figure 22B). The mean frequency of T cells (CD56-CD3+) among $CD45_{high}$ cells was 60.2 % in AML patients, while not significantly different to healthy BM donors (60.2 % vs. 52.7 %, $p=0.1499$, Figure 23A). The mean frequency of NK cells among $CD45_{high}$CD3- cells was 25.1 % in AML patients, while the mean frequency of NKT cells among $CD45_{high}$CD3+ cells was 4.9 % in patients' samples. Only the frequency of NK cells among CD3- cells was significantly reduced in healthy controls in comparison to AML patients (NK: 25.1 % vs. 14.0 %, $p=0.0320$, Figure 23B; NKT: 4.9 % vs. 4.4 %, $p=0.4166$, Figure 23C). Regarding CD3+ and CD3- cells among $CD45_{high}$ cells there were no differences observed between AML patients and healthy controls.

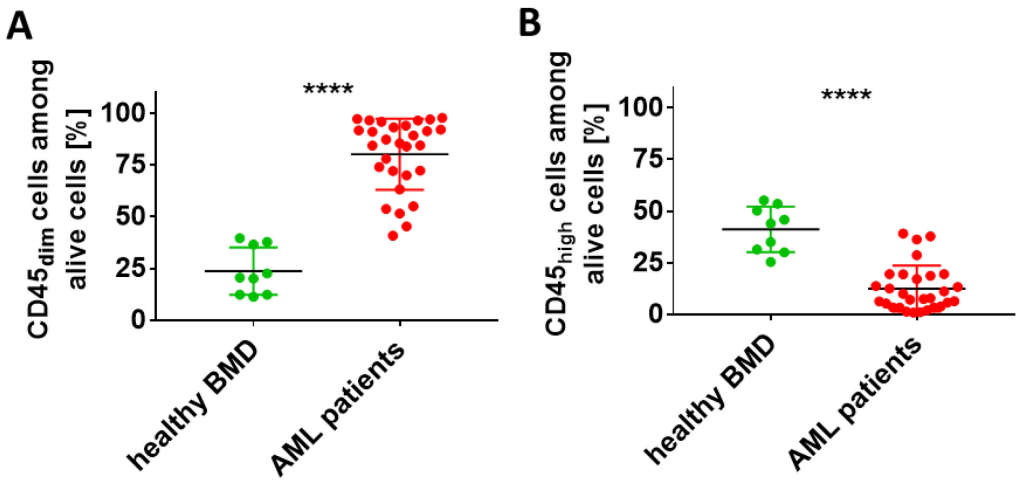

Figure 22: Cellular composition of alive cells in AML bone marrow samples in comparison to healthy BM donors' samples. A) Among alive cells in the bone marrow the mean frequency of $CD45_{dim}$ cells was increased in AML patients compared to healthy BM donors ($p<0.0001$). **B)** The number of $CD45_{high}$ cells among alive cells in the bone marrow was reduced in AML patients in comparison to healthy controls ($p<0.0001$). Healthy BMD: healthy bone marrow donors.

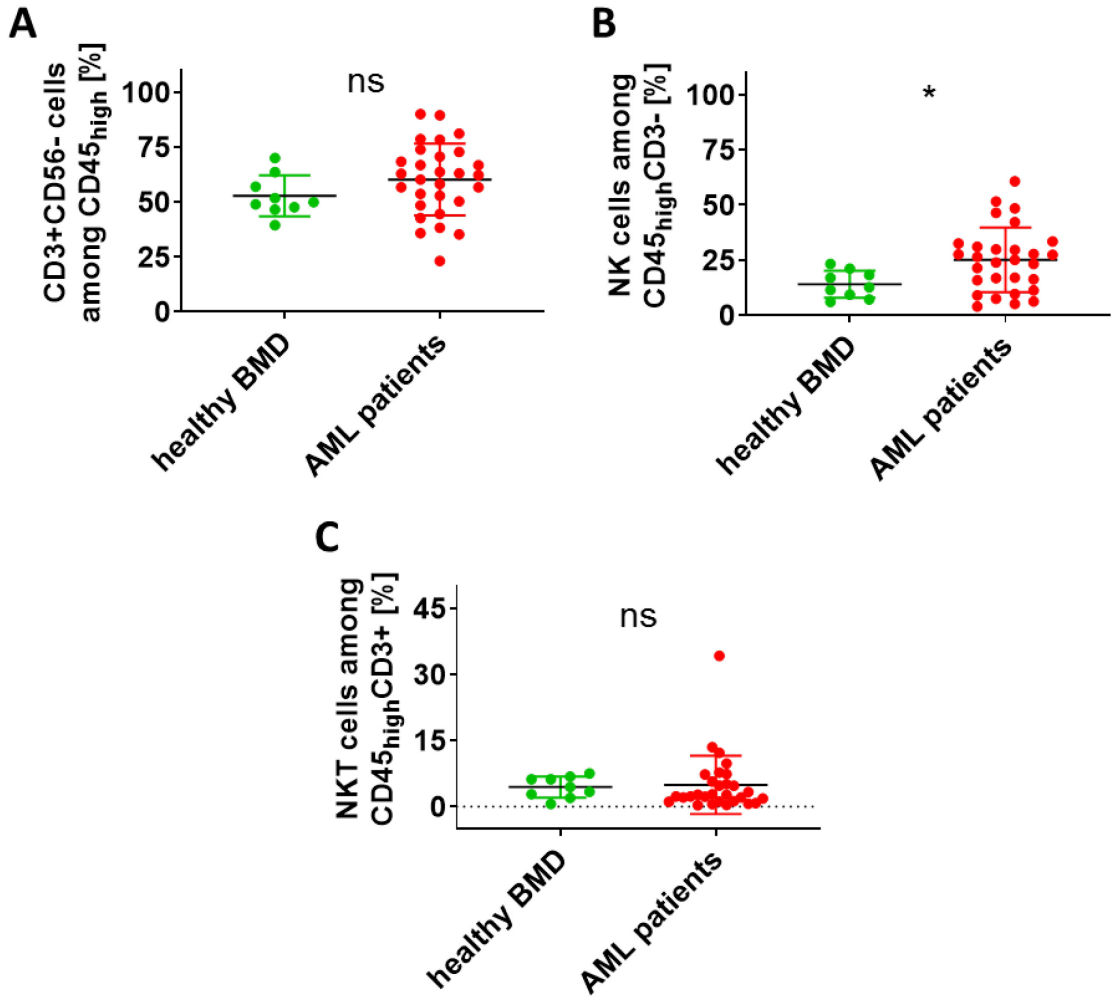

Figure 23: Cellular composition of CD45$_{high}$ cells in AML bone marrow samples and healthy BM donors' samples. A) Among CD45$_{high}$ cells in the bone marrow the mean frequency of T cells (CD3+CD56-) was not significantly different to healthy controls. **B)** Among CD45$_{high}$CD3- bone marrow cells the mean frequency of NK cells (CD56+, CD16+, CD56+CD16+) was increased compared to healthy BM donors (p=0.0320). **C)** In the frequency of NKT cells (CD56+, CD16+, CD56+CD16+) among CD45$_{high}$CD3+ bone marrow cells no statistical difference was observed between AML patients and healthy controls. Healthy BMD: healthy bone marrow donors.

6.2 Flow cytometric phenotype analysis of bone marrow T cells in AML patients

T cells in the bone marrow (bmT cells) were phenotypically analyzed for characteristics like T cell frequency and CD4/CD8 ratio, maturation stages and expression of co-inhibitory and co-stimulatory molecules. CD3+ bmT cells were differentiated further into CD3+CD4+ and CD3+CD8+ bmT cells. For convenience, the latter two were referred to as CD4+ and CD8+ bmT cells.

All initial AML samples were therapy naïve, but within the AML samples from 1st relapse (N=10) four relapses happened within the chemotherapy treatment of initial diagnosis, whereas four other relapses happened upon completion of the chemotherapy treatment of initial diagnosis. These sample groups were compared concerning the expression rates of different markers (Figure 24,

Figure 83). There were no significant differences determined, so all samples from 1st relapse were treated equally in analysis.

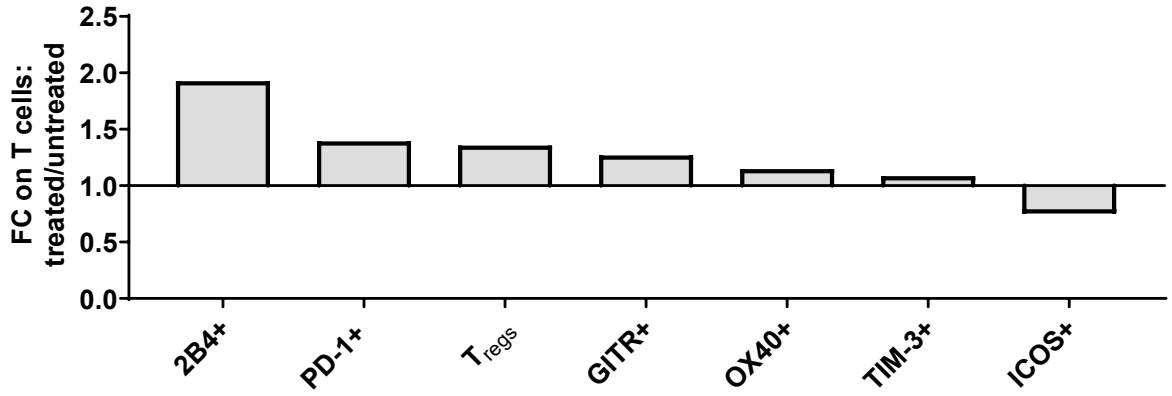

Figure 24: Comparison of relapsed AML samples (1st relapse) before chemotherapy completion (N=4) and after chemotherapy completion (N=4) of initial diagnosis. Between relapsed AML samples within chemotherapy treatment of initial diagnosis and relapsed AML samples upon completion of chemotherapy treatment of initial diagnosis expression rates of 2B4, PD-1, GITR, OX40, TIM-3 and ICOS on CD3+ bmT cells and the frequency of T_{regs} among CD4+ bmT cells were not significantly different. For other objects of comparison see Figure 83. Treated: relapsed AML samples before completion of primary AML chemotherapy, untreated: relapsed AML samples after completion of primary AML chemotherapy, FC: fold change.

6.2.1 Decreased frequency of bmT cells and increased frequency of late bmT cell differentiation stages in AML patients compared to healthy bone marrow donors

The frequency of CD3+ bmT cells was reduced in AML patients compared to healthy BM donors (8.4 % vs. 23.9 %, mean values, p<0.0001, Figure 25A), whereas the CD4/CD8 ratio of CD3+ bmT cells in patients was not altered in comparison to healthy controls (Figure 25B). The frequency of γδ T cells in AML patients was also not significantly different compared to healthy BM donors (Figure 25C).
Concerning the T cell maturation stages there was a shift towards a more mature phenotype in AML patients detectable in contrast to healthy BM donors. The following observations were based on CD62L, CD45RO and CD95 expression levels (Figure 26): The frequency of naïve (CD62L+CD45RO-CD95-) bmT cells (CD3+: 33.9 % vs. 57.5 %, p=0.0018; CD4+: 38.8 % vs. 62.9 %, p=0.0013; CD8+: 30.9 % vs. 54.3 %, p=0.0028) was reduced in AML patients in comparison to healthy controls, while the frequency of effector memory (CD62L-CD45RO+) bmT cells (CD3+: 21.5 % vs. 9.4 %, p=0.0010; CD4+: 21.1 % vs. 7.8 %, p=0.0018; CD8+: 19.6 % vs. 9.8 %, p=0.0491) was increased in AML patients. Moreover, the number of effector (CD62L-CD45RO-) CD4+ bmT cells was increased in AML patients (23.6 % vs. 12.1 %, p=0.0444). The comparison of stem cell-like memory (CD62L+CD45RO-CD95+) bmT cells, central memory (CD45RO+CD62L+) bmT cells and effector CD3+ bmT cells and effector

CD8+ bmT cells showed no significant differences in terms of frequency between AML patients and healthy donors.

Within the patient samples the only significant difference in frequency was a reduction in effector memory (CD62L-CD45RO+) CD8+ bmT cells in relapsed samples (1st relapse) in comparison to initial AML samples (11.4 % vs. 21.0 %, p=0.0247, not shown).

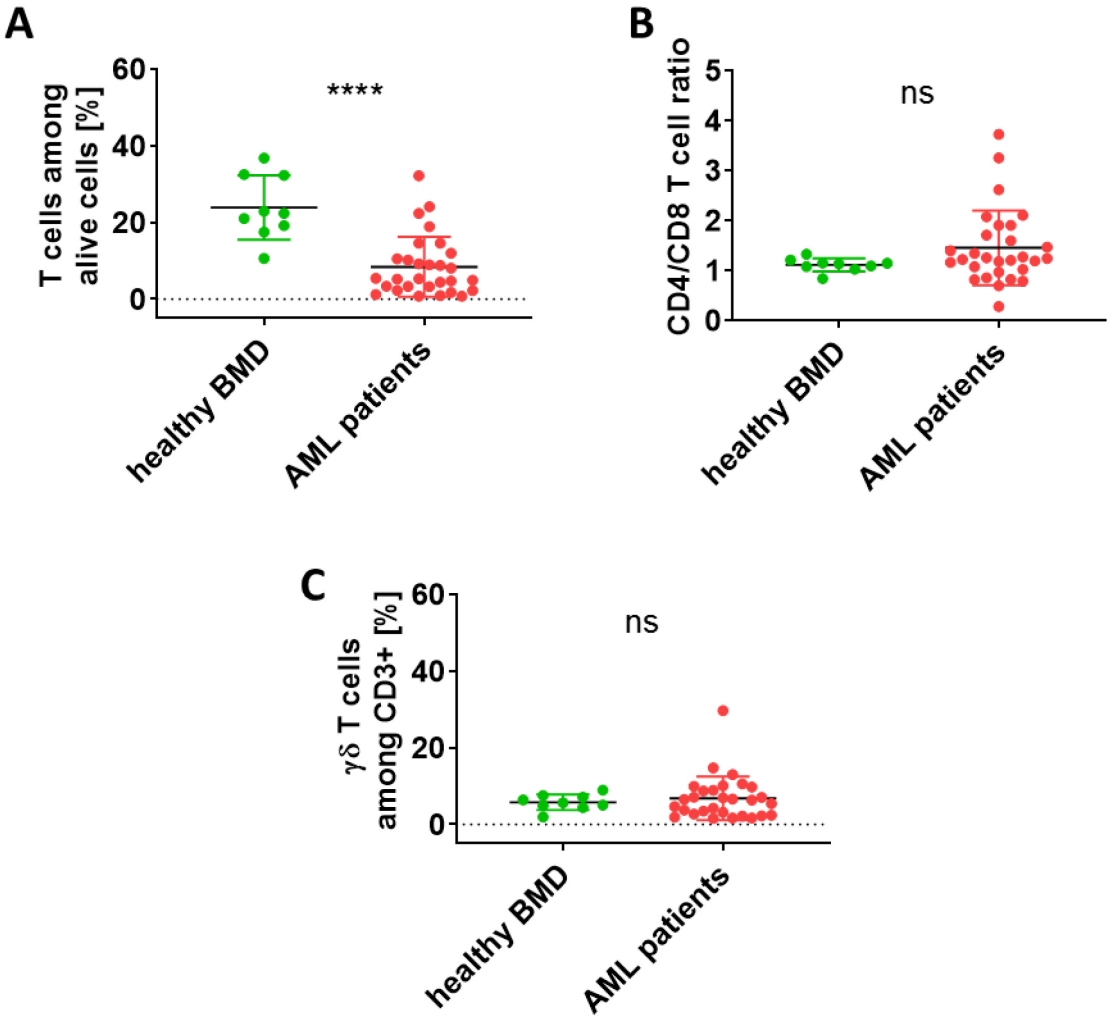

Figure 25: General characteristics of bmT cells in AML patients compared to healthy BM donors. A) The frequency of CD3+ bmT cells in AML patients was reduced compared to healthy bone marrow donors ($p<0.0001$). **B)** The CD4/CD8 ratio of CD3+ bmT cells in AML patients was not altered in comparison to healthy controls. **C)** The frequency of γδ T cells was not altered compared to healthy bone marrow donors. Healthy BMD: healthy bone marrow donors.

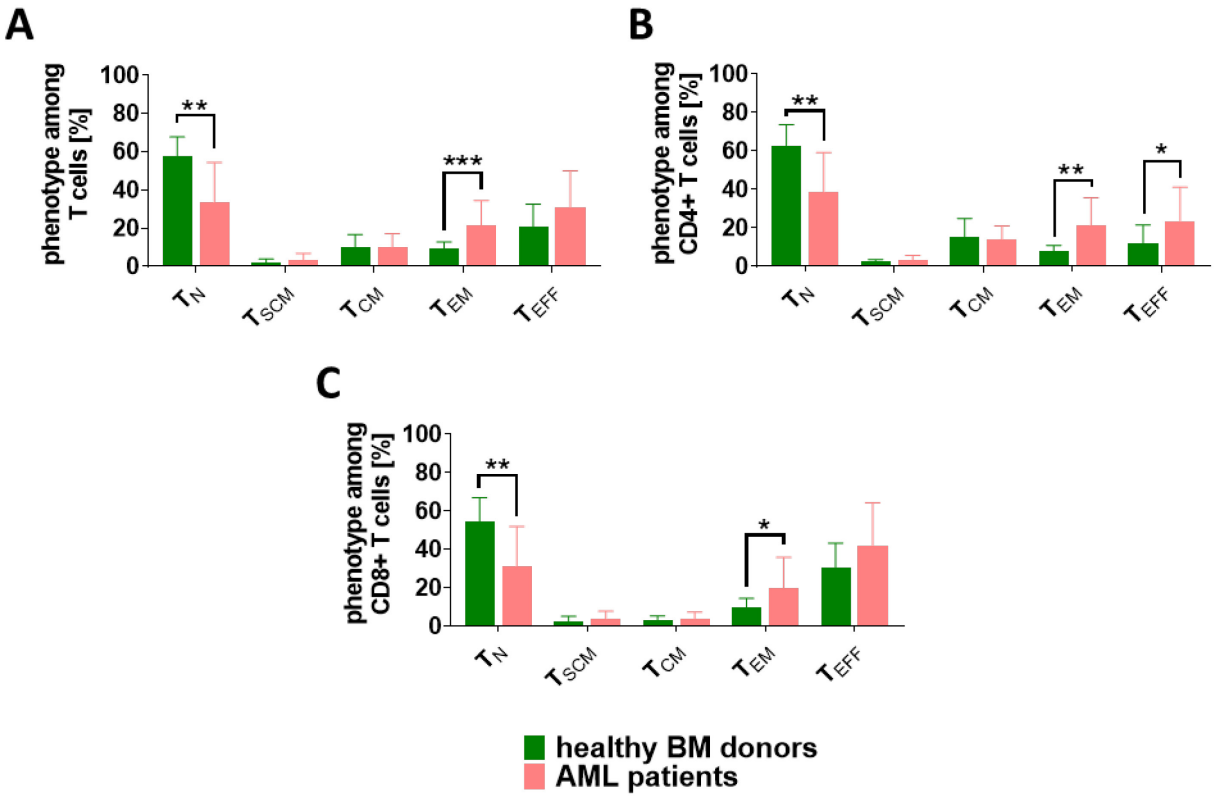

Figure 26: Shift to a more mature phenotype of bmT cells in AML patients (N=29) compared to healthy BM donors (N=9). Observations were based on CD62L, CD45RO and CD95 expression levels on bmT cells. **A)-C)** The frequency of naïve (CD62L+CD45RO-CD95-) bmT cells (CD3+: p=0.0018; CD4+: p=0.0013; CD8+: p=0.0028) was reduced in comparison to healthy controls, while the frequency of effector memory (CD62L-CD45RO+) bmT cells (CD3+: p=0.0010; CD4+: p=0.0018; CD8+: p=0.0491) was increased in AML patients. Moreover, the number of effector (CD62L-CD45RO-) CD4+ bmT cells was increased in AML patients (p=0.0444). The comparison of stem cell-like memory (CD62L+CD45RO-CD95+) bmT cells, central memory (CD45RO+CD62L+) bmT cells and effector CD3+ bmT cells and effector CD8+ bmT cells showed no significant differences in terms of frequency between AML patients and healthy donors. T_N: naïve bmT cells, T_{SCM}: T stem cell-like memory bmT cells, T_{CM}: central memory bmT cells, T_{EM}: effector memory bmT cells, T_{EFF}: effector bmT cells, healthy BM donors: healthy bone marrow donors.

6.2.2 Decreased frequency of Th0 cells and increased frequency of Th1 and Th1Th17 cells in AML patients compared to healthy bone marrow donors and increased frequency of Th2 and Th17 cells in relapsed AML samples compared to initial AML samples

Among CD4+ bmT cells the frequency of Th0 cells was reduced in AML patients compared to healthy bone marrow donors (55.0 % vs. 69.0 %, p=0.0126), whereas the frequencies of Th1 (12.6 % vs. 4.0 %, p=0.0044), CXCR3+ Th2 (2.5 % vs. 0.5 %, p=0.0006), CXCR3+ Th17 (0.6 % vs. 0.1 %, p=0.0030) and Th1Th17 cells (2.3 % vs. 0.6 %, p=0.0126) were increased in AML patients compared to healthy controls (Figure 27A).

Within AML patient samples Th2 (6.8 % vs. 4.0 %, p=0.0197), CXCR3+ Th2 (3.2 % vs. 2.1 %, p=0.0441), Th17 (2.9 % vs. 1.3 %, p=0.0197), CXCR3+ Th17 (0.9 % vs. 0.4 %, p=0.0270) and CCR6+ only cells

(2.1 % vs. 1.2 %, p=0.0249) showed higher frequencies in relapsed AML samples in comparison to initial AML samples (Figure 27B).

In comparison between initial AML samples with and without future relapse there were no differences reaching statistical significance (not shown).

These results supported the observation of a shift towards a more mature phenotype of bmT cells in AML patients shown in Figure 26.

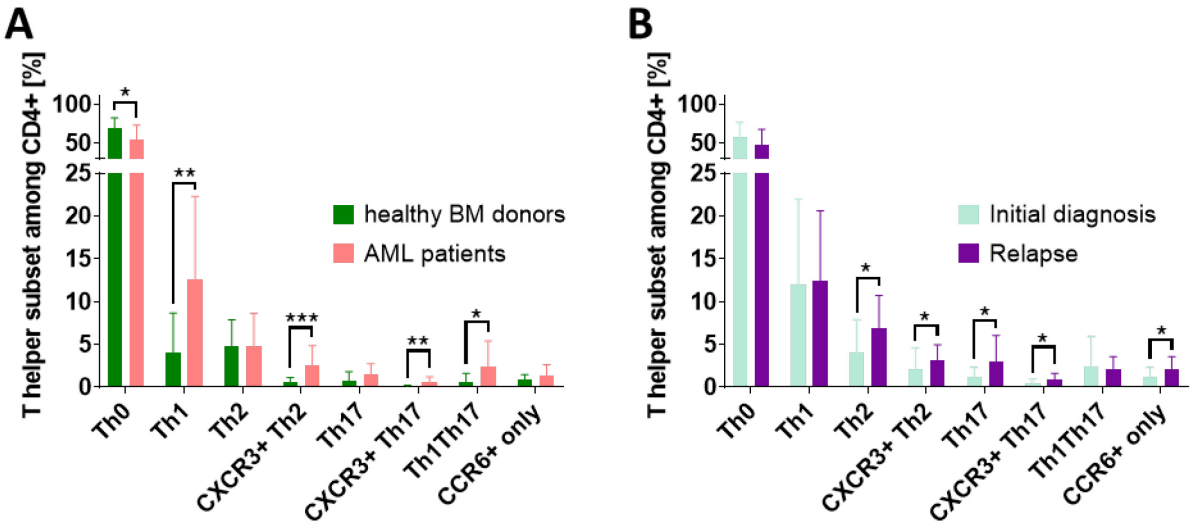

Figure 27: Distribution of T helper subsets Th0, Th1, Th2, TH17 and TH1Th17 among CD4+ bmT cells in AML patients. A) The frequency of Th0 cells was reduced (p=0.0126) in AML patients (N=29) compared to healthy BM donors (N=9), whereas the frequencies of Th1 (p=0.0044), CXCR3+ Th2 (p=0.0006), CXCR3+ Th17 (p=0.0030) and Th1Th17 cells (p=0.0126) were increased in AML patients compared to healthy controls. **B)** The frequencies of Th2 (p=0.0197), CXCR3+ Th2 (p=0.0441), Th17 (p=0.0197), CXCR3+ Th17 (p=0.0270) and CCR6+ only cells (p=0.0249) were increased in relapsed AML samples (N=12) in comparison to initial AML samples (N=21). Healthy BM donors: healthy bone marrow donors.

6.2.3 Increased frequency of bmT$_{regs}$ in relapsed AML samples compared to initial AML samples

The frequency of CD127$_{low}$CD25$_{high}$ cells (T$_{regs}$) among CD4+ bmT cells was significantly higher in relapsed AML samples in comparison to initial AML samples (9.5 % vs. 7.0 %, p=0.0215, Figure 28B). However, in all measured AML patient samples (N=29) the frequency of T$_{regs}$ did not influence survival of AML patients (not shown).

In AML patients compared to healthy BM donors (Figure 28A), as well as in initial AML samples with future relapse in comparison to initial AML samples without future relapse (not shown), the frequency of T$_{regs}$ was not significantly altered.

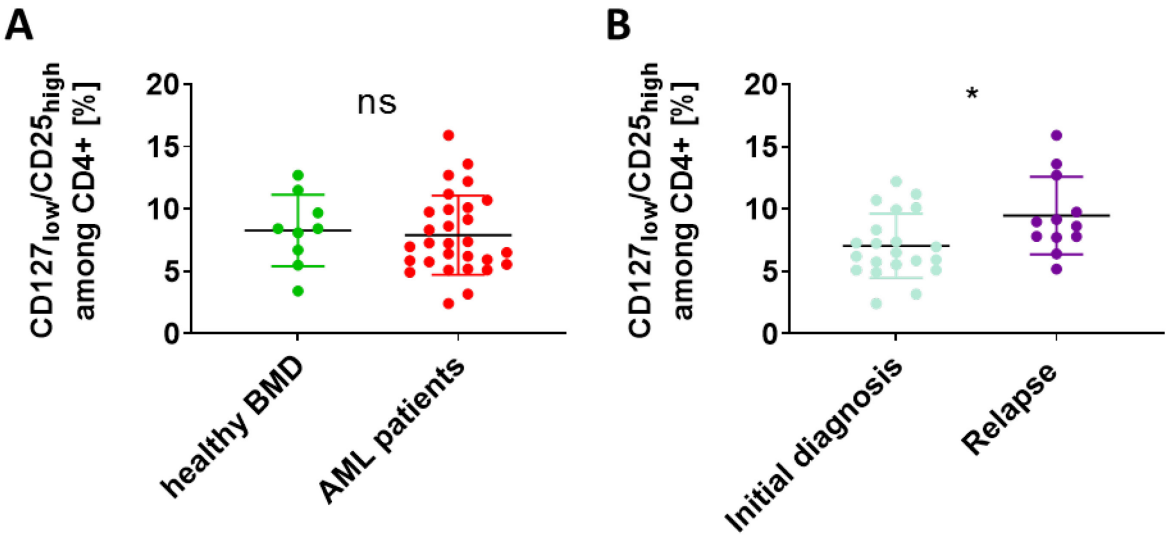

Figure 28: Increased frequency of bmT$_{regs}$ in relapsed AML samples compared to initial AML samples. A) The frequency of T$_{regs}$ (CD127$_{low}$CD25$_{high}$) among CD4+ bmT cells in AML patients was not significantly different compared to healthy BM donors. **B)** The frequency of T$_{regs}$ (CD127$_{low}$CD25$_{high}$) among CD4+ bmT cells was increased in relapsed AML samples in comparison to initial AML samples (p=0.0215). Healthy BMD: healthy bone marrow donors.

6.2.4 Overexpression of co-inhibitory and co-stimulatory molecules on bmT cells in AML patients compared to healthy bone marrow donors

As shown in Figure 29 (CD3+ bmT cells), Figure 32 (CD4+ bmT cells) and Figure 36 (CD8+ bmT cells) several co-inhibitory and co-stimulatory molecules were significantly overexpressed on CD3+ bmT cells as a whole, as well as on CD4+ and CD8+ bmT cells in AML patients in comparison to healthy BM donors.

Two co-inhibitory markers were found to be significantly overexpressed on all analyzed T cell subsets in AML patients compared to healthy controls. Those markers included TIM-3 (CD3+: 7.1 % vs. 1.7 %, p<0.0001; CD4+: 4.4 % vs. 1.0 %, p<0.0001; CD8+: 10.0 % vs. 2.4 %, p=0.0008) and PD-1 (CD3+: 34.8 % vs. 21.3 %, p=0.0016; CD4+: 30.6 % vs. 17.8 %, p=0.0031; CD8+: 38.4 % vs. 24.9 %, p=0.0215).
Also, the expression of the co-inhibitory marker CD39 (CD3+: 7.7 % vs. 2.0 %, p=0.0103; CD4+: 8.4 % vs. 2.6 %, p=0.0103; CD8+: 7.7 % vs. 1.8 %, p=0.0861) was increased on bmT cells in AML patients in comparison to healthy controls, but significantly differently only on CD3+ bmT cells and CD4+ bmT cells. LAG-3 (CD3+: 8.0 % vs. 2.9 %, p=0.0176; CD4+: 3.6 % vs. 1.7 %, p=0.0534; CD8+: 11.6 % vs. 4.2 %, p=0.0441) and CTLA-4 (CD3+: 3.9 % vs. 1.6 %, p=0.0024; CD4+: 7.6 % vs. 4.0 %, p=0.0916; CD8+: 1.0 % vs. 0.4 %, p=0.0240) were found to be statistically overexpressed only on CD8+ bmT cells and CD3+ bmT cells compared to healthy BM donors, but showed increased expression also on CD4+ bmT cells in AML patients. Co-inhibitory molecules 2B4 (CD4+: 9.9 % vs. 0.6 %, p=0.0004) and TIGIT (CD3+: 26.2 % vs. 17.3 %, p=0.0798; CD4+: 17.4 % vs. 10.8 %, p=0.0315; CD8+: 35.4 % vs. 24.1 %, p=0.0929) reached significant overexpression only on CD4+ bmT cells in AML patients in comparison to healthy controls.

Expression of co-stimulatory markers CD134 (CD3+: 8.7 % vs. 4.3 %, p=0.0058; CD4+: 17.3 % vs. 9.2 %, p=0.0159; CD8+: 1.0 % vs. 0.6 %, p=0.1933) and GITR (CD3+: 6.9 % vs. 3.5 %, p=0.0092; CD4+: 12.6 % vs. 6.0 %, p=0.0040) was significantly higher only on CD3+ bmT cells and CD4+ bmT cells in AML patients compared to healthy BM donors, with CD8+ bmT cells also showing a trend of an overexpression of CD134, but without reaching statistical significance. Furthermore, co-stimulatory markers ICOS and CD226 also tended to be higher expressed on bmT cells, while CD28 expression was rather reduced on bmT cells in AML patients compared to healthy controls (not significant).

Figure 30, Figure 31, Figure 33, Figure 34, Figure 37 and Figure 38 provide a more detailed description of differences in expression of co-inhibitory and co-stimulatory molecules on CD3+ bmT cells (Figure 30: co-inhibitory markers, Figure 31: co-stimulatory markers), CD4+ (Figure 33: co-inhibitory markers, Figure 34: co-stimulatory markers) and CD8+ bmT cells (Figure 37:

co-inhibitory markers, Figure 38: co-stimulatory markers) in AML patients in comparison to healthy controls.

Next, co-expression levels of co-inhibitory molecules on CD4+ (Figure 35) and CD8+ (Figure 39) bmT cells were compared in an attempt to further describe the phenotype of exhausted T cells. TIM-3/2B4 (CD4+: 0.7 % vs. 0.0 %, p<0.0001; CD8+: 6.6 % vs. 0.8 %, p<0.0001), TIM-3/PD-1 (CD4+: 3.9 % vs. 0.9 %, p=0.0004; CD8+: 7.8 % vs. 1.1 %, p=0.0010) and CTLA-4/CD39 (CD4+: 3.6 % vs. 1.1 %, p=0.0283; CD8+: 0.6 % vs. 0.1 %, p=0.0180) were in co-expression consistently higher on CD4+ bmT cells, as well as on CD8+ bmT cells in AML patients in comparison to healthy BM donors.
In addition, co-expression levels of 2B4/PD-1 (5.7 % vs. 0.5 %, p=0.0026) and LAG-3/PD-1 (3.0 % vs. 0.9 %, p=0.0211) were significantly increased on CD4+ bmT cells in AML patients compared to healthy BM donors.
However, due to a low frequency of co-inhibitory marker co-expressing T cells we reasoned that those small populations could bear only limited biological function. Thus, co-expression levels of co-inhibitory and co-stimulatory molecules were not investigated further.

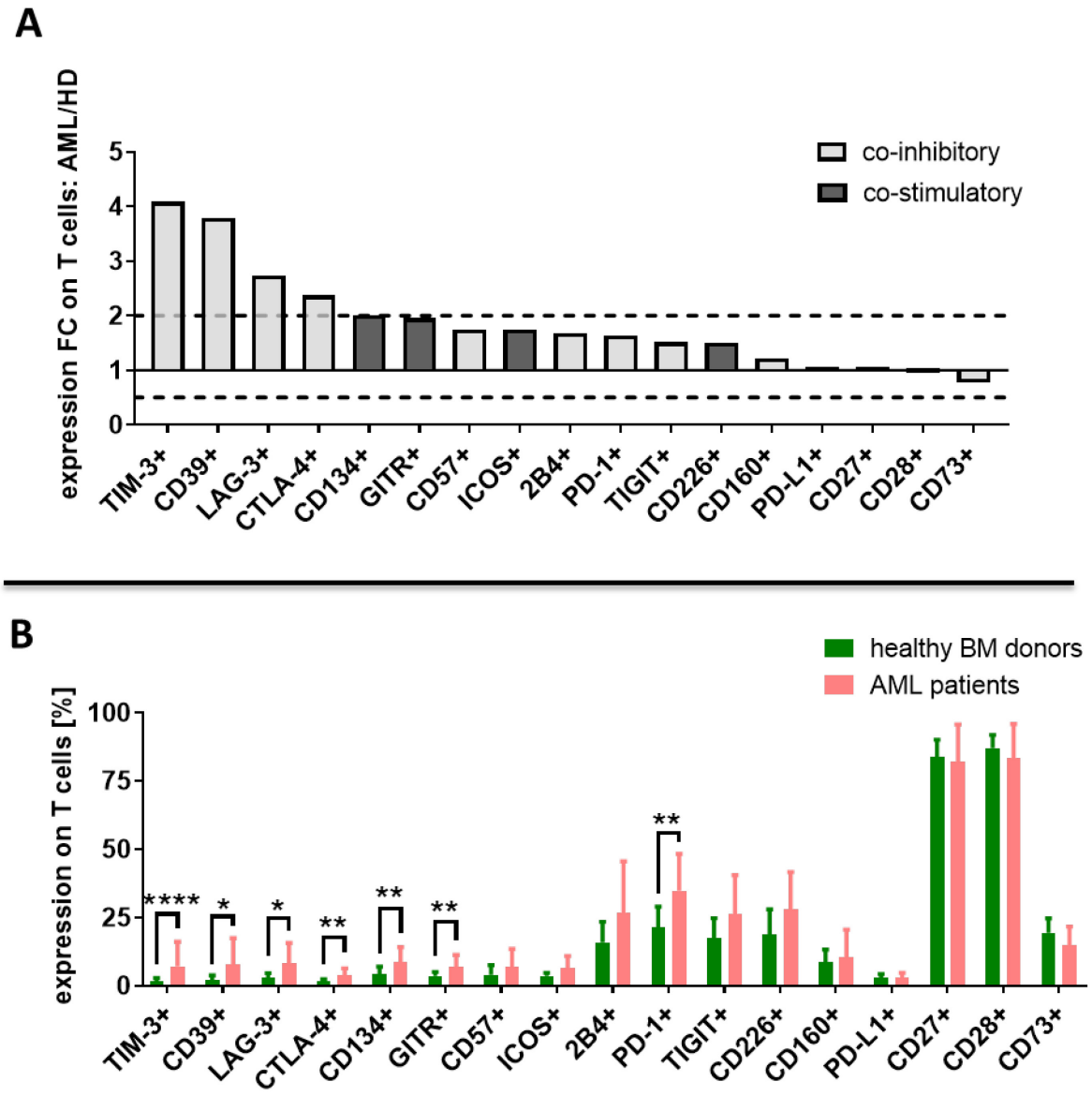

Figure 29: Overexpression of co-inhibitory and co-stimulatory molecules on CD3+ bmT cells in AML patients (N=29) in comparison to healthy BM donors (N=9). A) For each co-inhibitory or co-stimulatory molecule on CD3+ bmT cells the expression fold change AML/HD was defined as ratio of the mean expression on CD3+ bmT cells of all AML patients divided by the mean expression on CD3+ bmT cells of all healthy BM donors. **B)** Absolute expression levels of molecules on CD3+ bmT cells were arranged according to A. CTLA-4 and PD-L1 were stained intracellularly. Co-inhibitory markers TIM-3 ($p<0.0001$), CD39 ($p=0.0103$), LAG-3 ($p=0.0176$), CTLA-4 ($p=0.0024$) and PD-1 ($p=0.0016$) and co-stimulatory markers CD134 ($p=0.0058$) and GITR ($p=0.0092$) were significantly upregulated on CD3+ bmT cells in AML patients compared to healthy BM donors. HD/healthy BM donors: healthy bone marrow donors, FC: fold change.

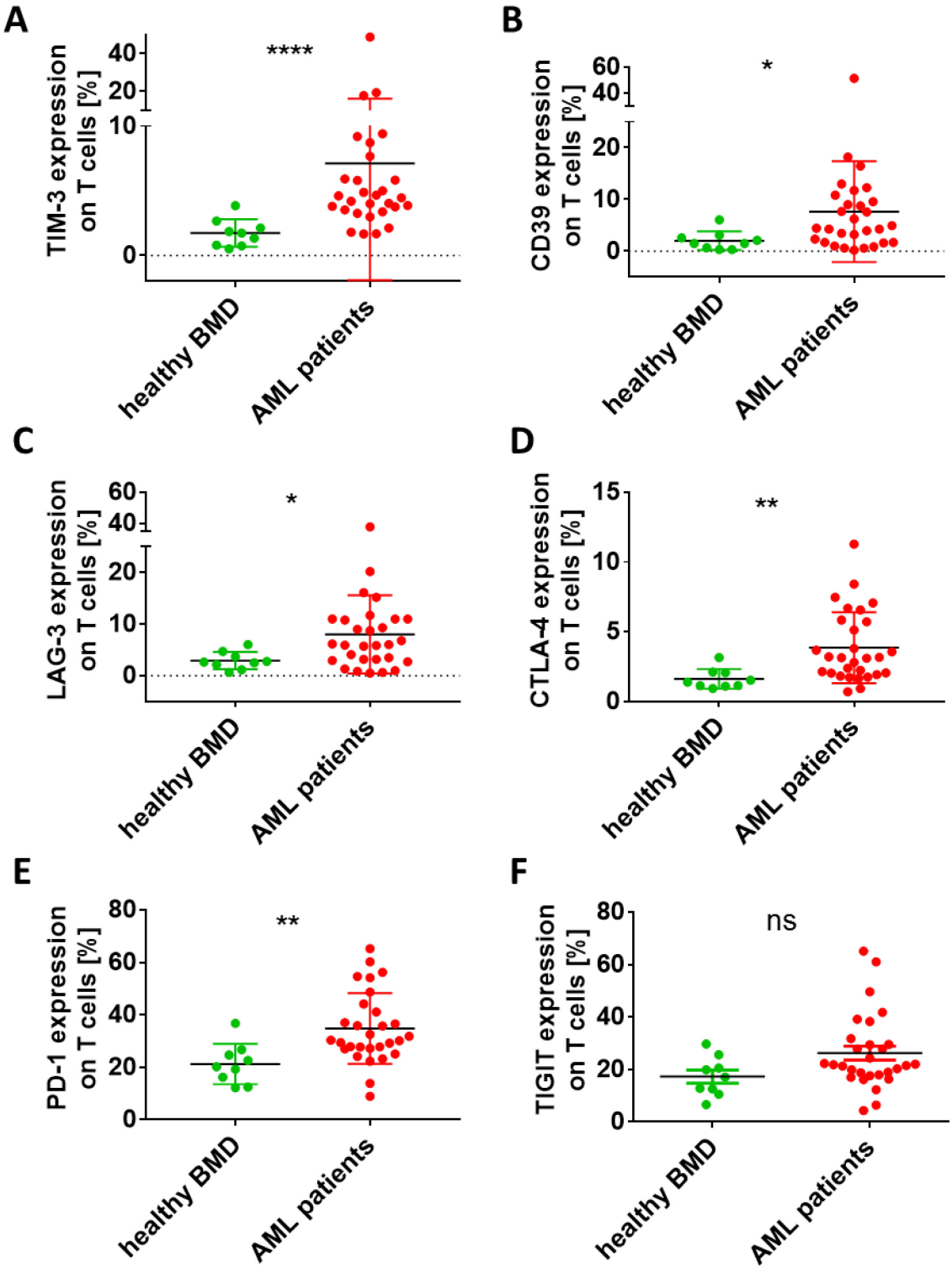

Figure 30: Detailed visualization of selected overexpressed co-inhibitory markers on CD3+ bmT cells in AML patients compared to healthy controls. A)-E) Co-inhibitory markers TIM-3 ($p<0.0001$, A), CD39 ($p=0.0103$, B), LAG-3 ($p=0.0176$, C), CTLA-4 ($p=0.0024$, D) and PD-1 ($p=0.0016$, E) showed significant upregulation on CD3+ bmT cells in AML patients compared to healthy BM donors. **F)** For TIGIT expression there was also a trend observable to be higher expressed on CD3+ bmT cells in AML patients in comparison to healthy BM donors, but without reaching statistical significance ($p=0.0798$). Healthy BMD: healthy BM donors. Results were based on same cohorts as in Figure 29.

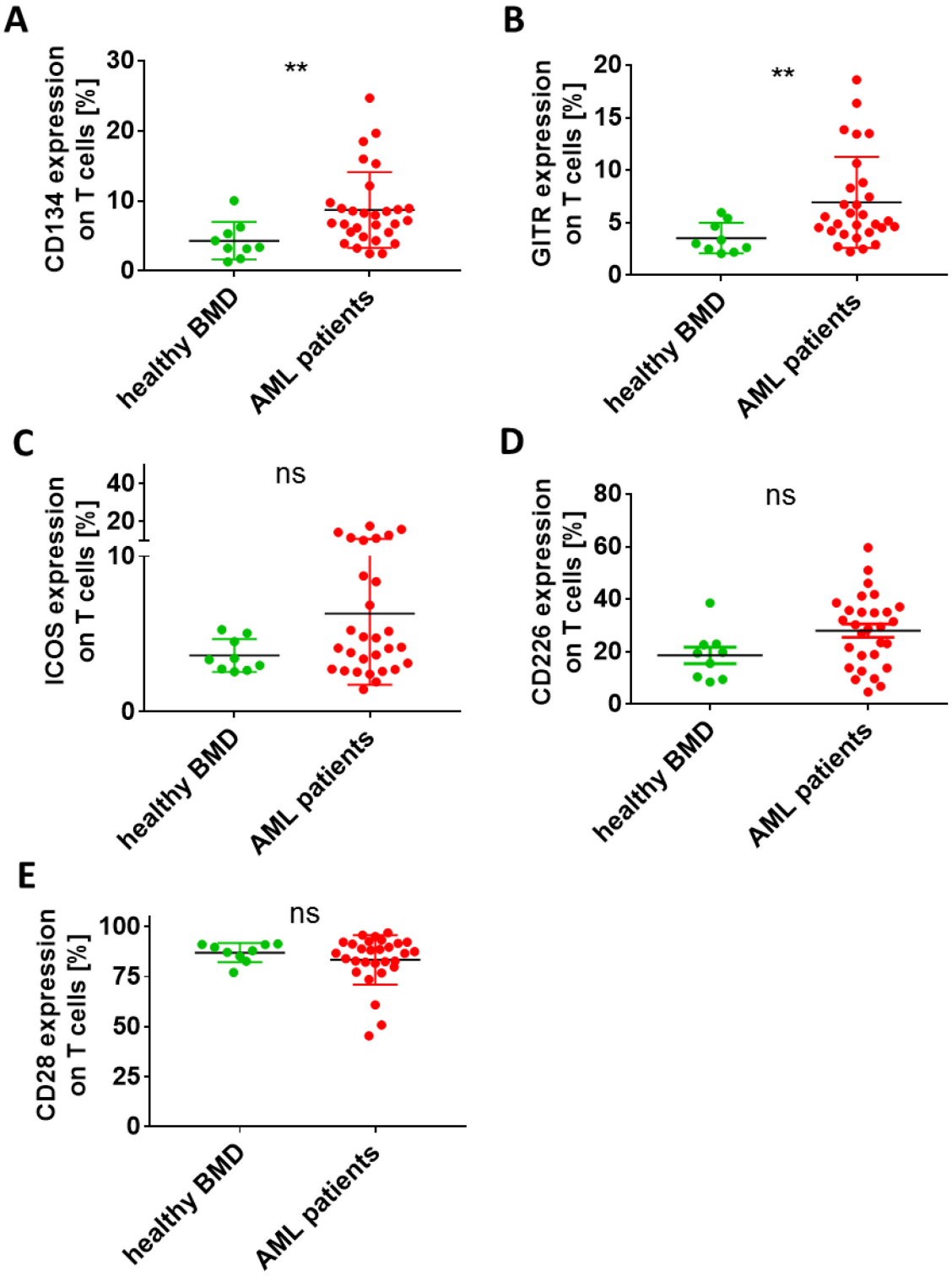

Figure 31: Detailed visualization of selected overexpressed co-stimulatory markers on CD3+ bmT cells in AML patients compared to healthy controls. A)-D) Co-stimulatory markers CD134 (p=0.0058, A), GITR (p=0.0092, B), ICOS (p=0.2479, C) and CD226 (p=0.0682, D) were overexpressed on CD3+ bmT cells in AML patients compared to healthy BM donors, with only CD134 and GITR reaching statistical significance. **E)** CD28 expression was reduced on CD3+ bmT cells in AML patients compared to healthy controls, without reaching statistical significance. Healthy BMD: healthy BM donors. Results were based on same cohorts as in Figure 29.

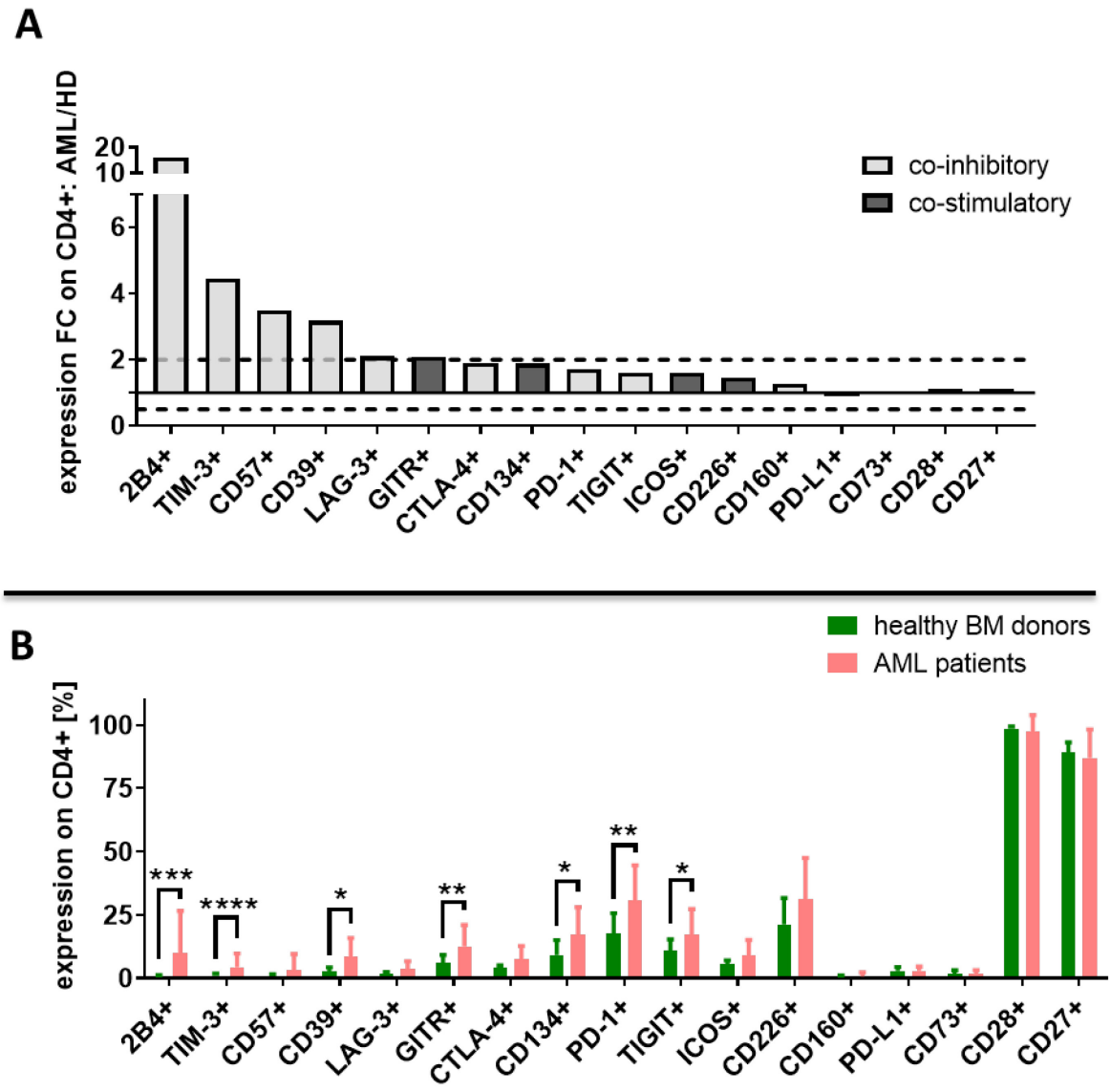

Figure 32: Overexpression of co-inhibitory and co-stimulatory molecules on CD4+ bmT cells in AML patients (N=29) in comparison to healthy BM donors (N=9). A) For each co-inhibitory or co-stimulatory molecule on CD4+ bmT cells the expression fold change AML/HD was defined as ratio of the mean expression on CD4+ bmT cells of all AML patients divided by the mean expression on CD4+ bmT cells of all healthy BM donors. **B)** Absolute expression levels of molecules on CD4+ bmT cells were arranged according to A. CTLA-4 and PD-L1 were stained intracellularly. Co-inhibitory markers 2B4 (p=0.0004), TIM-3 (p<0.0001), CD39 (p=0.0103), PD-1 (p=0.0031) and TIGIT (p=0.0315) and co-stimulatory markers GITR (p=0.0040) and CD134 (p=0.0159) were significantly upregulated on CD4+ bmT cells in AML patients compared to healthy BM donors. HD/healthy BM donors: healthy bone marrow donors, FC: fold change.

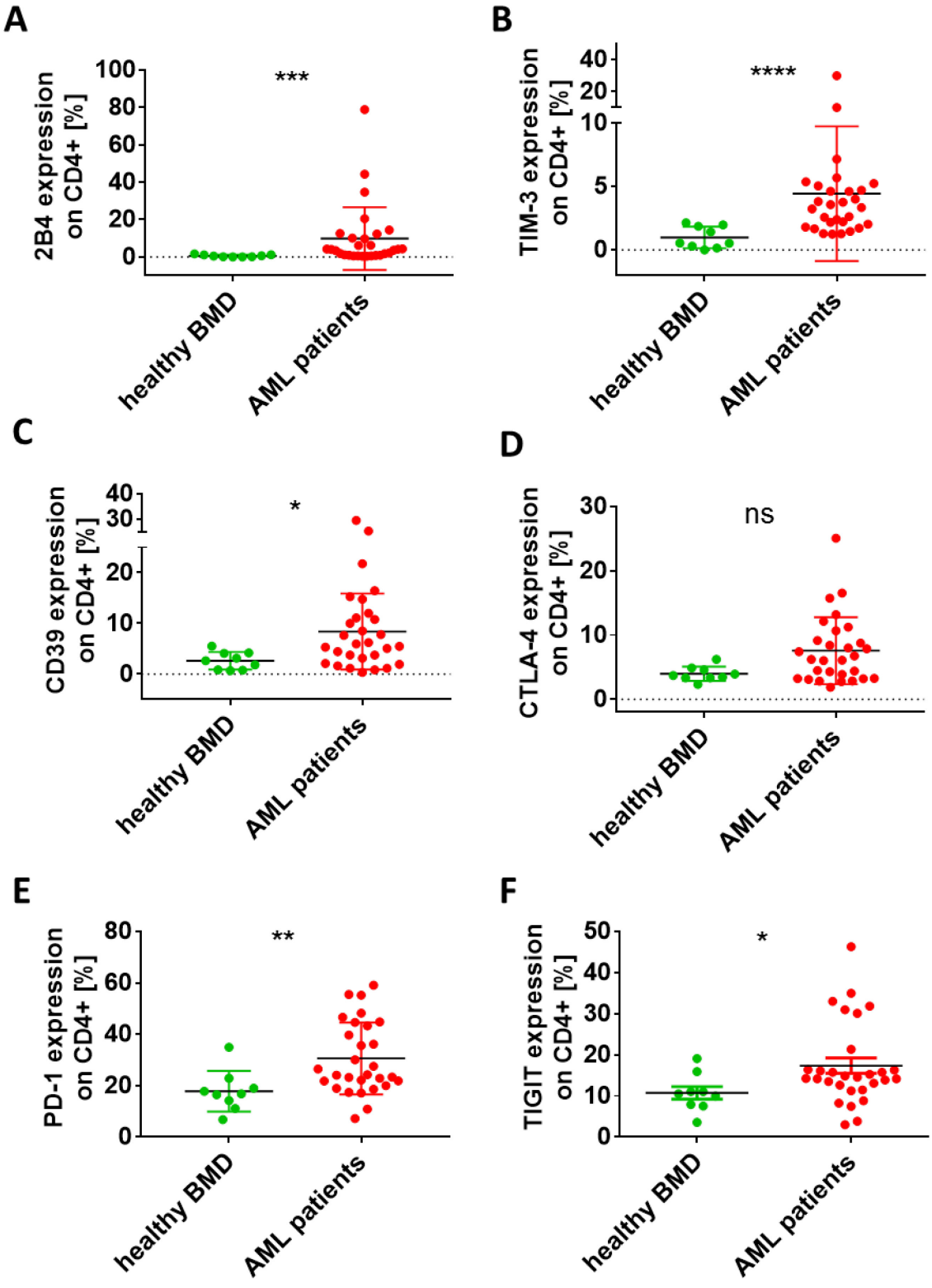

Figure 33: Detailed visualization of selected overexpressed co-inhibitory markers on CD4+ bmT cells in AML patients compared to healthy controls. A)-F) Co-inhibitory markers 2B4 (p=0.0004, A), TIM-3 (p<0.0001, B), CD39 (p=0.0103, C), CTLA-4 (p=0.0916, D), PD-1 (p=0.0031, E) and TIGIT (p=0.0315, F) were upregulated on CD4+ bmT cells in AML patients compared to healthy BM donors, with CTLA-4 expression only showing a trend to be higher on CD4+ bmT cells in AML patient samples without reaching statistical significance. Healthy BMD: healthy BM donors. Results were based on same cohorts as in Figure 32.

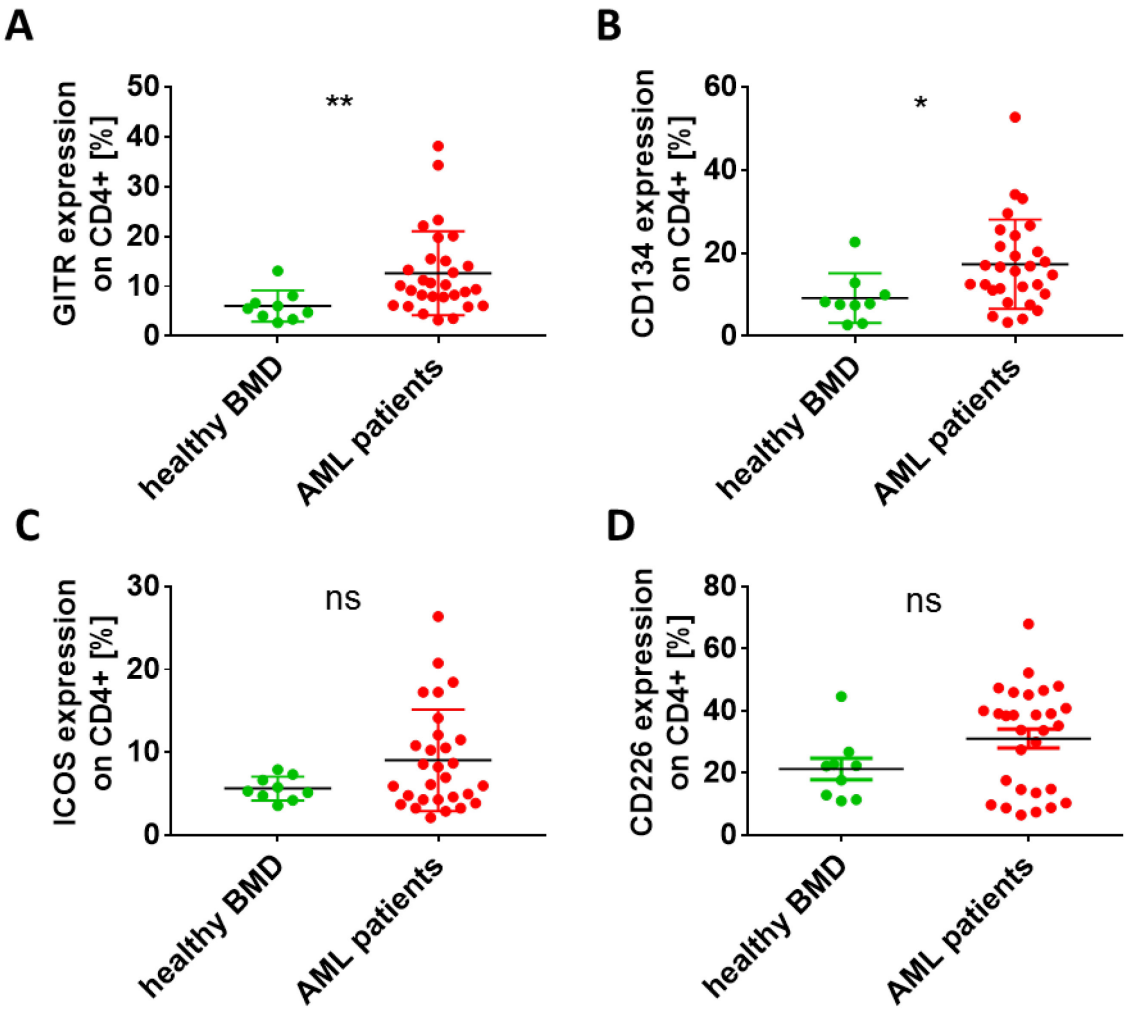

Figure 34: Detailed visualization of selected overexpressed co-stimulatory markers on CD4+ bmT cells in AML patients compared to healthy controls. A)-D) Co-stimulatory markers GITR (p=0.0040, A), CD134 (p=0.0159, B), ICOS (p=0.2479, C) and CD226 (p=0.1726, D) were overexpressed on CD4+ bmT cells in AML patients compared to healthy BM donors, with only CD134 and GITR reaching statistical significance. Healthy BMD: healthy BM donors. Results were based on same cohorts as in Figure 32.

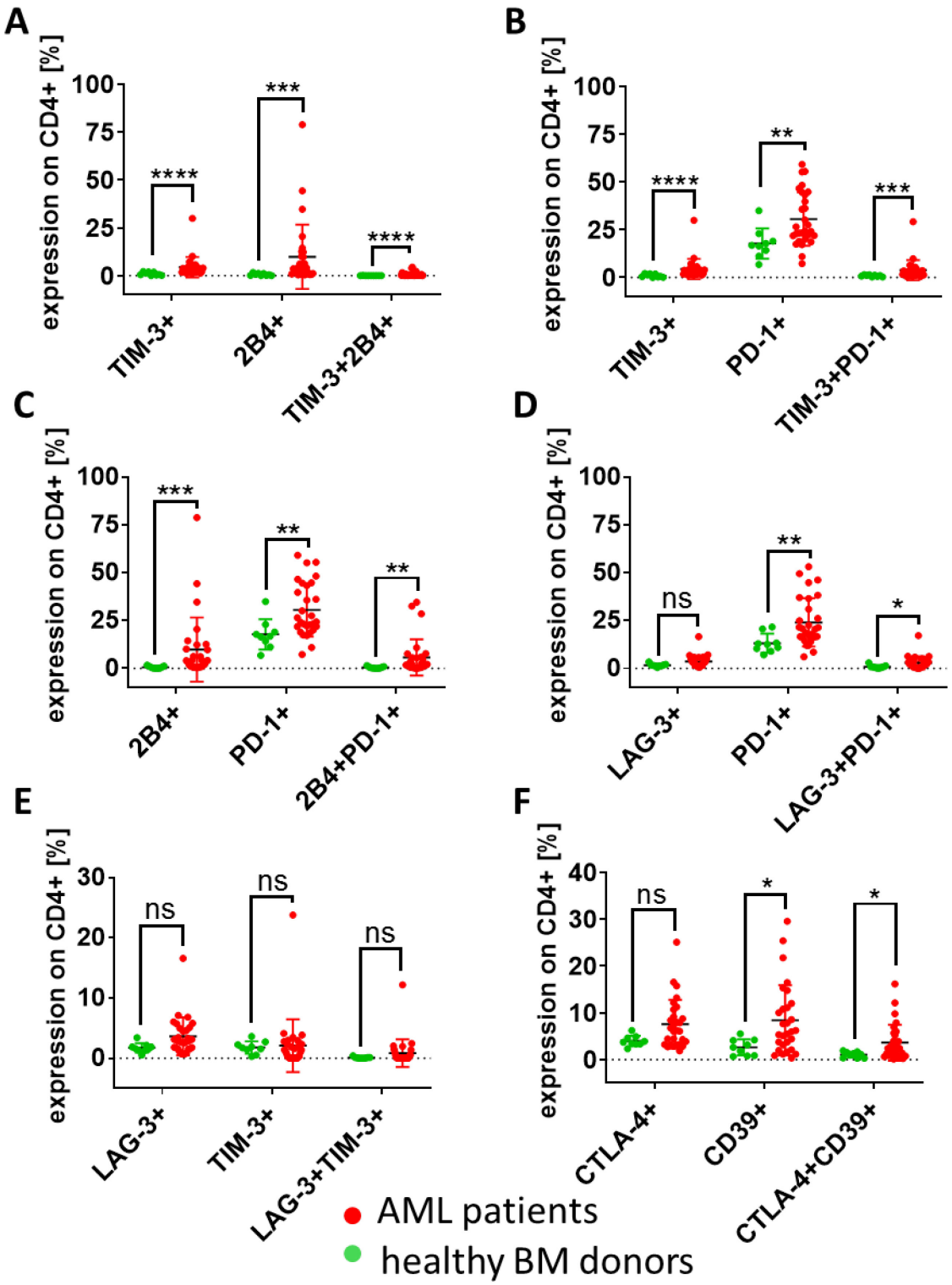

Figure 35: Co-expression of co-inhibitory molecules on CD4+ bmT cells in AML patients in comparison to healthy BM donors. Expression levels of single markers were compared to co-expression levels on CD4+ bmT cells. As TIM-3 expression was analyzed in two independent panels (5.3.1, Figure 6), the results measured with the brighter fluorochrome BB515 differ from the results measured with BV786. That is the reason why TIM-3 expression is not significantly different on bmT cells of AML patients compared to healthy controls in all the specimens above. Co-expression levels of TIM-3/2B4 ($p<0.0001$), TIM-3/PD-1 ($p=0.0004$), 2B4/PD-1 ($p=0.0026$), LAG-3/PD-1 ($p=0.0211$) and CTLA-4/CD39 ($p=0.0283$) were significantly higher on CD4+ bmT cells in AML patients in comparison to healthy controls. Healthy BM donors: healthy bone marrow donors. Results were based on same cohorts as in Figure 32.

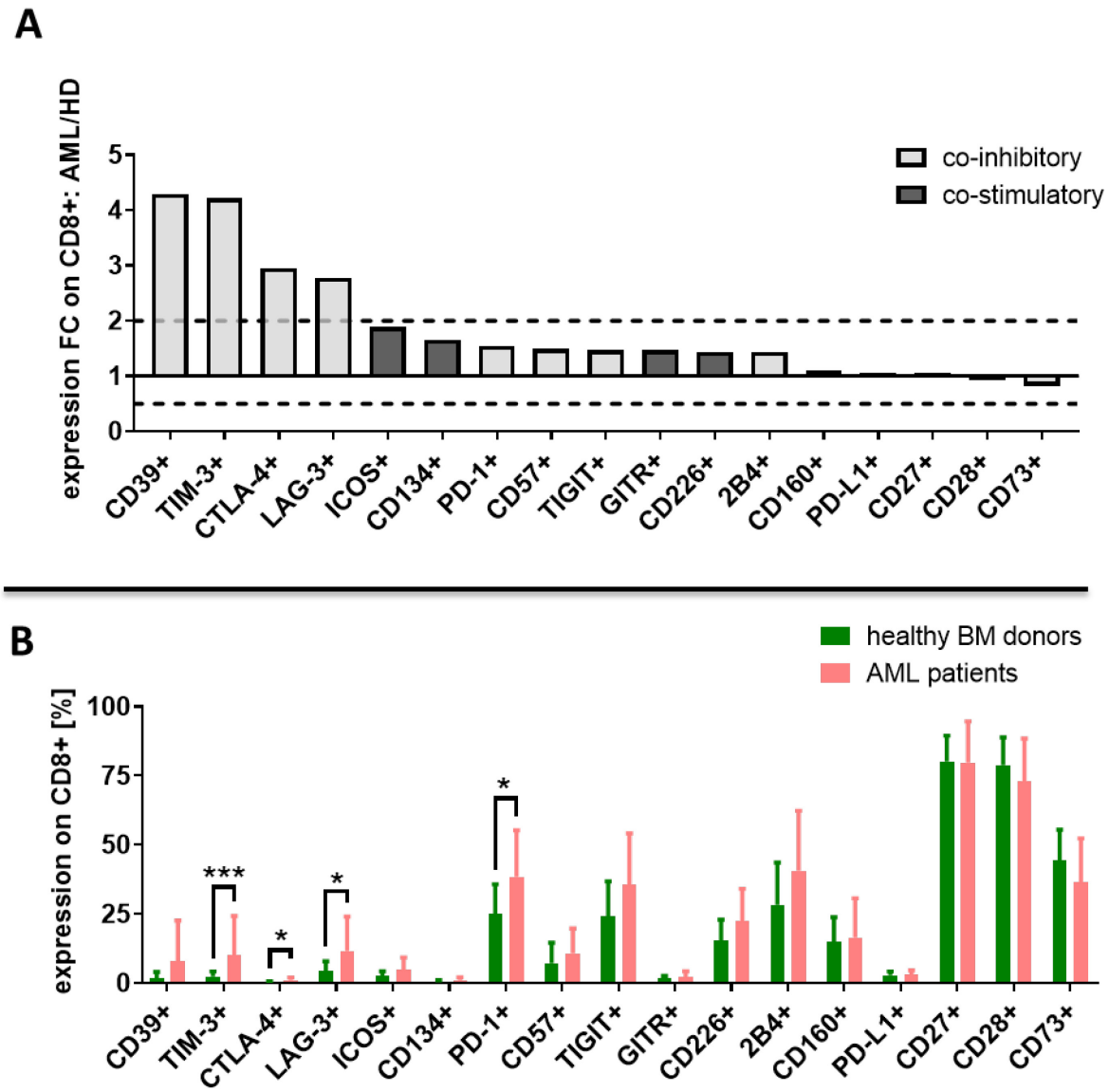

Figure 36: Overexpression of co-inhibitory molecules on CD8+ bmT cells in AML patients (N=29) in comparison to healthy BM donors (N=9). A) For each co-inhibitory or co-stimulatory molecule on CD8+ bmT cells the expression fold change AML/HD was defined as ratio of the mean expression on CD8+ bmT cells of all AML patients divided by the mean expression on CD8+ bmT cells of all healthy BM donors. **B)** Absolute expression levels of molecules on CD8+ bmT cells were arranged according to A. CTLA-4 and PD-L1 were stained intracellularly. Co-inhibitory markers TIM-3 (p=0.0008), CTLA-4 (p=0.0240), LAG-3 (p=0.0441) and PD-1 (p=0.0215) were significantly upregulated on CD8+ bmT cells in AML patients compared to healthy BM donors. HD/healthy BM donors: healthy bone marrow donors, FC: fold change.

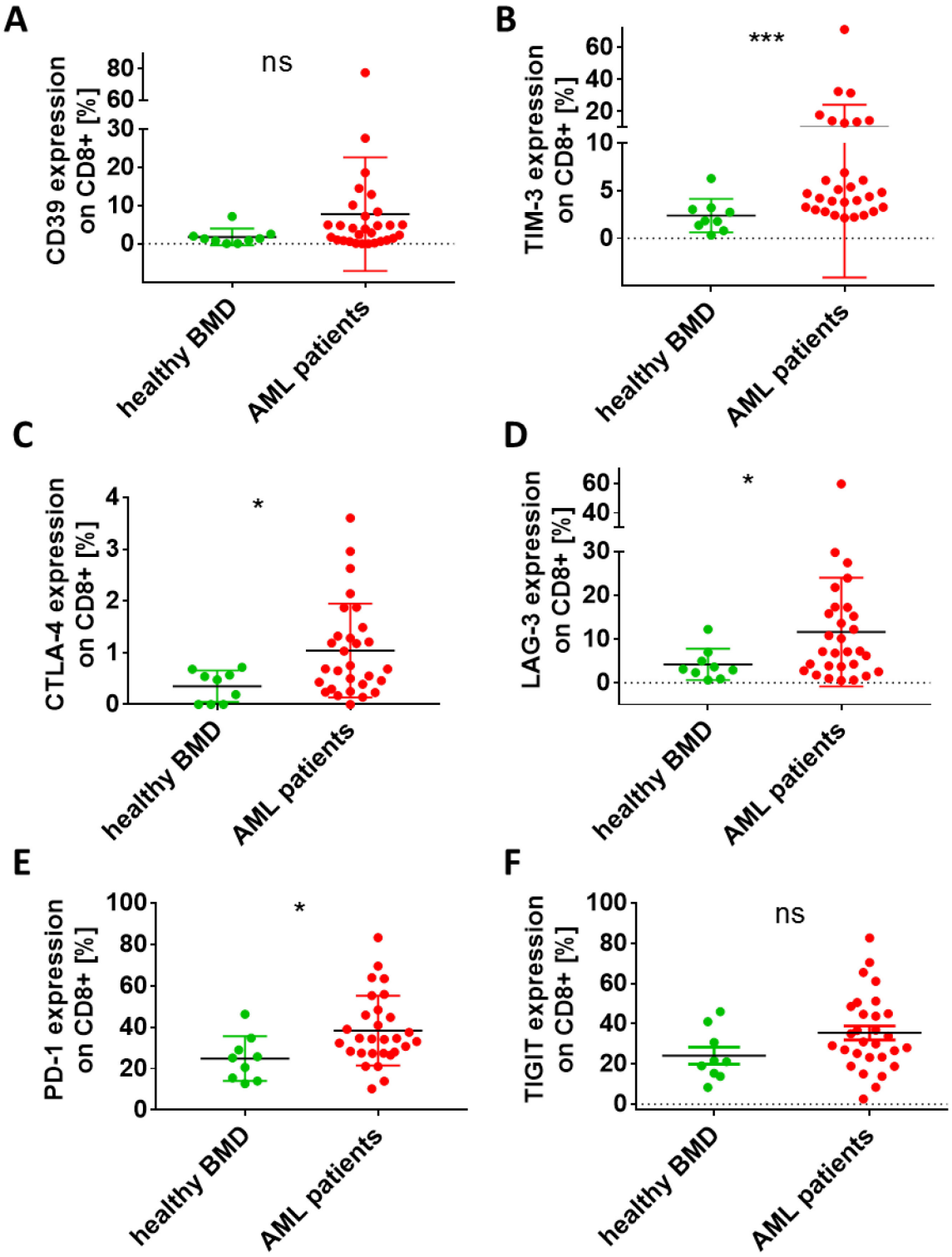

Figure 37: Detailed visualization of selected overexpressed co-inhibitory markers on CD8+ bmT cells in AML patients compared to healthy controls. A)-F) Co-inhibitory markers CD39 (p=0.0861, A), TIM-3 (p=0.0008, B), CTLA-4 (p=0.0240, C), LAG-3 (p=0.0441, D), PD-1 (p=0.0215, E) and TIGIT (p=0.0929, F) were upregulated on CD8+ bmT cells in AML patients compared to healthy BM donors, with CD39 and TIGIT expression only showing a trend to be higher in AML patients without reaching statistical significance. Healthy BMD: healthy BM donors. Results were based on same cohorts as in Figure 36.

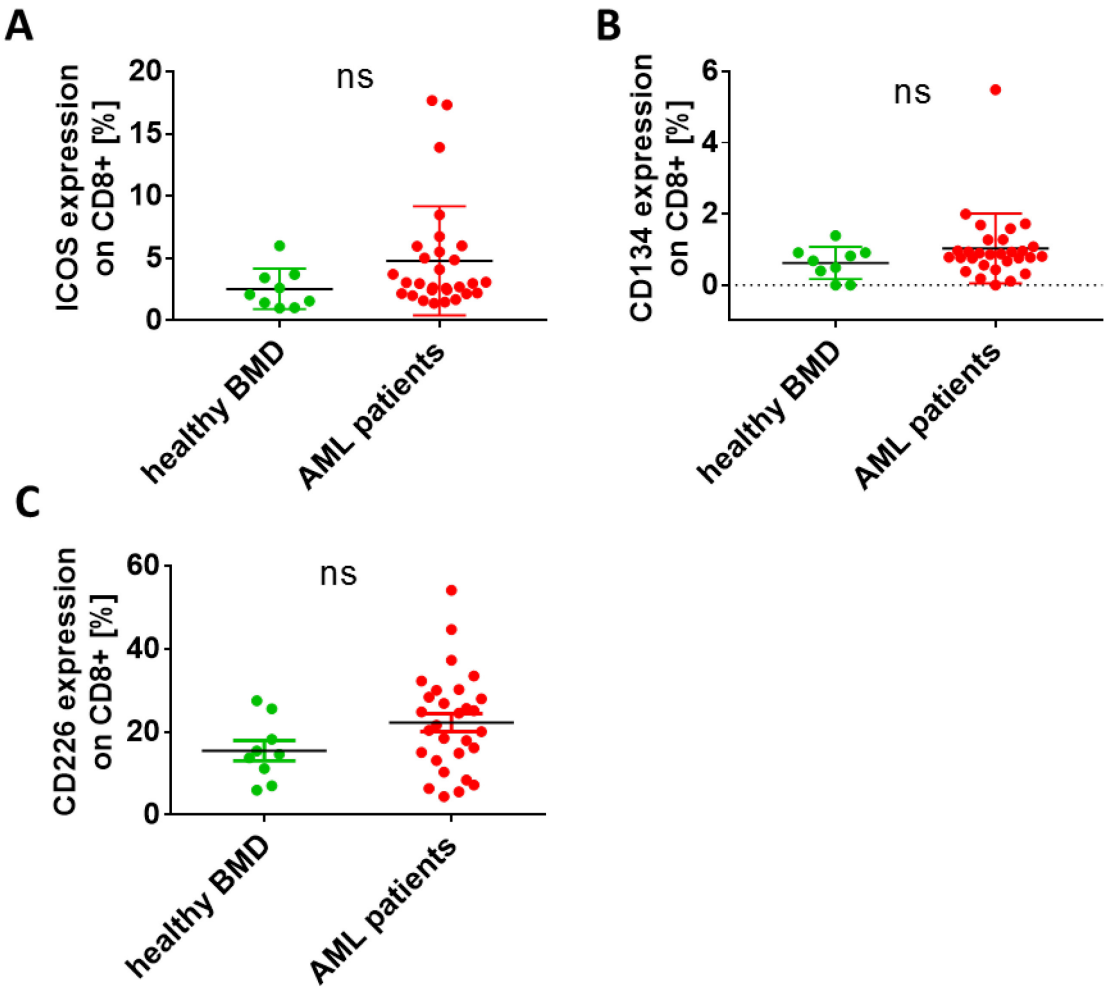

Figure 38: Detailed visualization of selected overexpressed co-stimulatory markers on CD8+ bmT cells in AML patients compared to healthy controls. A)-C) Co-stimulatory markers ICOS (p=0.0630, A), CD134 (p=0.1933, B) and CD226 (p=0.1075, C) showed a trend to be overexpressed on CD8+ bmT cells in AML patients compared to healthy BM donors, but without reaching any statistical significance. Healthy BMD: healthy BM donors. Results were based on same cohorts as in Figure 36.

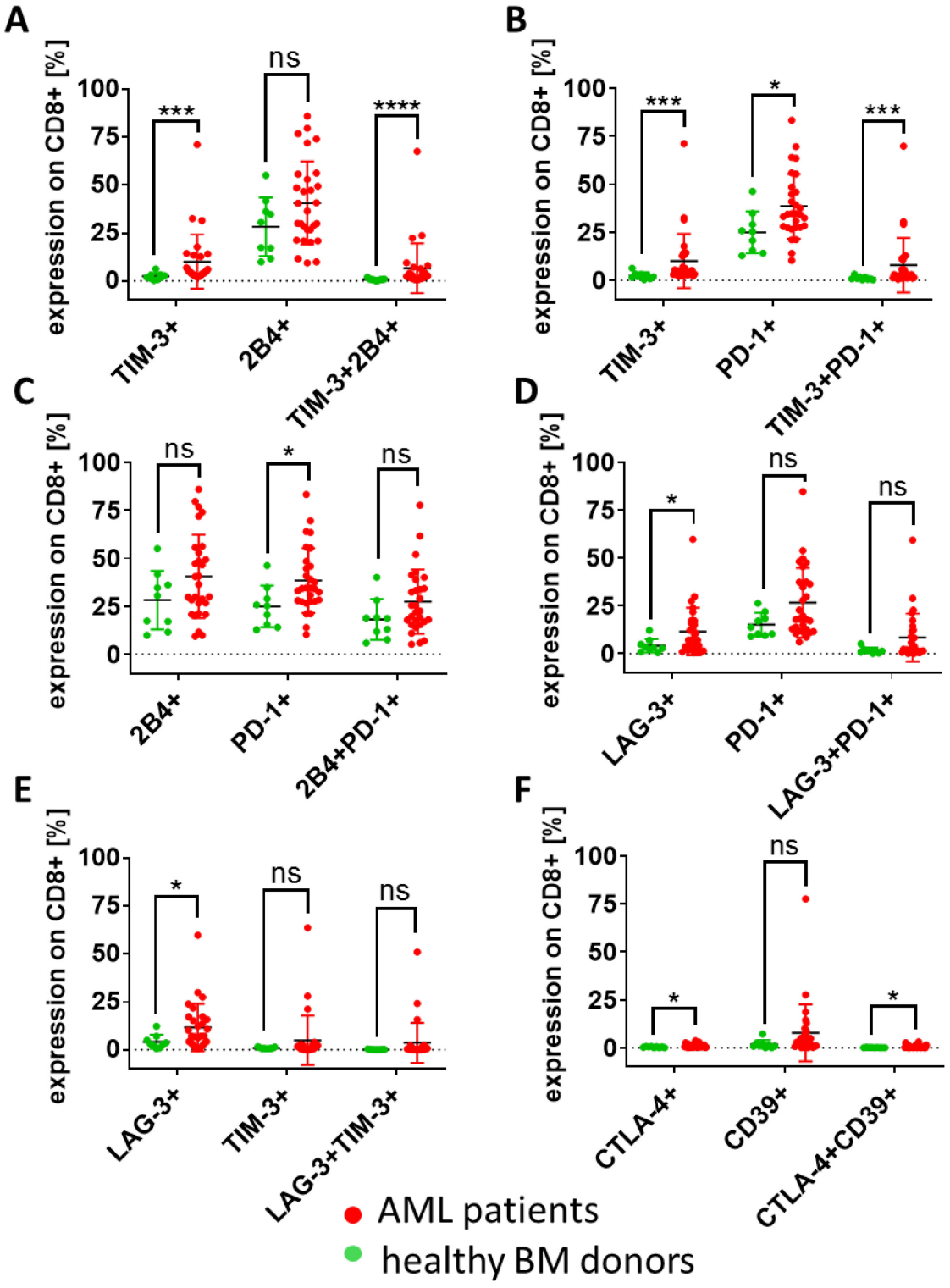

Figure 39: Co-expression of co-inhibitory molecules on CD8+ bmT cells in AML patients in comparison to healthy BM donors. Expression levels of single markers were compared to co-expression rates on CD8+ bmT cells. As TIM-3 and PD-1 expression levels were analyzed in two independent panels (5.3.1, Figure 6), the results measured with the brighter fluorochromes (BB515: TIM-3, BV421: PD-1) differ from the results measured with BV786 (TIM-3) or BV650 (PD-1). That is the reason why TIM-3 and PD-1 expression levels are not significantly different on bmT cells in AML patients compared to healthy controls in all the specimens above. Co-expression levels of TIM-3/2B4 ($p<0.0001$), TIM-3/PD-1 ($p=0.0010$) and CTLA-4/CD39 ($p=0.0180$) were significantly higher on CD8+ bmT cells in AML patients in comparison to healthy controls. Healthy BM donors: healthy bone marrow donors. Results were based on same cohorts as in Figure 36.

Multiple testing corrections were performed as described in 5.12.1. Corrected p values (q values) were listed and compared to uncorrected p values in Figure 40. Apart from that all mentioned p values are uncorrected in this chapter.

A

Antigen	p value	q value
TIM-3	0.0001	0.0017
CD160	0.9782	0.9782
2B4	0.1238	0.1913
PD-1	0.0016	0.0136
TIGIT	0.0798	0.1357
CD39	0.0103	0.0292
LAG-3	0.0176	0.0427
CTLA-4	0.0024	0.0136
PD-L1	0.7614	0.8685
CD27	0.8927	0.9485
CD134	0.0058	0.0247
CD28	0.7663	0.8685
ICOS	0.2479	0.3242
GITR	0.0092	0.0292
CD226	0.0682	0.1288
CD57	0.1517	0.2149
CD73	0.0580	0.1233

B

Antigen	p value	q value
TIM-3	0.0001	0.0017
CD160	0.4215	0.5512
2B4	0.0004	0.0034
PD-1	0.0031	0.0170
TIGIT	0.0315	0.0765
CD39	0.0103	0.0350
LAG-3	0.0534	0.1135
CTLA-4	0.0916	0.1730
PD-L1	0.9680	0.9680
CD27	0.8183	0.9274
CD134	0.0159	0.0451
CD28	0.7552	0.9170
ICOS	0.2479	0.3512
GITR	0.0040	0.0170
CD226	0.1726	0.2934
CD57	0.2307	0.3512
CD73	0.9659	0.9680

C

Antigen	p value	q value
TIM-3	0.0008	0.0136
CD160	0.9194	0.9194
2B4	0.1839	0.2528
PD-1	0.0215	0.1360
TIGIT	0.0929	0.2031
CD39	0.0861	0.2031
LAG-3	0.0441	0.1874
CTLA-4	0.0240	0.1360
PD-L1	0.8611	0.9149
CD27	0.7873	0.8923
CD134	0.1933	0.2528
CD28	0.2801	0.3401
ICOS	0.0630	0.2031
GITR	0.1056	0.2031
CD226	0.1075	0.2031
CD57	0.1839	0.2528
CD73	0.1818	0.2528

Figure 40: Corrected (q values) and uncorrected p values for analysis of CD3+ (A), CD4+ (B) and CD8+ bmT cells (C) in AML patients compared to healthy BM donors. Multiple testing correction was performed by using the Original FDR method of Benjamini and Hochberg (5.12.1). P and q values <0.05 are marked in green.

6.2.5 Overexpression of CD134 and PD-L1 on bmT cells in relapsed AML samples compared to initial AML samples

In contrast to the pronounced difference between AML patients and healthy BM donors, fewer differences were observed between primary AML samples and relapsed AML samples. For the expression of co-inhibitory and co-stimulatory molecules on bmT cells this is shown in Figure 41 (CD3+ bmT cells), Figure 42 (CD4+ bmT cells) and Figure 44 (CD8+ bmT cells).

The co-stimulatory marker CD134 was significantly overexpressed on CD3+ bmT cells (11.7 % vs. 6.9 %, p=0.0036) and CD4+ bmT cells (24.5 % vs. 14.1 %, p=0.0163) in relapsed AML samples compared to initial AML samples.

On CD4+ bmT cells also the co-inhibitory marker PD-L1 showed higher expression levels in relapsed AML samples in comparison to initial AML samples (4.0 % vs. 2.6 %, p=0.0092). Figure 43 illustrates those observations in greater detail.

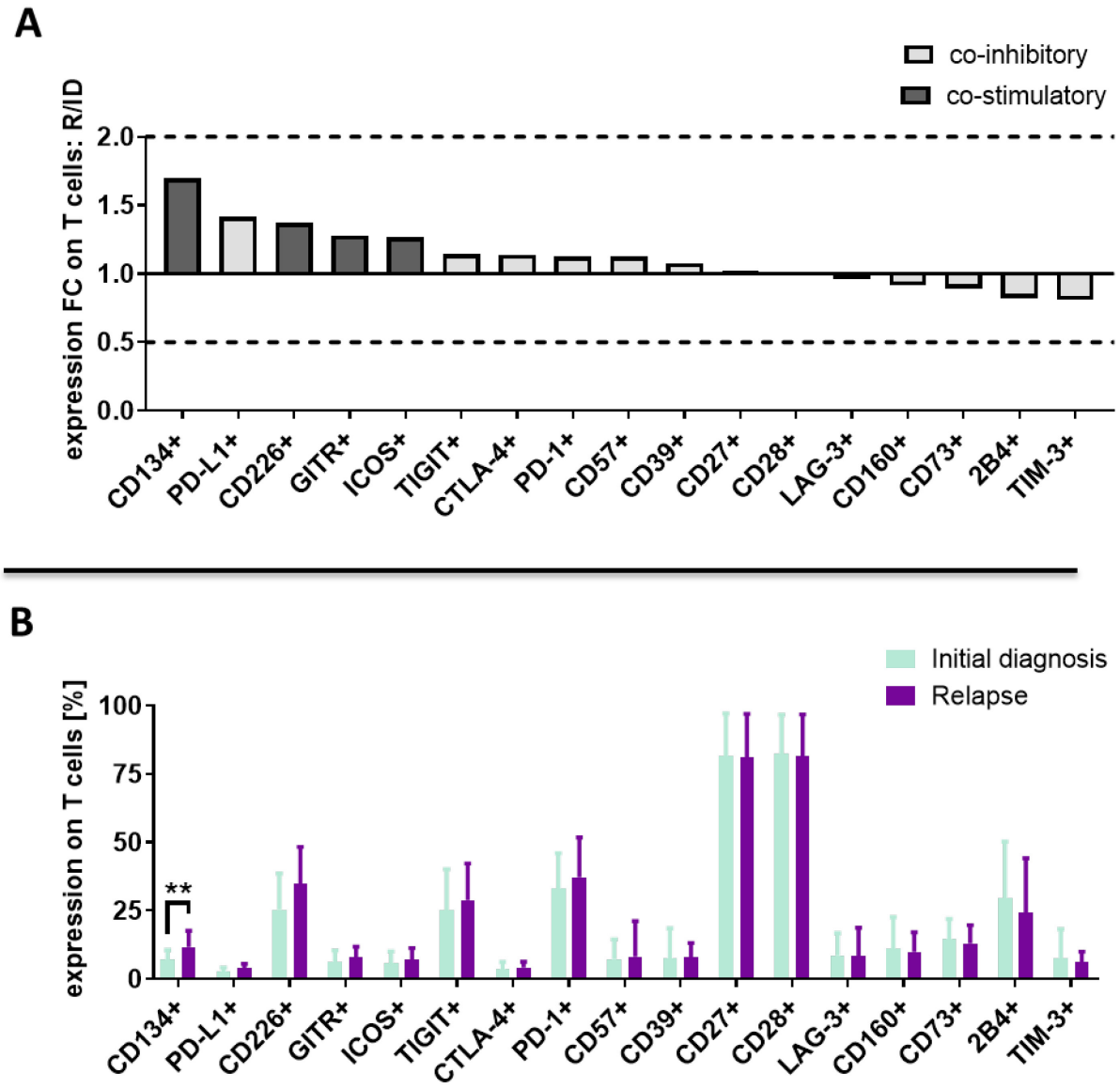

Figure 41: Expression of co-stimulatory and co-inhibitory molecules on CD3+ bmT cells in AML patients at initial diagnosis (N=21) and relapse (N≥11). A) For each co-inhibitory or co-stimulatory molecule on CD3+ bmT cells the expression fold change R/ID was defined as ratio of the mean expression on CD3+ bmT cells of all relapsed AML samples divided by the mean expression on CD3+ bmT cells of all initial AML samples. **B)** Absolute expression levels of molecules on CD3+ bmT cells were arranged according to A. CTLA-4 and PD-L1 were stained intracellularly. Co-stimulatory marker CD134 was significantly upregulated (p=0.0036) on CD3+ bmT cells in relapsed AML samples compared to initial AML samples. R: Relapse, ID: Initial diagnosis, FC: fold change.

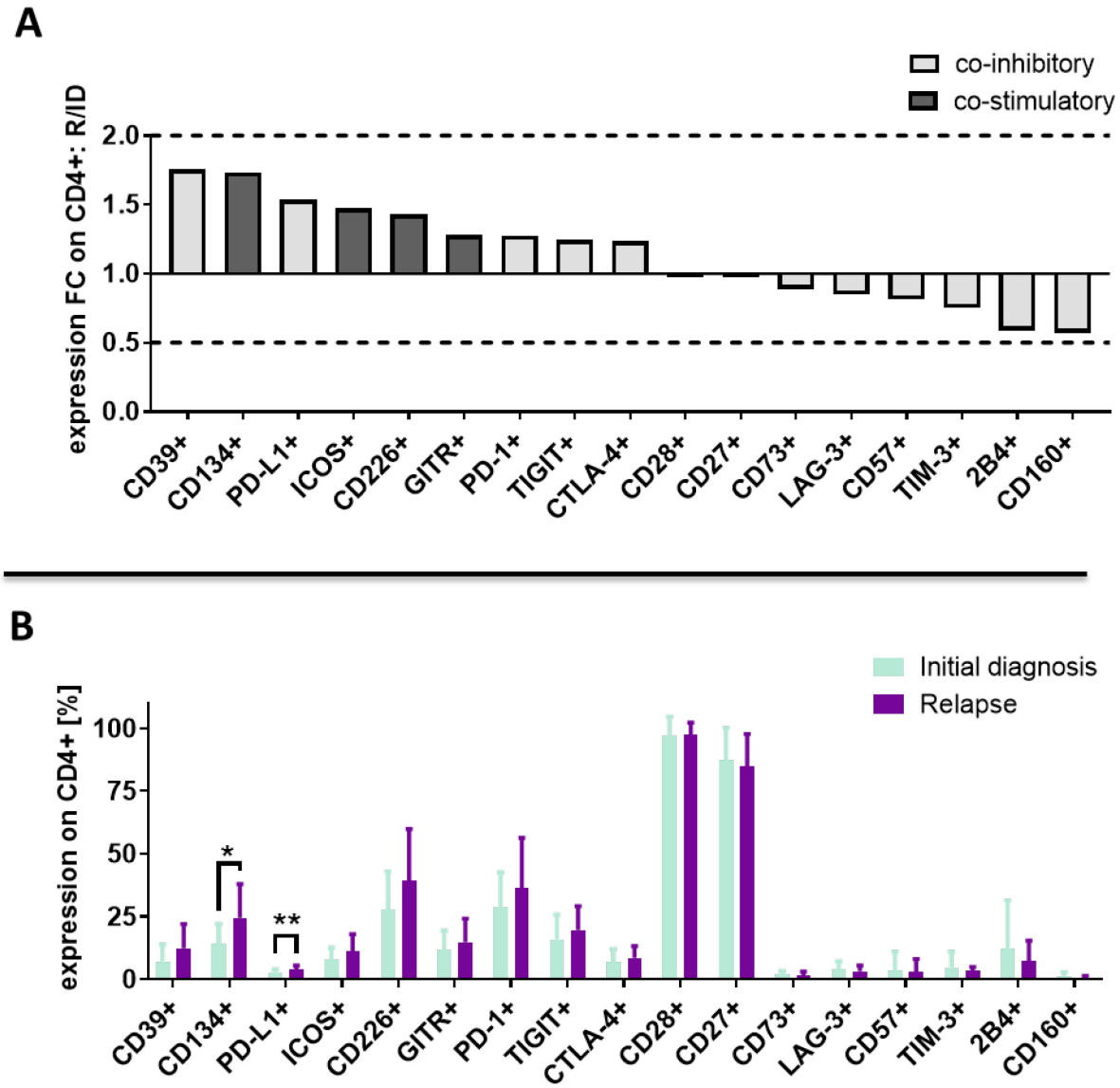

Figure 42: Expression of co-stimulatory and co-inhibitory molecules on CD4+ bmT cells in AML patients at initial diagnosis (N=21) and relapse (N≥11). A) For each co-inhibitory or co-stimulatory molecule on CD4+ bmT cells the expression fold change R/ID was defined as ratio of the mean expression on CD4+ bmT cells of all relapsed AML samples divided by the mean expression on CD4+ bmT cells of all initial AML samples. **B)** Absolute expression levels of molecules on CD4+ bmT cells were arranged according to A. CTLA-4 and PD-L1 were stained intracellularly. Co-stimulatory marker CD134 (p=0.0163) and co-inhibitory marker PD-L1 (p=0.0092) were significantly upregulated on CD4+ bmT cells in relapsed AML samples compared to initial AML samples. R: Relapse, ID: Initial diagnosis, FC: fold change.

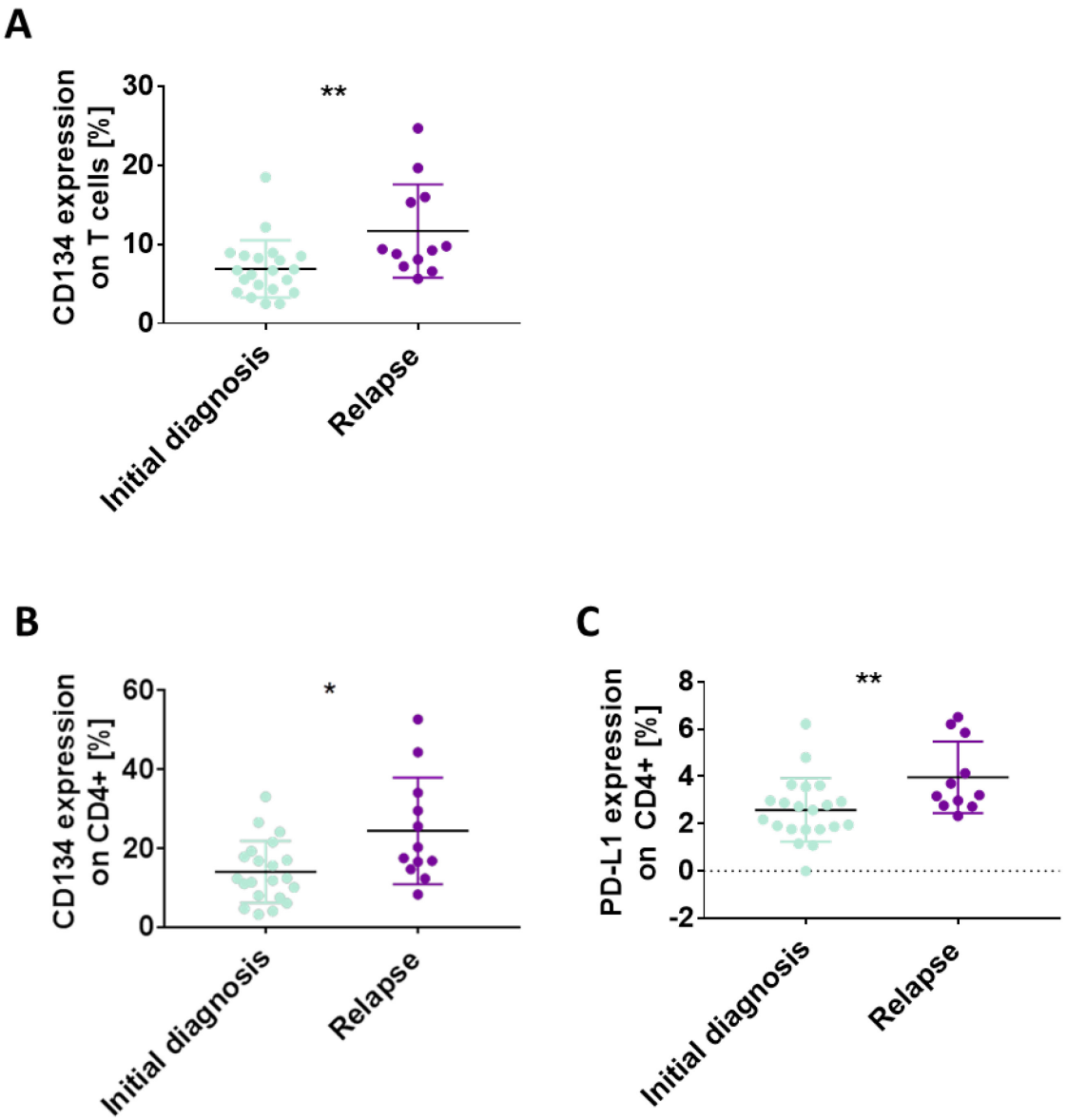

Figure 43: Overexpression of CD134 and PD-L1 on bmT cells in relapsed AML samples compared to initial AML samples. A) CD134 expression was significantly upregulated on CD3+ bmT cells in relapsed AML samples compared to initial AML samples (p=0.0036). **B), C)** CD134 (p=0.0163) and PD-L1 (p=0.0092) were significantly overexpressed on CD4+ bmT cells in relapsed AML samples compared to initial AML samples. Results were based on same cohorts as in Figure 41 and Figure 42.

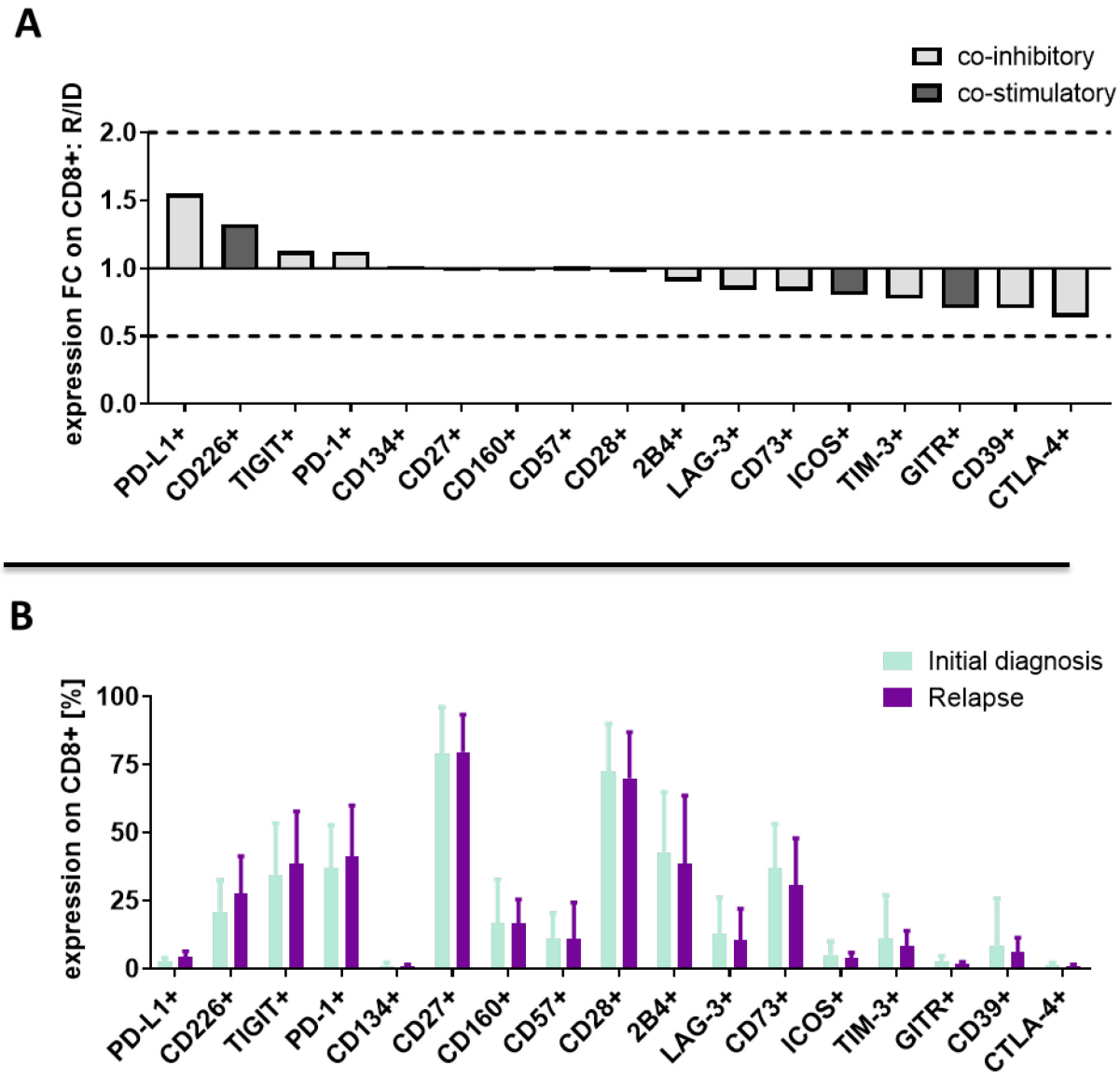

Figure 44: Expression of co-stimulatory and co-inhibitory molecules on CD8+ bmT cells in AML patients at initial diagnosis (N=21) and relapse (N≥11). A) For each co-inhibitory or co-stimulatory molecule on CD8+ bmT cells the expression fold change R/ID was defined as ratio of the mean expression on CD8+ bmT cells of all relapsed AML samples divided by the mean expression on CD8+ bmT cells of all initial AML samples. **B)** Absolute expression levels of molecules on CD8+ bmT cells were arranged according to A. CTLA-4 and PD-L1 were stained intracellularly. R: Relapse, ID: Initial diagnosis, FC: fold change.

Multiple testing corrections were performed as described in 5.12.1. Corrected p values (q values) were listed and compared to uncorrected p values in Figure 45. Apart from that all mentioned p values are uncorrected in this chapter.

A

Antigen	p value	q value
TIM-3	0.3646	0.6586
CD160	0.8683	0.8974
2B4	0.5424	0.6586
PD-1	0.4267	0.6586
TIGIT	0.3847	0.6586
CD39	0.2381	0.6586
LAG-3	0.3265	0.6586
CTLA-4	0.4335	0.6586
PD-L1	0.0508	0.3196
CD27	0.8974	0.8974
CD134	0.0036	0.0612
CD28	0.7261	0.8229
ICOS	0.1126	0.3828
GITR	0.0633	0.3196
CD226	0.0752	0.3196
CD57	0.5424	0.6586
CD73	0.5060	0.6586

B

Antigen	p value	q value
TIM-3	0.6447	0.8385
CD160	0.4105	0.6116
2B4	0.9266	0.9266
PD-1	0.2276	0.4511
TIGIT	0.2741	0.4660
CD39	0.1045	0.4295
LAG-3	0.7322	0.8385
CTLA-4	0.2381	0.4511
PD-L1	0.0092	0.1386
CD27	0.2388	0.4511
CD134	0.0163	0.1386
CD28	0.7892	0.8385
ICOS	0.0752	0.4261
GITR	0.1516	0.4295
CD226	0.1310	0.4295
CD57	0.4317	0.6116
CD73	0.7467	0.8385

C

Antigen	p value	q value
TIM-3	0.2242	0.7206
CD160	0.5672	0.7206
2B4	0.6714	0.7206
PD-1	0.5424	0.7206
TIGIT	0.4712	0.7206
CD39	0.3466	0.7206
LAG-3	0.5575	0.7206
CTLA-4	0.2932	0.7206
PD-L1	0.1065	0.7206
CD27	0.8974	0.8974
CD134	0.1126	0.7206
CD28	0.6714	0.7206
ICOS	0.3847	0.7206
GITR	0.6782	0.7206
CD226	0.2134	0.7206
CD57	0.6184	0.7206
CD73	0.4812	0.7206

Figure 45: Corrected (q values) and uncorrected p values for analysis of CD3+ (A), CD4+ (B) and CD8+ bmT cells (C) in AML patients at initial diagnosis compared to AML relapse samples. Multiple testing correction was performed by using the Original FDR method of Benjamini and Hochberg (5.12.1). P and q values <0.05 are marked in green.

6.2.6 Checkpoint expression on bmT cells during the course of AML in one patient with several relapses

Possible differences in antigen expression on bmT cells during the course of AML were investigated further on the basis of four sequential relapse samples of one AML patient (A501: 2nd relapse, A601: 3rd relapse, A701: 4th relapse and A801: 5th relapse, 5.1).

As in Figure 46 exemplarily shown, expression values of co-inhibitory markers TIM-3, PD-1 and CD39 and co-stimulatory marker CD226 on CD3+ bmT cells, as well as the frequency of T_{regs} among CD4+ bmT cells were in principle more increasing, whereas the expression level of co-stimulatory marker CD27 on bmT cells was more decreasing during the course of AML.

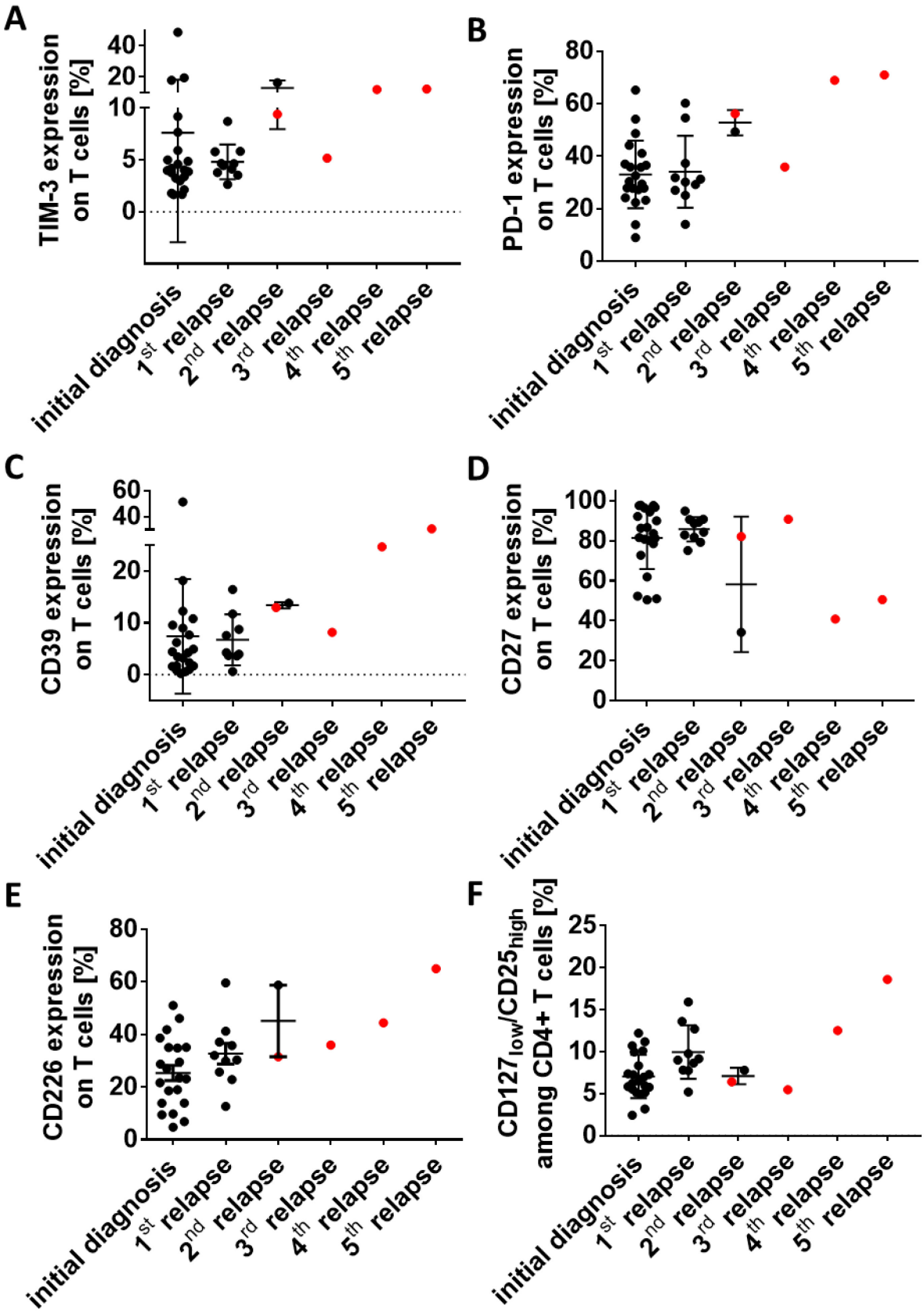

Figure 46: Differences in bmT cell phenotype during the course of multiple AML relapse samples from one patient. Samples marked in red are sequential relapse samples from one AML patient. These data points represent exemplarily a possible development in antigen expression during the course of AML.

6.2.7 Overexpression of ICOS on CD4+ bmT cells and downregulation of CD134 on CD8+ bmT cells in initial AML samples without future relapse compared to initial AML samples with future relapse

To investigate relevant prognostic factors in AML, initial AML samples with and without future relapse were compared concerning their expression levels of co-inhibitory and co-stimulatory molecules, as shown in Figure 47 (CD3+ bmT cells), 48 (CD4+ bmT cells) and 49 (CD8+ bmT cells).

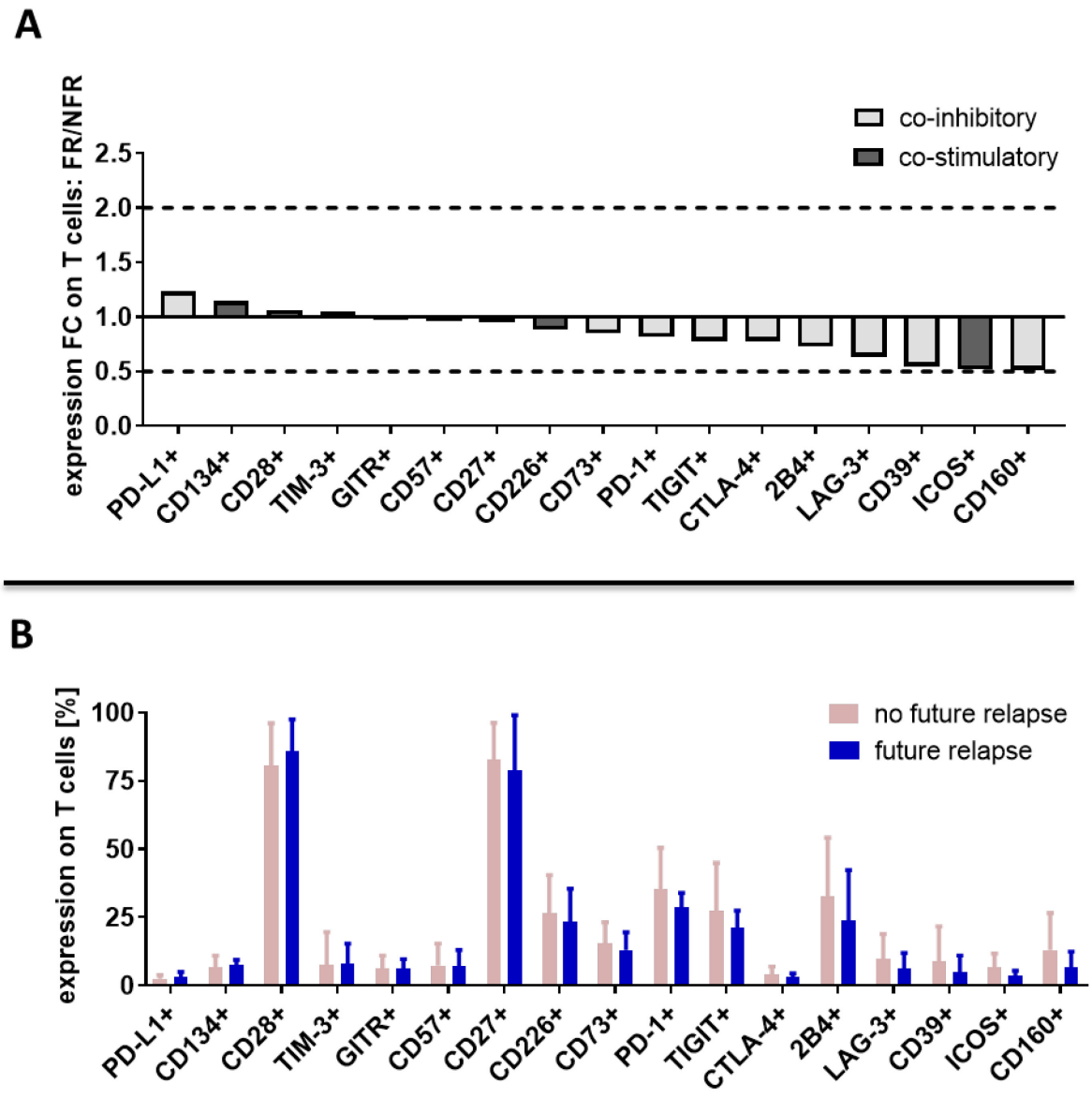

Figure 47: Expression of co-stimulatory and co-inhibitory molecules on CD3+ bmT cells in AML patients at the time of initial diagnosis with (N=7) and without (N=14) future relapse. A) For each co-inhibitory or co-stimulatory molecule on CD3+ bmT cells the expression fold change FR/NFR was defined as ratio of the mean expression on CD3+ bmT cells of all initial AML samples with future relapse divided by the mean expression on CD3+ bmT cells of all initial AML samples without future relapse. **B)** Absolute expression levels of molecules on CD3+ bmT cells were arranged according to A. CTLA-4 and PD-L1 were stained intracellularly. NFR: no future relapse, FR: future relapse, FC: fold change.

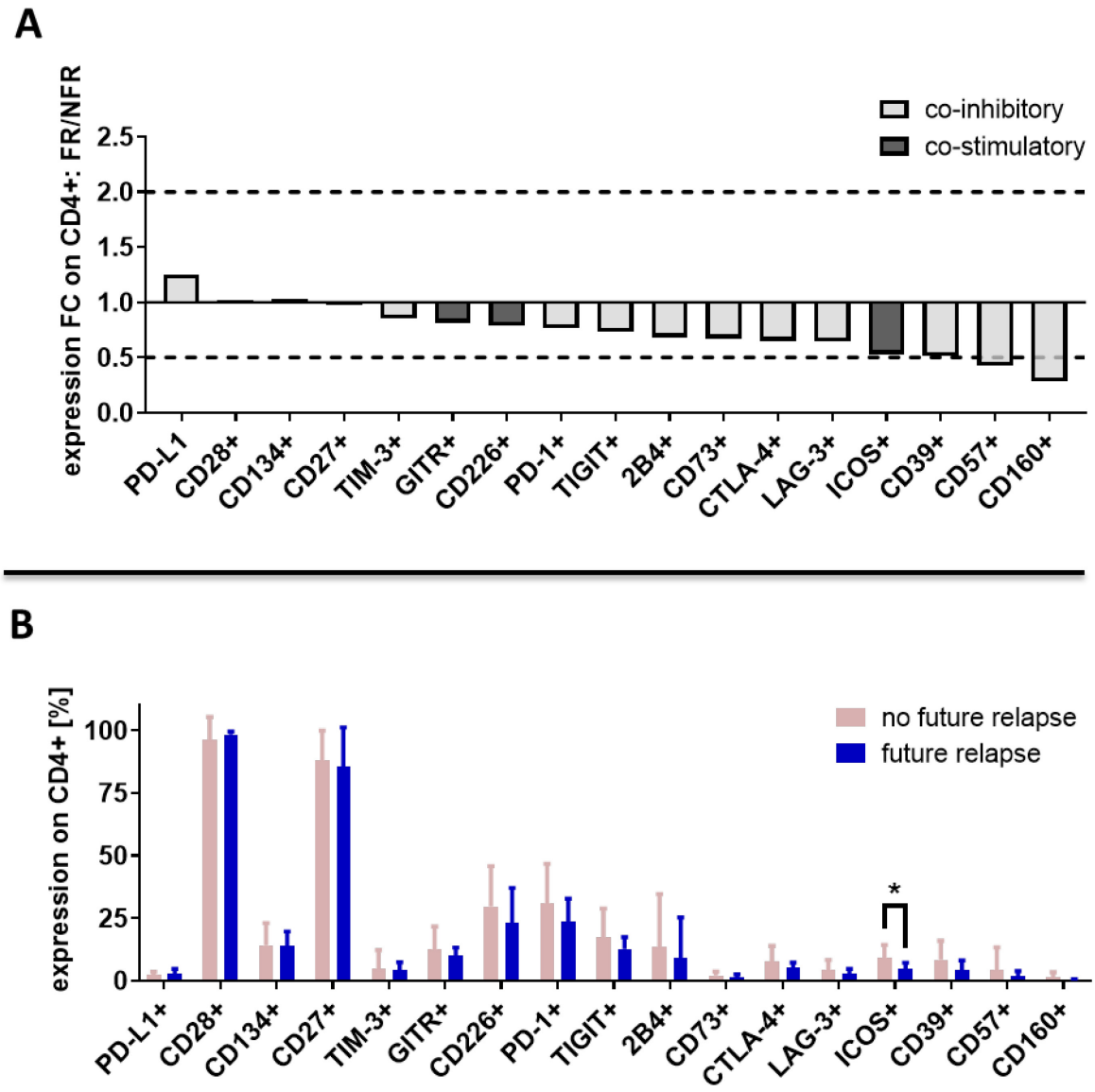

Figure 48: Expression of co-stimulatory and co-inhibitory molecules on CD4+ bmT cells in AML patients at the time of initial diagnosis with (N=7) and without (N=14) future relapse. A) For each co-inhibitory or co-stimulatory molecule on CD4+ bmT cells the expression fold change FR/NFR was defined as ratio of the mean expression on CD4+ bmT cells of all initial AML samples with future relapse divided by the mean expression on CD4+ bmT cells of all initial AML samples without future relapse. **B)** Absolute expression levels of molecules on CD4+ bmT cells were arranged according to A. CTLA-4 and PD-L1 were stained intracellularly. Expression of co-stimulatory marker ICOS was significantly upregulated in AML samples from initial diagnosis without future relapse compared to AML samples from initial diagnosis with future relapse (p=0.0309). NFR: no future relapse, FR: future relapse, FC: fold change.

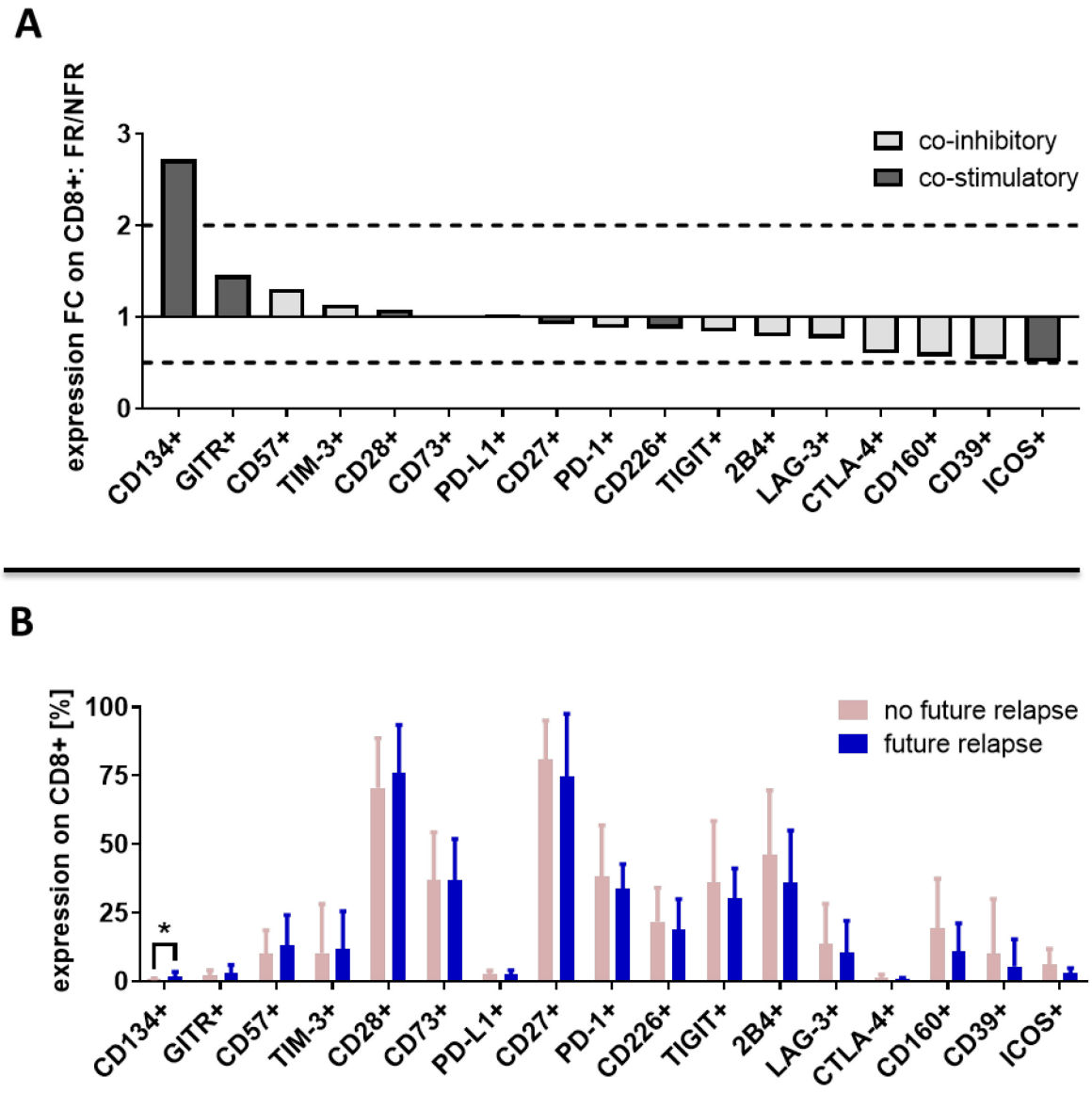

Figure 49: Expression of co-stimulatory and co-inhibitory molecules on CD8+ bmT cells in AML patients at the time of initial diagnosis with (N=7) and without (N=14) future relapse. A) For each co-inhibitory or co-stimulatory molecule on CD8+ bmT cells the expression fold change FR/NFR was defined as ratio of the mean expression on CD8+ bmT cells of all initial AML samples with future relapse divided by the mean expression on CD8+ bmT cells of all initial AML without future relapse. **B)** Absolute expression levels of molecules on CD8+ bmT cells were arranged according to A. CTLA-4 and PD-L1 were stained intracellularly. Co-stimulatory marker CD134 was significantly downregulated (p=0.0309) in AML samples from initial diagnosis without future relapse compared to AML samples from initial diagnosis with future relapse. NFR: no future relapse, FR: future relapse, FC: fold change.

The overexpression of ICOS on CD4+ bmT cells (9.1 % vs. 4.8 %, p=0.0309) and the downregulation of CD134 on CD8+ bmT cells (0.6 % vs. 1.7 %, p=0.0309) were the only differences reaching statistical significance in initial AML samples without future relapse compared to initial AML samples with future relapse. Figure 50 provides a more detailed insight into these observations.

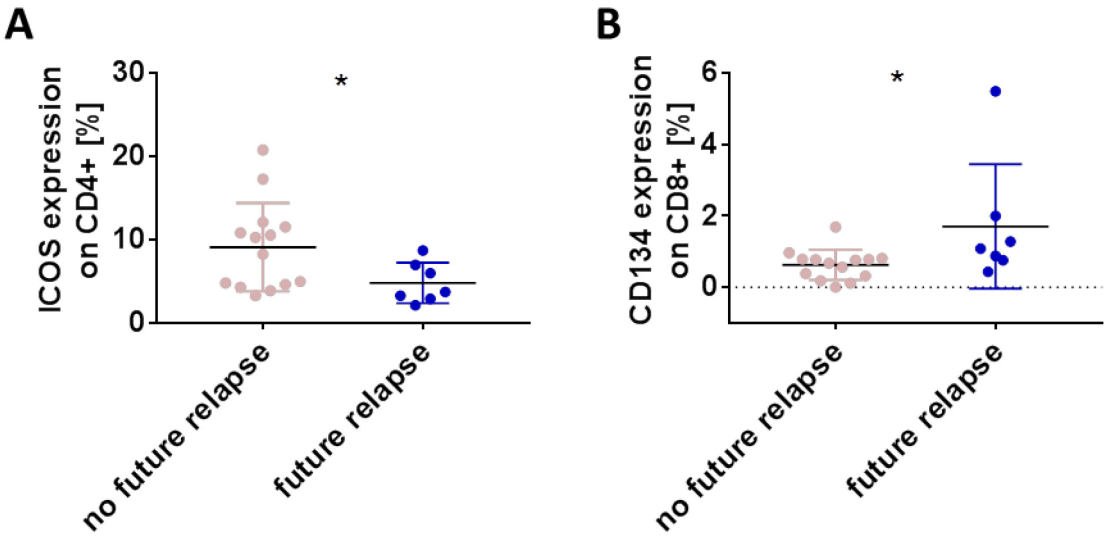

Figure 50: Overexpression of ICOS on CD4+ bmT cells and downregulation of CD134 on CD8+ bmT cells in initial AML samples without future relapse compared to initial AML samples with future relapse. A) The ICOS expression on CD4+ bmT cells was increased in initial AML samples without future relapse in comparison to initial AML samples with future relapse (p=0.0309). **B)** On CD8+ bmT cells CD134 was significantly downregulated in initial AML samples without future relapse compared to initial AML samples with future relapse (p=0.0309). Results were based on same cohorts as in Figure 48 and Figure 49.

Multiple testing corrections were performed as described in 5.12.1. Corrected p values (q values) were listed and compared to uncorrected p values in Figure 51. Apart from that, all mentioned p values are uncorrected in this chapter.

A

Antigen	p value	q value
TIM-3	0.6888	0.8489
CD160	0.2872	0.7652
2B4	0.3223	0.7652
PD-1	0.2545	0.7652
TIGIT	0.4880	0.8273
CD39	0.3601	0.7652
LAG-3	0.2865	0.7652
CTLA-4	0.7433	0.8489
PD-L1	0.7990	0.8489
CD27	0.9710	0.9710
CD134	0.1490	0.7652
CD28	0.3601	0.7652
ICOS	0.0793	0.7652
GITR	0.5353	0.8273
CD226	0.7990	0.8489
CD57	0.7433	0.8489
CD73	0.4430	0.8273

B

Antigen	p value	q value
TIM-3	0.7433	0.9026
CD160	0.0538	0.4573
2B4	0.4880	0.8296
PD-1	0.1969	0.7135
TIGIT	0.2545	0.7135
CD39	0.1969	0.7135
LAG-3	0.4003	0.8296
CTLA-4	0.4430	0.8296
PD-L1	0.7433	0.9026
CD27	0.9999	0.9999
CD134	0.9131	0.9702
CD28	0.6354	0.9026
ICOS	0.0309	0.4573
GITR	0.7990	0.9055
CD226	0.2545	0.7135
CD57	0.6492	0.9026
CD73	0.2938	0.7135

C

Antigen	p value	q value
TIM-3	0.9999	0.9999
CD160	0.2545	0.9007
2B4	0.3223	0.9007
PD-1	0.6359	0.9007
TIGIT	0.6359	0.9007
CD39	0.5846	0.9007
LAG-3	0.4880	0.9007
CTLA-4	0.4430	0.9007
PD-L1	0.7433	0.9026
CD27	0.6888	0.9007
CD134	0.0309	0.5253
CD28	0.4003	0.9007
ICOS	0.4880	0.9007
GITR	0.2872	0.9007
CD226	0.9999	0.9999
CD57	0.5846	0.9007
CD73	0.9710	0.9999

Figure 51: Corrected (q values) and uncorrected p values for analysis of CD3+ (A), CD4+ (B) and CD8+ bmT cells (C) in initial AML samples without future relapse compared to initial AML samples with future relapse. Multiple testing correction was performed by using the Original FDR method of Benjamini and Hochberg (5.12.1). P and q values <0.05 are marked in green.

6.2.8 High ICOS expression on CD4+ bmT cells as positive prognostic marker and high CD134 expression on CD8+ bmT cells as negative prognostic marker at initial diagnosis in terms of AML relapse

In comparison of initial AML samples with and without future relapse, ICOS on CD4+ bmT cells and CD134 on CD8+ bmT cells were the only markers differentially expressed (uncorrected p values, 6.2.7).

In that context, initial AML samples (initial AML samples with future relapse: N=7, initial AML samples without future relapse: N=14) were categorized into two groups using the mean value of ICOS and CD134 expression of all AML patients (N=29), respectively as cut-off value.
Subsequently, relapse-free survival rates were compared using Kaplan-Meier estimates, as shown in Figure 52.
During a median follow-up period of 7.0 years (0.8 – 14.4) a high ICOS expression on CD4+ bmT cells (> 9.0 %) at initial diagnosis was significantly correlated with favorable prognosis concerning AML relapse (100.0 % vs. 50.0 %, relapse-free survival in %, p=0.0265).
In contrast, a high CD134 expression (> 1.0 %) on CD8+ bmT cells at initial diagnosis was significantly correlated with an increased relapse risk (20.0 % vs. 81.3 %, p=0.0070).
P values of all Kaplan-Meier estimates calculated for single antigens (CD3+: TIM-3, ICOS, CD134, GITR; CD4+: TIM-3, ICOS, CD134, GITR; CD8+: TIM-3, ICOS, CD134, GITR, PD-1, LAG-3) were corrected as described in 5.12.1. After correction, a high CD134 expression on CD8+ bmT cells at initial diagnosis was still significantly correlated with increased relapse risk (q=0.0420), whereas ICOS expression was not correlated with favorable prognosis with regard to AML relapse, anymore (q=0.1060).

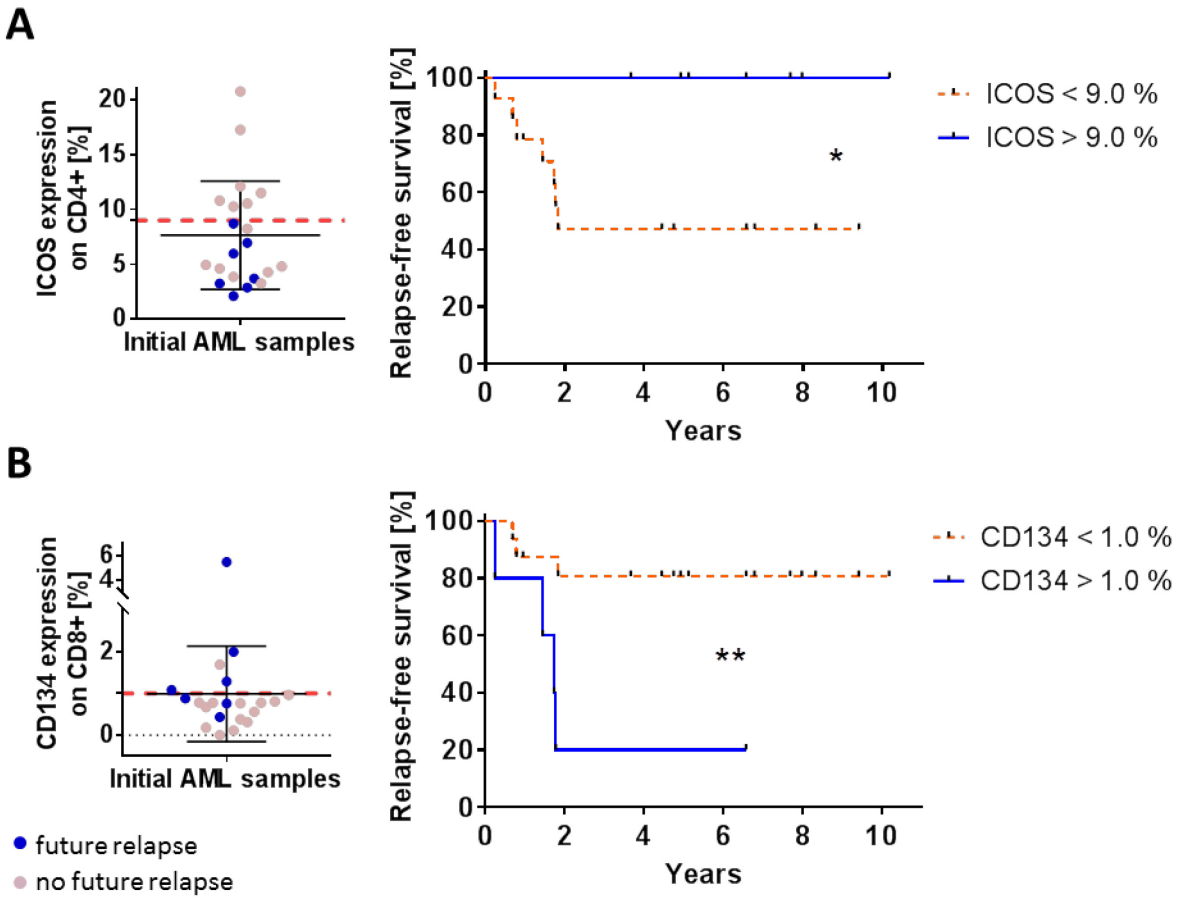

Figure 52: Relapse-free survival of AML patients in dependence of ICOS and CD134 expression on bmT cells at primary diagnosis. Initial AML samples were categorized into two groups using the mean value on CD4+ or CD8+ bmT cells of all AML patients (N=29) as cut-off value (left hand side, cut-off value in red). Relapse-free survival rates were analyzed using Kaplan-Meier estimates (right hand side). P values of all Kaplan-Meier estimates calculated for single antigens (CD4+: TIM-3, ICOS, CD134, GITR; CD8+: TIM-3, ICOS, CD134, GITR, PD-1, LAG-3) were corrected as described in 5.12.1. **A)** ICOS expression on CD4+ bmT cells at initial diagnosis was significantly correlated with favorable prognosis in terms of AML relapse. 7 out of 14 patients with an ICOS expression lower than 9.0 % had a relapse (RFS=50.0 %), while in the patient group with an ICOS expression higher than 9.0 % 0 out of 7 patients had a relapse (median follow-up period: 7.0 years (0.8 – 14.4), RFS=100.0 %, p=0.0265, corrected p value: q=0.1060). **B)** CD134 expression on CD8+ bmT cells at initial diagnosis was significantly correlated with an increased relapse risk. 3 out of 16 patients with a CD134 expression lower than 1.0 % had a relapse (RFS=81.3 %), whereas in the patient group with a CD134 expression higher than 1.0 % 4 out of 5 patients had a relapse (median follow-up period: 7.0 years (0.8 – 14.4), RFS=20.0 %, p=0.0070, corrected p value: q=0.0420). RFS: relapse-free survival.

In order to better describe the functional difference between CD134 and ICOS as co-stimulatory markers on bmT cells at initial diagnosis in context of relapse-free survival we developed so called *stimulation indices*. Those indices describe the relation of different co-stimulatory marker expression levels and were evaluated for prognostic use concerning “future relapse”.

For each patient sample indices were calculated by dividing the expression rate of one co-stimulatory marker (e.g. CD134) by the expression rate of another co-stimulatory marker (e.g. ICOS). Before, expression rates had been normalized by dividing them by the mean expression rate of all healthy BM donors.

As shown in Figure 53 GITR/ICOS indices of CD3+ bmT cells (2.1 vs. 1.1, p=0.0097), CD4+ (2.3 vs. 1.5, p=0.0250) and CD8+ bmT cells (1.6 vs. 0.9, p=0.0097) were significantly higher in initial AML samples with future relapse compared to initial AML samples without future relapse.

Furthermore, CD134/ICOS (2.0 vs. 0.8, p=0.0016) index of CD8+ bmT cells was increased in initial AML samples with future relapse compared to initial samples without future relapse.

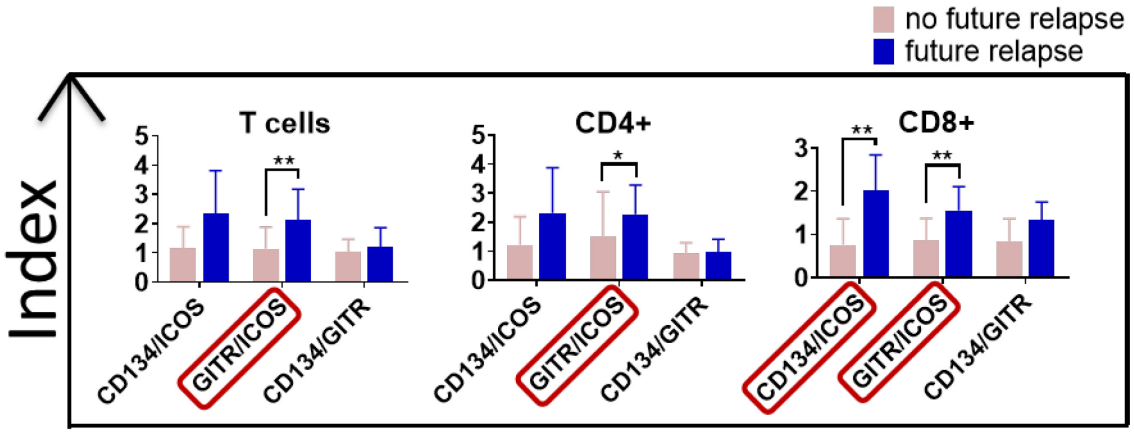

Figure 53: Stimulation indices of bmT cells in initial AML samples with (N=7) and without (N=14) future relapse. For each patient sample indices were calculated by dividing the expression rate of one co-stimulatory marker (e.g. CD134) by the expression rate of another co-stimulatory marker (e.g. ICOS). Before, expression rates had been normalized by dividing them by the mean expression rate of all healthy BM donors. In initial AML samples with future relapse the GITR/ICOS indices of CD3+ bmT cells (p=0.0097), CD4+ (p=0.0250) and CD8+ bmT cells (p=0.0097) were significantly increased in comparison to initial AML samples without future relapse (red boxes). Furthermore, the CD134/ICOS index (p=0.0016) of CD8+ bmT cells was increased in initial AML samples with future relapse compared to initial samples without future relapse (red box). A similar effect was observable for CD3+ bmT cells and CD4+ bmT cells, but without reaching statistical significance.

Again, initial AML samples were categorized into two groups according to the mean value of stimulation index of all AML patients and compared with respect to relapse-free survival, as described above.

As shown in Figure 54, a high GITR/ICOS index of CD3+ bmT cells (> 1.4) was significantly correlated with increased relapse risk (median follow-up period of 7.0 years (0.8 – 14.4), 42.9 % vs. 78.6 %, p=0.0457, corrected p value: q=0.0686). The same could be observed for CD4+ and CD8+ bmT cells (not shown).

Furthermore, a high CD134/ICOS index (> 1.2) of CD8+ bmT cells at initial diagnosis was significantly correlated with decreased relapse-free survival (37.5 % vs. 84.6 %, p=0.0213, corrected p value: q=0.0639, Figure 55).

Multiple testing corrections for indices were performed as described in 5.12.1 and 6.2.9.

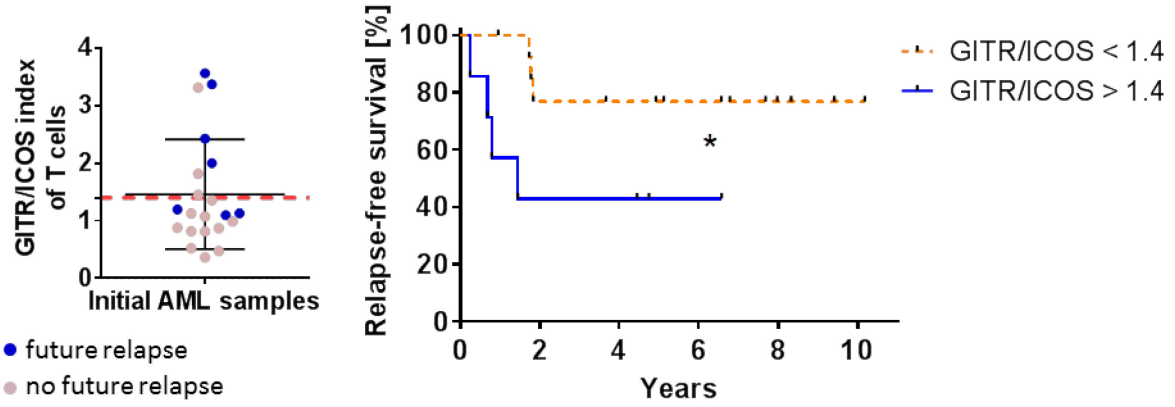

Figure 54: Relapse-free survival of AML patients in dependence of GITR and ICOS expression on CD3+ bmT cells at primary diagnosis. Initial AML samples were categorized into two groups using the mean value on CD3+ bmT cells of all AML patients (N=29) as cut-off value (left hand side, cut-off value in red). Relapse-free survival rates were analyzed using Kaplan-Meier estimates (right hand side). P values of all Kaplan-Meier estimates calculated for indices (CD3+: CD134/GITR, GITR/ICOS, ICOS/TIM-3) were corrected as described in 5.12.1. 4 out of 7 patients with a GITR/ICOS index higher than 1.4 had a recurrence (RFS=42.9 %), while in the patient group with a GITR/ICOS index lower than 1.4 only 3 out of 14 patients had a relapse during the entire follow up period (median follow-up period: 7.0 years (0.8 – 14.4), RFS=78.6 %, p=0.0457, corrected p value: q=0.0686). RFS: relapse-free survival.

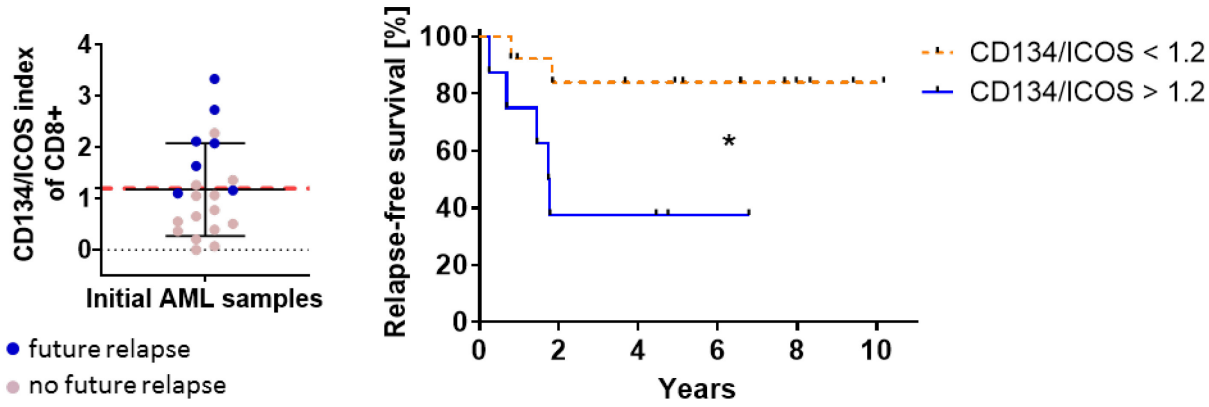

Figure 55: Relapse-free survival of AML patients in dependence of ICOS and CD134 expression on CD8+ bmT cells at primary diagnosis. Initial AML samples were categorized into two groups using the mean value on CD8+ bmT cells of all AML patients (N=29) as cut-off value (left hand side, cut-off value in red). Relapse-free survival rates were analyzed using Kaplan-Meier estimates (right hand side). P values of all Kaplan-Meier estimates calculated for indices (CD8+: CD134/ICOS, CD134/GITR, GITR/ICOS, CD134/TIM-3, CD134/PD-1, CD134/LAG-3) were corrected as described in 5.12.1. 5 out of 8 patients with a CD134/ICOS index higher than 1.2 had a recurrence (RFS=37.5 %), while in the patient group with a CD134/ICOS index lower than 1.2 only 2 out of 13 patients had a relapse (median follow-up period: 7.0 years (0.8 – 14.4), RFS=84.6 %, p=0.0213, corrected p value: q=0.0639). RFS: relapse-free survival.

In order to assess expression patterns of CD134 and ICOS on CD8+ bmT cells in even greater detail, co-expression levels were subsequently evaluated (Figure 56).

Within all AML patients the maximal co-expression level of CD134 and ICOS on CD8+ bmT cells was 1.7 % (mean: 0.2 %). No obvious relation could be shown between CD134 and ICOS single-expression, as well as between single-expression and co-expression rates in general on CD8+ bmT cells in the bone marrow.

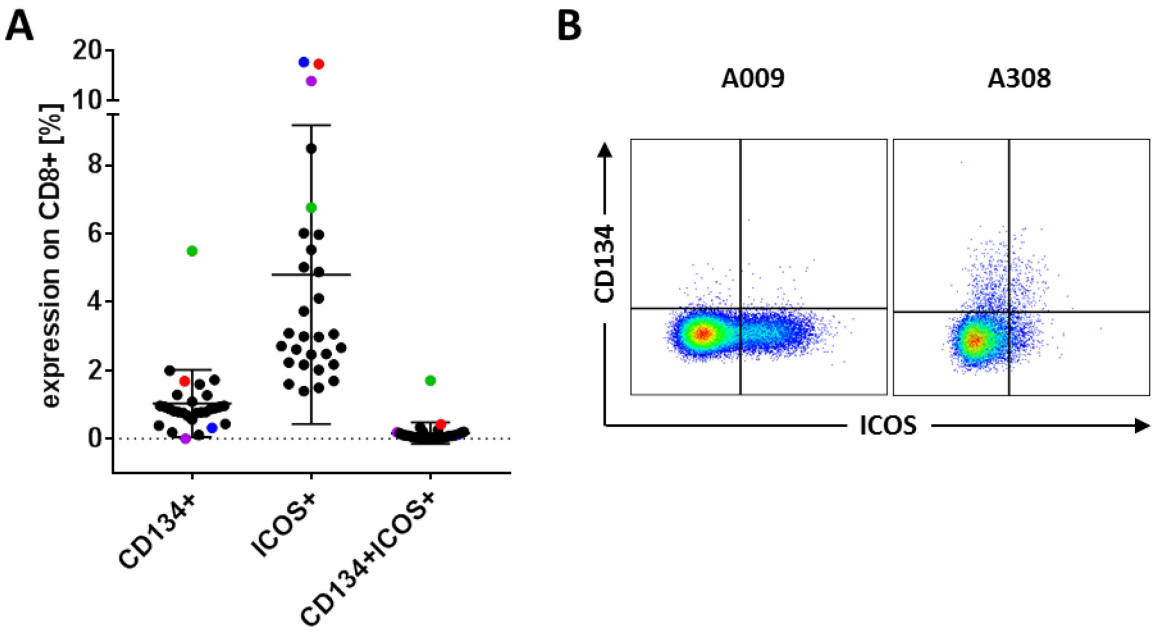

Figure 56: Co-expression levels of CD134 and ICOS on CD8+ bmT cells of AML patients in comparison to single-expression values. A) Co-expression levels of CD134 and ICOS were evaluated on CD8+ bmT cells. The maximal co-expression level within all AML patients was 1.7 % (mean: 0.2 %). The three patients` samples with the highest ICOS expression and the patient sample with the highest CD134 expression are color-coded to illustrate the relation between the CD134/ICOS single positive cell populations and the CD134+ICOS+ double positive cell populations in the bone marrow for these patient samples. **B)** Dot-plots showing the relation between CD134/ICOS single positive, as well as CD134+ICOS+ double positive CD8+ bmT cells of AML patients A009 and A308.

6.2.9 High ICOS/TIM-3 index of CD3+ bmT cells as positive prognostic marker and high CD134/PD-1 index of CD8+ bmT cells as negative prognostic marker at initial diagnosis in terms of AML relapse

The AML patient showing the highest expression of exhaustion marker TIM-3 on CD3+ bmT cells (48.8 %, mean: 7.1 %) also had the highest expression of co-stimulatory marker ICOS on CD3+ bmT cells (17.7 %, mean: 6.3 %) within all analyzed 29 AML patients (Figure 57). As this patient did not have a relapse nor a refractory AML, we reasoned that in this case the high TIM-3 expression on bmT cells was due to T cell activation rather than T cell exhaustion. In this context, a well-balanced

co-inhibitory/co-stimulatory marker expression on bmT cells could be of importance with regard to relapse-free survival.

So, in order to better describe the functionality of a bmT cell population we developed the so-called *exhaustion indices.* Those indices describe the relation of the co-inhibitory and co-stimulatory marker expression on bmT cells and were evaluated for prognostic use concerning "future relapse". For each patient sample indices were calculated by dividing the expression rate of a co-stimulatory marker (e.g. ICOS) by the expression rate of a co-inhibitory marker (e.g. TIM-3). Before, expression rates had been normalized by dividing them by the mean expression rate of all healthy BM donors.

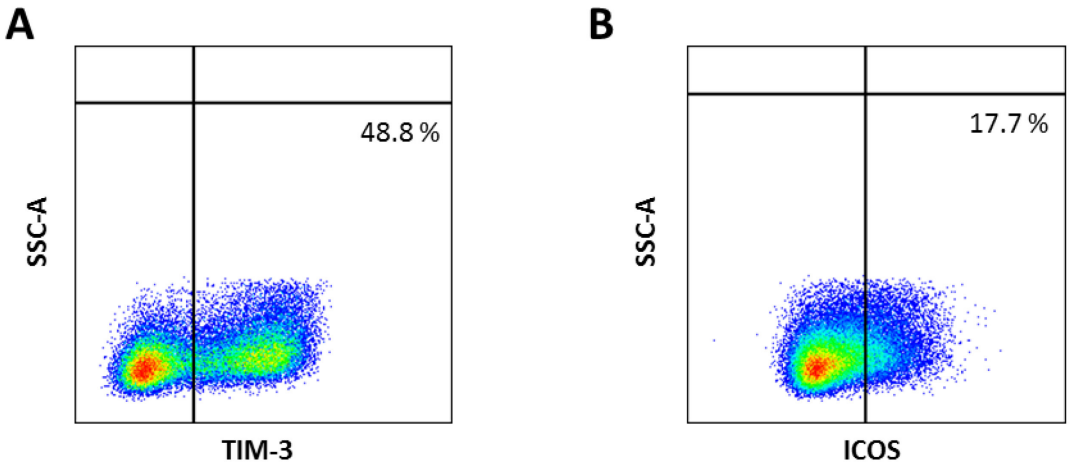

Figure 57: Dot plots showing the TIM-3 and ICOS expression on CD3+ bmT cells of patient A013. A)-B) Within all analyzed AML patient samples (N=29) patient A013 showed the highest TIM-3 expression (A: 48.8 %, mean: 7.1 %), as well as the highest ICOS expression (B: 17.7 %, mean: 6.3 %).

As shown in Figure 58 ICOS/TIM-3 index of CD3+ bmT cells (0.3 vs. 0.6, p=0.0200) and CD4+ bmT cells (0.3 vs. 0.5, p=0.0461) were significantly reduced in initial AML samples with future relapse compared to initial AML samples without future relapse.

Furthermore, CD134/TIM-3 (0.9 vs. 0.5, p=0.0309), CD134/PD-1 (1.9 vs. 0.8, p=0.0379) and CD134/LAG-3 (2.6 vs. 0.7, p=0.0074) indices of CD8+ bmT cells were increased in initial AML samples with future relapse compared to initial samples without future relapse.

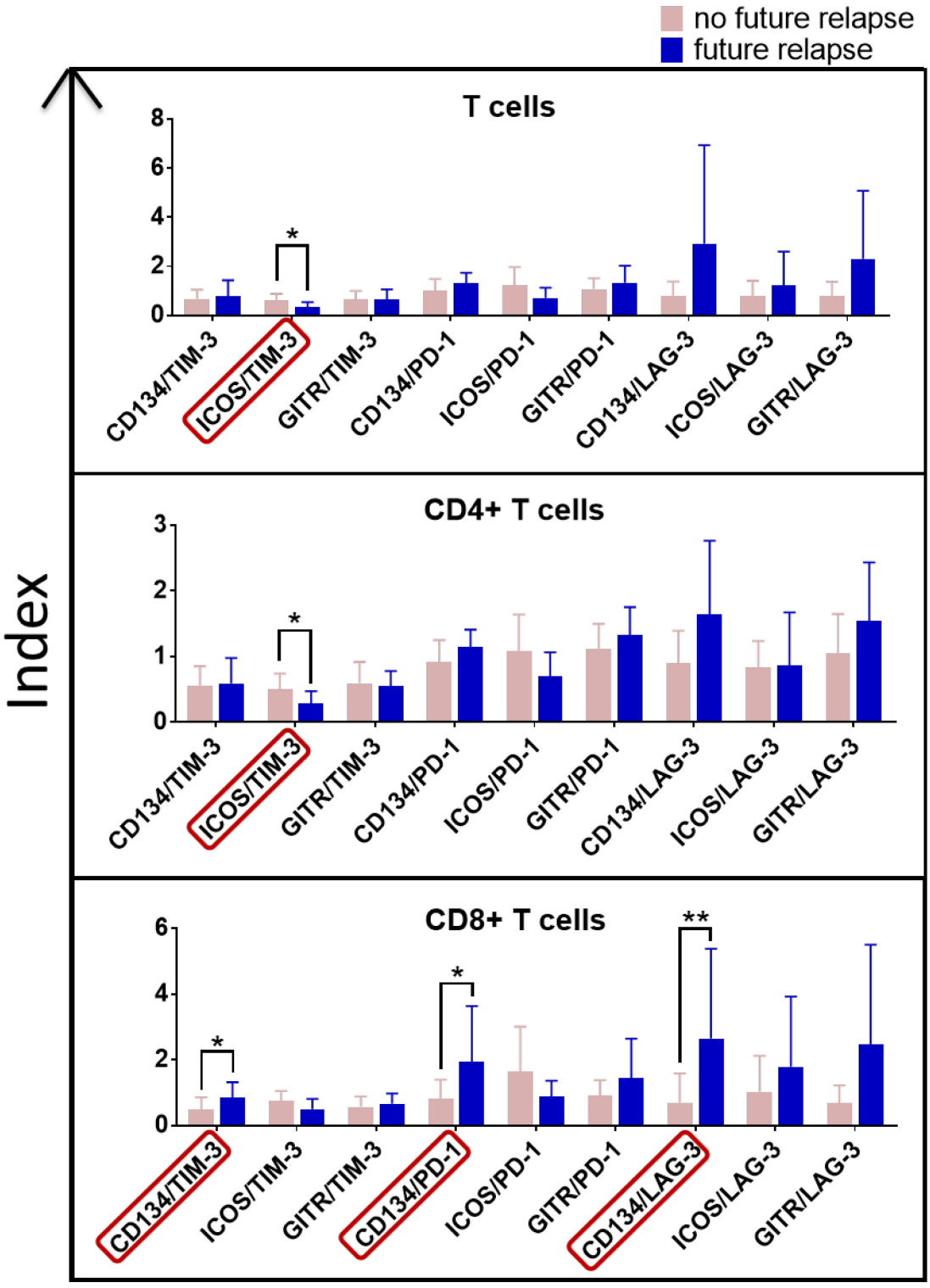

Figure 58: Exhaustion indices of bmT cells in initial AML samples with (N=7) and without (N=14) future relapse. For each patient sample indices were calculated by dividing the expression rate of a co-stimulatory marker (e.g. CD134) by the expression rate of a co-inhibitory marker (e.g. TIM-3). Before, expression rates had been normalized by dividing them by the mean expression rate of all healthy BM donors. In initial AML samples with future relapse the ICOS/TIM-3 indices of CD3+ bmT cells (p=0.0200) and CD4+ bmT cells (p=0.0461) were significantly decreased in comparison to initial AML samples without future relapse (red boxes). The CD134/TIM-3 (p=0.0309), CD134/PD-1 (p=0.0379) and CD134/LAG-3 (p=0.0074) indices of CD8+ bmT cells were increased in initial AML samples with future relapse compared to initial samples without future relapse (red boxes).

Subsequently, initial AML samples (initial AML samples with future relapse: N=7, initial AML samples without future relapse: N=14) were categorized into two groups using the mean value of the different indices of all AML patients (N=29) as cut-off value. Relapse-free survival rates were compared using Kaplan-Meier estimates.

As shown in Figure 59, a high ICOS/TIM-3 index of CD3+ bmT cells (> 0.6) at initial diagnosis of AML patients was significantly correlated with reduced relapse risk (median follow-up period: 7.0 years (0.8 – 14.4), 88.9 % vs. 50.0 %, p=0.0397).

Worthy of special mention is that the patient with the lowest ICOS/TIM-3 index of CD3+ bmT cells at initial diagnosis in our patient cohort (0.06, mean: 0.6) was the first patient to relapse (central nervous system relapse after 88 days).

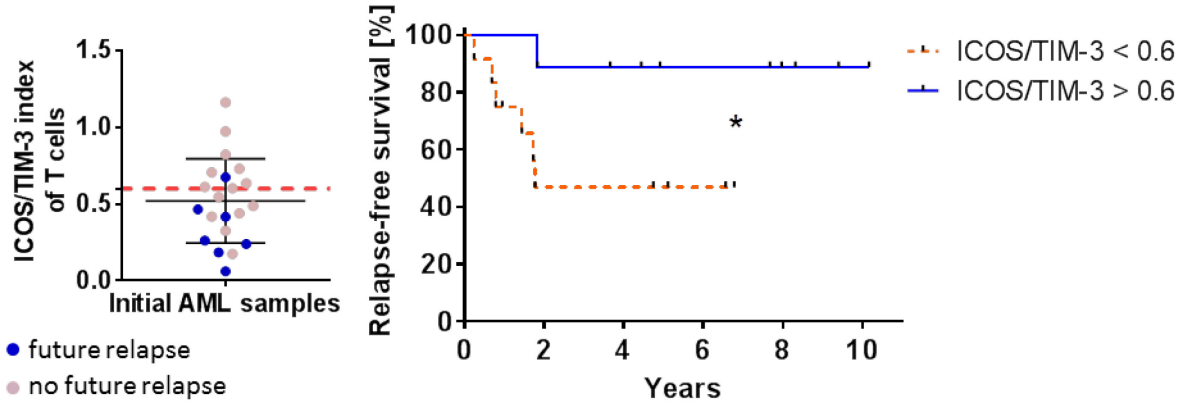

Figure 59: Relapse-free survival of AML patients in dependence of ICOS and TIM-3 expression on CD3+ bmT cells at primary diagnosis. Initial AML samples were categorized into two groups using the mean value on CD3+ bmT cells of all AML patients (N=29) as cut-off value (left hand side, cut-off value in red). Relapse-free survival rates were analyzed using Kaplan-Meier estimates (right hand side). P values of all Kaplan-Meier estimates calculated for indices (CD3+: CD134/GITR, GITR/ICOS, ICOS/TIM-3) were corrected as described in 5.12.1. Only 1 out of 9 patients with an ICOS/TIM-3 index higher than 0.6 had a recurrence (RFS=88.9 %), while in the patient group with an ICOS/TIM-3 index lower than 0.6 6 out of 12 patients had a relapse (median follow-up period: 7.0 years (0.8 – 14.4), RFS=50.0 %, p=0.0397, corrected p value: q=0.0686). RFS: relapse-free survival.

For CD8+ bmT cells a high CD134/PD-1 index at initial diagnosis proved to be correlated with AML relapse. During a median follow up period of 7.0 years (0.8 – 14.4) 4 out of 6 patients with a CD134/PD-1 index higher than 1.2 had a recurrence, while in the patient group with a CD134/PD-1 index lower than 1.2 only 3 out of 15 patients had a relapse (33.3 % vs. 80.0 %, p=0.0500, Figure 60).

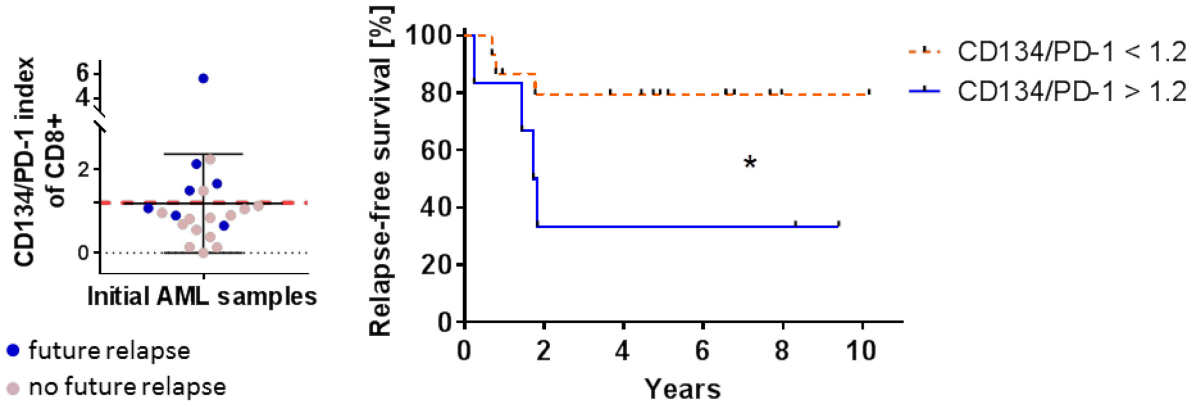

Figure 60: Relapse-free survival of AML patients in dependence of CD134 and PD-1 expression on CD8+ bmT cells at primary diagnosis. Initial AML samples were categorized into two groups using the mean value on CD8+ bmT cells of all AML patients (N=29) as cut-off value (left hand side, cut-off value in red). Relapse-free survival rates were analyzed using Kaplan-Meier estimates (right hand side). P values of all Kaplan-Meier estimates calculated for indices (CD8+: CD134/ICOS, CD134/GITR, GITR/ICOS, CD134/TIM-3, CD134/PD-1, CD134/LAG-3) were corrected as described in 5.12.1. 4 out of 6 patients with a CD134/PD-1 index higher than 1.2 had a recurrence (RFS=33.3 %), while in the patient group with a CD134/PD-1 index lower than 1.2 only 3 out of 15 patients had a relapse (median follow-up period: 7.0 years (0.8 – 14.4), RFS=80.0 %, p=0.0500, corrected p value: q=0.0908). RFS: relapse-free survival.

P values of all Kaplan-Meier estimates calculated for indices (CD3+: CD134/GITR, GITR/ICOS, ICOS/TIM-3; CD4+: CD134/GITR, GITR/ICOS, ICOS/TIM-3; CD8+: CD134/ICOS, CD134/GITR, GITR/ICOS, CD134/TIM 3, CD134/PD-1, CD134/LAG-3) were corrected as described in 5.12.1. After correction neither a low ICOS/TIM-3 index of CD3+ bmT cells (q=0.0686), nor a high CD134/PD-1 index of CD8+ bmT cells (q=0.0908) was still significantly correlated with increased relapse risk.

6.3 Flow cytometric phenotype analysis of AML blasts

In order to identify putative interaction nodes between T cells and malignant AML blasts, the latter population was phenotyped for ligands of those co-stimulatory and co-inhibitory surface molecules, that were measured on bmT cells. The results obtained from the analysis of AML samples were compared to $CD45_{dim}$ cells in the bone marrow of healthy BM donors to identify aberrant surface expression patterns of AML.

Additionally, expression levels of different AML target antigens were analyzed in order to identify possible target antigen combinations for synthetic immunotherapy such as combinatorial chimeric antigen receptor T cells (e.g. Tandem-CARs, synNotch-gated CARs).

All initial AML samples were therapy naïve, but within the AML samples from 1st relapse (N=10) four relapses happened during chemotherapy treatment of initial diagnosis, whereas four relapses happened upon completion of the chemotherapy of initial diagnosis. These sample groups were

compared concerning their expression levels of different markers (Figure 61, Figure 83). There were no significant differences determined, so all samples from 1st relapse were treated equally in analysis.

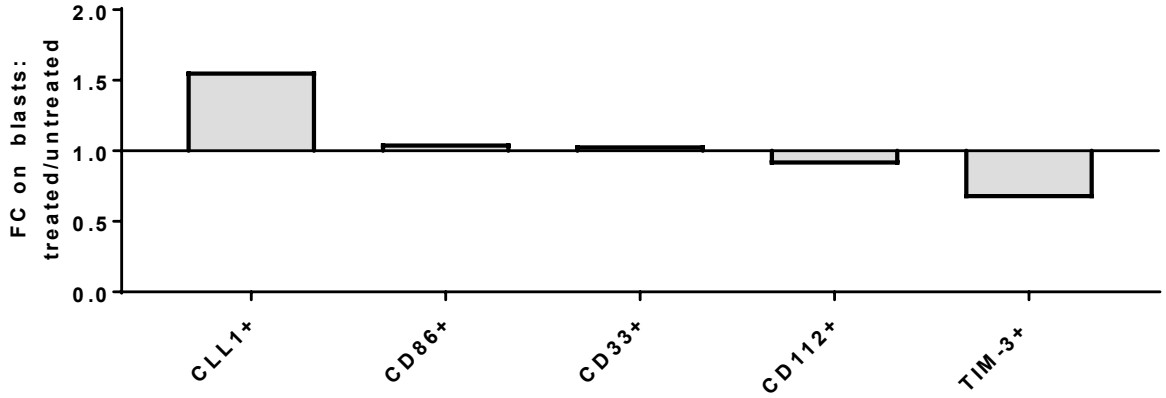

Figure 61: Comparison of relapsed AML samples (1st relapse) during ongoing chemotherapy and after completion of chemotherapy of initial diagnosis. Between relapsed AML samples within chemotherapy treatment of initial diagnosis (N=4) and relapsed AML samples upon completion of chemotherapy treatment of initial diagnosis (N=4) expression rates of CLL1, CD86, CD33, CD112 and TIM-3 on AML blasts were not significantly different. For other objects of comparison see Figure 83. Treated: relapsed AML samples within chemotherapy treatment of initial diagnosis, untreated: relapsed AML samples upon completion of chemotherapy treatment of initial diagnosis, FC: fold change.

6.3.1 Clonal CD34/CD38 phenotype of AML blasts

As shown in Figure 62A and B CD34/CD38 distribution within $CD45_{dim}$ cells in healthy BM donors was quite uniform: $CD45_{dim}$ cells were mostly CD34-CD38+ or CD34+CD38+ ($p<0.0001$).

In contrast to that AML patients showed a clonal distribution of CD34/CD38 phenotypes of blasts with a wide range within AML patients.

The significance of difference was determined using the Friedman test.

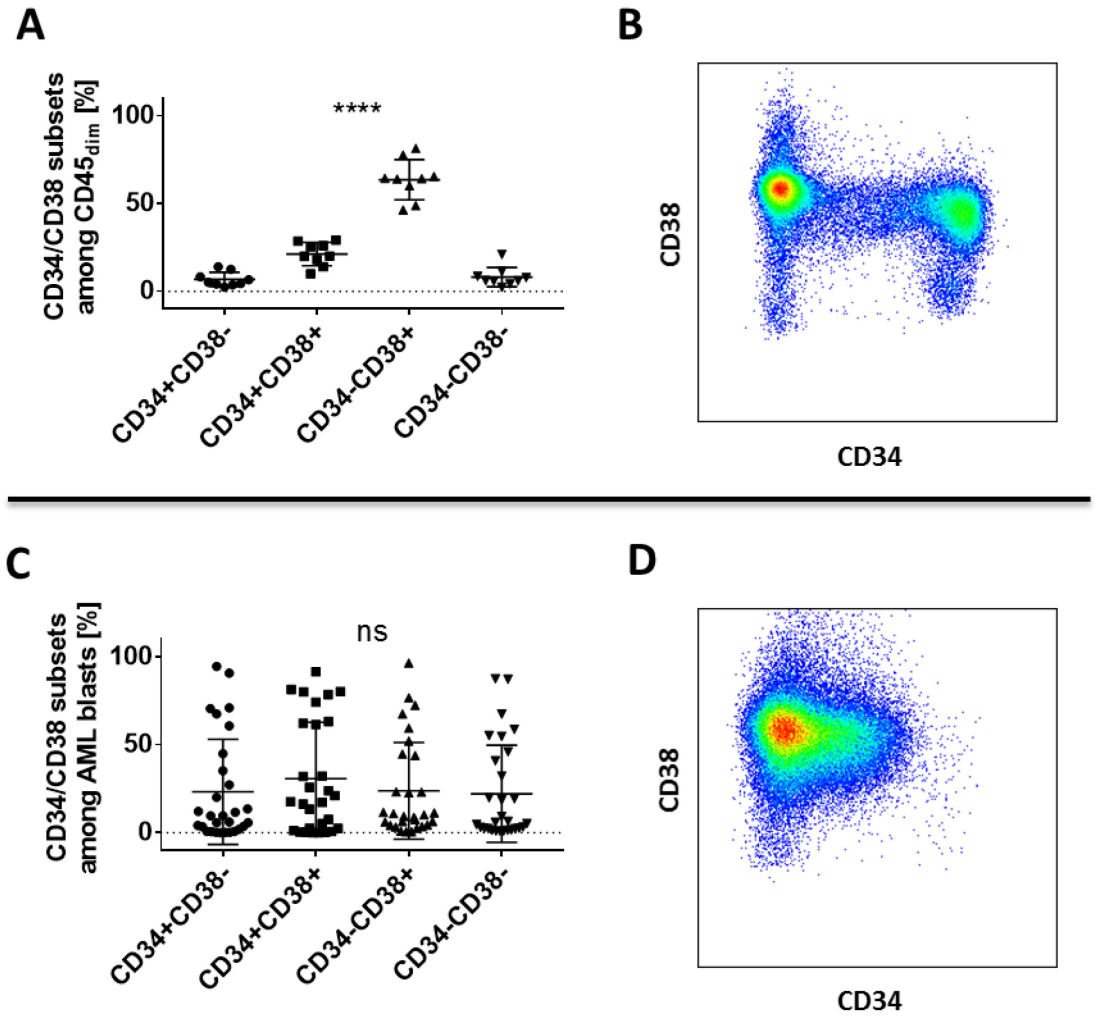

Figure 62: Clonal CD34/CD38 phenotype of AML blasts. A) $CD45_{dim}$ cells in healthy BM donors showed a uniform distribution of CD34/CD38 phenotypes: $CD45_{dim}$ cells were mostly CD34-CD38+ or CD34+CD38+ cells. The significance of difference was determined using the Friedman test ($p<0.0001$). **B)** Representative dot plot shows usual distribution of CD34/CD38 phenotypes within $CD45_{dim}$ cells in healthy BM donors. **C)** AML patients showed a clonal distribution of CD34/CD38 phenotypes of blasts. The significance of difference was determined using the Friedman test. **D)** Exemplary dot plot shows clonal CD38+CD34- blast phenotype of an AML patient. There was a wide range of CD34/CD38 phenotypes of AML blasts within our patient cohort.

6.3.2 Overexpression of CD86, TIM-3, CD112 and CD39 on AML blasts

Figure 63 shows antigen expression levels on AML blasts compared to $CD45_{dim}$ cells in healthy BM donors. Expression of CD86 (13.3 % vs. 0.1 %, mean values, $p<0.0001$), TIM-3 (37.5 % vs. 1.5 %, $p=0.0002$), CD112 (55.4 % vs. 6.6 %, $p=0.0002$) and co-inhibitory marker CD39 (32.5 % vs. 6.0 %, $p=0.0064$) was significantly higher on AML blasts in comparison to healthy controls.

Expression levels of CD47 (97.3 % vs. 99.7 %, $p=0.0384$), PD-1 (0.3 % vs. 0.7 %, $p=0.0023$) and co-inhibitory markers PD-L1 (1.9 % vs. 3.1 %, $p=0.0173$) and CD73 (1.3 % vs. 3.6 %, $p=0.0003$), as well

as expression of co-stimulatory marker ICOS-L (1.6 % vs. 2.3 %, p=0.0145) were downregulated on AML blasts compared to $CD45_{dim}$ cells in healthy BM donors.

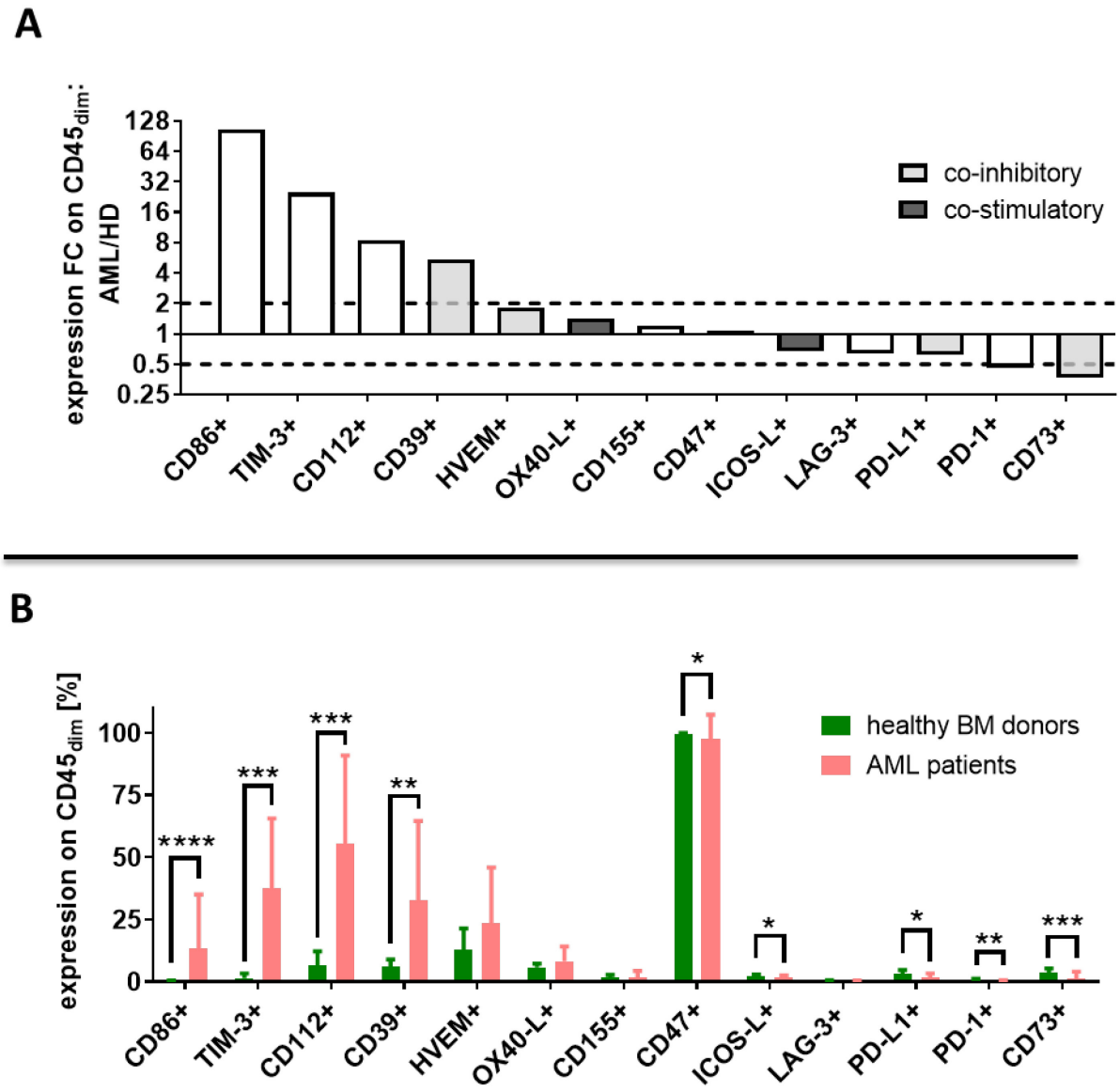

Figure 63: Overexpression of CD86, TIM-3, CD112 and CD39 on blasts in AML patients (N=29) compared to $CD45_{dim}$ cells in healthy BM donors (N=9). A) For each co-inhibitory or co-stimulatory molecule the expression fold change AML/HD was defined as ratio of the mean expression on blasts of all AML patients divided by the mean expression on $CD45_{dim}$ cells of all healthy BM donors. Markers not marked in grey could be either co-inhibitory and co-stimulatory or their function has not been clarified so far regarding blast-T cell interaction in AML. **B)** Absolute expression levels of molecules on blasts/$CD45_{dim}$ cells were arranged according to A. PD-L1 was stained intracellularly. CD86 ($p<0.0001$), TIM-3 ($p=0.0002$), CD112 ($p=0.0002$) and co-inhibitory marker CD39 ($p=0.0064$) were significantly overexpressed on AML blasts in comparison to $CD45_{dim}$ cells in healthy BM donors. Expression levels of CD47 ($p=0.0384$), PD-1 ($p=0.0023$) and co-inhibitory markers PD-L1 ($p=0.0173$) and CD73 ($p=0.0003$), as well as expression of co-stimulatory marker ICOS-L ($p=0.0145$) were significantly downregulated on AML blasts compared to $CD45_{dim}$ cells in healthy BM donors. HD/healthy BM donors: healthy bone marrow donors, FC: fold change.

Analysis of initial AML samples with (N=7) and without future relapse (N=14) showed that CD155 was significantly differently expressed (overexpression of CD155 on blasts of initial AML samples without future relapse compared to initial AML samples with future relapse, 2.8 % vs. 0.8 %, p=0.0461, Figure 64). Nevertheless, differences are rather small.

During the course of AML (initial AML samples vs. relapsed AML samples) there were no differences in antigen expression observed (not shown).

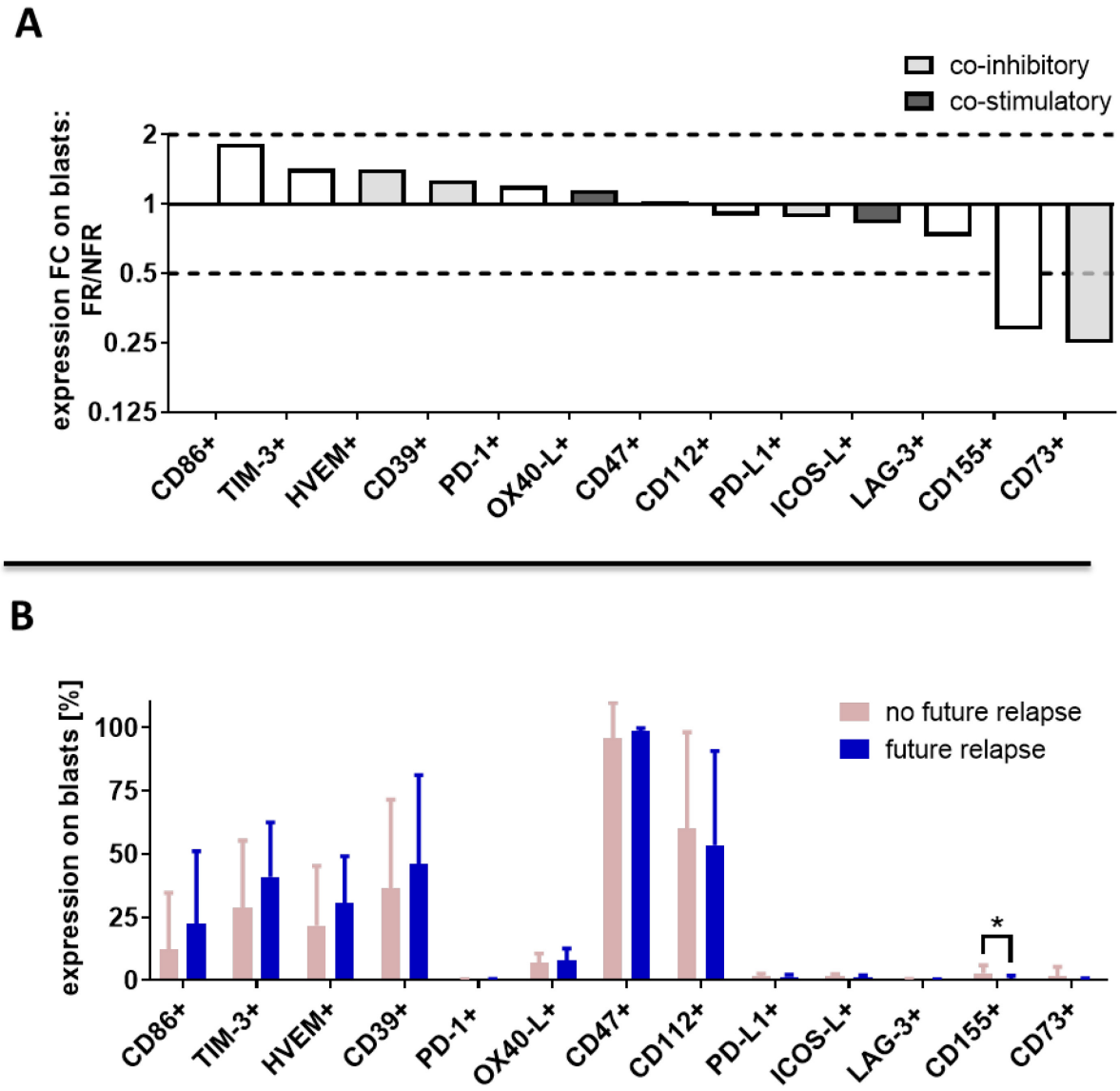

Figure 64: Overexpression of CD155 on blasts in initial AML samples without future relapse (N=14) compared to initial AML samples with future relapse (N=7). A) For each co-inhibitory or co-stimulatory molecule the expression fold change FR/NFR was defined as ratio of the mean expression on blasts in all initial AML samples with future relapse divided by the mean expression on blasts in all initial AML samples without future relapse. Markers not marked in grey could be either co-inhibitory and co-stimulatory or their function has not been clarified so far with reference to blast-T cell interaction in AML. **B)** Absolute expression levels of molecules on AML blasts were arranged according to A. PD-L1 was stained intracellularly. CD155 expression was borderline significantly higher on blasts in initial AML samples without future relapse compared to initial AML samples with future relapse (p=0.0461). FR: future relapse, NFR: no future relapse, FC: fold change.

6.3.3 Identification of CD135, EMR2, CLL1, CD123, CD33 and TIM-3 as possible combinatorial CAR targets on AML blasts

In parts, the following results have already been published in an adapted form by our working group in Willier et al., 2021.

To identify possible target antigen combinations out of AML associated antigens for combinatorial CAR T-cell therapy, expression values of single markers were analyzed on AML blasts and compared to $CD45_{dim}$ cells in healthy BM donors. CD135 (38.0 % vs. 7.2 %, p=0.0128), CD123 (38.0 % vs. 7.6 %, p<0.0001), CLL1 (71.7 % vs. 10.6 %, p=0.0004), CD33 (82.6 % vs. 6.2 %, p<0.0001) and TIM-3 (37.5 % vs. 1.5 %, p=0.0002) showed significant overexpression on AML blasts compared to $CD45_{dim}$ cells in healthy BM donors. For CCR1, CD85d and EMR2 expression, no healthy BM donors were analyzed as control. Nevertheless, EMR2 was highly expressed on AML blasts (mean expression: 41.6 %), while CCR1 and CD85d were expressed on less than 20% of AML blasts (mean expression values, CCR1: 2.0 %, CD85d: 10.7 %).

CD96 was initially analyzed as potential immunotherapy target in AML. However, due to a high CD96 expression on bmT cells it was finally excluded from the panel. In case of the antigens listed in Figure 65 expression on bmT cells was evaluated for 4 AML patients. Here, all antigens except TIM-3 were not expressed on bmT cells.

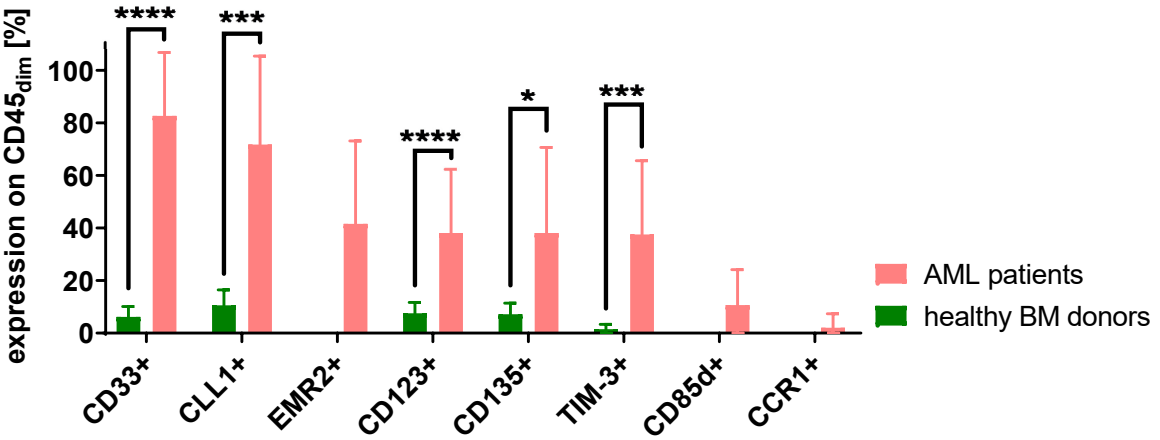

Figure 65: Antigen expression on blasts in AML patients (N≥21) compared to $CD45_{dim}$ cells in healthy BM donors (N=9). CD135 (p=0.0128), CD123 (p<0.0001), CLL1 (p=0.0004), CD33 (p<0.0001) and TIM-3 (p=0.0002) were significantly overexpressed on AML blasts compared to $CD45_{dim}$ cells in healthy BM donors. For CCR1, CD85d and EMR2 expression no healthy BM donors were analyzed as control. Healthy BM donors: healthy bone marrow donors.

During the course of AML (initial AML samples vs. relapsed AML samples), CD33 showed a trend to be higher expressed on AML blasts in relapsed AML samples compared to initial AML samples, but without reaching statistical significance (90.2 % vs. 79.5 %, p=0.0736, Figure 66).

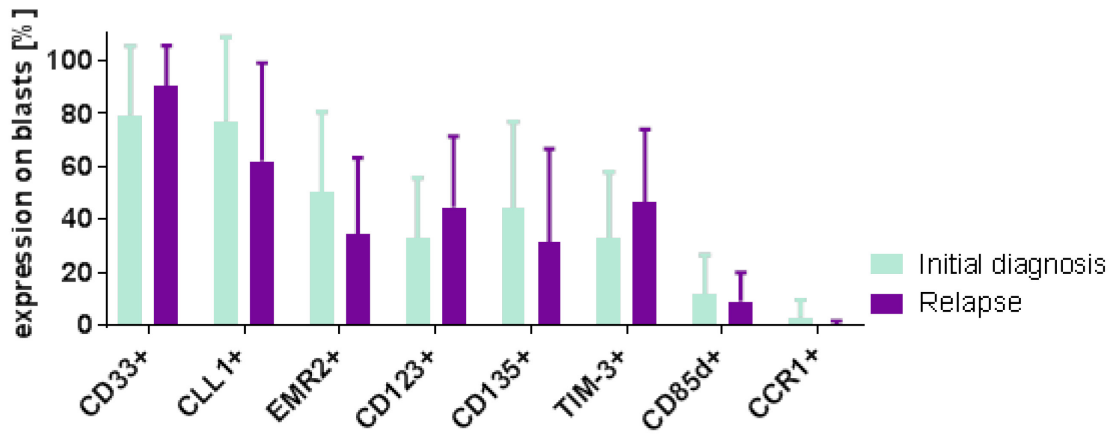

Figure 66: Antigen expression on AML blasts in initial AML samples (N≥13) compared to relapsed AML samples (N=12). There were no significant differences observed, with CD33 showing only a trend to be higher expressed on AML blasts in relapsed AML samples compared to initial AML samples without reaching statistical significance (p=0.0736).

Analysis of initial AML samples with and without future relapse did not show any significant differences concerning antigen expression on AML blasts (not shown).

6.3.3.1 Identification of CD33-CLL1 as best target antigen combination for a Tandem-CAR

In parts, the following results have already been published in an adapted form by our working group in Willier et al., 2021.

On basis of the single marker expression levels, different antigen combinations were chosen for combinatorial AML targeting. In context of a Tandem-CAR (2.3) target cells need to express both target antigens at the same time. Therefore, the percentages of double positive AML blasts were determined for each target antigen combination. Cut-off was arbitrarily set at 50 % double positive blasts.

Here, CD33/CLL1 turned out to be the combination, for which the most AML patients of our cohort (21/29 patients, 72 %) had at least 50 % double positive blasts (Figure 67A).

Of the remaining 8 AML patients, which could not be covered using CD33/CLL1, another 2 patients had at least 50 % double positive blasts for the combination out of CD33 and TIM-3 and 1 patient each could be covered by the usage of CD33/CD135 and CLL1/CD135. So, in the context of a

Tandem-CAR with the cut-off set at 50 % double positive blasts 86 % (25/29 patients) of our patient cohort could be covered by using one of the mentioned target antigen combinations (Figure 67B).

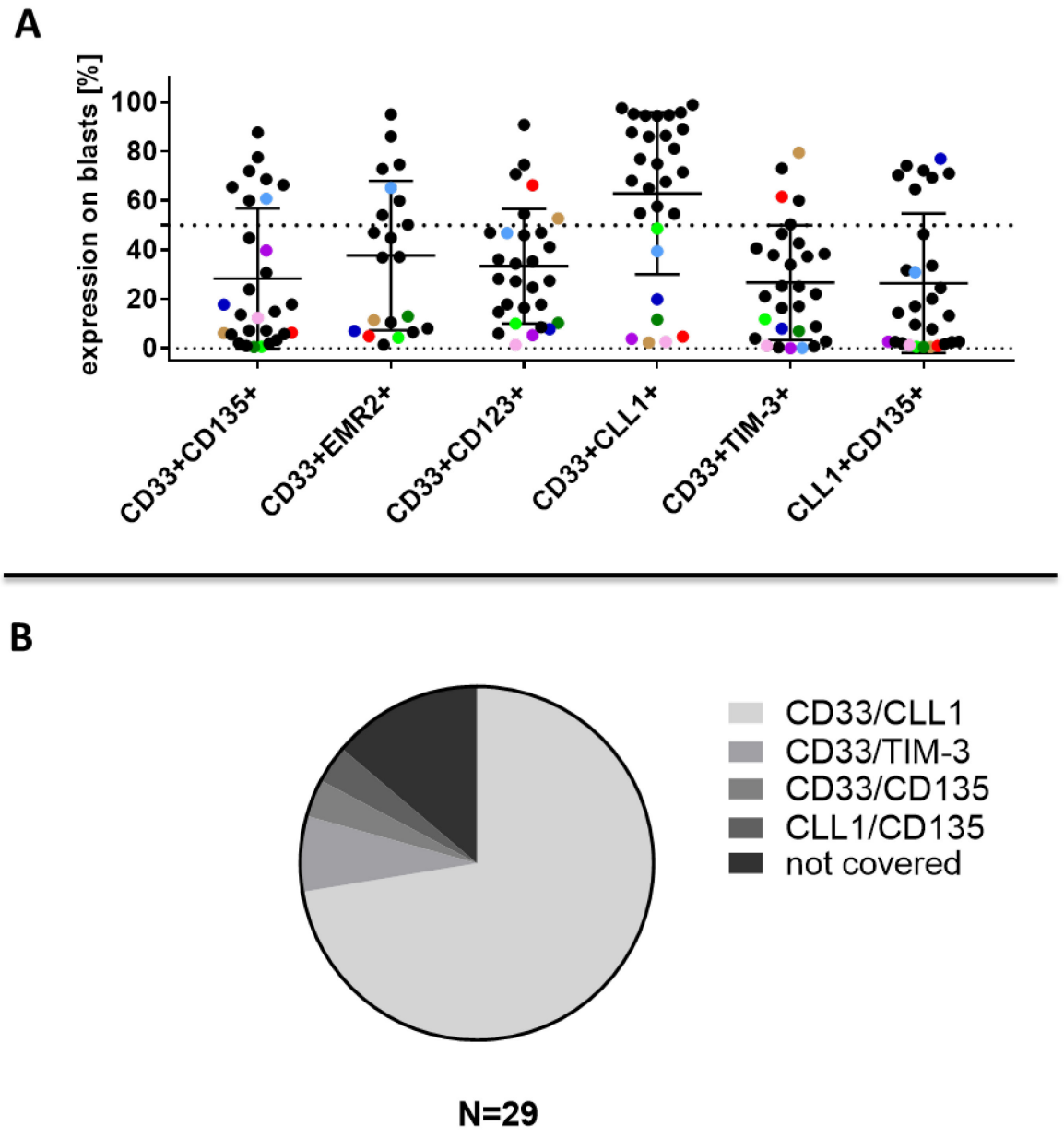

Figure 67: Antigen co-expression on AML blasts. A) For each combination of antigens the percentage of double positive AML blasts was determined. Cut-off was set at 50% double positive blasts. For CD33-CLL1 the most AML patients of our cohort (21/29, 72 %) had at least 50 % double positive blasts in comparison to the other tested antigen combinations. AML patients with less than 50 % CD33/CLL1 double positive blasts were color-coded in order to evaluate those also in terms of expression of the other target antigen combinations. **B)** Under the condition that at least 50 % of all AML blasts were double positive, 21 out of 29 patients could be covered by using CD33/CLL1 (72 %). By the additional usage of CD33/TIM-3, CD33/CD135 and CLL1/CD135 25/29 patients (86 %) could be covered. 4 patients (14 %) would not be coverable with mentioned antigen combinations.

In the project, $CD45_{dim}$ cells in AML patient samples were defined as AML blasts (5.6.1, Figure 11). This gating is widely used for isolating blasts by flow cytometry, even though it was shown that other cells contaminate this "blast gate" (Harrington et al., 2012). However, due to the lack of common specific antigens of all AML subtypes, we decided to stay with this method in order to classify AML blasts.

In this context, it was analyzed, whether the blast count documented at the time point of AML diagnosis, was correlated with the percentage of CD33/CLL1 double positive blasts (not shown). In case, that a low blast count would indicate a higher probability of contamination of the identified "blast population", a low percentage of CD33/CLL1 double positive blasts could be correlated with a low blast count at AML diagnosis, but no significant correlation could be shown.

6.3.3.2 Identification of CD33-CLL1 as best combination for a synNotch-gated CAR

In parts, the following results have already been published in an adapted form by our working group in Willier et al., 2021.

An alternative approach for dual targeting CAR T cells is the synNotch-gated CAR (2.3). As the mechanism of action differs from the Tandem-CAR, the following criteria were taken into account: at least 20 % blasts had to be positive for the antigen 1 (inductor antigen), whereas for the antigen 2 (target antigen) more than 80 % blasts had to be positive. Cut-off values were set arbitrarily, but with respect to the mechanism of action of a synNotch-gated CAR.

Under these conditions, the most patients of our cohort (19/29, 66 %) could be covered by using CLL1 as inductor (I) and CD33 as target (T) antigen (Figure 68A).

Of the remaining 10 patients 2 additional patients each could be covered by the usage of CD135I/CLL1T, TIM-3I/CD33T and TIM-3I/CLL1T. By using CD135 as inductor antigen and CD33 as target antigen coverage of 1 more patient was possible. So, in the context of a synNotch-gated CAR 90 % (26/29 patients) of all analyzed patients could be covered by the usage of one of the mentioned target antigen combinations under the set conditions (Figure 68B).

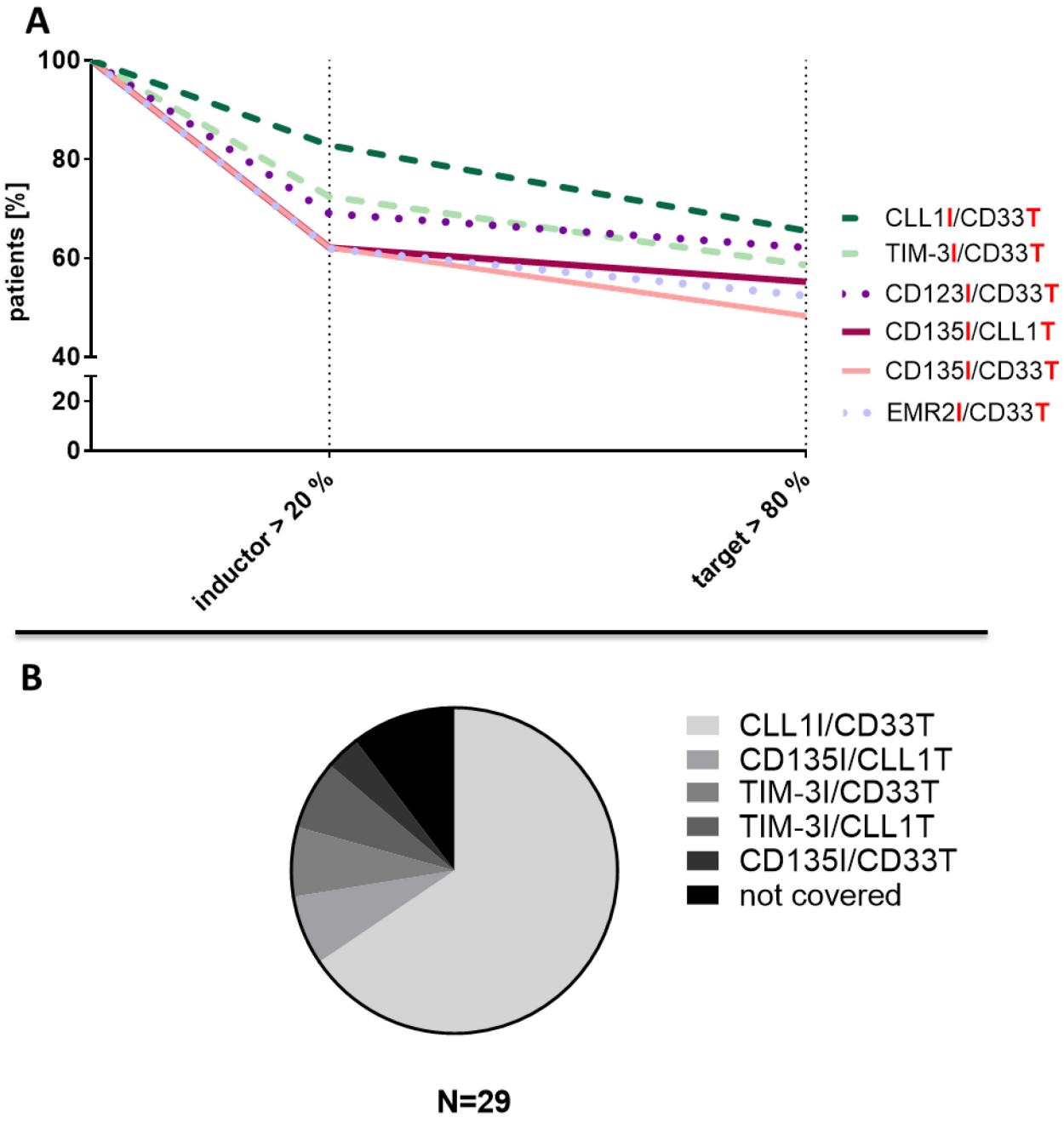

Figure 68: Identification of CD33I/CLL1T as best combination for a synNotch-gated CAR. For a synNotch-gated CAR the following criteria were taken into account: at least 20 % of all blasts had to be positive for the inductor antigen, for the target antigen more than 80 % blasts had to be positive. For EMR2I/CD33T only 21 patients were tested, whereas for all other combinations 29 patients were evaluated. **A)** Using CLL1 as inductor and CD33 as target the most patients (19/29, 66 %) could be covered in comparison to other tested combinations. **B)** By additional usage of CD135I/CLL1T, TIM-3I/CD33T, TIM-3I/CLL1T and CD135I/CD33T 26/29 patients (90 %) could be covered. 3 patients (10 %) would not be covered by using mentioned antigen combinations. I: inductor antigen, T: target antigen.

6.3.3.3 EOL-1 as appropriate human AML cell line for functionality measurement of a CD33/CLL1 Tandem-CAR and a CLL1I/CD33T synNotch-gated CAR

In context of possible functionality assays CAR target antigen expression levels were evaluated on the human AML cell lines EOL-1, OCI-AML, THP-1 and MOLM-13 (N=1). Under the same conditions as in 6.3.3.1 and 6.3.3.2 EOL-1 would be an appropriate cell line to use in functionality measurement of a CD33/CLL1 Tandem-CAR, as well as of a CLL1I/CD33T synNotch-gated CAR (Figure 69).

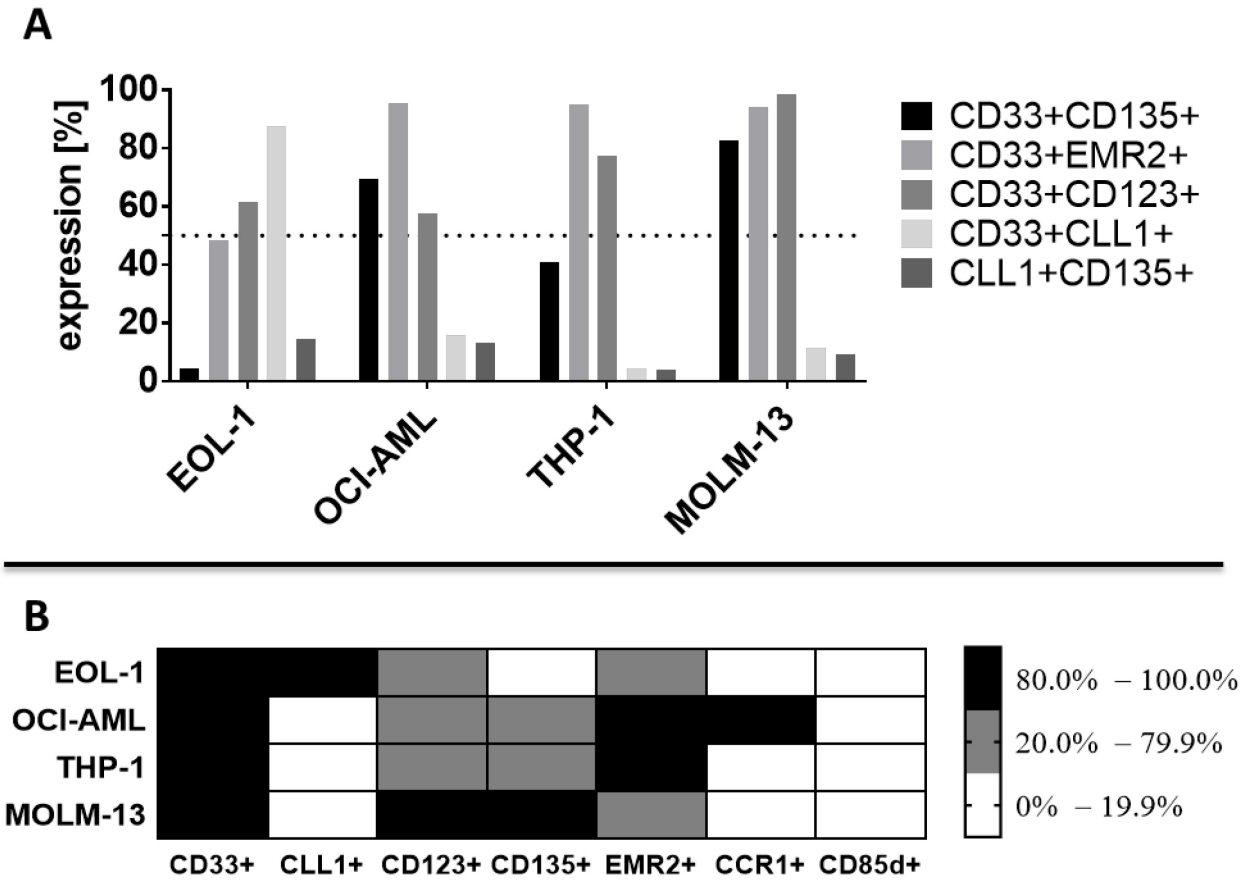

Figure 69: Antigen expression on human AML cell lines EOL-1, OCI-AML, THP-1 and MOLM-13 (N=1). A) For each combination of antigens the percentage of double positive cells was determined. Cut-off was set at 50% double positive blasts in context of a Tandem-CAR. Under this condition EOL-1 would be an appropriate cell line to use in a functionality assay for a CD33/CLL1 Tandem-CAR. **B)** In context of a synNotch-gated CAR expression levels of single antigens were evaluated on cell lines. With a CLL1 expression level higher than 20 % and CD33 higher expressed than 80 %, EOL-1 could be used in functionality measurement of a CLL1I/CD33T synNotch-gated CAR. I: inductor antigen, T: target antigen.

6.3.3.4 Reduced Expression of CD33 and CLL1 and increased expression of TIM-3 on leukemic stem cells compared to bulk AML cells

In parts, the following results have already been published in an adapted form by our working group in Willier et al., 2021.

As shown in Figure 70 AML associated antigens CD33, TIM-3 and CLL1 were additionally analyzed for expression on leukemic stem cells (LSCs). Comparing antigen expression levels on AML bulk cells and LSCs using Wilcoxon matched-pairs signed rank test, mean expression (N=29) of CD33 (74.3 % vs. 82.6 %, p=0.0689) and CLL1 (58.9 % vs. 71.7 %, p=0.0005) was reduced on LSCs in comparison to AML bulk cells, whereas TIM-3 was slightly higher expressed on LSCs (39.1 % vs. 37.5 %, p=0.2470). Only the reduction of CLL1 on LSCs compared to AML bulk cells reached statistical significance. Other possible CAR target antigens were not analyzed on LSCs.

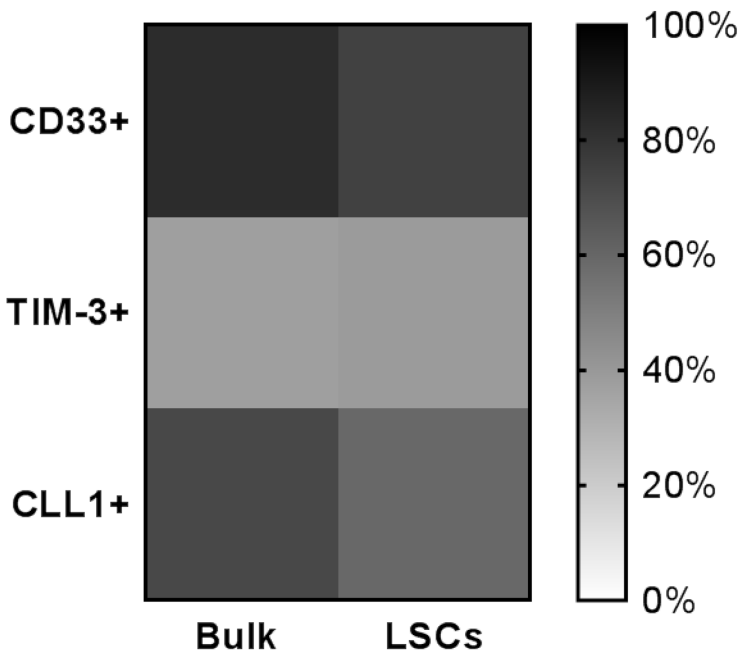

Figure 70: Antigen expression on LSCs and AML bulk cells. Summary of antigen expression levels (mean expression rate within all analyzed patients in %, N=29): Mean expression of CD33 and CLL1 was reduced on LSCs in comparison to AML bulk cells, whereas TIM-3 was slightly higher expressed on LSCs. Only the reduction of CLL1 on LSCs compared to AML bulk cells was reaching statistical significance (p=0.0005). For comparison Wilcoxon matched-pairs signed rank test was used. LSCs: Leukemic stem cells, Bulk: Bulk AML cells

6.4 Flow cytometric phenotype analysis of NK and NKT cells in the bone marrow of AML patients

NK and NKT cells in the bone marrow were phenotypically analyzed for frequency, maturation stages and expression of immune-modulatory surface molecules.

6.4.1 Increased frequency of NK cells and increased frequency of late NK cell differentiation stages in the bone marrow of AML patients

As shown in Figure 23, the frequency of NK cells among $CD45_{high}CD3$- cells was increased in AML patients compared to healthy BM donors (25.1 % vs. 14.0 %, mean values, p=0.0320).

Furthermore, concerning their differentiation stages, within NK cells there was a shift towards a more mature phenotype in AML patients compared to healthy controls (Figure 71A): The frequency of NK cells with a high proliferation capacity and a rather low cytolytic activity (CD16-CD57-) was significantly reduced in AML patients compared to healthy BM donors (14.7 % vs. 24.4 %, p=0.0159), whereas the number of NK cells with an intermediate proliferation capacity and cytolytic activity (CD16+CD57-) was increased in AML patients (66.8 % vs. 53.3 %, p=0.0233).
In relapsed AML samples the frequency of CD16-CD57- NK cells was increased (22.0 % vs. 12.6 %, p=0.0330, Figure 71B) in comparison to initial AML samples, while the number of NK cells with a low proliferation capacity and a high cytolytic activity (CD16+CD57+) was reduced in relapsed AML samples (7.5 % vs. 22.1 %, p=0.0047, Figure 71B).
Between initial AML samples with and without future relapse there were no significant differences determined concerning maturation stages of NK cells (not shown).

Regarding CD16/CD56 distribution (Figure 71C) within NK cells the frequency of CD16-CD56+ NK cells was significantly higher (21.4 % vs. 9.3 %, p=0.0080) in relapsed AML samples in comparison to initial AML samples. Between initial AML samples with and without future relapse there were no differences detected (not shown). The difference of the CD16/CD56 distribution between AML patients and healthy BM donors was not analyzed.

Concerning the expression of TIGIT, CD226 and CD57 on NK cells in the bone marrow (Figure 72), the only difference detected was a decreasing CD57 expression in relapsed AML samples compared to initial AML samples (7.2 % vs. 18.4 %, p=0.0345). The difference of CD57 single expression between AML patients and healthy BM donors was not analyzed.

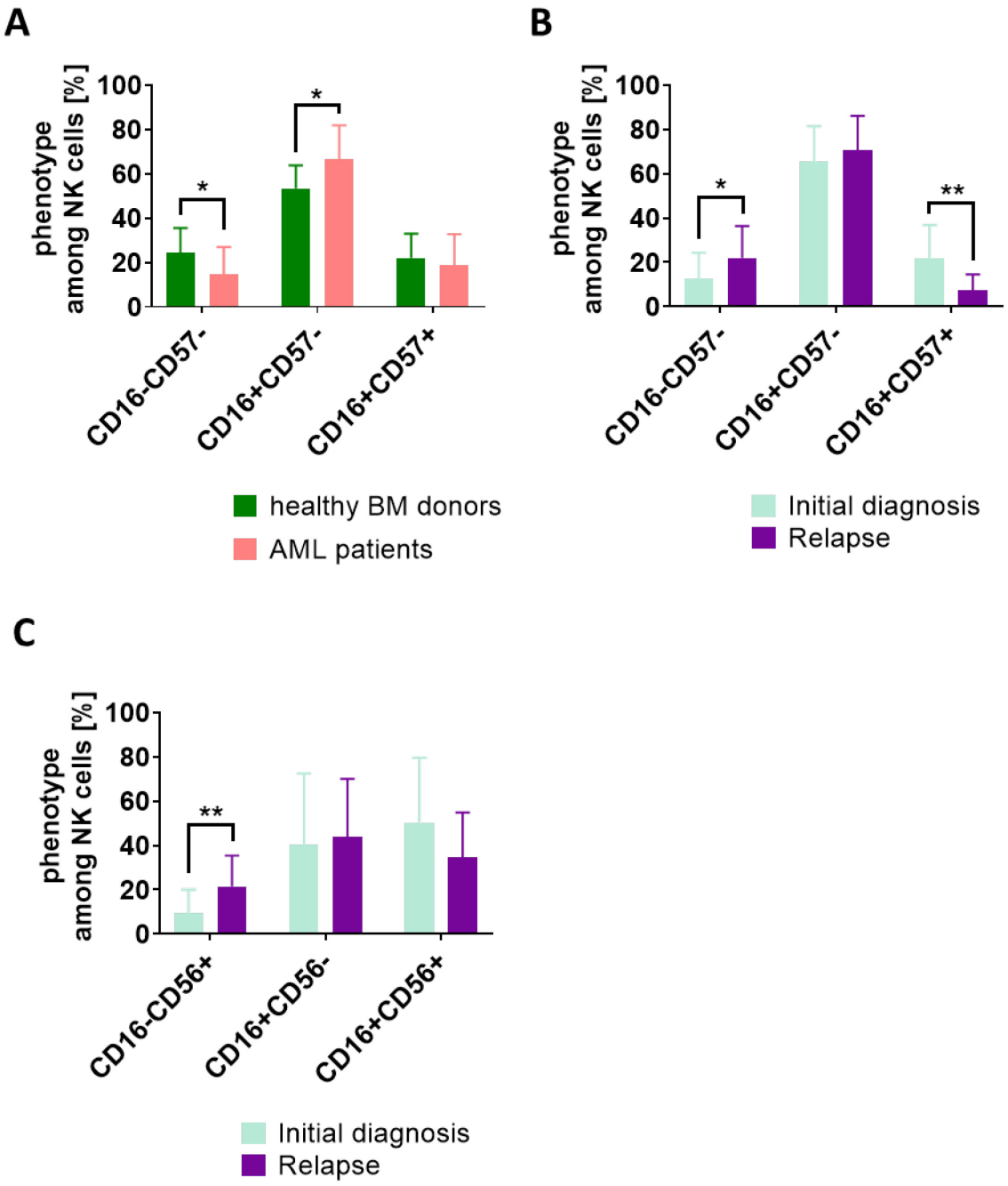

Figure 71: Alteration of the NK cell phenotype in AML bone marrow compared to healthy controls. A) The frequency of CD16-CD57- NK cells (high proliferation capacity, low cytolytic activity) was significantly reduced (p=0.0159) in AML patients (N=29) compared to healthy BM donors (N=9), whereas the number of CD16+CD57- NK cells (intermediate proliferation capacity, intermediate cytolytic activity) was increased in AML patients (p=0.0233). **B)** In relapsed AML samples (N=12) the frequency of CD16-CD57- NK cells was increased (p=0.0330) in comparison to initial AML samples (N=21), while the number of CD16+CD57+ NK cells (low proliferation capacity, high cytolytic activity) was reduced in relapsed AML samples (p=0.0047). **C)** The frequency of CD16-CD56+ NK cells was significantly higher (p=0.008) in relapsed AML samples (N=12) in comparison to initial AML samples (N=13). Healthy BM donors: healthy bone marrow donors.

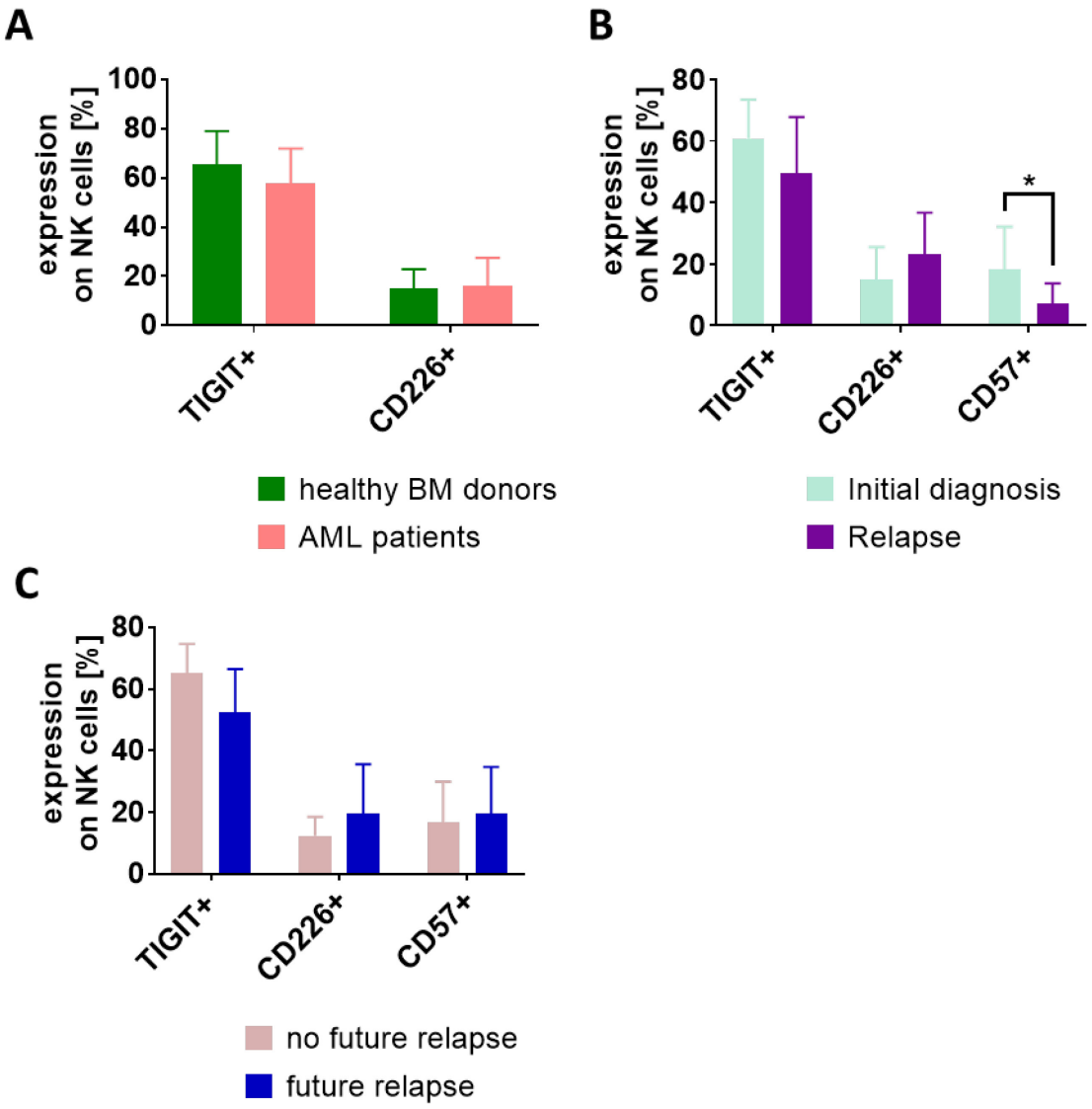

Figure 72: Antigen expression on NK cells in AML patients. A)-C) CD57 expression was significantly reduced (p=0.0345) in relapsed AML samples (N=12) compared to initial AML samples (N≥13). Healthy BM donors: healthy bone marrow donors.

6.4.2 NKT cells in the bone marrow of AML patients

The frequency of NKT cells among $CD45_{high}CD3+$ cells in the bone marrow of AML patients was not altered in comparison to healthy BM donors (Figure 23).

With regard to their CD56/CD16 distribution (Figure 73) the frequency of CD16+CD56+ NKT cells was increased in initial AML samples without future relapse compared to initial AML samples with future relapse (5.4 % vs. 1.7 %, p=0.0350). Between initial AML samples and relapsed AML samples there were no differences detected (not shown). The difference between AML patients and healthy BM donors concerning the CD56/CD16 distribution was not analyzed.

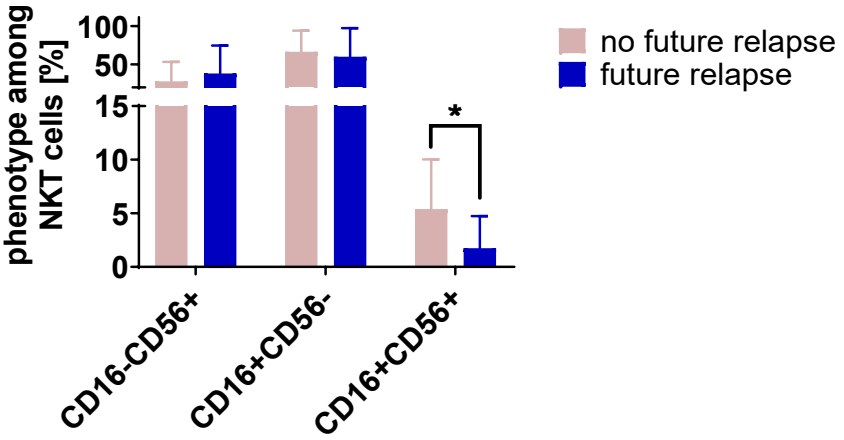

Figure 73: General characteristics of NKT cells in AML patients. The frequency of CD16+CD56+ NKT cells was higher (p=0.0350) in initial AML samples without future relapse (N=6) compared to initial AML samples with future relapse (N=7).

Concerning the expression of TIGIT, CD226 and CD57 on NKT cells there were no differences reaching statistical significance (Figure 74).

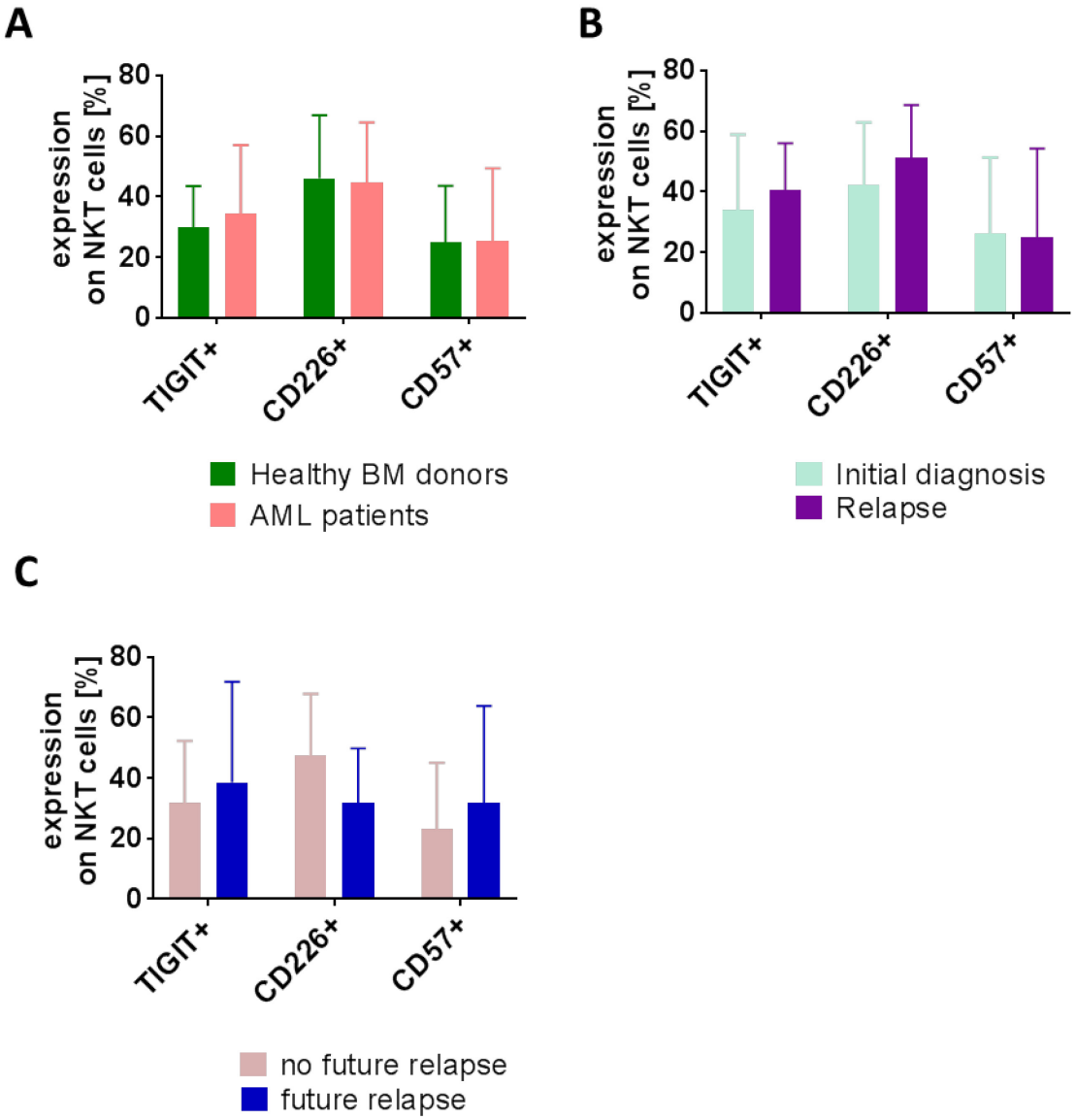

Figure 74: Antigen expression on NKT cells in AML patients. A)-C) There were no significant differences detected in terms of antigen expression. Healthy BM donors: healthy bone marrow donors.

6.5 Interaction of AML blasts with T cells, NK and NKT cells in patient bone marrow

Finally, we examined whether the observed changes in phenotype of physiologic immune cells (T cells, NK and NKT cells) were linked to blast phenotype. Thus, to determine whether AML blasts do induce e.g. T cell phenotype changes we analyzed two common axes of interaction between antigen-presenting cells (APCs) and T cells in the context of AML. To that end, we correlated the expression of CD86 and CD112/CD155 on AML blasts to the respective expression of CTLA-4/CD28 on bmT cells and TIGIT/CD226 on bmT cells, NK and NKT cells (6.5.1 and 6.5.2).

6.5.1 Missing correlation of increased CD86 expression on AML blasts with a change in CD28/CTLA-4 expression on bmT cells

CD86 was significantly overexpressed on AML blasts compared to healthy controls (13.3 % vs. 0.1 %, mean values, p<0.0001). Here, patients A007 (83.2 %), A302 (75.1 %) and A308 (46.6 %) showed the highest CD86 expression in our patient cohort (Figure 75A). To determine, if there was any connection between a high CD86 expression on AML blasts and the CTLA-4/CD28 expression on bmT cells, CD28 expression rates were plotted against CTLA-4 expression rates. But as Figure 75B shows, mentioned linkage was not detectable, nor could be shown that for example a reduced CD28 expression on bmT cells was connected with an increased CTLA-4 expression on bmT cells.

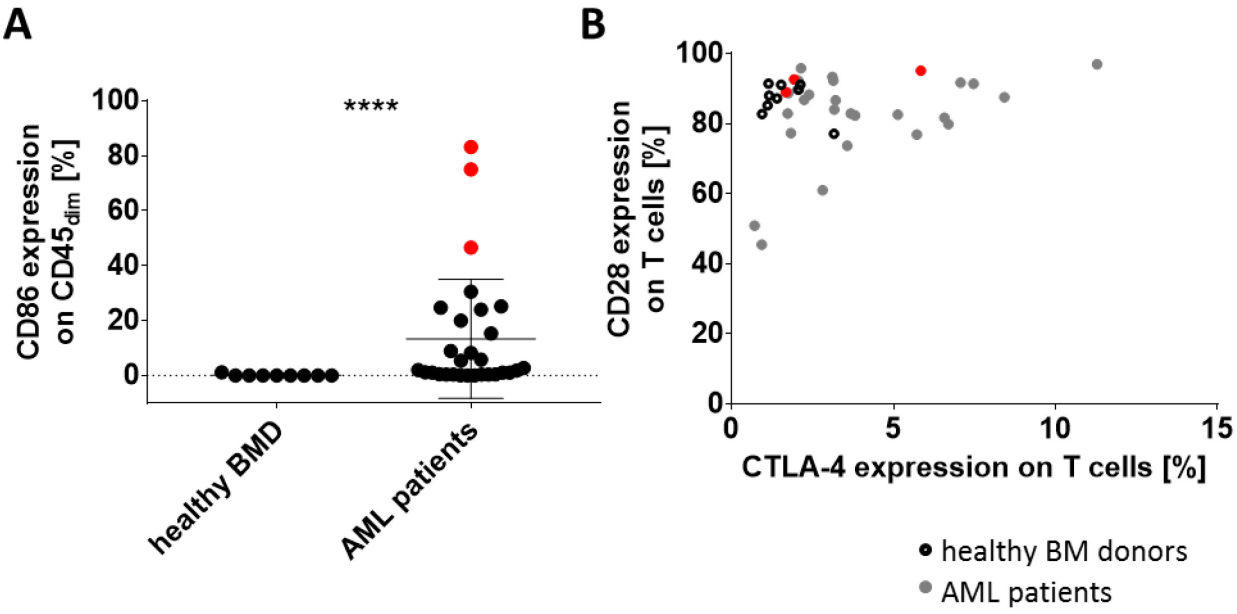

Figure 75: Missing correlation of increased CD86 expression on AML blasts with a change in CD28/CTLA-4 expression on bmT cells. A) CD86 was significantly overexpressed on AML blasts compared to $CD45_{dim}$ cells in healthy BM donors (p<0.0001). Patients A007 (83.2 %), A302 (75.1 %) and A308 (46.6 %) showed the highest CD86 expression (marked in red). **B)** CD28 expression rates on bmT cells were plotted against CTLA-4 expression rates on bmT cells. Mentioned patients A007, A302 and A308 are marked in red. Healthy BMD/healthy BM donors: healthy bone marrow donors.

6.5.2 Correlation of a high CD112 expression on AML blasts with a low expression of CD226 on bmT cells, NK and NKT cells

CD112 was significantly overexpressed on AML blasts compared to $CD45_{dim}$ cells in healthy BM donors (55.4 % vs. 6.6 %, p=0.0002), whereas CD155 showed only low expression levels on AML blasts. As shown in Figure 76, within our patient cohort CD112 expression showed a trimodal

distribution on AML blasts. In context to that AML patients were divided into three groups: AML patients with low ($CD112_{low}$), intermediate ($CD112_{int}$) and high CD112 expression ($CD112_{high}$) on blasts. Divided into these three groups AML patients were compared in relation to their TIGIT and CD226 expression on bmT cells, NK and NKT cells (Figure 77):

Regarding TIGIT expression levels there were no significant differences determined within AML patients, with the exception of a significant higher TIGIT expression on NK cells of AML patients with $CD112_{high}$ blasts compared to AML patients with $CD112_{int}$ blasts (62.7 % vs. 49.0 %, p=0.0309).

CD226 was significantly downregulated on bmT cells of AML patients with $CD112_{high}$ blasts in comparison to AML patients with $CD112_{int}$ (20.1 % vs. 32.2 %, p=0.0379) and $CD112_{low}$ (20.1 % vs. 38.2 %, p=0.0064) blasts.

On NK (11.4 % vs. 21.6 %, p=0.0421) and NKT cells (38.2 % vs. 59.4 %, p=0.0064) CD226 was significantly lower expressed in AML patients with $CD112_{high}$ blasts compared to AML patients with $CD112_{low}$ blasts.

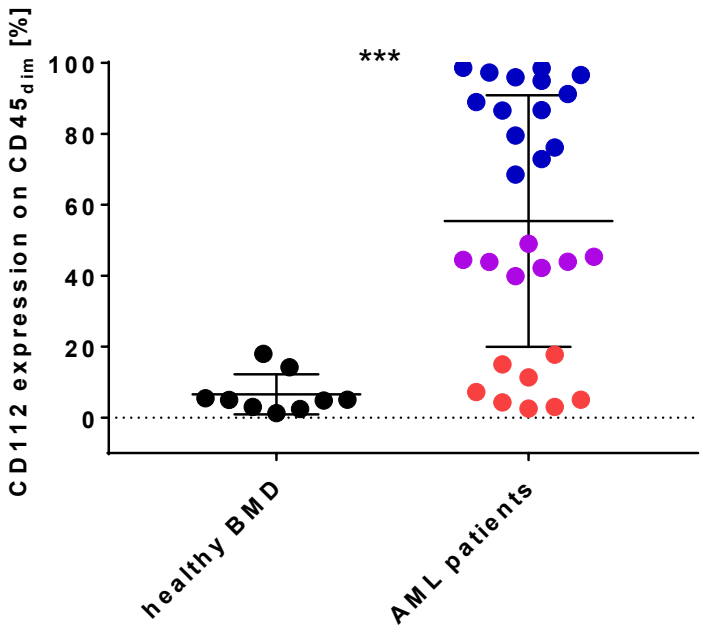

Figure 76: CD112 expression on AML blasts compared to $CD45_{dim}$ cells in healthy BM donors. CD112 was significantly overexpressed on AML blasts compared to $CD45_{dim}$ cells in healthy BM donors (p=0.0002). AML patients showed a trimodal distribution of CD112 expression on AML blasts: $CD112_{low}$ (in red), $CD112_{int}$ (in purple) and $CD112_{high}$ (in blue) AML blasts. Int: intermediate, healthy BMD: healthy bone marrow donors.

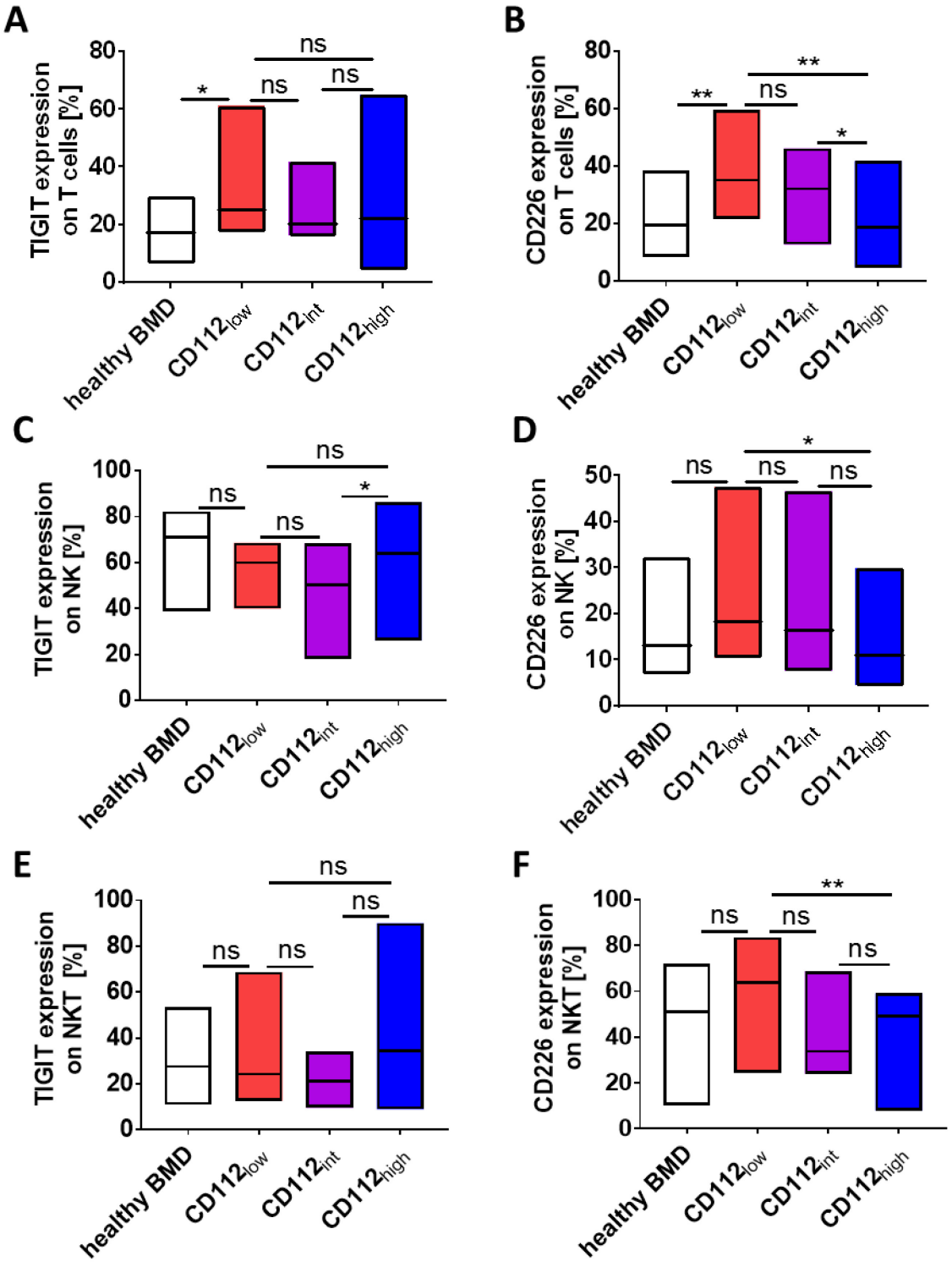

Figure 77: Interaction of CD112 on AML blasts with TIGIT/CD226 on bmT cells, NK and NKT cells. AML patients were divided into three groups according to their CD112 expression level on blasts and compared concerning their TIGIT/CD226 expression rates on bmT cells, NK and NKT cells. **A), C) and E)** With regards to TIGIT expression levels there were no significant differences determined within AML patients, with the exception of a significant higher TIGIT expression on NK cells of AML patients with $CD112_{high}$ blasts compared to AML patients with $CD112_{int}$ blasts (p=0.0309). **B), D) and F)** CD226 was significantly downregulated on bmT cells of AML patients with $CD112_{high}$ blasts in comparison to AML patients with $CD112_{int}$ (p=0.0379) and $CD112_{low}$ (p=0.0064) blasts. On NK (p=0.0421) and NKT cells (p=0.0064) CD226 was significantly lower expressed in AML patients with $CD112_{high}$ blasts compared to AML patients with $CD112_{low}$ blasts. Healthy BMD: healthy bone marrow donors, int: intermediate.

6.6 Bridging the gap between phenotype and genotype of CD8+ bmT cells via RNA-seq

Flow cytometry analysis of CD8+ bmT cells showed some pronounced differences between AML patient samples and healthy BM donors (6.2.4). Bridging the gap between phenotype and genotype of CD8+ bmT cells, RNA-seq and gene expression analyses were performed. RNA-seq and filtering of sequenced genes was performed by Dr. med. Semjon Willier. Analysis of filtered genes was performed by me.

Filtering of sequenced genes was performed in two steps. Firstly, all genes with RPKM≥2 in both groups were exported. Secondly, the 11022 exported genes were filtered under the following conditions: (1) RPKM≥2 in AML patient samples, (2) RPKM≥2 in healthy BM donor samples, (3) FC≥2, (4) $p<0.05$. Filtering revealed 234 genes. Consequently, filtered genes were scanned manually with regard to general and CD8+ T cell-specific functional relevance (Figure 78). PRF1 (Perforin 1, p=0.0007, FC=3.04) and GZMB (Granzyme B, p=0.0025, FC=3.94) were higher expressed by CD8+ bmT cells in AML patient samples in comparison to healthy BM donors. CREM (reported enhancer of IL21 expression, Ohl et al., 2016, p=0.0008, FC=0.22), IL21R (IL21 receptor, p=0.0005, FC=0.37), REL (c-Rel, NF-κB subunit, p=0.0012, FC=0.34), IFRD1 (Interferon related developmental regulator 1, shown to suppress NF-κB, Tummers et al., 2015, p=0.0024, FC=0.28), NFKBIA (NF-κB inhibitor alpha, p=0.0341, FC=0.43), TRIM39 (Tripartite motif containing 39, reported to negatively regulate NF-κB-mediated signaling pathway, Suzuki et al., 2016, p=0.0439, FC=0.46) and RARA (Retinoic acid receptor alpha, shown to be required for CD8+ T cell survival and expression of effector molecules, Guo et al., 2014, p=0.0039, FC=0.38) were less expressed by CD8+ bmT cells in AML patient samples.

In Figure 79, the only genes shown are coding for molecules from the flow cytometry analysis of CD8+ bmT cells. In contrast to the differences detected there, in RNA-seq analysis CD27 (p=0.0167, FC=2.47) and LAG3 (p=0.0494, FC=2.37) were the only genes significantly higher expressed in AML patient samples in comparison to healthy BM donors. ENTPD1 and B3GAT1 coding for CD39 and CD57 were not part of the filtered genes and were therefore added in this graph.

For gene expression analyses of initial AML samples without future relapse in comparison to initial AML samples with future relapse, we proceeded in the same way as described above. Filtering of 11328 exported genes revealed 13 genes. Depending on their functional relevance, genes were selected and color-coded (Figure 80): TNFRSF4 (CD134, p=0.0476, FC=3.80) was higher expressed in initial AML samples with future relapse, whereas DYNLT1 (Dynein light chain Tctex-type 1, reported to play a role in hypoxic cytoprotection, Fang et al., 2011, p=0.0386, FC=0.29) was less expressed in comparison to initial AML samples without future relapse.

As one can see in Figure 81, TNFRSF4 was also the single significantly differently expressed gene within the other genes coding for molecules from the flow cytometry analysis of CD8+ bmT cells. This is consistent with the flow cytometry results.

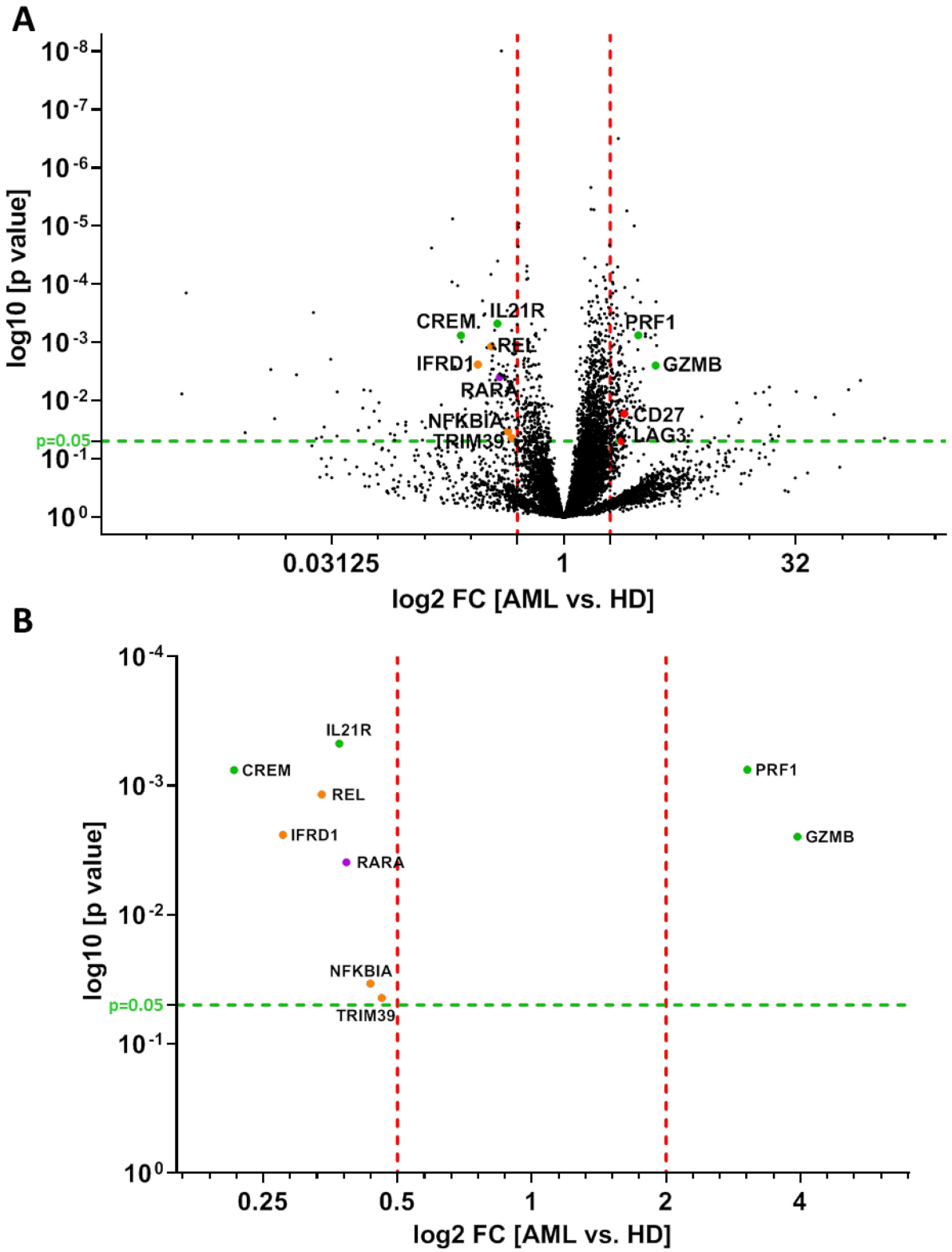

Figure 78: Differential gene expression of CD8+ bmT cells in AML patients (N=20) in comparison to healthy BM donors (N=14). Gene expression data from RNA sequencing. **A)** Volcano plot showing differential expression of coding genes in CD8+ bmT cells in AML patient samples compared to healthy BM donors. Genes were filtered under the following conditions: (1) RPKM≥2 in AML patient samples, (2) RPKM≥2 in healthy BM donor samples, (3) FC≥2, (4) p<0.05. Filtering revealed 234 genes. Depending on their functional relevance, filtered genes were selected and color-coded. Red lines show fold change cut-off of 2 (p<0.05). For multiple testing correction, Student's t-test and Benjamini Hochberg were used. **B)** Volcano blot showing only the color-coded genes. PRF1 (Perforin 1, p=0.0007, FC=3.04) and GZMB (Granzyme B, p=0.0025, FC=3.94) were higher expressed by CD8+ bmT cells in AML patient samples in comparison to healthy BM donors. CREM (reported enhancer of IL21 expression, Ohl et al., 2016, p=0.0008, FC=0.22), IL21R (IL21 receptor, p=0.0005, FC=0.37), REL (c-Rel, NF-κB subunit, p=0.0012, FC=0.34), IFRD1 (Interferon related developmental regulator 1, shown to suppress NF-κB, Tummers et al., 2015, p=0.0024, FC=0.28), NFKBIA (NF-κB inhibitor alpha, p=0.0341, FC=0.43), TRIM39 (Tripartite motif containing 39, reported to negatively regulate NF-κB-mediated signaling pathway, Suzuki et al., 2016, p=0.0439, FC=0.46) and RARA (Retinoic acid receptor alpha, shown to be required for CD8+ T cell survival and expression of effector molecules, Guo et al., 2014, p=0.0039, FC=0.38) were less expressed by CD8+ bmT cells in AML patient samples. RPKM: reads per kilo base per million mapped reads, FC: fold change, HD: healthy bone marrow donors.

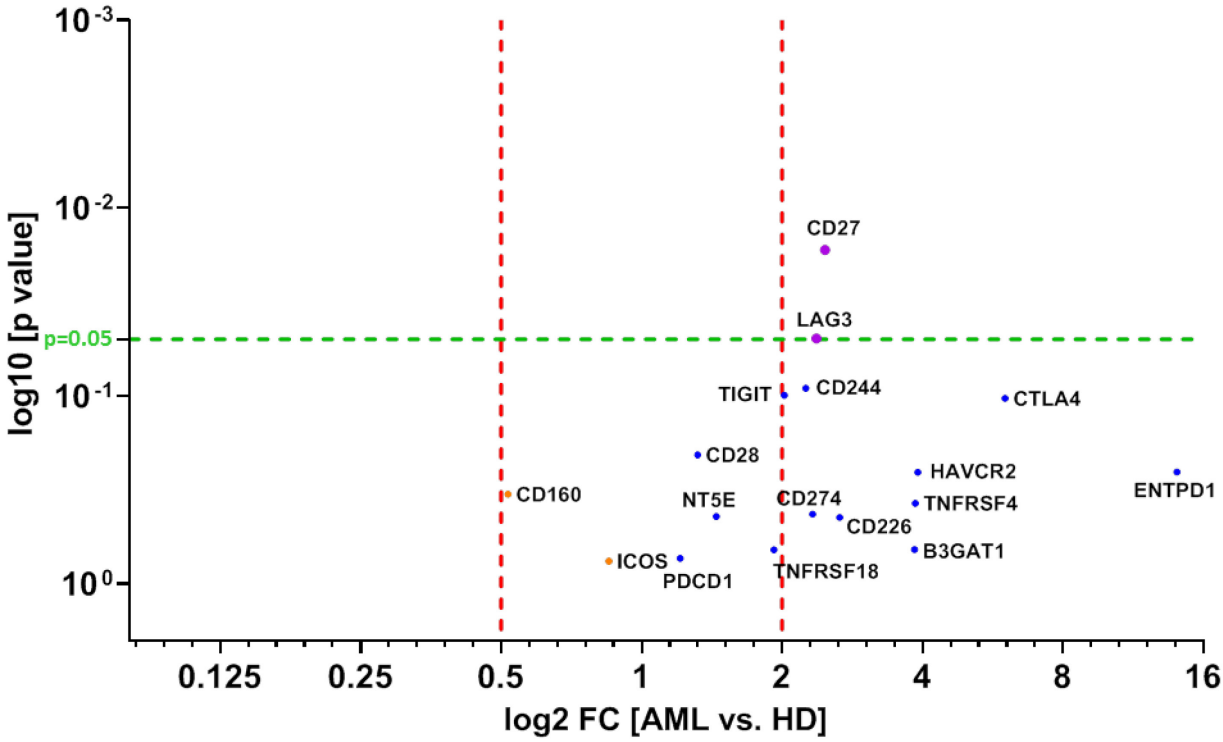

Figure 79: Differential gene expression of CD8+ bmT cells in AML patients (N=20) in comparison to healthy BM donors (N=14). Gene expression data from RNA sequencing. The only genes shown are coding for molecules from the flow cytometry analysis of CD8+ bmT cells. Red lines show fold change cut-off of 2 (p<0.05). For multiple testing correction, Student's t-test and Benjamini Hochberg were used. CD27 (p=0.0167, FC=2.47) and LAG3 (p=0.0494, FC=2.37) coding for CD27 and LAG-3 were the only genes significantly higher expressed in AML patient samples in comparison to healthy BM donor samples (marked in purple). Blue dots indicate upregulated genes in AML patient samples, orange dots indicate downregulated genes (not statistically significant). ENTPD1 and B3GAT1 coding for CD39 and CD57 were not part of the filtered genes and were therefore added in this graph. FC: fold change, HD: healthy bone marrow donors.

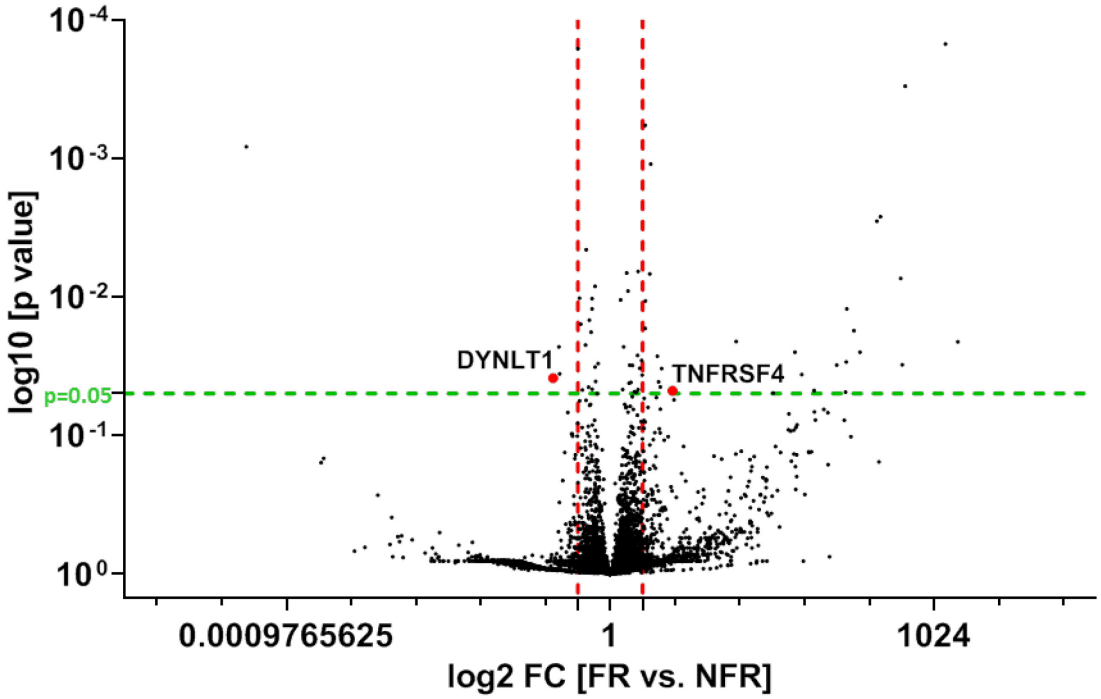

Figure 80: Differential gene expression of CD8+ bmT cells in initial AML samples with (N=4) and without (N=10) future relapse. Gene expression data from RNA sequencing. Volcano plot showing differential expression of coding genes in CD8+ bmT cells in initial AML samples with future relapse compared to initial AML samples without future relapse. Genes were filtered under the following conditions: (1) RPKM≥2 in initial AML samples without future relapse, (2) RPKM≥2 in initial AML samples with future relapse, (3) FC≥2, (4) $p<0.05$. Filtering revealed 13 genes. Depending on their functional relevance, filtered genes were color-coded: TNFRSF4 ($p=0.0476$, FC=3.80) coding for CD134 and DYNLT1 ($p=0.0386$, FC=0.29) coding for Dynein light chain Tctex-type 1 (reported to play a role in hypoxic cytoprotection, Fang et al., 2011). Red lines show fold change cut-off of 2 ($p<0.05$). For multiple testing correction, Student's t-test and Benjamini Hochberg were used. RPKM: reads per kilo base per million mapped reads, FC: fold change, FR: future relapse, NFR: no future relapse.

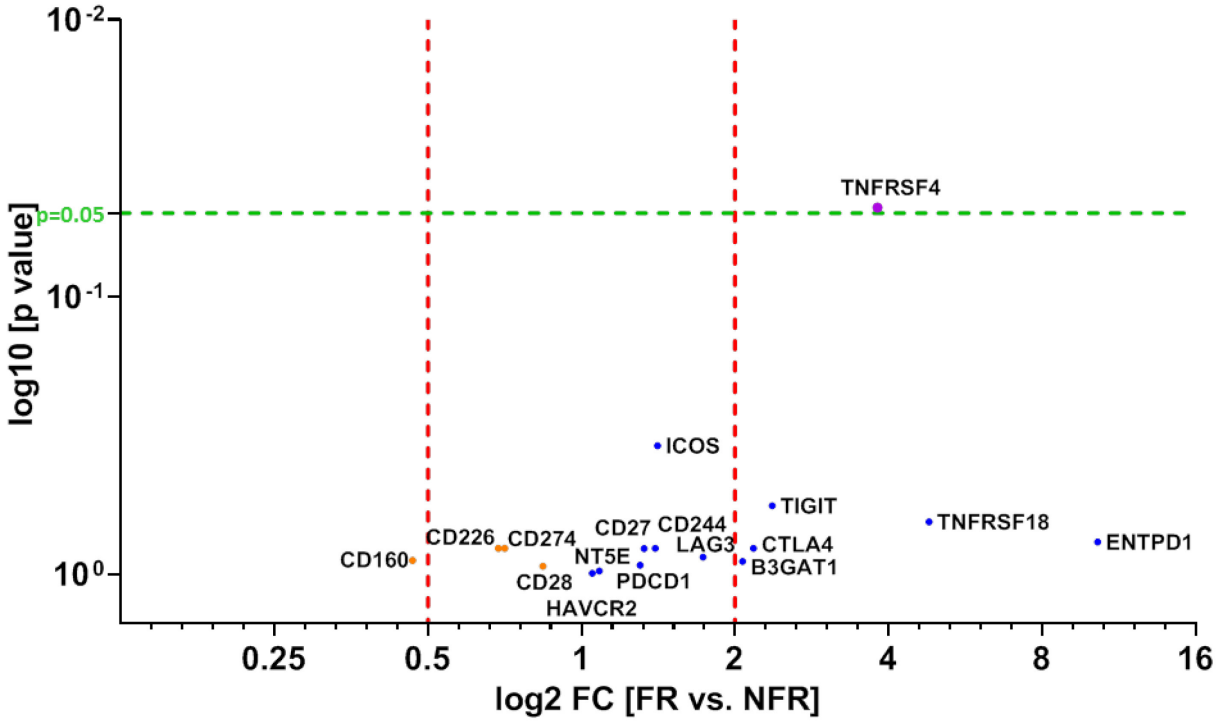

Figure 81: Differential gene expression of CD8+ bmT cells in initial AML samples with (N=4) and without (N=10) future relapse. Gene expression data from RNA sequencing. The only genes shown are coding for molecules from the flow cytometry analysis of CD8+ bmT cells. Red lines show fold change cut-off of 2 ($p<0.05$). For multiple testing correction, Student's t-test and Benjamini Hochberg were used. TNFRSF4 ($p=0.0476$, FC=3.80) coding for CD134 was the only gene significantly higher expressed in initial AML samples with future relapse compared to initial AML samples without future relapse (marked in red). Blue dots indicate upregulated genes in initial AML samples with future relapse, orange dots indicate downregulated genes (not statistically significant). FC: fold change, FR: future relapse, NFR: no future relapse.

6.7 Additional (negative) findings

Fluorochrome	Antigen	Cell type	Function	Problem
BV785	LAG-3	T cells	exhaustion marker	weak fluorochrome
BV650	PD-1	T cells	exhaustion marker	weak fluorochrome
PerCP-Cy5.5	CD70	blasts	AML associated antigen	lack of expression
APC	CD80	blasts	AML associated antigen	lack of expression
BV785	TIM-3	T cells + blasts	exhaustion marker + AML associated antigen	weak fluorochrome
BV421	PD-L1 ec	blasts	ligand for PD-1	lack of expression
APC	MUC1 5E5	blasts	CAR target	lack of expression
PE	MUC1 5E10	blasts	control for MUC1 5E5	lack of expression
BB515	CD96	blasts	CAR target	expression on T cells

Figure 82: Summary of additionally stained antigens. Listed antigens had been omitted from integrated analysis due to mentioned issues. Ec: extracellularly stained.

Antigens listed in Figure 82 had been stained additionally in the study for several reasons, but finally had been omitted from integrated analysis due to mentioned issues.

Figure 83 shows all objects of comparison between relapsed AML samples (1st relapse) within chemotherapy treatment (N=4) and upon completion of chemotherapy treatment of initial diagnosis (N=4): As there were no significant differences for all objects of comparison detected, all samples from 1st relapse were treated equally.

Object of comparison	Cell type
TIM-3 expression	T cells
2B4 expression	T cells
PD-1 expression	T cells
CD134 expression	T cells
ICOS expression	T cells
GITR expression	T cells
TCRγδ expression	T cells
proportion of Tregs	CD4+ T cells
proportion of Th0	CD4+ T cells
proportion of Th1	CD4+ T cells
proportion of Th2	CD4+ T cells
CD25 expression	CD4+ T cells
proportion of CD16-CD57+	NK cells
proportion of CD16+CD57+	NK cells
proportion of CD16+CD57-	NK cells
proportion of CD16-CD57-	NK cells

Object of comparison	Cell type
CLL1 expression	blasts
CD33 expression	blasts
CD112 expression	blasts
CD86 expression	blasts
TIM-3 expression	blasts

Figure 83: Objects of comparison between relapsed AML samples (1st relapse) within chemotherapy treatment (N=4) and upon completion of chemotherapy treatment of initial diagnosis (N=4). As there were no significant differences for all objects of comparison detected, all samples from 1st relapse were treated equally in analysis.

7 Discussion

The impressive success of T-cell-mediated immunotherapy in the treatment of pediatric B-ALL emphasizes the irrefutable benefit of anti-cancer immunotherapy in children (Majzner et al., 2017; Maude et al., 2018). As indicated in pediatric ALL patients by Zamora et al. in 2019, pediatric leukemia patients do generate functional neoantigen-specific antitumor T cell responses. However, in pediatric AML, there are still many hurdles to overcome in order to accelerate progress in immunotherapy, especially due to the unknown immunogenicity of AML (Perna et al., 2017) and lacking usable AML-specific target antigens (Haubner et al., 2019; Mardiana and Gill, 2020). The low number of pediatric AML patients further complicates the situation (Klein et al., 2018), as new findings in immunotherapy of AML have been mainly obtained in adults (Koedijk et al., 2021).
As shown by Alexandrov et al. in 2013, AML was found to have one of the lowest mutational burden within different malignant entities (average of 13 somatic gene mutations in de novo AML patients). Based on the supposition that mutational burden directly correlates with immunogenicity, this indicates a quite low immunogenicity of AML blasts (Austin et al., 2016).
However, tumor-specific antigens could also derive from allegedly noncoding regions and would be missed by standard exome-based approaches, as used e.g. by Alexandrov et al. Here it is to be expected that many further tumor-specific antigens could possibly be identified (Laumont et al., 2018). Furthermore, the question arises whether the mutational quality rather than the overall mutational burden may be more important (Austin et al., 2016; Strickler et al., 2021).
Up until now, not only the successful treatment of AML patients by allogeneic hematopoietic stem cell transplantation (allo-HSCT; Barrett and Le Blanc, 2010; Bleakley and Riddell, 2004), but also rare cases of spontaneous remission in AML patients associated with bacterial infections and resulting triggered immune responses (Müller et al., 2004; Mozafari et al., 2017), have shown the ability of the immune system to eradicate AML blasts. Nevertheless, effective specific immunotherapies for (pediatric) AML are still missing.

To investigate possible interactions between AML blasts and healthy immune cell populations in our patient cohort, we analyzed defined populations within bone marrow samples of 29 pediatric AML patients and 9 healthy bone marrow donors (healthy BM donors). In particular, we analyzed CD4+ T cells, CD8+ T cells, NK cells, NKT cells and leukemic blasts for protein expression by flow cytometry, for RNA expression by RNA-sequencing and for chromatin accessibility by ATAC-sequencing.

In leukemia, the bone marrow serves as tumor microenvironment (TME) for leukemic development with most leukemic cells finally residing in the BM.

Bone marrow T cells have been recognized to comprise relevant populations such as memory CD8+ T cells and tissue-resident memory T cells. Bone marrow memory T cells are largely circulatory, using BM niches as “stopping point”, where they receive survival signals, before re-entering the circulation to contribute to systemic cellular memory immunity, while tissue-resident memory T cells participate in immediate local protection as sessile non-migratory cells (Di Rosa and Gebhardt, 2016). Besides regulating immunity, bmT cells also regulate hematopoietic and bone remodeling systems (Bonomo et al., 2016).

By leukemia onset, those bmT cells are within the site of tumor development and will share characteristics of tumor infiltrating lymphocytes (TILs), even if it is unclear whether additional T cell populations immigrate to the BM due to leukemia or only preexisting populations are present in leukemic BM.

In solid tumors, the presence of tumor-infiltrating lymphocytes has been associated with increased survival (Sato et al., 2005; Oble et al., 2009; Hwang et al., 2012; Barnes and Amir, 2017). For AML patients, a good lymphocyte recovery after chemotherapy is an indicator of good prognosis (Austin et al., 2016). Consequently, we want to establish the relevance of bmT cells in pediatric AML by asking three questions in this study: (7.1) are bmT cell populations changed by the presence of leukemia - and if this is the case - (7.2) are those changes in bmT cells mirrored by expression profiles of AML blasts as a sign of specific blast - T cell - interactions - rather than unspecific bystander effects and finally - (7.3) does T cell phenotype correlate with clinical features such as future relapse. Additionally, we want to examine which AML antigens described for synthetic immunotherapy in adult patients might be of relevance for pediatric AML patients e.g. for CAR T cell approaches (7.4).

7.1 Alteration of bmT cells in AML patients compared to healthy BM donors

Firstly, we assessed whether bmT cell populations are changed in AML patients by comparing bmT cells in AML patients with healthy controls.

7.1.1 Increased frequency of late bmT cell differentiation stages and overexpression of co-inhibitory and co-stimulatory molecules on bmT cells in AML patients compared to healthy bone marrow donors

In flow cytometry, an increased frequency of late bmT cell differentiation stages could be detected in AML patients when comparing with healthy BM donors. Namely, the frequency of naïve bmT cells was reduced, while the frequency of effector memory bmT cells and effector CD4+ bmT cells was increased in AML patients in comparison to healthy controls.

In RNA-seq, CD8+ bmT cells of AML patients showed higher expression rates of the pore-forming protein Perforin and the serine protease Granzyme B compared to healthy BM donors. These two are key players in cytotoxic lymphocyte-mediated target cell lysis, including antitumor cytotoxicity and are particularly highly expressed in effector T cells (Hlongwane et al., 2018; Voskoboinik et al., 2015).
Genes coding for the IL21 receptor and CREM, a reported enhancer of IL21 expression (Ohl et al., 2016), were lower expressed in AML patient samples in comparison to healthy BM donors. IL21 is closely related to IL2, but in the context of adaptive immunotherapy for example it was reported to suppress the maturation of naïve CD8+ T cells into Granzyme B expressing effector CD8+ T cells (Hinrichs et al., 2008).
Therefore, this transcriptomic data aligns with flow cytometry data, where a shift towards a more mature phenotype could be documented in AML patients when comparing with healthy BM donors.
However, IL21 was also shown to exert pleiotropic functions by facilitating the maturation and enhancing the cytotoxicity of CD8+ T cells and NK cells, promoting the differentiation of memory CD8+ T cells and suppressing the induction and function of T_{regs} (Deng et al., 2020). Thus, the role of IL21 pathway in bmT cells needs to be further investigated in the context of pediatric AML before making any more detailed evaluation here.

As described by Xu and colleagues in 2018, the shift from less differentiated T cells to a higher ratio of effector memory and effector T cells, both in peripheral blood and in the bone marrow, especially in younger AML patients (< 60 years), may be due to the constant exposure of T cells to AML blasts and the leukemia microenvironmental physiology.
In case of a leukemia-induced phenomenon via indirect or direct blast-T-cell-interaction, the bmT cells could either present altered tissue-resident memory T cells (Di Rosa and Gebhardt, 2016) or different immigrated populations. Moreover, leukemia leads to increased cell death in the bone marrow and thus could cause an elevated extracellular potassium concentration, which was reported to limit T cell function in context of other tumors (Eil et al., 2016; Ong et al., 2019). Therefore, a rather adaptive response to the tumor microenvironment would be another possible reason for this observation.
Nevertheless, mechanisms reported to be employed by the AML cells to impair anti-leukemic immune responses and therefore to interact with the immune cells have been the high expression of inhibitory ligands on AML blasts and the downregulation of activating ligands and receptors on T cells (Austin et al., 2016; Taghiloo and Asgarian-Omran, 2021).

Consistent with that in our study, the two co-inhibitory markers TIM-3 and PD-1 were found to be significantly overexpressed on all analyzed T cell subsets (CD3+, CD4+ and CD8+ bmT cells), as well as

in co-expression on CD4+ and CD8+ bmT cells in our AML patient cohort compared to healthy controls based on the flow cytometry analysis. In addition, co-inhibitory molecules LAG-3 and CTLA-4 showed higher expression rates in AML patients in comparison to healthy BM donors (statistically significant only on CD3+ and CD8+ bmT cells). For LAG-3 on CD8+ bmT cells, this could also be shown in RNA-seq.

In the literature, PD-1/PD-L1 (Okazaki et al., 2013) and TIM-3/GAL-9 (Austin et al., 2016; Wang et al., 2021) axes are described as important co-inhibitory pathways suppressing T cell function. Additionally, increased co-expression of TIM-3 and PD-1 on T cells is associated with an exhausted T cell phenotype in AML (Zhou et al., 2011; Kong et al., 2015). CTLA-4 is another well described co-inhibitory marker inhibiting T cell activation via binding to ligands CD80 and CD86 after out-competing their co-stimulatory counterpart CD28 (Pardoll, 2012) and plays a role in immunoescape of AML (Ok and Young, 2017). Showing a striking synergy with PD-1 (Woo et al., 2012), also LAG-3 has been reported to suppress T cell activation and cytokine secretion (Andrews et al., 2017).

Putting it all together, late differentiation stages of bmT cells are enriched in the bone marrow of pediatric AML patients and accordingly those cells might express high levels of exhaustion markers, possibly representing the outcome of AML induced T cell exhaustion as immunoescape mechanism.

However, besides co-inhibitory molecules, also the expression of co-stimulatory molecules was altered at protein level on bmT cells of AML patients in comparison to healthy controls: Expression rates of CD134, GITR and ICOS were increased, whereas CD28 expression was reduced in AML patients (statistically significant only CD134 and GITR expression on CD3+ and CD4+ bmT cells).

At RNA level, NF-κB transcription factor c-Rel was found to be lower expressed by CD8+ bmT cells in AML patient samples compared to healthy BM donors. NF-κB pathway is an important signaling axis in T cells shown to be required for tumor control in vivo (Barnes et al., 2015). Especially in CD8+ T cells, impaired NF-κB activation was reported to be correlated with anergic condition (Clavijo and Frauwirth, 2012). c-Rel is a member of the NF-κB family predominantly found in cells of hematopoietic origin. In T cells, c-Rel is an important regulator of certain genes essential for immune function such as IL2 and Foxp3 (Visekruna et al., 2012). However, NF-κB inhibitor alpha and other proteins like Tripartite motif containing 39 (TRIM 39, Suzuki et al., 2016) and Interferon related developmental regulator 1 (IFRD1, Tummers et al., 2015) that were reported to rather inhibit NF-κB activation were also downregulated at RNA level in CD8+ bmT cells of AML patients. Therefore, the

role of NF-κB pathway in CD8+ bmT cells needs to be further investigated in the context of pediatric AML before making any more detailed evaluation here.

7.1.2 Increased frequency of bmT_{regs} in relapsed AML samples compared to initial AML samples

In contrast to numerous other studies (Szczepanski et al., 2009; Bansal et al., 2020; Wang et al., 2005), in which regulatory T cells (T_{regs}) have been shown to be overrepresented in AML patients (peripheral blood, bone marrow), in our pediatric patient cohort, the frequency of T_{regs} was not significantly altered compared to healthy controls in flow cytometry. Here it must be borne in mind that those results can differ depending on phenotypic definition of populations and conclusions are limited due to the small sample size in our study. However, there was an increased frequency of T_{regs} in relapsed AML samples in comparison to initial AML samples, indicating the recruitment of T_{regs} as mechanism of AML persistence, as described by Zhou et al. in 2009.

7.2 CD112 expression on AML blasts impacts CD226 expression on T cells, NK and NKT cells

Until now, we could show that the bmT cell phenotype of AML patients is altered in comparison to healthy controls. Despite some indications there is still the question, whether the differences in expression on bmT cells of AML patients and healthy BM donors are caused by an indirect or direct blast-T cell-interaction or whether they only represent the adaptive response of the bmT cells to the tumor microenvironment.

To investigate that further, we examined whether the observed changes in phenotype of physiologic immune cells (T cells, NK and NKT cells) were linked to blast phenotype. Thus, to determine whether AML blasts do induce e.g. T cell phenotype changes we analyzed two common axes of interaction between antigen presenting cells (APCs) and immune cells in the context of AML. To that end, we correlated the expression of CD86 and CD112/CD155 on AML blasts to the respective expression of CTLA-4/CD28 on bmT cells and TIGIT/CD226 on bmT cells, NK and NKT cells.

TIGIT and CD226, expressed by T cells, NK and NKT cells, are surface antigens with shared ligands CD112 and CD155. While the engagement of CD226 has a positive effect on immune cell function, TIGIT exerts immunosuppressive effects via outcompeting CD226 (Lozano et al., 2012; Yeo et al., 2021).

In our patient cohort, CD155 showed only low expression levels on AML blasts, whereas CD112 was overexpressed, with a trimodal distribution on AML blasts. Therefore, AML patients were divided into three groups: AML patients with low, intermediate and high CD112 expression on blasts. Divided into these three groups AML patients were compared in relation to their TIGIT and CD226 expression on bmT cells, NK and NKT cells. Indeed, CD112 expression on AML blasts was negatively correlated with CD226 expression on bmT cells, NK and NKT cells.

As shown by Wang and colleagues in 2018, CD8+ T cells expressing both TIGIT and PD-1, but not CD226, had significantly reduced capacity of producing IFN-γ, TNF-α and IL-2 in AML patients indicating that those cells may be dysfunctional.
Therefore, AML blasts in some patients might use this axis to impair immune cell function in sense of an immunoescape strategy.

Additionally, RNA-seq analysis showed that expression of DYNLT1 of CD8+ bmT cells was downregulated in initial AML samples with future relapse in comparison to initial AML samples without future relapse. DYNLT1 coding for Dynein light chain Tctex-type 1 was reported to play a role in hypoxic cytoprotection (Fang et al., 2011). This could be another mechanism used by AML blasts in some patients to inhibit T cell function.

A correlation of an increased CD86 expression on AML blasts with a change in CD28/CTLA-4 expression on bmT cells was not observed. In summary, the axis of TIGIT/CD226 seems a more suitable target for immune response amplifier therapy than the CTLA-4/CD28 axis.

7.3 Prognostic relevance of bmT cell phenotype

As a next step, this chapter elaborates the question whether bmT cell phenotype in AML correlates with clinical features such as future relapse. All of the following correlations with the clinical course of patients are based on a rather small patient cohort. Therefore, even from significant differences conclusions are limited due to the lack of a larger validation cohort. In addition, the results are limited by the lack of multivariate analyses. Nevertheless, the following results provide a unique set of information for future mechanistic experiments on the interaction between AML blasts and the immune system.

7.3.1 High ICOS expression on CD4+ bmT cells as positive prognostic marker and high CD134 expression on CD8+ bmT cells as negative prognostic marker at initial diagnosis in terms of AML relapse

At protein level, ICOS on CD4+ bmT cells and CD134 on CD8+ bmT cells were the only markers differentially expressed between initial AML samples with and without future relapse. For CD8+ bmT cells this could be also confirmed at RNA level.
In that context, AML patients were divided into two groups according to their ICOS or CD134 expression and compared with regards to their relapse-free survival using Kaplan-Meier estimates. In our patient cohort, a high ICOS expression on CD4+ bmT cells was shown to be a positive prognostic marker, whereas a high CD134 expression on CD8+ bmT cells was correlated with decreased relapse-free survival (only CD134 on CD8+ bmT cells remained statistically significant after multiple testing correction, see 6.2.8).
In order to better describe the functional difference between CD134 and ICOS as co-stimulatory markers on bmT cells so called *stimulation indices* were developed (described in 6.2.8) and patient groups were compared again using Kaplan-Meier estimates. Those indices describe the relation of different co-stimulatory marker expression levels and were evaluated for prognostic use concerning "future relapse". A high CD134/ICOS index of CD8+ bmT cells at initial diagnosis was significantly correlated with decreased relapse-free survival (not statistically significant after multiple testing correction, see 6.2.8), supporting the potential negative correlation between CD134 expression on CD8+ bmT cells at initial diagnosis and relapse-free survival.

For CD134 as a co-stimulatory molecule, which promotes expansion of CD8+ bmT cells, this seems paradoxical. However, as shown in a mouse model by Shrimali et al. in 2017, the antitumor effects of CD134 Agonist Antibody could be annulled by additional PD-1 blockade with consequently reduced survival. This was caused by an increased IFNγ expression leading to apoptosis of lymphocytes.
In our patient cohort, high CD134 expression could have led to apoptosis of the T cells via an exceptionally strong T cell activation and therefore, might be correlated with reduced relapse-free survival.

7.3.2 High ICOS/TIM-3 index of CD3+ bmT cells as positive prognostic marker and high CD134/PD-1 index of CD8+ bmT cells as negative prognostic marker at initial diagnosis regarding AML relapse

The so-called *tide* model, published by Zhu et al. in 2011, dealing with cell surface signaling molecules, and how they are involved in the control of immune responses, states that each

inflammatory response is tightly controlled with co-stimulatory and co-inhibitory molecules as modulators, which decide the direction and magnitude of the immune response. It serves as an addition to the traditional *two-signal* model.

The AML patient showing the highest expression of exhaustion marker TIM-3 on CD3+ bmT cells also had the highest expression of co-stimulatory marker ICOS on CD3+ bmT cells within all analyzed 29 AML patients.

Considering that ICOS was reported to support T cell function (Pourakbari et al., 2021; Wikenheiser and Stumhofer, 2016), this seems to contradict the hypothesis that AML drives bmT cells into exhaustion. However, as described by Esendagli in 2013, AML blasts may express potent co-stimulatory molecules (e.g. ICOSL) resulting in upregulation of T cell activation markers and T cell expansion, but the provoked T cell response would then finally enable the AML blasts to acquire an inhibitory phenotype. In contrast to that, it might be the case, that the overexpression of co-inhibitory molecules on bmT cells is not induced de novo, but upregulated upon T cell activation in the presence of co-stimulation, as part of a negative feedback response (Zhu et al., 2011).

As this patient did not have a relapse nor a refractory AML, we reasoned that in this case the high expression of the co-inhibitory molecule was rather a sign of T cell activation than T cell exhaustion. With regard to the *tide* model (Zhu et al., 2011), a well-balanced co-inhibitory/co-stimulatory marker expression on bmT cells could be consequently of importance for relapse-free survival.

So, in order to better describe the functionality of a bmT cell population we developed the so-called *exhaustion indices* (described in 6.2.9) and patient groups were compared using Kaplan-Meier estimates. Those indices describe the relation of the co-inhibitory and co-stimulatory marker expression on bmT cells and were evaluated for prognostic use concerning “future relapse”.
In our patient cohort, a high CD134/PD-1 index of CD8+ bmT cells was shown to be a negative prognostic marker regarding AML relapse, whereas a high ICOS/TIM-3 index of CD3+ bmT cells was correlated with increased relapse-free survival (not statistically significant after multiple testing correction, see 6.2.9). Worthy of special mention is that the patient with the lowest ICOS/TIM-3 index of CD3+ bmT cells at initial diagnosis in our patient cohort was the first patient to relapse.

To sum up, transferring the above-described *tide* model (Zhu et al., 2011) to our exhaustion indices, this would mean that the resulting T cell response might depend on whether the co-inhibitory or the co-stimulatory signal predominates (for exhaustion indices index of 1 as critical value). However,

numerous other prognostic markers have not been taken into account in our analysis and will have to be analyzed in prospective studies in larger patient cohorts.

7.4 Synthetic Immunotherapy for AML: Identification of CD33 and CLL1 as appropriate CAR antigens in combinatorial CAR T-cell therapy

Partially, the following has already been published in an adapted form by our working group in Willier et al., 2021.

To additionally identify possible target antigens in context of immunotherapy, AML blasts were phenotyped for respective expression levels. The results obtained from the analysis of AML samples were compared to $CD45_{dim}$ cells in the bone marrow of healthy BM donors.

Considering AML as malignant entity with one of the lowest mutational burden, targeting of AML-specific neo-antigens (ASNAs) arising directly from genetic alterations may not be that effective. AML associated antigens (AAAs), which are self-antigens that are abnormally expressed by AML cells, might represent more promising immune targets in context of CAR T-cell therapy for example (Austin et al., 2016).

Therefore, expression values of described AAAs were analyzed on AML blasts in our patient cohort and compared to $CD45_{dim}$ cells in healthy BM donors. CD135, CD123, CLL1, CD33 and TIM-3 showed significant overexpression in AML patients. Also, EMR2 was highly expressed on AML blasts.

However, as the majority of reported AAAs is also expressed in healthy bystander tissues, especially on normal myeloid progenitors, single targeting approaches could lead to severe on-target off-leukemia toxicity (Haubner et al., 2019; Mardiana and Gill, 2020). Here, combinatorial therapies might enhance efficacy of this immunotherapeutic approach without increasing on-target off-leukemia effects (Perna et al., 2017).

In this context, different antigen combinations were chosen on basis of the single marker expression levels. In our patient cohort, we checked the respective requirements for two different approaches of combinatorial CAR T-cell therapy.

In context of a Tandem-CAR target cells need to express both target antigens at the same time (Navai and Ahmed, 2016).

Therefore, the percentages of double positive AML blasts were determined for each target antigen combination. Cut-off was arbitrarily set at 50 % double positive blasts. Here, CD33/CLL1 turned out to be the combination, for which the most AML patients of our cohort (21/29 patients) had at least 50 % double positive blasts.

An alternative approach for dual targeting CAR T cells is the synNotch-gated CAR. Here, a synNotch receptor for one antigen (inductor antigen) controls the inducible expression of a CAR for a second antigen (target antigen, Roybal et al., 2016).

As the mechanism of action differs from the Tandem-CAR, the following criteria were considered: at least 20 % blasts had to be positive for the inductor antigen, whereas for the target antigen more than 80 % blasts had to be positive. Cut-off values were set arbitrarily, but with respect to the mechanism of action of a synNotch-gated CAR. Under these conditions, the most patients of our cohort (19/29) could be covered by using CLL1 as inductor and CD33 as target antigen.

The difference here to the Tandem-CAR is that synNotch-gated CAR T cells do not necessarily require both target antigens to be co-expressed on the same target cell and were shown to induce tumor regression without causing toxicity when the antigen-expressing normal cells and tumor cells were segregated (Srivastava et al., 2019).

Another possibility for dual targeting CAR T cells is the compound CAR (cCAR), a construct bearing two complete CAR constructs (ablation of leukemic cells expressing either or both CAR antigens, Petrov et al., 2018). Here, CLL1-CD33 cCAR T cells have already been shown to lead to good response in patients with refractory AML in a first-in-human phase 1 clinical trial (Liu et al., 2018).

In comparison to a compound CAR construct, Tandem- and synNotch-gated CAR-T cell therapies might be more specific approaches associated with less on-target off-leukemia toxicity, while probably showing reduced killing capacity. Nevertheless, all possibilities for combinatorial CAR T-cell therapy of pediatric AML need to be further investigated.

Furthermore, leukemic stem cells (LSCs) play an important role in disease progression and relapse of AML, implying that approaches to treatment have to eradicate LSCs for cure (van Gils et al., 2021; Thomas and Majeti, 2017).

Therefore, AML associated antigens CD33, TIM-3 and CLL1 were additionally analyzed for expression on LSCs. The mean expression of CD33 and CLL1 was reduced on LSCs in comparison to AML bulk cells, whereas TIM-3 was slightly higher expressed on LSCs (statistically significant only the reduction of CLL1 on LSCs compared to AML bulk cells).

This is more or less consistent with the findings in adult AML published by Haubner et al. in 2019, except that they found TIM-3 to be reduced on LSCs in comparison to AML bulk cells.

However, in our patient cohort, CD33 and CLL1 showed in general higher mean expression levels both on AML bulk cells and LSCs compared to TIM-3, although there was a reduction on LSCs. Consequently, CD33 and CLL1 were still considered to be the best suited CAR antigens in our patient cohort.

7.5 Outlook

In summary, we observed several differences comparing bmT cells, NK and NKT cells of pediatric AML patients and healthy BM donors. Some of these differences could be also of prognostic relevance. This, together with the fact, that observed changes might also be linked to blast phenotype, shown in our patient cohort for example via the TIGIT/CD226 axis, is indicative of a possible interaction between bmT cells and AML blasts. Moreover, for such an interaction to take place, a TCR engagement seems likely and consequently our data hint at a possible immunogenicity of pediatric AML.

CD33 and CLL1 were identified as appropriate target antigens in context of combinatorial CAR T-cell therapy. With regards to possible functionality assays, CAR target antigen expression levels were evaluated on human AML cell lines. Under the same conditions as in 7.4 EOL-1 would be a suitable cell line to use in functionality measurement of a CD33/CLL1 Tandem-CAR, as well as of a CLL1I/CD33T synNotch-gated CAR.

CD8+ bmT cells were shown to overexpress co-inhibitory molecule LAG-3, both at protein and RNA level. Therefore, it could be investigated for example whether a LAG-3 knockout could improve the cytotoxity of CAR T cells in pediatric AML, like it had been already studied for B cell acute lymphoblastic leukemia (e.g. Zhang et al., 2017). In contrast to that, IL21 receptor was less expressed by CD8+ bmT cells in AML patients at RNA level. As IL21 was reported to markedly enhance the ability of cells to mediate tumor regression upon adoptive transfer (Hinrichs et al., 2008), the engineering of an IL21 receptor could be another interesting approach which we are already trying to implement in our working group.

However, it remains to be assessed how to master the difficult balancing act between adequate killing capacity of CAR T cells and lacking specificity with resulting on-target off-leukemia toxicity.
The usage of adjuvant immunotherapeutic approaches in addition to conventional chemotherapy of AML might be a possible solution, for example, as standard chemotherapies were reported to induce immunogenic cell death (Fabian et al., 2021; Vincent et al., 2010).

7.6 Limitations of the study

After all, some limitations of our study should be noted. First, AML is a rather heterogeneous disease and can be differentiated into multiple subtypes (Goldman et al., 2019). Due to the small number of available pediatric AML patient samples this could not be considered in patient selection and might cause bias in our results. This issue is caused by the low frequency of pediatric AML with about 70 new cases per year in Germany. Moreover, patients diagnosed with MDS-related AML were excluded from the study. Nevertheless, since the transition is fluent, it was sometimes difficult to identify those samples. Thirdly, although results from AML samples were compared to age-matched and gender-matched healthy BM donors, as good as possible, age and gender bias may be still an issue, especially in comparison of different AML patient groups (no future relapse vs. future relapse, initial diagnosis vs. relapse), in which no gender and age balancing could be performed due to low sample size. Furthermore, expression levels were often very low in flow cytometry and the question arises which expression rates may be considered as relevant and which are insignificant.

8 Summary

While accounting for only approximately 15 % of pediatric leukemia, patients with acute myeloid leukemia (AML) have still a worse prognosis than the average of pediatric cancers. Over the last decades, immunotherapy has developed from a promising therapeutic option to a robust clinical reality for treating cancer patients. AML has been excluded from this development. Here, the possible interaction of pediatric AML with the immune system is investigated. Therefore, this work analyzed bmT cells (T cells in the bone marrow), AML blasts, NK and NKT cells within bone marrow samples of 29 pediatric AML patients and 9 healthy bone marrow (BM) donors for protein expression by flow cytometry, for RNA expression by RNA-sequencing and for chromatin accessibility by ATAC-sequencing. Firstly, bmT cell phenotype was altered in AML compared to healthy BM donors. Concerning the T cell maturation stages, there was a shift towards a more mature phenotype in AML patients detectable in contrast to healthy BM donors. This was shown at protein level in flow cytometry, but also in RNA-seq within the scope of reduced IL21R and upregulated Perforin 1 and Granzyme B expression by CD8+ bmT cells in AML patients. Moreover, bmT cells of AML patients showed overexpression of several co-inhibitory and co-stimulatory molecules at protein level in comparison to healthy BM donors. Here, TIM-3 and PD-1 are worthy of special mention being consistently overexpressed on all T cell subsets (CD3+, CD4+ and CD8+ bmT cells). On CD8+ bmT cells also LAG-3 expression was upregulated, both at protein and RNA level. Secondly, to investigate, whether the observed alterations in phenotype of physiologic immune cells (T cells, NK and NKT cells) were linked to blast phenotype, we analyzed two common axes of interaction between antigen presenting cells and immune cells in the context of AML. Here, CD226 expression on bmT cells, NK and NKT cells was shown to be negatively correlated with CD112 expression on AML blasts. This might indicate that the described alterations are rather caused by a direct or indirect blast-T cell-interaction also in sense of immunoescape strategies than the results of an adaptive response to the tumor microenvironment. Thirdly, CD134 expression on CD8+ bmT cells at initial diagnosis was shown to be of potential prognostic relevance in context of AML relapse, even after multiple testing correction. In RNA-seq this could be reaffirmed. In order to better describe the functionality of a bmT cell population we developed the so-called *exhaustion indices.* Those indices describe the relation of the co-inhibitory and co-stimulatory marker expression on bmT cells and were evaluated for prognostic relevance concerning “future relapse”. A high CD134/PD-1 index of CD8+ bmT cells was shown to be a potential negative prognostic marker concerning AML relapse, whereas a high ICOS/TIM-3 index of CD3+ bmT cells was correlated with increased relapse-free survival. Even with the limitation in mind of a small sample size and lack of a validation cohort, the results are indicative for an immune-interaction of pediatric AML blasts. Finally, targets for synthetic immunotherapy were

investigated. Considering co- and single-expression values on AML blasts, as well as expression levels on leukemic stem cells CD33 and CLL1 were shown to be the best suited target antigens in context of combinatorial CAR-T cell therapies (synNotch-CAR, Tandem-CAR). However, prospective clinical trials will have to confirm clinical relevance.

9 Zusammenfassung

Die akute myeloische Leukämie (AML) im Kindesalter ist mit ca. 15 % aller pädiatrischen Leukämien ein zwar eher selteneres Ereignis, zählt jedoch zu den vergleichsweise prognostisch ungünstigeren malignen Erkrankungen in diesem Lebensabschnitt. In der Krebstherapie hat in den letzten Jahrzehnten vor allem die Immuntherapie eine paradigmatische Entwicklung vollzogen. Heute sind immuntherapeutische Verfahren bereits fest in den Behandlungsplan einiger Krebserkrankungen integriert. Diese Arbeit beschäftigt sich mit der möglichen Interaktion des Immunsystems mit pädiatrischen AML Blasten. Es wurde eine Analyse von T-Zellen im Knochenmark von 29 pädiatrischen AML-Patienten und 9 gesunden Knochenmarksspendern durchgeführt. Mittels Durchflusszytometrie, RNA-Sequenzierung und ATAC-Sequenzierung untersuchten wir neben den T-Lymphozyten zudem AML-Blasten, NK- und NKT-Zellen. Erstens zeigten T-Zellen in AML-Patienten dabei im Allgemeinen einen weiter fortgeschrittenen Reifezustand als in gesunden Spendern. Dies zeigte sich auf Proteinebene mittels Durchflusszytometrie, aber konnte für CD8+ T-Zellen auch in der RNA-Sequenzierung im Rahmen der reduzierten IL21R-Expression und der erhöhten Expression von Perforin 1 und Granzym B bestätigt werden. T-Lymphozyten von AML-Patienten zeigten daneben in der Durchflusszytometrie eine Überexpression sowohl von kostimulatorischen, als auch von koinhibitorischen Molekülen im Vergleich zu Gesunden. Hier sind insbesondere die Moleküle TIM-3 und PD-1 zu erwähnen, die verglichen mit Knochenmarksspendern einheitlich auf allen drei T-Zell-Subtypen (CD3+, CD4+ und CD8+ T-Zellen) von AML-Patienten höher exprimiert waren. Auf CD8+ T-Zellen war zudem LAG-3 auf Protein-, wie auch auf RNA-Ebene hochreguliert. Um zu beurteilen, inwieweit die beobachteten Unterschiede des Phänotyps der physiologischen Immunzellen (T-Zellen, NK- und NKT-Zellen) in Zusammenhang mit dem Phänotypen der AML-Blasten stehen, wurden als nächster Schritt zwei geläufige Achsen der Interaktion zwischen Antigenpräsentierenden Zellen und Immunzellen im Kontext der AML analysiert. Hier zeigte sich eine negative Korrelation von CD226-Expression auf T-Zellen, NK- und NKT-Zellen und CD112-Expression auf AML-Blasten. Dies ist ein Hinweis, dass beschriebene Unterschiede eher durch eine direkte oder indirekte Blasten-T-Zellen-Interaktion auch im Rahmen einer möglichen Immunevasionsstrategie verursacht sind und nicht nur als eine bloße Anpassungsreaktion der Immunzellen an das Mikromilieu der AML zu verstehen sind. Außerdem zeigte sich die CD134-Expression auf CD8+ T-Zellen bei Erstdiagnose als potentiell prognostisch relevant im Kontext eines AML-Rezidivs, was sich auch in der RNA-Sequenzierung bestätigen ließ. Um die Funktionalität einer T-Zellpopulation im Knochenmark noch besser beschreiben zu können, entwickelten wir zudem die sogenannten *Exhaustion-Indizes* (*exhaustion indices*). Diese Indizes beschreiben das Verhältnis aus von T-Zellen exprimierten koinhibitorischen und kostimulatorischen Markern und wurden hinsichtlich des

Rezidivrisikos berechnet und bewertet. Ein hoher CD134/PD-1 Index von CD8+ T-Zellen stellte sich dabei als potentiell prognostisch ungünstig heraus, während ein hoher ICOS/TIM-3 Index von CD3+ T-Zellen mit einem eher niedrigen Rezidivrisiko korrelierte. Auch unter Berücksichtigung der begrenzten Stichprobengröße, sowie bislang fehlender Validierungskohorte, ist diese Arbeit hinweisend auf eine Interaktion von AML-Blasten mit dem Immunsystem. Abschließend wurden außerdem mögliche Zielproteine für synthetische Immuntherapie untersucht. Unter Berücksichtigung von Ko- und Einzelexpressionswerten auf AML-Blasten, sowie Expressionsraten auf leukämischen Stammzellen erwiesen sich CD33 und CLL1 als die am besten geeigneten Zielantigene im Rahmen einer kombinatorischen CAR-T-zell-Therapie (synNotch-CAR, Tandem-CAR). Prospektive klinische Studien werden die klinische Relevanz der Ergebnisse zu bestätigen haben.

10 Literature

Alexandrov, L.B., Nik-Zainal, S., Wedge, D.C., Aparicio, S.A.J.R., Behjati, S., Biankin, A.V., Bignell, G.R., Bolli, N., Borg, A., Børresen-Dale, A.-L., Boyault, S., Burkhardt, B., Butler, A.P., Caldas, C., Davies, H.R., Desmedt, C., Eils, R., Eyfjörd, J.E., Foekens, J.A., Greaves, M., Hosoda, F., Hutter, B., Ilicic, T., Imbeaud, S., Imielinski, M., Jäger, N., Jones, D.T., Jones, D., Knappskog, S., Kool, M., Lakhani, S.R., López-Otín, C., Martin, S., Munshi, N.C., Nakamura, H., Northcott, P.A., Pajic, M., Papaemmanuil, E., Paradiso, A., Pearson, J.V., Puente, X.S., Raine, K., Ramakrishna, M., Richardson, A.L., Richter, J., Rosenstiel, P., Schlesner, M., Schumacher, T.N., Span, P.N., Teague, J.W., Totoki, Y., Tutt, A.N., Valdés-Mas, R., van Buuren, M.M., van 't Veer, L., Vincent-Salomon, A., Waddell, N., Yates, L.R.; Australian Pancreatic Cancer Genome Initiative; ICGC Breast Cancer Consortium; ICGC MMML-Seq Consortium; ICGC PedBrain, Zucman-Rossi, J., Futreal, P.A., McDermott, U., Lichter, P., Meyerson, M., Grimmond, S.M., Siebert, R., Campo, E., Shibata, T., Pfister, S.M., Campbell, P.J., and Stratton, M.R. (2013). Signatures of mutational processes in human cancer. Nature *500*, 415–421.

Andrews, L.P., Marciscano, A.E., Drake, C.G., and Vignali, D.A.A. (2017). LAG3 (CD223) as a Cancer Immunotherapy Target. Immunol Rev *276*, 80–96.

Austin, R., Smyth, M.J., and Lane, S.W. (2016). Harnessing the immune system in acute myeloid leukaemia. Critical Reviews in Oncology/Hematology *103*, 62–77.

Bansal, A.K., Sharawat, S.K., Gupta, R., Vishnubhatla, S., Dhawan, D., and Bakhshi, S. (2020). Regulatory T cells in pediatric AML are associated with disease load and their serial assessment suggests role in leukemogenesis. Am J Blood Res *10*, 90–96.

Barnes, T.A., and Amir, E. (2017). HYPE or HOPE: the prognostic value of infiltrating immune cells in cancer. Br J Cancer *117*, 451–460.

Barnes, S.E., Wang, Y., Chen, L., Molinero, L.L., Gajewski, T.F., Evaristo, C., and Alegre, M.-L. (2015). T cell-NF-κB activation is required for tumor control in vivo. J Immunother Cancer *3*.

Barrett, A.J., and Le Blanc, K. (2010). Immunotherapy prospects for acute myeloid leukaemia. Clin Exp Immunol *161*, 223–232.

Bleakley, M., and Riddell, S.R. (2004). Molecules and mechanisms of the graft-versus-leukaemia effect. Nature Reviews Cancer *4*, 371–380.

Bonomo, A., Monteiro, A.C., Gonçalves-Silva, T., Cordeiro-Spinetti, E., Galvani, R.G., and Balduino, A. (2016). A T Cell View of the Bone Marrow. Front Immunol *7*.

Clavijo, P.E., and Frauwirth, K.A. (2012). Anergic CD8+ T Lymphocytes Have Impaired NF-κB Activation with Defects in p65 Phosphorylation and Acetylation. J Immunol *188*, 1213–1221.

Corces, M.R., Trevino, A.E., Hamilton, E.G., Greenside, P.G., Sinnott-Armstrong, N.A., Vesuna, S., Satpathy, A.T., Rubin, A.J., Montine, K.S., Wu, B., Kathiria, A., Cho, S.W., Mumbach, M.R., Carter, A.C., Kasowski, M., Orloff, L.A., Risca, V.I., Kundaje, A., Khavari, P.A., Montine, T.J., Greenleaf, W.J., and Chang H.Y. (2017). An improved

ATAC-seq protocol reduces background and enables interrogation of frozen tissues. Nat Methods *14*, 959–962.

Daver, N., Alotaibi, A.S., Bücklein, V., and Subklewe, M. (2021). T-cell-based immunotherapy of acute myeloid leukemia: current concepts and future developments. Leukemia *35*, 1843–1863.

Deng, S., Sun, Z., Qiao, J., Liang, Y., Liu, L., Dong, C., Shen, A., Wang, Y., Tang, H., Fu, Y.-X., and Peng, H. (2020). Targeting tumors with IL-21 reshapes the tumor microenvironment by proliferating PD-1intTim-3-CD8+ T cells. JCI Insight *5*, 132000.

Di Rosa, F., and Gebhardt, T. (2016). Bone Marrow T Cells and the Integrated Functions of Recirculating and Tissue-Resident Memory T Cells. Front. Immunol. *7*.

Eil, R., Vodnala, S.K., Clever, D., Klebanoff, C.A., Sukumar, M., Pan, J.H., Palmer, D.C., Gros, A., Yamamoto, T.N., Patel, S.J., Guittard, G.C., Yu, Z., Carbonaro, V., Okkenhaug, K., Schrump, D.S., Linehan, W.M., Roychoudhuri, R., and Restifo, N.P. (2016). Ionic immune suppression within the tumour microenvironment limits T cell effector function. Nature *537*, 539–543.

Elgarten, C.W., and Aplenc, R. (2020). Pediatric acute myeloid leukemia: updates on biology, risk stratification, and therapy. Current Opinion in Pediatrics *32*, 57–66.

Esendagli, G. (2013). A co-stimulatory trap set by myeloid leukemia cells. Oncoimmunology *2*.

Fabian, K.P., Wolfson, B., and Hodge, J.W. (2021). From Immunogenic Cell Death to Immunogenic Modulation: Select Chemotherapy Regimens Induce a Spectrum of Immune-Enhancing Activities in the Tumor Microenvironment. Front Oncol *11*, 728018.

Fang, Y., Xu, X., Dang, Y., Zhang, Y., Zhang, J., Hu, J., Zhang, Q., Dai, X., Teng, M., Zhang, D., and Huang, Y.S. (2011). MAP4 mechanism that stabilizes mitochondrial permeability transition in hypoxia: microtubule enhancement and DYNLT1 interaction with VDAC1. PLoS ONE *6*, e28052.

Fidler, M.M., Reulen, R.C., Winter, D.L., Kelly, J., Jenkinson, H.C., Skinner, R., Frobisher, C., and Hawkins, M.M. (2016). Long term cause specific mortality among 34 489 five year survivors of childhood cancer in Great Britain: population based cohort study. BMJ i4351.

van Gils, N., Denkers, F., and Smit, L. (2021). Escape From Treatment; the Different Faces of Leukemic Stem Cells and Therapy Resistance in Acute Myeloid Leukemia. Front Oncol *11*, 659253.

Goldman, S.L., Hassan, C., Khunte, M., Soldatenko, A., Jong, Y., Afshinnekoo, E., and Mason, C.E. (2019). Epigenetic Modifications in Acute Myeloid Leukemia: Prognosis, Treatment, and Heterogeneity. Front Genet *10*.

Guo, Y., Lee, Y.-C., Brown, C., Zhang, W., Usherwood, E., and Noelle, R.J. (2014). Dissecting the Role of Retinoic Acid Receptor Isoforms in the CD8 Response to Infection. J Immunol *192*, 3336–3344.

Harrington, A.M., Olteanu, H., and Kroft, S.H. (2012). A Dissection of the CD45/Side Scatter “Blast Gate.” Am J Clin Pathol *137*, 800–804.

Haubner, S., Perna, F., Köhnke, T., Schmidt, C., Berman, S., Augsberger, C., Schnorfeil, F.M., Krupka, C.,

Lichtenegger, F.S., Liu, X., Kerbs, P., Schneider, S., Metzeler, K.H., Spiekermann, K., Hiddemann, W., Greif, P.A., Herold, T., Sadelain, M., and Subklewe, M. (2019). Coexpression profile of leukemic stem cell markers for combinatorial targeted therapy in AML. Leukemia *33*, 64–74.

Hegde, P.S., and Chen, D.S. (2020). Top 10 Challenges in Cancer Immunotherapy. Immunity *52*, 17–35.

Hinrichs, C.S., Spolski, R., Paulos, C.M., Gattinoni, L., Kerstann, K.W., Palmer, D.C., Klebanoff, C.A., Rosenberg, S.A., Leonard, W.J., and Restifo, N.P. (2008). IL-2 and IL-21 confer opposing differentiation programs to CD8+ T cells for adoptive immunotherapy. Blood *111*, 5326–5333.

Hlongwane, P., Mungra, N., Madheswaran, S., Akinrinmade, O.A., Chetty, S., and Barth, S. (2018). Human Granzyme B Based Targeted Cytolytic Fusion Proteins. Biomedicines *6*, 72.

Howlader, N., Noone, A.M., Krapcho, M., Miller, D., Brest, A., Yu, M., Ruhl, J., Tatalovich, Z., Mariotto, A., Lewis, D.R., Chen, H.S., Feuer, E.J., and Cronin, K.A. (eds). SEER Cancer Statistics Review, 1975-2016, National Cancer Institute. Bethesda, MD, https://seer.cancer.gov/csr/1975_2016/, based on November 2018 SEER data submission, posted to the SEER web site, April 2019.

Hwang, W.-T., Adams, S.F., Tahirovic, E., Hagemann, I.S., and Coukos, G. (2012). Prognostic Significance of Tumor-infiltrating T-cells in Ovarian Cancer: a Meta-analysis. Gynecol Oncol *124*, 192–198.

Kaspers, G.J.L., and Creutzig, U. (2005). Pediatric acute myeloid leukemia: international progress and future directions. Leukemia *19*, 2025–2029.

Klein, K., de Haas, V., and Kaspers, G.J.L. (2018). Clinical challenges in *de novo* pediatric acute myeloid leukemia. Expert Review of Anticancer Therapy *18*, 277–293.

Koedijk, J.B., van der Werf, I., Calkoen, F.G., Nierkens, S., Kaspers, G.J.L., Zwaan, C.M., and Heidenreich, O. (2021). Paving the Way for Immunotherapy in Pediatric Acute Myeloid Leukemia: Current Knowledge and the Way Forward. Cancers (Basel) *13*, 4364.

Kong, Y., Zhang, J., Claxton, D.F., Ehmann, W.C., Rybka, W.B., Zhu, L., Zeng, H., Schell, T.D., and Zheng, H. (2015). PD-1^{hi}TIM-3^{+} T cells associate with and predict leukemia relapse in AML patients post allogeneic stem cell transplantation. Blood Cancer Journal *5*, e330.

Lamble, A.J., and Tasian, S.K. (2019). Opportunities for immunotherapy in childhood acute myeloid leukemia. Blood Adv *3*, 3750–3758.

Larkin, J., Chiarion-Sileni, V., Gonzalez, R., Grob, J.-J., Rutkowski, P., Lao, C.D., Cowey, C.L., Schadendorf, D., Wagstaff, J., Dummer, R., Ferrucci, P.F., Smylie, M., Hogg, D., Hill, A., Márquez-Rodas, I., Haanen, J., Guidoboni, M., Maio, M., Schöffski, P., Carlino, M.S., Lebbé, C., McArthur, G., Ascierto, P.A., Daniels, G.A., Long, G.V., Bastholt, L., Rizzo, J.I., Balogh, A., Moshyk, A., Hodi, F.S., and Wolchok, J.D. (2019). Five-Year Survival with Combined Nivolumab and Ipilimumab in Advanced Melanoma. New England Journal of Medicine.

Laumont, C.M., Vincent, K., Hesnard, L., Audemard, É., Bonneil, É., Laverdure, J.-P., Gendron, P., Courcelles, M., Hardy, M.-P., Côté, C., Durette, C., St-Pierre, C., Benhammadi, M., Lanoix, J., Vobecky, S., Haddad, E., Lemieux, S., Thibault, P., and Perreault, C. (2018). Noncoding regions are the main source of targetable tumor-specific

antigens. Sci. Transl. Med. *10*, eaau5516.

Liu, F., Cao, Y., Pinz, K., Ma, Y., Wada, M., Chen, K., Ma, G., Shen, J., Tse, C.O., Su, Y., Xiong, Y., He, G., Li, Y., and Ma, Y. (2018). First-in-Human CLL1-CD33 Compound CAR T Cell Therapy Induces Complete Remission in Patients with Refractory Acute Myeloid Leukemia: Update on Phase 1 Clinical Trial. Blood *132*, 901–901.

Lozano, E., Dominguez-Villar, M., Kuchroo, V., and Hafler, D.A. (2012). The TIGIT/CD226 axis regulates human T cell function. J Immunol *188*, 3869–3875.

Majzner, R.G., Heitzeneder, S., and Mackall, C.L. (2017). Harnessing the Immunotherapy Revolution for the Treatment of Childhood Cancers. Cancer Cell *31*, 476–485.

Mardiana, S., and Gill, S. (2020). CAR T Cells for Acute Myeloid Leukemia: State of the Art and Future Directions. Front Oncol *10*, 697.

Maude, S.L., Frey, N., Shaw, P.A., Aplenc, R., Barrett, D.M., Bunin, N.J., Chew, A., Gonzalez, V.E., Zheng, Z., Lacey, S.F., Mahnke, Y.D., Melenhorst, J.J., Rheingold, S.R., Shen, A., Teachey, D.T., Levine, B.L., June, C.H., Porter, D.L., and Grupp, S.A. (2014). Chimeric Antigen Receptor T Cells for Sustained Remissions in Leukemia. N Engl J Med *371*, 1507–1517.

Maude, S.L., Laetsch, T.W., Buechner, J., Rives, S., Boyer, M., Bittencourt, H., Bader, P., Verneris, M.R., Stefanski, H.E., Myers, G.D., Qayed, M., De Moerloose, B., Hiramatsu, H., Schlis, K., Davis, K.L., Martin, P.L., Nemecek, E.R., Yanik, G.A., Peters, C., Baruchel, A., Boissel, N., Mechinaud, F., Balduzzi, A., Krueger, J., June, C.H., Levine, B.L., Wood, P., Taran, T., Leung, M., Mueller, K.T., Zhang, Y., Sen, K., Lebwohl, D., Pulsipher, M.A., and Grupp, S.A. (2018). Tisagenlecleucel in Children and Young Adults with B-Cell Lymphoblastic Leukemia. New England Journal of Medicine.

Mozafari, R., Moeinian, M., and Asadollahi-Amin, A. (2017). Spontaneous Complete Remission in a Patient with Acute Myeloid Leukemia and Severe Sepsis. Case Rep Hematol *2017*.

Müller, C.I., Trepel, M., Kunzmann, R., Lais, A., Engelhardt, R., and Lübbert, M. (2004). Hematologic and molecular spontaneous remission following sepsis in acute monoblastic leukemia with translocation (9;11): a case report and review of the literature. European Journal of Haematology *73*, 62–66.

Navai, S.A., and Ahmed, N. (2016). Targeting the tumour profile using broad spectrum chimaeric antigen receptor T-cells. Biochemical Society Transactions *44*, 391–396.

Oble, D.A., Loewe, R., Yu, P., and Mihm, M.C. (2009). Focus on TILs: Prognostic significance of tumor infiltrating lymphocytes in human melanoma. Cancer Immun *9*.

Ohl, K., Wiener, A., Lippe, R., Schippers, A., Zorn, C., Roth, J., Wagner, N., and Tenbrock, K. (2016). CREM Alpha Enhances IL-21 Production in T Cells In Vivo and In Vitro. Front Immunol *7*.

Ok, C.Y., and Young, K.H. (2017). Checkpoint inhibitors in hematological malignancies. J Hematol Oncol *10*.

Okazaki, T., Chikuma, S., Iwai, Y., Fagarasan, S., and Honjo, T. (2013). A rheostat for immune responses: the unique properties of PD-1 and their advantages for clinical application. Nature Immunology *14*, 1212–1218.

Ong, S.T., Ng, A.S., Ng, X.R., Zhuang, Z., Wong, B.H.S., Prasannan, P., Kok, Y.J., Bi, X., Shim, H., Wulff, H., Chandy, K.G., and Verma, N.K. (2019). Extracellular K+ Dampens T Cell Functions: Implications for Immune Suppression in the Tumor Microenvironment. Bioelectricity *1*, 169–179.

Pardoll, D.M. (2012). The blockade of immune checkpoints in cancer immunotherapy. Nat Rev Cancer *12*, 252–264.

Perna, F., Berman, S.H., Soni, R.K., Mansilla-Soto, J., Eyquem, J., Hamieh, M., Hendrickson, R.C., Brennan, C.W., and Sadelain, M. (2017). Integrating Proteomics and Transcriptomics for Systematic Combinatorial Chimeric Antigen Receptor Therapy of AML. Cancer Cell *32*, 506-519.e5.

Petrov, J.C., Wada, M., Pinz, K.G., Yan, L.E., Chen, K.H., Shuai, X., Liu, H., Chen, X., Leung, L.-H., Salman, H., Hagag, N., Liu, F., Jiang, X., and Ma, Y. (2018). Compound CAR T-cells as a double-pronged approach for treating acute myeloid leukemia. Leukemia *32*, 1317.

Pourakbari, R., Hajizadeh, F., Parhizkar, F., Aghebati-Maleki, A., Mansouri, S., and Aghebati-Maleki, L. (2021). Co-stimulatory agonists: An insight into the immunotherapy of cancer. EXCLI J *20*, 1055–1085.

Roybal, K.T., Rupp, L.J., Morsut, L., Walker, W.J., McNally, K.A., Park, J.S., and Lim, W.A. (2016). Precision Tumor Recognition by T Cells With Combinatorial Antigen Sensing Circuits. Cell *164*, 770–779.

Samstein, R.M., Lee, C.-H., Shoushtari, A.N., Hellmann, M.D., Shen, R., Janjigian, Y.Y., Barron, D.A., Zehir, A., Jordan, E.J., Omuro, A., Kaley, T.J., Kendall, S.M., Motzer, R.J., Hakimi, A.A., Voss, M.H., Russo, P., Rosenberg, J., Iyer, G., Bochner, B.H., Bajorin, D.F., Al-Ahmadie, H.A., Chaft, J.E., Rudin, C.M., Riely, G.J., Baxi, S., Ho, A.L., Wong, R.J., Pfister, D.G., Wolchok, J.D., Barker, C.A., Gutin, P.H., Brennan, C.W., Tabar, V., Mellinghoff, I.K., DeAngelis, L.M., Ariyan, C.E., Lee, N., Tap, W.D., Gounder, M.M., D'Angelo, S.P., Saltz, L., Stadler, Z.K., Scher, H.I., Baselga, J., Razavi, P., Klebanoff, C.A., Yaeger, R., Segal, N.H., Ku, G.Y., DeMatteo, R.P., Ladanyi, M., Rizvi, N.A., Berger, M.F., Riaz, N., Solit, D.B., Chan, T.A., and Morris, L.G.T. (2019). Tumor mutational load predicts survival after immunotherapy across multiple cancer types. Nat. Genet. *51*, 202–206.

Sanchez-Correa, B., Gayoso, I., Bergua, J.M., Casado, J.G., Morgado, S., Solana, R., and Tarazona, R. (2012). Decreased expression of DNAM-1 on NK cells from acute myeloid leukemia patients. Immunol. Cell Biol. *90*, 109–115.

Sato, E., Olson, S.H., Ahn, J., Bundy, B., Nishikawa, H., Qian, F., Jungbluth, A.A., Frosina, D., Gnjatic, S., Ambrosone, C., Kepner, J., Odunsi, T., Ritter, G., Lele, S., Chen, Y.T., Ohtani, H., Old, L.J., and Odunsi, K. (2005). Intraepithelial CD8+ tumor-infiltrating lymphocytes and a high CD8+/regulatory T cell ratio are associated with favorable prognosis in ovarian cancer. Proc Natl Acad Sci U S A *102*, 18538–18543.

Shrimali, R.K., Ahmad, S., Verma, V., Zeng, P., Ananth, S., Gaur, P., Gittelman, R.M., Yusko, E., Sanders, C., Robins, H., Hammond, S.A., Janik, J.E., Mkrtichyan, M., Gupta, S., and Khleif, S.N. (2017). Concurrent PD-1 Blockade Negates the Effects of OX40 Agonist Antibody in Combination Immunotherapy through Inducing T-cell Apoptosis. Cancer Immunol Res *5*, 755–766.

Srivastava, S., Salter, A.I., Liggitt, D., Yechan-Gunja, S., Sarvothama, M., Cooper, K., Smythe, K.S., Dudakov, J.A., Pierce, R.H., Rader, C., and Riddell, S.R. (2019). Logic-Gated ROR1 Chimeric Antigen Receptor Expression

Rescues T Cell-Mediated Toxicity to Normal Tissues and Enables Selective Tumor Targeting. Cancer Cell *35*, 489-503.e8.

Strickler, J.H., Hanks, B.A., and Khasraw, M. (2021). Tumor Mutational Burden as a Predictor of Immunotherapy Response: Is More Always Better? Clin Cancer Res *27*, 1236–1241.

Suzuki, M., Watanabe, M., Nakamaru, Y., Takagi, D., Takahashi, H., Fukuda, S., and Hatakeyama, S. (2016). TRIM39 negatively regulates the NFκB-mediated signaling pathway through stabilization of Cactin. Cellular and Molecular Life Sciences *73*, 1085–1101.

Szczepanski, M.J., Szajnik, M., Czystowska, M., Mandapathil, M., Strauss, L., Welsh, A., Foon, K.A., Whiteside, T.L., and Boyiadzis, M. (2009). Increased Frequency and Suppression by Regulatory T Cells in Patients with Acute Myelogenous Leukemia. Clin Cancer Res *15*, 3325–3332.

Taghiloo, S., and Asgarian-Omran, H. (2021). Immune evasion mechanisms in acute myeloid leukemia: A focus on immune checkpoint pathways. Critical Reviews in Oncology/Hematology *157*, 103164.

Thomas, D., and Majeti, R. (2017). Biology and relevance of human acute myeloid leukemia stem cells. Blood *129*, 1577–1585.

Tummers, B., Goedemans, R., Pelascini, L.P.L., Jordanova, E.S., van Esch, E.M.G., Meyers, C., Melief, C.J.M., Boer, J.M., and van der Burg, S.H. (2015). The interferon-related developmental regulator 1 is used by human papillomavirus to suppress NFκB activation. Nat Commun *6*.

Vincent, J., Mignot, G., Chalmin, F., Ladoire, S., Bruchard, M., Chevriaux, A., Martin, F., Apetoh, L., Rébé, C., and Ghiringhelli, F. (2010). 5-Fluorouracil Selectively Kills Tumor-Associated Myeloid-Derived Suppressor Cells Resulting in Enhanced T Cell–Dependent Antitumor Immunity. Cancer Res *70*, 3052–3061.

Visekruna, A., Volkov, A., and Steinhoff, U. (2012). A Key Role for NF-κB Transcription Factor c-Rel in T-Lymphocyte-Differentiation and Effector Functions. Clin Dev Immunol *2012*.

Voskoboinik, I., Whisstock, J.C., and Trapani, J.A. (2015). Perforin and granzymes: function, dysfunction and human pathology. Nature Reviews Immunology *15*, 388–400.

Wang, M., Bu, J., Zhou, M., Sido, J., Lin, Y., Liu, G., Lin, Q., Xu, X., Leavenworth, J.W., and Shen, E. (2018). CD8+T cells expressing both PD-1 and TIGIT but not CD226 are dysfunctional in acute myeloid leukemia (AML) patients. Clinical Immunology *190*, 64–73.

Wang, X., Zheng, J., Liu, J., Yao, J., He, Y., Li, X., Yu, J., Yang, J., Liu, Z., and Huang, S. (2005). Increased population of CD4(+)CD25(high), regulatory T cells with their higher apoptotic and proliferating status in peripheral blood of acute myeloid leukemia patients. Eur. J. Haematol. *75*, 468–476.

Wang, Z., Chen, J., Wang, M., Zhang, L., and Yu, L. (2021). One Stone, Two Birds: The Roles of Tim-3 in Acute Myeloid Leukemia. Front Immunol *12*, 618710.

Wikenheiser, D.J., and Stumhofer, J.S. (2016). ICOS Co-Stimulation: Friend or Foe? Front Immunol *7*.

Willier, S., Rothämel, P., Hastreiter, M., Wilhelm, J., Stenger, D., Blaeschke, F., Rohlfs, M., Kaeuferle, T., Schmid,

I., Albert, M.H., Binder, V., Subklewe, M., Klein, C., and Feuchtinger, T. (2021). CLEC12A and CD33 coexpression as a preferential target for pediatric AML combinatorial immunotherapy. Blood *137*, 1037–1049.

Woo, S.-R., Turnis, M.E., Goldberg, M.V., Bankoti, J., Selby, M., Nirschl, C.J., Bettini, M.L., Gravano, D., Vogel, P., Liu, C.L., Tangsombatvisit, S., Grosso, J.F., Netto, G., Smeltzer, M.P., Chaux, A., Utz, P.J., Workman, C.J., Pardoll, D.M., Korman, A.J., Drake, C.G., and Vignali, D.A. (2012). Immune inhibitory molecules LAG-3 and PD-1 synergistically regulate T cell function to promote tumoral immune escape. Cancer Res *72*, 917–927.

Xu, L., Yao, D., Tan, J., He, Z., Yu, Z., Chen, J., Luo, G., Wang, C., Zhou, F., Zha, X., Chen, S., and Li, Y. (2018). Memory T cells skew toward terminal differentiation in the CD8+ T cell population in patients with acute myeloid leukemia. J Hematol Oncol *11*.

Yeo, J., Ko, M., Lee, D.-H., Park, Y., and Jin, H.-S. (2021). TIGIT/CD226 Axis Regulates Anti-Tumor Immunity. Pharmaceuticals (Basel) *14*, 200.

Zamora, A.E., Crawford, J.C., Allen, E.K., Guo, X.J., Bakke, J., Carter, R.A., Abdelsamed, H.A., Moustaki, A., Li, Y., Chang, T.-C., Awad, W., Dallas, M.H., Mullighan, C.G., Downing, J.R., Geiger, T.L., Chen, T., Green, D.R., Youngblood, B.A., Zhang, J., and Thomas, P.G. (2019). Pediatric patients with acute lymphoblastic leukemia generate abundant and functional neoantigen-specific CD8+ T cell responses. Sci Transl Med *11*.

Zhang, Y., Zhang, X., Cheng, C., Mu, W., Liu, X., Li, N., Wei, X., Liu, X., Xia, C., and Wang, H. (2017). CRISPR-Cas9 mediated LAG-3 disruption in CAR-T cells. Frontiers of Medicine *11*, 554–562.

Zhou, Q., Bucher, C., Munger, M.E., Highfill, S.L., Tolar, J., Munn, D.H., Levine, B.L., Riddle, M., June, C.H., Vallera, D.A., Weigel, B.J., and Blazar, B.R. (2009). Depletion of endogenous tumor-associated regulatory T cells improves the efficacy of adoptive cytotoxic T-cell immunotherapy in murine acute myeloid leukemia. Blood *114*, 3793–3802.

Zhou, Q., Munger, M.E., Veenstra, R.G., Weigel, B.J., Hirashima, M., Munn, D.H., Murphy, W.J., Azuma, M., Anderson, A.C., Kuchroo, V.K., and Blazar, B.R. (2011). Coexpression of Tim-3 and PD-1 identifies a CD8+ T-cell exhaustion phenotype in mice with disseminated acute myelogenous leukemia. Blood *117*, 4501–4510.

Zhu, Y., Yao, S., and Chen, L. (2011). CELL SURFACE SIGNALING MOLECULES IN THE CONTROL OF IMMUNE RESPONSES: A TIDE MODEL. Immunity *34*, 466–478.

Zwaan, C.M., Kolb, E.A., Reinhardt, D., Abrahamsson, J., Adachi, S., Aplenc, R., De Bont, E.S.J.M., De Moerloose, B., Dworzak, M., Gibson, B.E.S., Hasle, H., Leverger, G., Locatelli, F., Ragu, C., Ribeiro, R.C., Rizzari, C., Rubnitz, J.E., Smith, O.P., Sung, L., Tomizawa, D., van den Heuvel-Eibrink, M.M., Creutzig, U., and Kaspers, G.J. (2015). Collaborative Efforts Driving Progress in Pediatric Acute Myeloid Leukemia. J Clin Oncol *33*, 2949–2962.

11 Acknowledgements

Firstly, I would like to express my sincere gratitude to Prof. Dr. Tobias Feuchtinger for providing me the opportunity to complete my doctoral thesis in his laboratory and for trusting me with this great project. I am deepest grateful for all his encouragement and kind support during the last few years.

My deepest appreciation also goes to Dr. Semjon Willier. He provided me the best supervision and support I could have during the process of researching and thesis writing. I am very grateful for providing his invaluable guidance, comments and suggestions throughout the course of the project. I deeply appreciate any time he donated for discussions, particularly in his precious spare time. I enjoyed his professional and concomitant sincere, as well as often humorous way of supervision. Furthermore, RNA-sequencing and analysis could not have been accomplished without his support.

Additionally, I would like to thank Jonas Wilhelm for being my lab partner and for all his support and encouragement during this time.
Furthermore, I would like to extend my sincere thanks to Raffaele Conca and Susanne Wullinger for helping with FACS procedure and for providing all required technical devices.
Also, I would like to offer special thanks to Dr. Meino Rohlfs for his great support with RNA- and ATAC-sequencing procedure, as well as operation of the bioanalyzer.
Additionally, I would like to thank Dr. Matthias Heinig, Dr. Thomas Walzthöni and Dr. Lukas Friedrich for their great support with RNA-seq analysis. I also take this opportunity to express a deep sense of gratidude to Prof. Dr. Dr. Christoph Klein, without whom RNA-seq would not have been possible to afford so quickly.
Moreover, I am grateful for Tanja Weißer and Nicola Habjan for their guidance during my training.
I am deeply grateful for Dr. Franziska Blaeschke, Dr. Theresa Käuferle, Dana Stenger, Tanja Stief, Nadine Stoll, Florian Jurgeleit, Tanja Rossmann, Larissa Deisenberger, Jasmin Mahdawi, Lena Jablonowski, Antonia Apfelbeck and the entire working group for all their kind support, their help and motivations. I am grateful for integrating me in their research group and for providing such a pleasant working atmosphere.

Finally, I am particularly grateful for all the mental support and encouragements given by my boyfriend Andreas, my friends and my family.

This work was supported by a doctoral fellowship of the *Kind-Philipp-Stiftung für pädiatrisch-onkologische Forschung*.